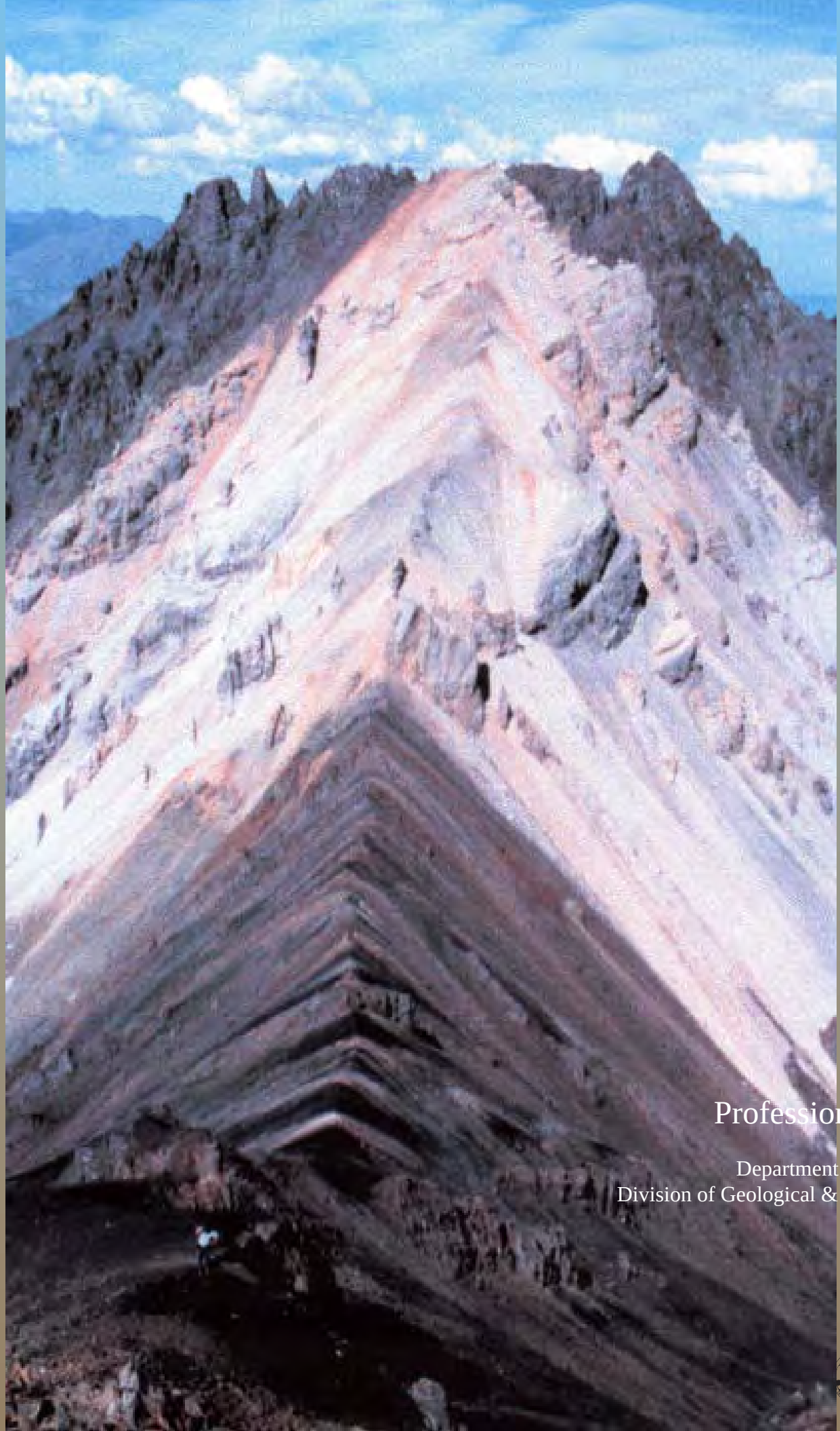

Short Notes on Alaska Geology 1999

Professional Report 119

State of Alaska
Department of Natural Resources
Division of Geological & Geophysical Surveys

Milton A. Wiltse
State Geologist

1999

Alaska Department of
NATURAL
RESOURCES

Editorial Policy

Short Notes on Alaska Geology is a collection of brief scientific papers describing recent geological investigations of limited scope. This publication is widely distributed to a state, national, and international audience that represents industry, academia, government agencies, and the general public. Manuscripts are accepted for consideration with the understanding that they have not been previously published and are not being submitted for publication elsewhere, that all persons listed as authors have given their approval for submission of the paper, and that any person cited as a source of personal communication has approved such a citation. Authors are encouraged to suggest appropriate reviewers and provide reviewers' telephone numbers.

Submission of Manuscripts

Authors should submit three paper copies of their draft manuscripts to Short Notes Editor, Alaska Division of Geological & Geophysical Surveys, 794 University Avenue, Suite 200, Fairbanks, Alaska 99709-3645. Contributors should retain one copy of all materials submitted. DGGS is not responsible for materials lost in the mail. In general, articles are limited to about 10 manuscript pages (approximately 2,000 words of text), including references, figures, and tables.

All draft manuscripts will be examined and approved by the DGGS editor and at least two reviewers. After technical reviews are completed, copies of review forms and reviewed manuscript pages will be returned to the author for revision (if required) and resubmittal. Conflicts between reviewers and authors must be resolved to the satisfaction of the DGGS editor before final acceptance of manuscripts. Final submittals must be provided as double-spaced paper copy and on high-density IBM-compatible diskette (Microsoft Word or WordPerfect). Questions should be directed to the DGGS editor 907-451-5053. Major changes by the author—whether scientific or editorial—are not permitted after the manuscript is in galley form.

Text Preparation

Manuscripts should be double spaced with 1-inch margins on all sides. The title page should include the title of the article and the name(s) and affiliation(s) of the author(s). Because of the brevity of *Short Notes* articles, tables of contents, lists of illustrations, and abstracts are not required. Words to be printed in italics should be typed in italics. Use upper and lower case type as appropriate; ***do not use all caps.***

Specific guidelines for units of measure, abbreviations, and references are provided in *Suggestions to Authors of Reports of the United States Geological Survey* (7th edition) or *Government Printing Office Style Manual 1973*. Potential authors are also encouraged to consult the latest issue of *Short Notes* for information.

Preparation of Illustrations

Figures should be provided on an IBM-compatible diskette (either high-density 3½" floppy disk or 100MB Zip disk). Computer-generated drawings should be of a resolution of at least 300 dpi and saved in a format compatible with CorelDraw 7.0 or later, or as a TIF or EPS file if produced from another drawing program. Scans of printed figures or drawings should be saved as TIF or EPS format at 300 dpi resolution at approximately the size they will be shown. If figures are hand drafted and scanning technology is not available to the author at a reasonable cost, please supply high-resolution camera-ready prints of your figures.

Line figures are generally published in black and white. Color art may be accepted with the understanding that the author will pay additional printing costs for colored figures. Current page-cost information can be obtained from the DGGS editor. Maximum size for figures is 6½" x 8½".

SHORT NOTES ON ALASKA GEOLOGY 1999

Edited by DeAnne S. Pinney and Paula K. Davis

Division of Geological & Geophysical Surveys
Professional Report 119
Recent research on Alaska geology
Fairbanks, Alaska
2000

Front cover photo: *Marine sedimentary rocks of the Nutzotin Mountains sequence (black strata in the foreground) in fault contact with the Wrangellia composite terrane in the Nutzotin Mountains, eastern Alaska Range. White strata in the midground is the Nizina Limestone. Gray strata in the background at the ridge crest is the Nikolai Greenstone. For scale, a person with a blue shirt can be seen on the ridgeline. View is to the north. (Photo by Jeffrey D. Manuszak)*

Back cover photo (top): *View eastward along the west fork of Atigun River of prominent anticlinal hinge in the upper Kanayut Conglomerate (Lower Mississippian to Upper Devonian) within the Toyuk thrust zone, a major thrust zone in the central Brooks Range. See Chmielowski and others (this volume), "Duplex structure and Paleocene displacement of the Toyuk thrust zone near the Dalton Highway, north-central Brooks Range." (Photo by Reia M. Chmielowski)*

Back cover photo (bottom): *Excavator and bulldozer trench on Lewis Ridge, Donlin Creek property, southwestern Alaska. Trench is approximately 1,300 feet long and part of a 3.7-mile trenching program by Placer Dome Exploration Inc. during the 1997 and 1998 field seasons. Light-colored rocks are igneous dikes and sills, and darker rocks are Kuskokwim Group shale and graywacke. Note the core drill rig in the background to the right of center. (Photo by David J. Szumigala)*

STATE OF ALASKA
Tony Knowles, *Governor*

DEPARTMENT OF
NATURAL RESOURCES
John T. Shively, *Commissioner*

DIVISION OF GEOLOGICAL &
GEOPHYSICAL SURVEYS
Milton A. Wiltse
State Geologist and Director

Division of Geological & Geophysical Surveys publications may be inspected at the following locations. Address mail orders to the Fairbanks office.

Alaska Division of Geological &
Geophysical Surveys
Attn: Geologic Communications Section
794 University Avenue, Suite 200
Fairbanks, Alaska 99709-3645
http://wwwdggs.dnr.state.ak.us
dggspubs@dnr.state.ak.us

Department of Natural Resources
Public Information Center
550 W 7th Ave., Suite 1250
Anchorage, Alaska 99501-3557

This publication, released by the Division of Geological & Geophysical Surveys, was produced and printed in Fairbanks, by Commerical Printing, at a cost of $9.00 per copy. Publication is required by Alaska Statute 41, "to determine the potential of Alaskan land for production of metals, minerals, fuels, and geothermal resources; the location and supplies of groundwater and construction materials; the potential geologic hazards to buildings, roads, bridges, and other installations and structures; and shall conduct such other surveys and investigations as will advance knowledge of the geology of Alaska."

FOREWORD

The biennial *Short Notes on Alaska Geology* volume is a publication supported by Alaska's entire geologic community. Alaska has a large and extended community of highly talented earth scientists, many of whom encounter geologic issues of great interest in the course of performing work associated with their primary obligations. In the press to meet organizational mandates, many of these stories could be lost in spite of the interest they hold for all of us. This realization led the Alaska Division of Geological & Geophysical Surveys to establish the *Short Notes on Alaska Geology* series so that there would be a vehicle to share these insights. By intent and tradition the *Short Notes on Alaska Geology* series has been an inclusive publication. Contributors to this biennial publication step forward from the ranks of private-sector firms, academia, and government agencies.

This volume of *Short Notes on Alaska Geology 1999* is the culmination of two years of predominantly volunteer efforts by your colleagues to author 11 articles about stratigraphic, structural, geochronologic, mineral deposit, and paleontologic geologic phenomena observed within the state. These papers contain significant observations and new data with regional implications that advance the knowledge of Alaska's geologic framework and will be cited frequently in years to come.

Editing the "Short Notes" volume, like authoring the papers it contains, is an extra duty placed on top of ongoing work. This year we owe our thanks to DeAnne Pinney, who graciously stepped up to that task. I believe that everyone who has participated in keeping the DGGS *Short Notes on Alaska Geology* publication series viable over the years has demonstrated a commitment to the finest traditions of collegial science. Authors, editors, reviewers, and publication staff have labored diligently for our benefit. To all of them, I say thank you.

Milton A. Wiltse
State Geologist and Director

CONTENTS

THE SODA CREEK LIMESTONE, A NEW UPPER LOWER DEVONIAN FORMATION IN THE MEDFRA QUADRANGLE, WEST-CENTRAL ALASKA

Robert B. Blodgett,[1] David M. Rohr,[2] Elizabeth A. Measures,[2]
Norman M. Savage,[3] Alan E. H. Pedder,[4] and Robert W. Chalmers[2]

ABSTRACT

The Soda Creek Limestone, a new stratigraphic unit of formation rank, is proposed here for a distinctive succession of richly fossiliferous, upper Lower Devonian (Emsian) limestone, shaly limestone, and minor shale exposed throughout much of the Medfra B-3 Quadrangle. The formation, bounded above and below by dolostone, is excellently exposed along a north-trending ridge in the eastern half of the SW¼ of sec. 23, T. 24 S., R. 23 E., Medfra B-3 Quadrangle. On this ridge, long known informally as "Reef Ridge" by mineral company geologists, the Emsian succession is repeated once by thrust faulting. The southernmost section on this ridge is designated as the type section, while the northern section is designated as the reference section. The 149.3-m-thick type section of limestone, shaly limestone, and minor shale represents shallow, subtidal to open-shelf depositional environments. Carbonate rocks consist of packstone, wackestone, and mudstone, and contain open-marine faunas consisting of brachiopods, rugose and tabulate corals, echinoderms, ostracodes, gastropods, and rare trilobites. Favositid tabulate corals up to 1 m in diameter are locally abundant. The lowermost beds of the unit are weakly dolomitized. Some channels of probable tidal origin with reworked bioclasts and intraclasts are present. Four prominent fossiliferous shale intervals occur interbedded with the carbonate rocks. Fossils from the new formation (notably brachiopods, corals, and conodonts) indicate an early Emsian age. This formation appears to have been deposited in an inner shelf setting of the platform carbonate complex that comprises the Nixon Fork subterrane of the Farewell terrane. Recent biogeographic studies of Devonian age faunas from the Farewell terrane, including the richly diverse fauna of the Soda Creek Limestone, indicate that this terrane probably originated as a rift block derived from the Siberian (or Angaraland) paleocontinent.

INTRODUCTION

The northern Kuskokwim Mountains of the Medfra Quadrangle, west-central Alaska, contains a richly fossiliferous succession of early to middle Paleozoic age strata, mostly deposited on a carbonate platform. Although these rocks are well exposed, very few investigations have been carried out upon them until recently. The basic stratigraphic framework for the Ordovician to Devonian succession was established in the formal naming paper of Dutro and Patton (1982), and a generalized geologic map was published by Patton and others (1980). Since this pioneering stratigraphic work, numerous paleontologic and stratigraphic papers have appeared which have addressed various parts of the Paleozoic succession in further detail (Blodgett and Rohr, 1989; Blodgett and others, 1988; Frýda and Blodgett, 1998; Hahn and Hahn, 1993; Measures and others, 1992a, b; Rohr, 1993; Rohr and Blodgett, 1988; Rohr and others, 1991, 1992; Rohr and Gubanov, 1997; Savage and others, 1995; Stock, 1981). In addition, Blodgett (1992) and Blodgett and Johnson (1992) described several Devonian gastropods that occur in the Medfra Quadrangle, though the focus of both papers was on faunas from other regions. The Paleozoic stratigraphic succession of the northern Kuskokwim Mountains served as the type area for the definition of the Nixon Fork terrane of Patton (1978), which is characterized primarily by a distinctive succession of lower and middle Paleozoic platform carbonate rocks. Subsequently, the Nixon Fork terrane (fig. 1) was reduced in rank by Decker and others (1994) to that of a subterrane of the newly established Farewell terrane, a larger tectonostratigraphic entity, also including the genetically related Dillinger and Mystic subterranes. These subterranes are now commonly believed to be in close stratigraphic juxtaposition (that is, facies relations) with one another. Recent work on the biogeographic affinities of Devonian age faunas of the Farewell terrane indicate that it probably originated as a rift block from the Siberian (or Angaraland) paleocontinent (Blodgett, 1998; Blodgett and Boucot, 1999; Blodgett and Brease, 1997; Blodgett and others, 1999).

In this paper, we define a new formation of late Early Devonian (early Emsian) age which forms a distinctive

[1]Departments of Zoology and Geosciences, Oregon State University, Corvallis, Oregon 97331.
Email for Robert Blodgett: blodgetr@bcc.orst.edu
[2]Department of Geology, Sul Ross State University, Alpine, Texas 79832.
[3]Department of Geological Sciences, University of Oregon, Eugene, Oregon 97403.
[4]8859 Park Pacific Terrace, Sidney, British Columbia V8L 4S1, Canada.

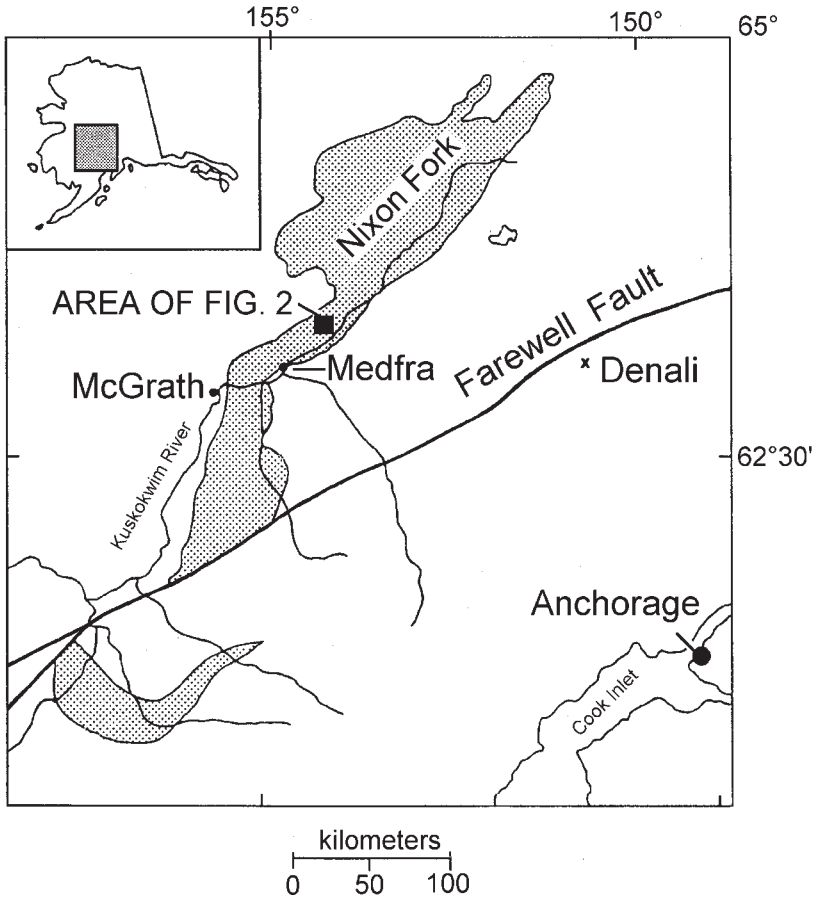

Figure 1. *Index map of part of west-central and southwestern Alaska showing location of Nixon Fork subterrane (stippled areas) of the Farewell terrane and the location of the "Reef Ridge" area in the Medfra B-3 Quadrangle; modified from Blodgett and Gilbert (1992) and Babcock and others (1995).*

marker unit of limestone and minor shale in the Medfra B-3 Quadrangle of west-central Alaska. This unit is part of the previously described Whirlwind Creek Formation of Dutro and Patton (1982), which they described as "an Upper Silurian to Upper Devonian sequence of predominantly shallow-water carbonate rocks, 1,000–1,500 m thick" (p. H19). The type section was designated as a south-dipping sequence exposed on the ridge between Whirlwind and Soda creeks in sec. 23, T. 24 S., R. 23 E., Medfra B-3 Quadrangle. An additional supplemental section was designated for the higher beds of the formation on the north flank of the syncline in secs. 29 and 30, T. 23 S., R. 25 E., Medfra B-3 Quadrangle. The Soda Creek Limestone (here named) corresponds to the Emsian–Siegenian age interval of limestones with coral biostromes shown in figure 5 of Dutro and Patton (1982). Although not mentioned in their naming paper, this distinctive unit is repeated once along their designated type section ridge of the Whirlwind Creek Formation. Several abstracts (Blodgett and others, 1995; Chalmers and others, 1995) have been published previously on the biostratigraphic and depositional environments, respectively, of this distinctive new formation named herein the Soda Creek Limestone. The Whirlwind Creek Formation of Dutro and Patton (1982) includes several distinctive stratigraphic units, and is considered here to represent a stratigraphic unit of Group rank. Its uppermost strata as recognized by the authors are stratigraphically equivalent to the Cheeneetnuk Limestone of Blodgett and Gilbert (1983) of the McGrath A-4 and A-5 quadrangles, west-central Alaska. The upper part (early Eifelian age) of the Cheeneetnuk Limestone contains the same fauna and similar lithology as that found in the uppermost strata of the Whirlwind Creek Formation. The uppermost part of the Whirlwind Creek was indicated by Dutro and Patton (1982) to be of early Late Devonian (Frasnian) age. Examination by R.B. Blodgett of the site indicated to him by W.W. Patton, Jr. (USGS locality 9755-SD; field locality 76APa65c of W.W. Patton, Jr.) to be of Frasnian age, shows that these strata belong to the herein-named Soda Creek Limestone of Emsian age. No rugose corals

belonging to the genus *Smithiphyllum*, the age indicator for the Frasnian age noted in Dutro and Patton (1982, p. H21), or the reported accompanying stick-like stromatoporoid *Amphipora*, were recovered. Instead, a diverse fauna of Emsian age corals was found at the site where *Smithiphyllum* was indicated to occur. The stromatoporoid *Amphipora* has a long stratigraphic range throughout much of the Devonian, and is commonly found in both Emsian and Eifelian age strata of the Medfra Quadrangle. Based on field studies totaling at least four weeks in duration, the youngest beds we have recognized in the Devonian succession in the Medfra B-3 and B-4 quadrangles are Eifelian (early Middle Devonian) age limestones. These beds are similar both lithologically and faunally to the upper part of the Cheeneetnuk Limestone of the McGrath A-4 and A-5 quadrangles, the Cheeneetnuk comprising the highest Devonian carbonate unit recognized in Nixon Fork subterrane strata in that region.

The Devonian strata at "Reef Ridge" and the surrounding area have long been of interest to mineral exploration companies because of the occurrence of Mississippi Valley-type lead–zinc deposits. It is our aim in this paper to provide a more detailed description of the Lower Devonian stratigraphic succession of the Medfra B-3 Quadrangle, in order to better constrain the age of the intervals hosting the lead–zinc deposits in this region.

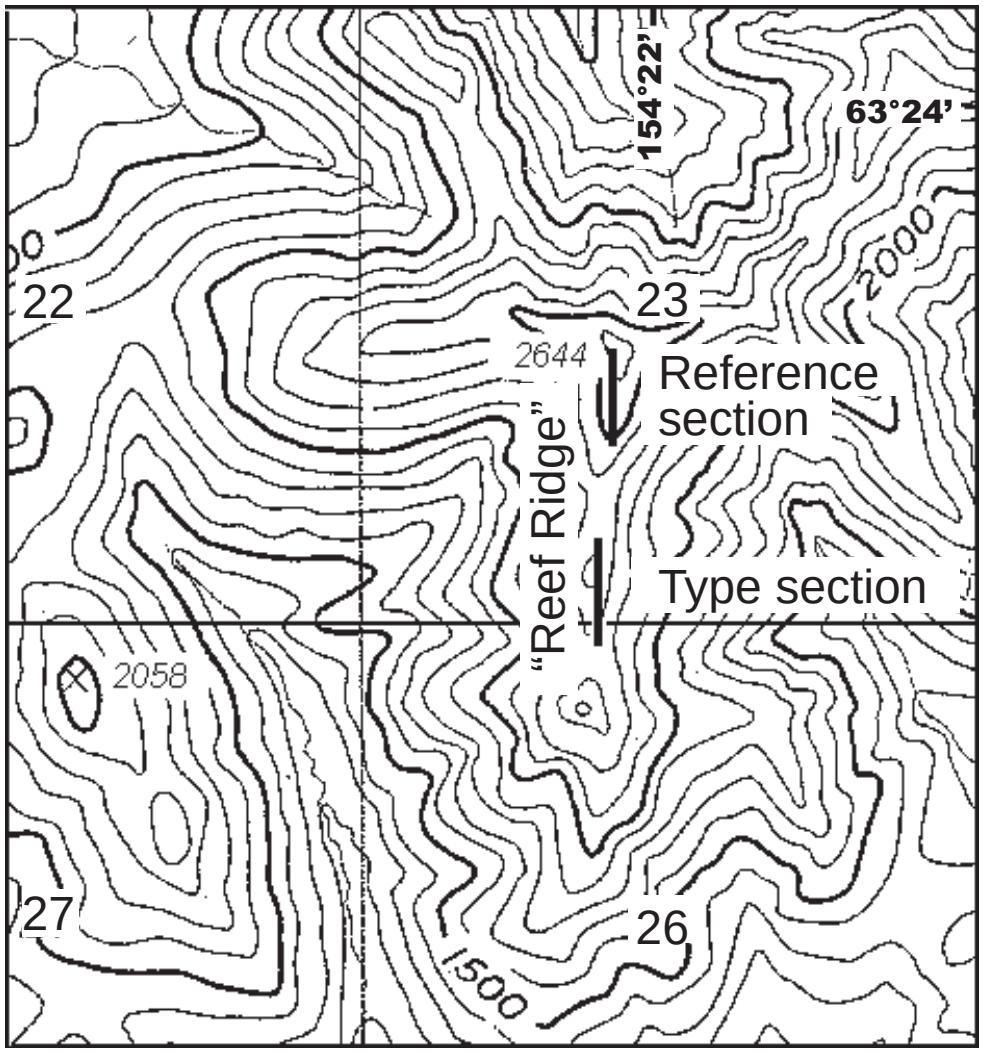

Figure 2. *Map showing the location of the type and reference sections of the Soda Creek Limestone along "Reef Ridge" in sec. 23 and northern part of sec. 26, T. 24 S., R. 23 E., Medfra B-3 Quadrangle. Base is at the north end of both the type and reference sections. Contour interval 100 feet. Base map from U.S. Geological Survey, 1955, Medfra B-3 1:63,360-scale topographic map.*

SODA CREEK LIMESTONE (NEW NAME)

The name "Soda Creek Limestone" is here assigned to a distinctive succession of richly fossiliferous, upper Lower Devonian (Emsian) limestone and minor shale exposed throughout much of the Medfra B-3 Quadrangle. The new unit is 149.3 m (490 ft) thick at its type section, which is situated along a north-trending ridge in the SE¼ SW¼ sec. 23, T. 24 S., R. 23 E., Medfra B-3 Quadrangle (see fig. 2 for location). The unit is repeated once along the ridge due to imbricate low-angle thrust faulting (figs. 3, 4). The southern section is designated as the type section, whereas the northern section is designated as the reference section. The northern section is situated along the same ridge in the NE¼ SW¼ sec. 23, T. 24 S., R. 23 E., Medfra B-3 Quadrangle (see fig. 2 for location), and is 157.0 m (515 ft) thick. The formation derives its name from nearby Soda Creek, a tributary of the North Fork of the Kuskokwim River, which is south and east of the type section.

The lower contact of the Soda Creek Limestone with the underlying unnamed dolostone-dominated unit (fig. 5) is sharp and conformable and can be well observed at the base of both sections of the unit along the crest of "Reef Ridge." The underlying dolostone unit is composed of thin- to thick-bedded light-yellowish gray weathering (medium gray on fresh surfaces), dolomudstone to dolowackestone and lime mudstone. The

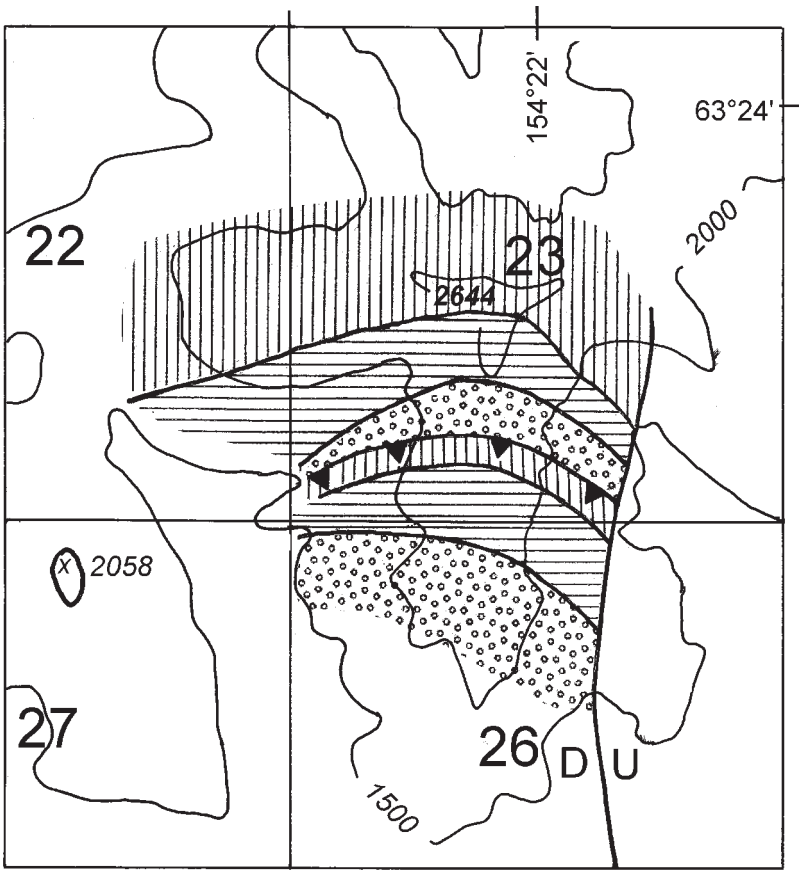

Figure 3. *Geologic map of "Reef Ridge," showing distribution of geologic unit in the vicinity of the type and reference sections of the Soda Creek Limestone. Map includes all or parts of secs. 22–23 and 26–27 of T. 24 S., R. 23 E., Medfra B-3 Quadrangle. Contour interval 500 ft. Base map from U.S. Geological Survey, 1955, Medfra B-3 1:63,360-scale topographic map.*

Dark to light gray weathering dolostone with lenses of silicified fossil (*Amphipora*, small brachiopods, and molluscs) (late Early Devonian, post-early Emsian)

SODA CREEK LIMESTONE
(early Emsian, late Early Devonian)

Interbedded dolostone and limestone, weathering light to dark gray and buff in color (pre-Emsian)

dolostone underlying the Soda Creek Limestone is a bioclastic mudstone to wackestone with resistant, wavy dolomite stringers roughly parallel with the bedding. Bedding is thin overall, varying from 0.1–0.3 m (0.3–1.0 ft). Large leperditiid ostracodes are locally present in the underlying unnamed unit. The uppermost bed of the underlying unit in contact with the Soda Creek Limestone is a rudstone composed of branching, highly digitate favositid tabulate corals. This bed varies from 0.3–0.9 m (1–3 ft) in thickness as a result of hardground formation prior to deposition of the overlying Soda Creek Limestone. Truncation of bioclasts and sharp erosional relief occurs along strike. This disconformity represents a hiatus of uncertain length between the deposition of the underlying unit and the Soda Creek Limestone.

The Soda Creek Limestone is composed predominantly of dark gray limestone (ranging from packstone to wackestone, with minor mudstone), but with prominent, thinner, recessive, weathering intervals of shale and shaly limestone. The unit at its type section is 149.3 m (490 ft) thick (fig. 6). Abundant free weathering fossils, notably brachiopods and corals, are readily available in the shaly, recessive intervals. The Soda Creek Limestone is primarily carbonate, but there are four significant occurrences of shaly interbeds which create saddles in "Reef Ridge," as well as in other outcrops of the unit regionally. The uppermost shaly

Figure 4. *Ridge with type and reference sections of the Soda Creek Limestone along "Reef Ridge." View is from the northeast.*

Figure 5. *View looking south showing base of the type section of the Soda Creek Limestone.*

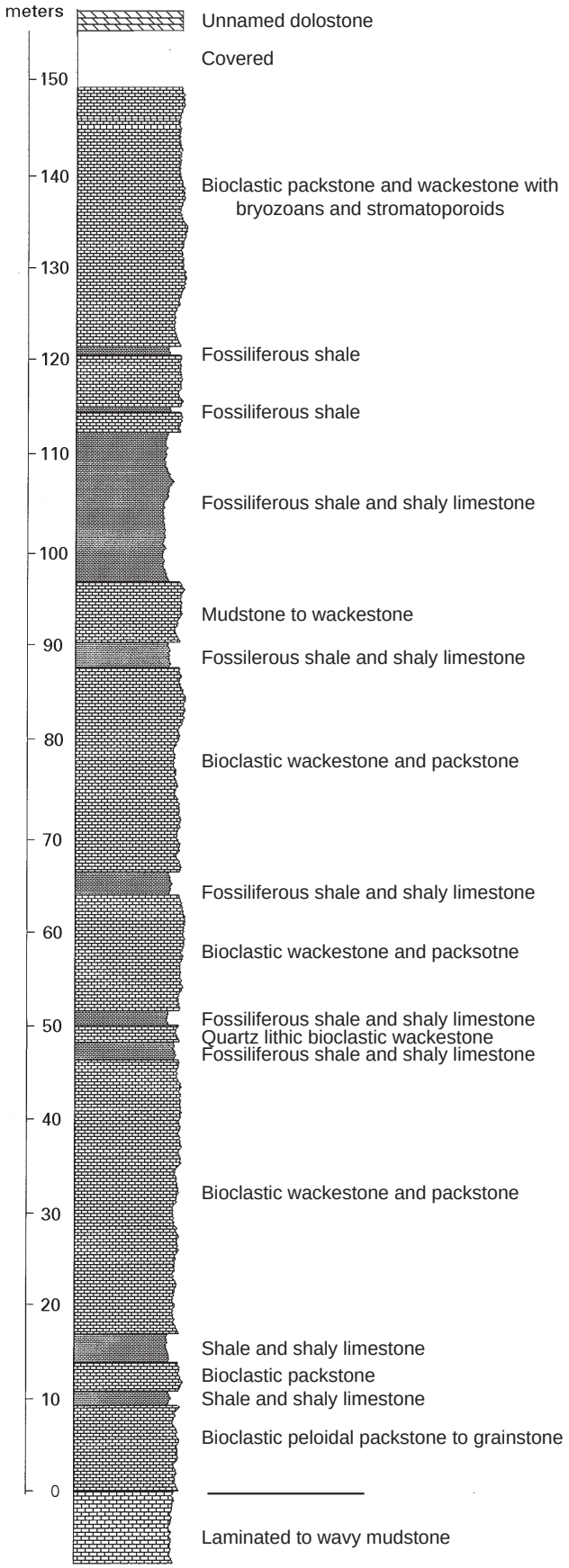

interval is the most prominent and is approximately 18.3 m (60 ft) thick.

The limestones of Soda Creek contain an abundant and diverse fauna. In outcrop, fossiliferous mudstones are most common, but there are also wackestones, packstones, rudstones, floatstones, and bafflestones. Thin sections reveal that many of the mudstones are actually peloidal packstones and grainstones. Contacts between the limestones and shales are primarily sharp, but some contacts do show gradation. Some of the limestones are thin-bedded and less resistant and have a substantial argillaceous component. Yellow marly intervals and individual beds also occur. What makes this formation so diagnostic and gives name to the ridge itself is the abundance of large reef-like corals and stromatoporoids. The tabulate corals are digitate to hemispherical, and include branches 5.0 cm (2 in.) in diameter and heads varying in diameter up to 0.3 m (1 ft), rarely 1.0 m (3 ft). The bulbous heads are commonly in place (fig. 7). The branching forms are rarely in place, commonly overturned and reworked. The stromatoporoids are commonly bulbous and hemispherical. They are commonly 0.15–0.3 m (0.5–1.0 ft) in diameter. These coral and stromatoporoid heads sometimes occur isolated in beds or form beds continuous along strike. Solitary rugose corals are also common and occur with the other "reefal" forms.

The contact of the Soda Creek Limestone with the overlying unnamed dolostone unit is sharp, but conformable. The upper contact in the type section is poorly exposed in a saddle as the resistant carbonate appears to grade into the overlying, non-resistant dolomitic formation (fig. 8). Dolostones of the overlying unnamed unit vary from medium to dark gray, and are locally black in color. These strata are typically well-bedded, but commonly contain solution-collapse breccia. The stick-like stromatoporoid *Amphipora* is locally common in the unit. Some zones of cherty silicification occur in the lower part of this unit, and commonly contain silicified megafossils, consisting primarily of small-sized brachiopods and molluscs. The dolostone unit was not measured, but it appears to have a minimum thickness of 200 m. The lower part of the unnamed, overlying dolostone unit is of major interest to mineral company geologists, because it is typically the host horizon for lead–zinc deposits in the region. The unnamed dolostone unit is succeeded by a succession of limestones bearing Eifelian (early

Figure 6. *Stratigraphic column of the type section of the Soda Creek Limestone.*

Figure 7. *Large favositid tabulate coral head, typical of the more carbonate-rich intervals within the Soda Creek Limestone.*

Figure 8. *View looking north showing top of the type section of the Soda Creek Limestone.*

Middle Devonian) age megafossils. This limestone unit forms the uppermost part of the Devonian carbonate succession in the Medfra B-3 and B-4 quadrangles, and is equivalent in age and lithology to the Cheeneetnuk Limestone of Blodgett and Gilbert (1983) defined to the south in the McGrath Quadrangle.

ENVIRONMENT OF DEPOSITION

The presence of an open-marine, diverse fauna throughout the formation, especially such stenohaline forms as brachiopods and echinoderms, suggests that the unit was deposited under normal marine conditions. The presence of numerous, but poorly preserved gastropods, and also locally large leperditiid ostracodes indicate relatively shallow-water paleoenvironments. However, although this formation appears to be of shallow-water origin, regionally it represents an interval of slightly deeper water sedimentation than that found in both the underlying and overlying units. Both of these units are dominated by dolostone, lack shaly interbeds and are notably lacking in well-developed open-marine faunas. This is especially evident in the overlying dolostone unit, which commonly contains locally abundant *Amphipora*. This stick-like stromatoporoid genus is thought by many workers to be most common in semi-restricted or restricted lagoonal environments. In summary, it appears that the Soda Creek Limestone represents a local transgressive-regressive cycle within the upper part of the Lower Devonian stratigraphic succession.

AGE

Faunal age control is amply provided by the abundant megafossils and conodonts found throughout the unit. Megafossils are particularly abundant in the more shaly intervals, and include brachiopods, rugose and tabulate corals, echinoderm ossicles, leperdiitid ostracodes, bivalves, gastropods, and trilobites. Favositid tabulate corals are especially notable in the more carbonate rich intervals (fig. 7). Their large size (some up to 1 m in diameter) and abundance, together with the abundant weathered-free solitary rugose corals of the shaly intervals, provide the origin of the informal term "Reef Ridge" for the ridge bearing the type and reference sections.

Brachiopods include over 30 species, of which the most common elements are rhynchonellids (notably uncinulids). Genera present include *Plicogypa*, *Stenorhynchia*, *Taimyrrhynx*, "*Uncinulus*", *Nordotoechia*?, *Spinatrypa*, *Nucleospira*, *Protathyris*, *Howellella*, and *Aldanispirifer*. Diagnostic species are *Plicogypa* cf. *kayseri* (Peetz), *Taimyrrhynx taimyrica* (Nikiforova), "*Uncinulus*" *polaris* Nikiforova, and *Howellella yacutica* Alekseeva. The latter three species show their closest affinities with faunas from Arctic Russia (Novaya Zemlya, Taimyr, and Kolyma).

Conodonts were recovered only from the lower half of the type section and indicate an early Emsian age (*Polygnathus dehiscens* Zone). These include the following species: *Polygnathus eberleini*, *Ozarkodina* cf. *remscheidensis* at 21.3 m; *Icriodus taimyricus*, *Pandorinellina exigua philipi*, and *O*. cf. *remscheidensis* at 30.5 m; *P. exigua philipi* at 46.9–48.5 m; and *Icriodus taimyricus* at 54.6 m.

Rugose corals from 21.3 to 57.3 m above the base of the type section are dominated by relatively undiagnostic *Pseudoamplexus altaicus*, *Lythophyllum* spp., and rare *Zonophyllum* sp. From 65.2 to 111.9 m corals include *Rhizophyllum schischkaticum*, *Lythophyllum* spp., and *Pseudamplexus altaicus*, new species of *Zelophyllia*, *Acanthophyllum* and a new genus. Although undescribed, these higher faunas are related to early Emsian coral faunas from the Kolyma region of northeastern Siberia. A weakly colonial version of the new *Acanthophyllum* species, occurring at 123.7 m, is the only colonial rugosan from the type section.

ACKNOWLEDGMENTS

D.M. Rohr thanks the National Geographic Society Committee for Research and Exploration for supporting the 1994 summer field work conducted in the vicinity of Reef Ridge. R.B. Blodgett thanks Patiño, Inc. for introducing him to the geology of this region in 1981; he also thanks Sohio Oil Company, Union Oil Company, and the Alaska Division of Geological & Geophysical Surveys (DGGS) for site visits to the type section and surrounding area in the years of 1983–1985, and 1991. Field work in 1994 was supported by National Geographic Society Research Grant 5188-94. We are grateful to Bill Beebe, Area Forester, Alaska Department of Natural Resources, Division of Forestry, McGrath, Alaska, for arranging helicopter support that permitted us to conduct our field study in the Reef Ridge area during the summer of 1994. We also thank David L. LePain and Arthur J. Boucot for their reviews of this manuscript.

REFERENCES

Blodgett, R.B., 1992, Taxonomy and paleobiogeographic affinities of an early Middle Devonian (Eifelian) gastropod faunule from the Livengood quadrangle, east-central Alaska: Palaeontographica Abteilung A, v. 221, p. 125–168.

———1998, Emsian (late Early Devonian) fossils indicate a Siberian origin for the Farewell terrane, *in* Clough, J.G., and Larson, F., eds., Short Notes on Alaska Geology 1997: Alaska Division of Geological & Geophysical Surveys Professional Report 118, p. 53–61.

Blodgett, R.B., and Boucot, A.J., 1999, Late Early Devonian (Late Emsian) eospiriferinid brachiopods from Shellabarger Pass, south-central Alaska and their biogeographic importance; further evidence for a Siberian origin of the Farewell and allied Alaskan accreted terranes: Senckenbergiana lethaea, v. 79, no. 1, p. 209–221.

Blodgett, R.B., and Brease, P.F., 1997, Emsian (late Early Devonian) brachiopods from Shellabarger Pass, Talkeetna C-6 quadrangle, Denali National Park, Alaska indicate Siberian origin for Farewell terrane: Geological Society of America Abstracts with Programs, v. 29, no. 5, p. 5.

Blodgett, R.B., and Gilbert, W.G., 1983, The Cheeneetnuk Limestone; A new Early(?) to Middle Devonian formation in the McGrath A-4 and A-5 quadrangles, west-central Alaska: Alaska Division of Geological & Geophysical Surveys Professional Report 85, 6 p, 1 sheet, scale 1:63,360.

Blodgett, R.B., and Johnson, J.G., 1992, Early Middle Devonian (Eifelian) gastropods of central Nevada: Palaeontographica Abteilung A, v. 222, p. 85–139.

Blodgett, R.B., and Rohr, D.M., 1989, Two new Devonian spine-bearing pleurotomariacean gastropod genera from Alaska: Journal of Paleontology, v. 63, p. 47–52.

Blodgett, R.B., Rohr, D.M., and Boucot, A.J., 1988, Lower Devonian gastropod biogeography of the Western Hemisphere, *in* McMillan, N.J., Embry, A.F., Glass, D.J., eds., Devonian of the World:

Canadian Society of Petroleum Geologists Memoir 14, v. 3, p. 285–305.

Blodgett, R.B., Savage, N.M., Pedder, A.E.H., and Rohr, D.M., 1995, Biostratigraphy of an Upper Lower Devonian (Emsian) limestone unit at "Reef Ridge", Medfra B-3 quadrangle, west-central Alaska: Geological Society of America Abstracts with Programs, v. 27, no. 5, p. 6.

Blodgett, R.B., Sullivan, R., Clough, J.G., and LePain, D.L., 1999, Paleozoic paleontology of the Holitna Lowland, southwest Alaska: Geological Society of America Abstracts with Programs, v. 31, no. 6, p. A39.

Chalmers, R.W., Measures, E.A., Rohr, D.M., and Blodgett, R.B., 1995, Depositional environments of an upper Lower Devonian (Emsian) limestone unit at "Reef Ridge," Medfra B-3 quadrangle, west-central Alaska: Geological Society of America Abstracts with Programs, v. 27, no. 5, p. 9.

Decker, John, Bergman, S.C., Blodgett, R.B., Box, S.E., Bundtzen, T.K., Clough, J.G., Coonrad, W.L., Gilbert, W.G., Miller, M.L., Murphy, J.M., Robinson, M.S., and Wallace, W.K., 1994, Geology of southwestern Alaska, *in* Plafker, George, and Berg, H.C., eds., The Geology of Alaska: Boulder, Colorado, Geological Society of America, The Geology of North America, v. G-1, p. 285–310.

Dutro, J.T., Jr., and Patton, W.W., Jr., 1982, New Paleozoic platform formations in the northern Kuskokwim Mountains, west-central Alaska: U.S. Geological Survey Bulletin 1529-H, p. H13–H22.

Frýda, J., and Blodgett, R.B., 1998, Two new cirroidean genera (Vetigastropoda, Archaeogastropoda) from the Emsian (late Early Devonian) of Alaska with notes on the early phylogeny of Cirroidea: Journal of Paleontology, v. 72, p. 265–273.

Hahn, G., and Hahn, R., 1993. Neue Trilobiten-Funde aus dem Karbon und Perm Alaskas: Geologica et Palaeontologica, v. 27, p.141–163.

Measures, E.A., Blodgett, R.B., and Rohr, D.M., 1992a, Depositional setting and fauna of Middle Ordovician rocks of the Telsitna Formation, northern Kuskokwim Mountains, Alaska: Geological Society of America Abstracts with Programs, v. 24, no. 5, p. 70.

Measures, E.A., Rohr, D.M., and Blodgett, R.B., 1992b, Depositional environments and some aspects of the fauna of Middle Ordovician rocks of the Telsitna Formation, northern Kuskokwim Mountains, Alaska, *in* Bradley, D.C., and Dusel-Bacon, C., eds., Geologic Studies in Alaska by the U.S. Geological Survey, 1991: U.S. Geological Survey Bulletin 2041, p. 186–201.

Patton, W.W., Jr., 1978, Juxtaposed continental and oceanic-island arc terranes in the Medfra quadrangle, west-central Alaska, *in* Johnson, K.M., ed., The United States Geological Survey in Alaska: Accomplishments during 1977: U.S. Geological Survey Circular 772-B, p. B38–B39.

Patton, W.W., Jr., Moll, E.J., Dutro, J.T., Jr., Silberman, M.L., and Chapman, R.M., 1980. Preliminary geologic map of the Medfra Quadrangle, Alaska: U.S. Geological Survey Open-File Report 80-811A, 1 sheet, scale 1:250,000.

Rohr, D.M., 1993, Middle Ordovician carrier shell *Lytospira* (Mollusca, Gastropoda) from Alaska: Journal of Paleontology, v. 67, p. 959–962.

Rohr, D.M., and Blodgett, R.B., 1988, First occurrence of *Helicotoma* Salter (Gastropoda) from the Ordovician of Alaska: Journal of Paleontology, v. 62, p. 304–306.

Rohr, D.M., Dutro, J.T., Jr., and R.B. Blodgett, 1991, Gastropods and brachiopods from the Ordovician Telsitna Formation, northern Kuskokwim Mountains, west-central Alaska: Sixth International Symposium on the Ordovician System - Abstracts - University of Sydney, Sydney, Australia, July 15–19, 1991. Australia Bureau of Mineral Resources, Geology and Geophysical Record 1991/47, p. 29.

———1992, Gastropods and brachiopods from the Ordovician Telsitna Formation, northern Kuskokwim Mountains, west-central Alaska, *in* Webby, B.D., and Laurie, J.R., eds., Global perspectives on Ordovician Geology: Proceedings of the Sixth International Symposium on the Ordovician System, Sydney, Australia. Balkema Press, p. 499–512.

Rohr, D.M., and Gubanov, A.P., 1997, Macluritid opercula (Gastropoda) from the Middle Ordovician of Siberia and Alaska: Journal of Paleontology, v. 71, p. 394–400.

Savage, N.M., Rohr, D.M., and Blodgett, R.B., 1995, Late Silurian condonts from the Medfra B-4 quadrangle, west-central Alaska: Geological Society of America Abstracts with Programs, v. 27, no. 5, p. 76.

Stock, C.W., 1981, *Cliefdenella alaskanensis* n. sp. (Stromatoporoidea) from the Middle/Upper Ordovician of central Alaska: Journal of Paleontology, v. 55, p. 998–1005.

DUPLEX STRUCTURE AND PALEOCENE DISPLACEMENT OF THE TOYUK THRUST ZONE NEAR THE DALTON HIGHWAY, NORTH-CENTRAL BROOKS RANGE

Reia M. Chmielowski,[1] Wesley K. Wallace,[2] and Paul B. O'Sullivan[3]

ABSTRACT

The Toyuk thrust zone is a regional tectonic boundary in the central Brooks Range of northern Alaska that has been interpreted previously as a single large-displacement fault. Just west of the Dalton Highway, the thrust zone is defined by several north-vergent imbricate thrust faults. These faults have cut detachment folds formed in the competent Kanayut Conglomerate between detachments in the underlying Hunt Fork Shale and overlying Kayak Shale, thereby forming a duplex. The exposed structural geometry suggests two end-member models of duplex geometry. In model one, each linking thrust has roughly the same small displacement and the roof thrust is overlain by a normal stratigraphic succession. In model two, the uppermost and hindmost fault has greater displacement than the other faults and so forms a duplex roof above which the stratigraphic section is duplicated. Discrimination between these models is not possible because the duplex roof has been eroded in the field area.

Apatite fission-track analyses of samples collected within the Toyuk thrust zone record two distinct episodes of cooling interpreted to represent unroofing in response to tectonic deformation. The initial episode occurred at ~100 Ma, while the later episode occurred at ~60 Ma. These two cooling/denudation events have been documented previously in the region, but the samples from the thrust zone are the first to document displacement on a specific fault during the ~60 Ma event so far south of the front of the central Brooks Range. The results suggest that at least part of the growth of the Toyuk thrust zone accommodated structural thickening within the orogenic wedge coeval with deformation at the range front.

INTRODUCTION

The folds in many fold-and-thrust belts have been interpreted to be fault-bend or fault-propagation folds, in which faulting predates or is synchronous with folding (Suppe, 1983; Jamison, 1987; Suppe and Medwedeff, 1990). However, in many areas those models may not apply. Recent studies in the Brooks Range of northern Alaska have documented the formation of duplexes in which folds formed before being cut by thrust faults (Wallace and others, 1997; Homza and Wallace, 1991; Homza, 1992). This study examines the structural geometry and evolution of the Toyuk thrust zone, an example of just such a duplex within the Endicott Mountains allochthon in the Brooks Range (fig. 1).

The lower part of the Endicott Mountains allochthon consists dominantly of the Upper Devonian Hunt Fork Shale, the Upper Devonian to Lower Mississippian (?) Kanayut Conglomerate, and the Mississippian Kayak Shale (Brosgé and others, 1979a, 1979b; Mull and others, 1989; Moore and others, 1989, 1994a, 1997). The contrast in competency between the Kanayut and its overlying and underlying units has resulted in formation of a combination of map-scale detachment folds and thrust faults within the Kanayut during the evolution of the northern Brooks Range (Wallace and others, 1997). These structures form duplexes in the Kanayut Conglomerate, with a floor thrust in the Hunt Fork Shale and a roof thrust in the Kayak Shale, both of which are relatively incompetent units.

Previous workers have generally assumed that the regional boundary between exposures dominated by the Hunt Fork Shale to the south and the Kanayut Conglomerate to the north (fig. 2), is a single thrust fault, the Toyuk thrust (Moore and others 1989, 1997; Kelley and Brosgé, 1995). This study explores the alternative hypothesis that the regional boundary between the Hunt Fork and the Kanayut is not simply a single thrust fault that is continuous along strike, but instead reflects the local intersection of the erosion surface with a duplex in the Kanayut, referred to here as the Toyuk thrust zone (Wallace and others, 1997). This hypothesis allows an estimate to be made of the minimum possible displacement across the zone.

Detailed geologic mapping (1:25,000 scale) of an approximately 23-square-km portion of the Toyuk thrust zone was completed during an 8-week field season during the summer of 1995. The field area is north of Atigun Pass

[1]Geology Department, University of Alaska Anchorage, 3211 Providence Drive, Anchorage, Alaska 99508-8338. Now at: 1910 Mt. Vernon Ct., Mountain View, California 94040.
Email for Reia M. Chmielowski: kareinatt@yahoo.com
[2]Department of Geology & Geophysics, University of Alaska Fairbanks, P.O. Box 755780, Fairbanks, Alaska 99775-5780.
[3]LaTrobe University, Department of Geology, Bundoora, VIC 3083 Australia.

between the east and west forks of the Atigun River along the northern flanks of James Dalton Mountain just south of the west fork of the Atigun River (fig. 2). The Dalton Highway is about 9.6 km due east of the area. The mapping concentrated on precisely delineating folds and faults in the area and determining their relationship to the stratigraphy. Several parallel steep gullies on the north flank of James Dalton Mountain are perpendicular to the strike of the faults. These gullies provide a three-dimensional picture of the structure, which facilitated the construction of cross sections.

To constrain the timing of activity on the faults, a series of samples for apatite fission-track analysis were collected from outcrop localities spanning the thrust zone (fig. 3). This approach potentially provides a powerful tool for elucidating the history of movement of major faults, especially in areas of reactivation where cross-cutting relations are lacking (O'Sullivan and others, 1998a).

REGIONAL GEOLOGY

Most of the Brooks Range is part of the Arctic Alaska terrane (Jones and others, 1987; Silberling and others, 1994). The area of this study is in the northern part of the central Brooks Range, and is wholly within the Endicott Mountains allochthon, one of the subterranes of the Arctic Alaska terrane (Moore and others, 1994a) (fig. 1). A number of regional cross sections illustrate the structural style and stratigraphy of the Endicott Mountains allochthon and the northern Brooks Range (Mull and others, 1987; Oldow and others, 1987; Grantz and others, 1991; Moore and others, 1994b).

DEFORMATION HISTORY

The initial phase of the Brookian orogeny began with the collision of an intraoceanic arc represented by the Angayucham and Koyukuk terranes with the south-facing passive continental margin of the Arctic Alaska

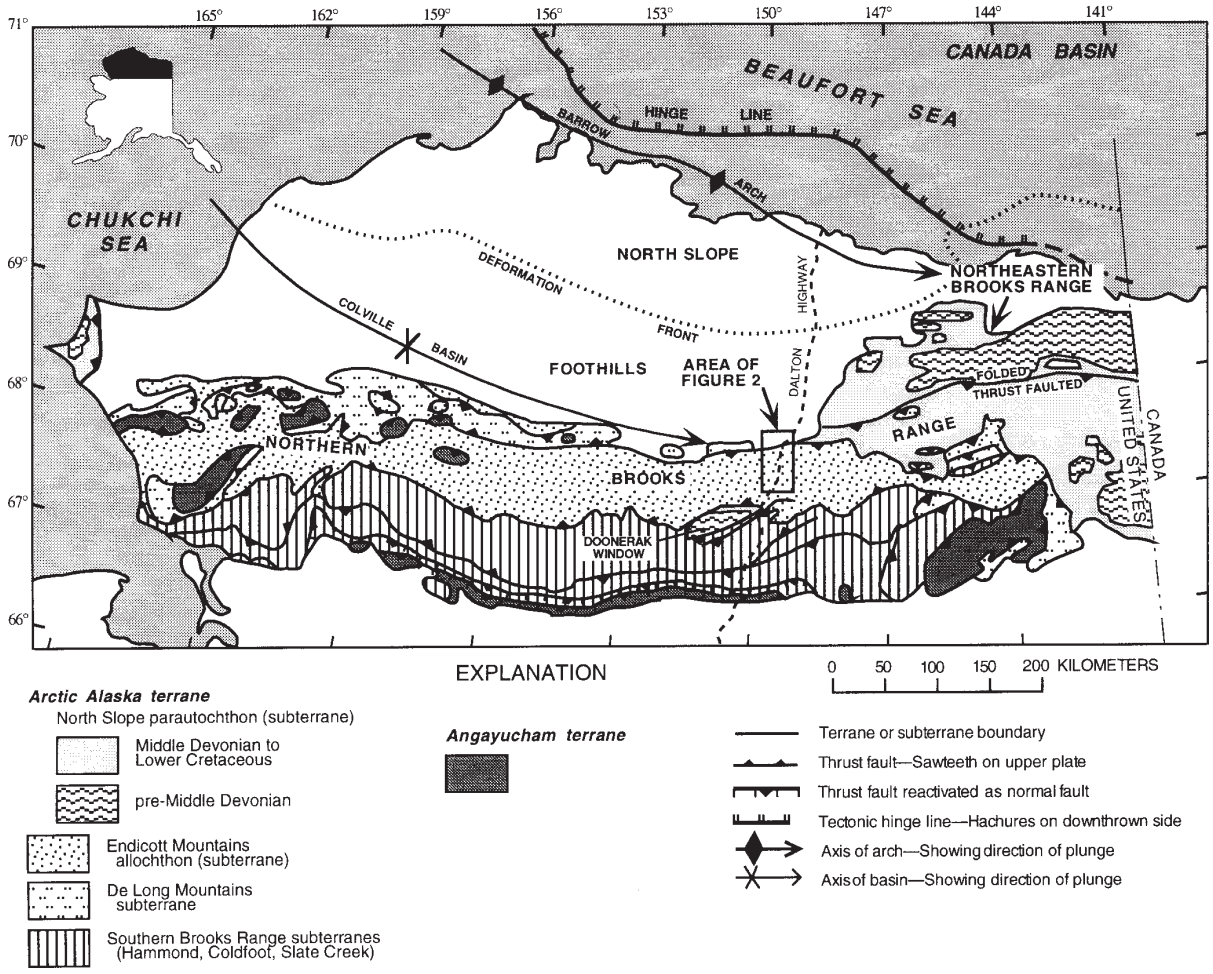

Figure 1. *Location map, showing the terranes and major tectonic elements of northern Alaska as well as the Dalton Highway. Location of geologic map (fig. 2) is outlined. Modified from figure 2 of Wallace and others (1997).*

terrane in Middle Jurassic to Early Cretaceous time (Moore and others, 1994a). The partial subduction of the Arctic Alaska terrane involved hundreds of kilometers of shortening that resulted in northward delamination and imbrication of the continental superstructure to form a stacked series of allochthons (Moore and others, 1994a). The Endicott Mountains allochthon is the structurally lowest of these allochthons (fig. 1) (Mull, 1982; Mayfield and others, 1988).

The Endicott Mountains allochthon was displaced at least 88 km northward over less deformed rocks that compose the North Slope parautochthon (Mull and others, 1989). In addition to the displacement of the entire allochthon, the units within the allochthon have undergone significant internal shortening via map-scale thrust faults and folds.

The second phase of the Brookian orogeny, from mid-Cretaceous and into the Neogene, involved tens of kilometers of post-collisional shortening that resulted in uplift and unroofing along the main axis of the Brooks Range and its northern foothills (Moore and others, 1994a). Apatite fission-track cooling ages of ~100 Ma, ~60 Ma, and ~24 Ma from the Brooks Range and its foothills suggest that discrete deformational events contributed to that unroofing (O'Sullivan, 1996; O'Sullivan and others, 1997, 1998b).

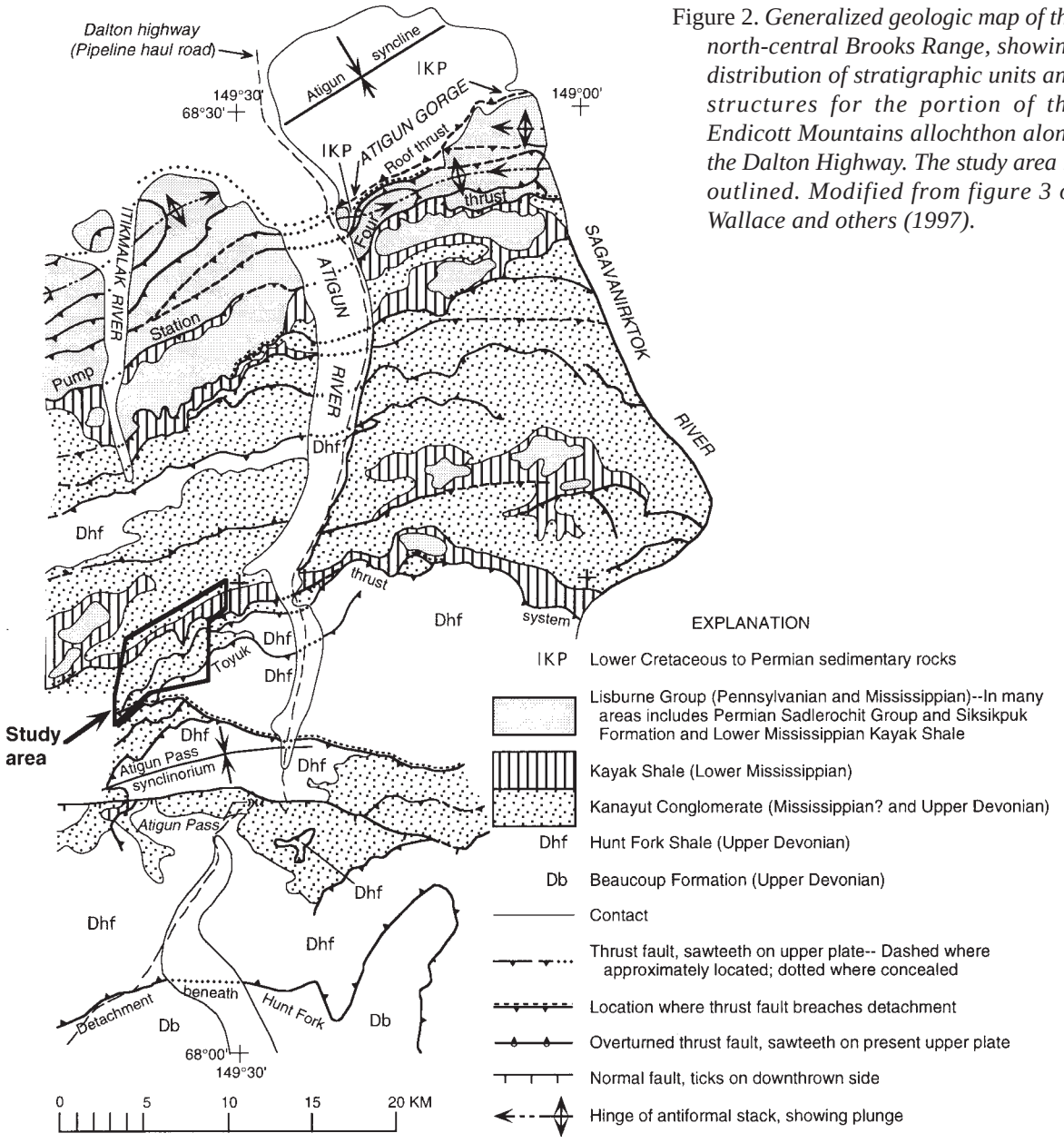

Figure 2. *Generalized geologic map of the north-central Brooks Range, showing distribution of stratigraphic units and structures for the portion of the Endicott Mountains allochthon along the Dalton Highway. The study area is outlined. Modified from figure 3 of Wallace and others (1997).*

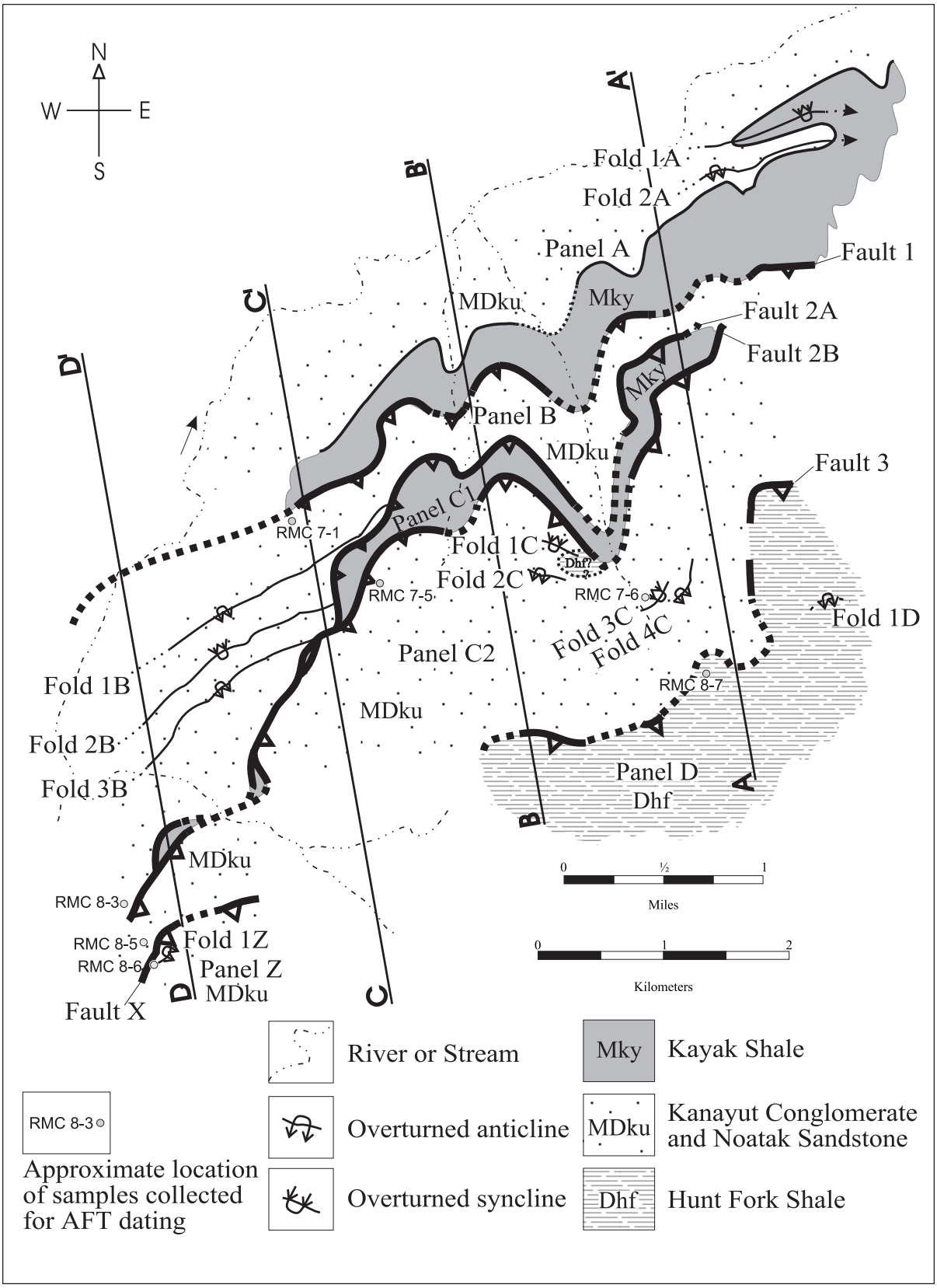

Figure 3. *Simplified geologic map of the field area. Shows the location of cross-section lines and fission-track samples, and identifies the faults and thrust-bound panels.*

STRUCTURAL STYLE

The structural style of the Endicott Mountains allochthon is fundamentally influenced by its mechanical stratigraphy. Relatively incompetent shale units serve as detachment intervals and alternate with competent units of conglomerate and sandstone or of limestone (Brosgé and others, 1979a; Mull and Adams, 1989; Wallace and others, 1997). The relative thickness and competency of these units control the size and location of folds and thrusts, as well as the spacing and orientation of the ramps and flats within the faults. The rocks of the allochthon are stacked in south-dipping thrust fault-bounded sheets, with displacements ranging from tens of meters to a few kilometers, and map distances between faults of about 0.5 to 5 km (fig. 2). Map-scale north-vergent folds and smaller parasitic folds reflect structural thickening within the sheets. Leading hanging-wall anticlines truncated by underlying thrust faults are common and trailing footwall synclines are exposed less commonly. However, large unbroken fold pairs are seen only locally within the sheets. The folds in the Kanayut Conglomerate, a thick, competent unit, are larger in amplitude and wavelength than those in the Hunt Fork Shale, an incompetent unit. Within the southern part of the allochthon, including the study area, folds and thrust faults within the competent Kanayut Conglomerate are bounded below by a detachment in the Hunt Fork Shale and above by a detachment in the Kayak Shale (Wallace and others, 1997).

The map-scale folds in the Kanayut Conglomerate have been interpreted to have originated as detachment folds (Wallace and others, 1997). The contrast in competency between the Kanayut Conglomerate and the underlying Hunt Fork facilitated the formation of these folds. Although folds that have not been cut by thrusts are rare, the abundant folds cut by thrusts are similar in character to thrust-truncated detachment folds that display a transition into unfaulted detachment folds in the northeastern Brooks Range (Homza, 1992; Wallace, 1993).

The thrust faults cut the steep limbs of hanging-wall anticlines and footwall synclines at a high angle to bedding. These thrust faults form a duplex (Wallace and others, 1997). The thrust flats, where exposed, are in the Hunt Fork Shale and Kayak Shale so that the stratigraphic section included within the thrust sheets is generally limited to Hunt Fork Shale through Kayak Shale. Where the overlying Lisburne Group is not eroded, disharmony exists in structures across the Kayak. These characteristics suggest that the thrust faults broke through (truncated) the steep to overturned limbs of asymmetrical folds in the Kanayut Conglomerate to form a duplex of thrust-truncated folds between the Hunt Fork Shale and the Kayak Shale (Wallace and others, 1997).

THE TOYUK THRUST ZONE

Although it is mentioned extensively in the literature, the Toyuk thrust has only been loosely defined and identified in previous works. The name originally applied to a single thrust fault which is exposed on the southern flanks of Toyuk Mountain, near Anaktuvuk Pass (Porter, 1966). However, the name now applies to a regional boundary within the Endicott Mountains allochthon that separates exposures that consist predominantly of Hunt Fork Shale to the south and Kanayut Conglomerate to the north (Brosgé and others, 1979b; Mull and Adams, 1989). The Toyuk thrust zone has been mapped ~300 km to the west and ~140 km to the east of the field area. The Toyuk thrust zone tends to be thought of as a single traceable fault along strike, but existing mapping shows that it actually is a zone that consists of multiple faults along its length (Brosgé and others, 1979a, b; Mull, 1989; Kelley, 1990; Mull and others, 1994; Wallace and others, 1997). This zone appears to mark a regional change in depositional facies within the Endicott Mountains allochthon, most notably the change between the southern facies of the Kanayut Conglomerate and the thicker, more proximal northern facies (Kelley and Brosgé, 1995; Moore and others, 1997). However, the exact location and character of the facies change with respect to the Toyuk thrust zone has not been determined in detail along the length of the zone. At different places along strike, it could lie within the fault zone itself or nearby to the north or south of the zone.

The Toyuk thrust zone has been suggested to be a major large-displacement thrust within the Endicott Mountains allochthon on the basis of its length and because it separates different facies in the Kanayut (Moore and others, 1997). Minimum displacements of 18 km (Moore and others, 1997), 8 km (Kelley and Brosgé, 1995), and 5 km (Wallace and others, 1997) have been reported for individual faults in the zone, from west to east. However, near the Dalton Highway, Wallace and others (1997) described the zone to consist of a series of different thrust faults, none of which continues along strike for the entire length of the fault zone and that juxtapose Hunt Fork Shale to the south against Kanayut Conglomerate to the north (fig. 2). They interpret this to reflect different horses in a duplex of thrust-truncated detachment folds being revealed by changes in the level of erosion along strike. This interpretation requires only relatively small displacement on most of the individual thrust faults in the duplex, although it does not preclude a larger displacement on the southern, structurally highest fault.

LOCAL GEOLOGY

MECHANICAL STRATIGRAPHY

The stratigraphic units in the study include, from bottom to top, the Upper Devonian Hunt Fork Shale, Upper Devonian Noatak Sandstone, Upper Devonian and Lower Mississippian (?) Kanayut Conglomerate, and Lower Mississippian Kayak Shale. The relative competency of the units strongly influences the structure of the area. The regional and local characteristics of these units are summarized in table 1.

STRUCTURAL ORGANIZATION OF THE FIELD AREA

The field area is divided into panels bounded by thrust faults that strike between N 65° E and N 77° E and dip gently (15° to 30°) to the south (figs. 3, 4; table 2). The faults are designated from bottom to top by numbers 1 to 3, except for the southernmost thrust to the west, which is labeled "X" because its relationship to fault 3 is unclear in the field area. However, fault X is shown by Wallace and others (1997) to cut across fault 3. Faults 2A and 2B are here interpreted to be splays of the same fault. The panels separated by these faults are designated A, B, C1, C2, D, and Z, from lowest to highest (north to south).

GEOMETRY AND SEQUENCE OF STRUCTURES

Thrust Truncation of Detachment Folds

Detachment folds may develop in deformed areas where incompetent units underlie competent units (Poblet and McClay, 1996; Homza and Wallace, 1997). Contraction causes the competent layers to fold and the incompetent layers to flow into the core of the fold above a detachment that bounds the fold below. This is in contrast to fault-bend folds, in which folding is in response to bends in the underlying fault (Suppe, 1983), or fault-propagation folds, in which folding is in response to deformation preceding a propagating ramp tip (Suppe and Medwedeff, 1990; Mitra, 1990). As detachment folds tighten, they may be truncated by thrust faults, which leave anticlines in the hanging walls and synclines in the footwalls (Morley, 1994; Liu and Dixon, 1995; Wallace and Homza, 1996, 1997). Further shortening may cause the process to be repeated, which can result in a structural stack of fault-bounded panels of folded rock.

Figure 5 illustrates a schematic example of detachment folding and the truncation of a fold by a thrust fault. An anticline in the hanging wall and a syncline in the footwall result from displacement on a thrust fault that has cut the steep limb of an asymmetrical fold pair. Most of the panels in the field area contain a series of folds. The foremost anticline of each series of folds has been truncated in this manner (fig. 4). No truncated footwall synclines are exposed in the field area, although they have been observed elsewhere in the region (Wallace and others, 1997).

No direct evidence indicates the type of folds present in the field area. However, the contrast in competency between the units, the thickening of the incompetent units, the trains of multiple folds in several panels, and the indication that at least some of the folds pre-date the faults all favor the interpretation that these folds formed as detachment folds. The regional presence of detachment folds (Wallace, 1993; Wallace and others, 1997) further supports this interpretation. Fault-bend folding and fault-propagation folding are less likely alternatives because of the presence of an underlying incompetent unit, the presence of fold trains, and the local decapitation of folds, which indicates that the folds pre-date the faults.

In the study area, the folds are truncated by faults in two distinct manners. In panels B and Z (figs. 3, 4) the steep, short limbs of anticlines are clearly truncated by the underlying fault. The other manner of fold truncation is present only in panel B, where the tops of the folds have been cut off by the overlying fault (fig. 4). In this case, both the back limbs and forelimbs of several folds have been cut. While it could be argued that folding was contemporaneous with faulting where only the forelimb is truncated, as in fault-propagation folds (Suppe and Medwedeff, 1990; Mitra, 1990), the decapitation of the fold triplet in panel B (fig. 3; fig. 4 sec. C–C') clearly shows that those folds pre-date the fault that cut them.

The truncation of bedding at high angles and the decapitation of some folds by thrust faults both suggest that pre-existing folds were cut by thrust faults. These observations are consistent with the interpretation that the folds in the area are thrust-truncated detachment folds, as has also been suggested by Wallace and others (1997).

Duplex Thrust System

The thrust faults cut and repeat a limited stratigraphic interval (Dhf to Mky). Each panel consists of folded strata. Fault 3 parallels bedding in Hunt Fork at the base of panel D, and fault 1 parallels the Kanayut–Kayak contact at the top of panel A (fig. 4). These relations suggest that the thrusts of the area are bounded below by a floor thrust in Hunt Fork and above by a roof thrust in Kayak, although neither are exposed in the study area. In this interpretation, the structure of the area constitutes a duplex of thrust-truncated detachment folds (fig. 6B), which is consistent with a similar interpretation for the structure of the region proposed by Wallace and others (1997). The interpretation that the horses in this duplex contain pre-existing folds that were cut by the linking thrusts of the duplex differs from more familiar duplex interpretations, in which folds within the duplex are limited to fault-bend folds or, rarely, fault-propagation

Table 1. *Summary of mechanical stratigraphy*

Unit	Rock types	Structure	Comments
• **Lower Mississippian Kayak Shale** (Mky)	Black fissile clay shale with rare limestone marker beds in its upper part	Incompetent. Internally thickened by small folds and thrust faults. Forms flats of major thrust faults. In fault-bounded slivers in panel C1.	Upper detachment unit.
• **Upper Devonian to Lower Mississippian (?) Kanayut Conglomerate** (MDku =undifferentiated Kanayut unless specific member [below] is named). North facies divided into members: Ear Peak (MDke) (lower), Shainin Lake (middle, not identified in field area), and Stuver (MDks) (upper). Southern facies not divided into members	Conglomerate, sandstone, siltstone, and shale in Ear Peak and Stuver. (Shainin Lake, which is not identified in the field area, consists only of conglomerate and sandstone.)	Competent. Forms large folds and ramps of thrust faults.	Competent unit. The northern facies is thicker than the southern facies. The field area is in the boundary zone between the two, and could include either or both facies.
• **Upper Devonian Noatak Sandstone** (Dns)	Calcareous sandstone that shows rusty orange nodules. a single shale exposure as the underlying Dhf unit (panel C2). However, Noatak is treated as part of the overlying Kanayut for development of models.	Competent. Forms large folds and ramps of thrust faults.	Possibly present in the field area based on identification of
• **Upper Devonian Hunt Fork Shale** (Dhf)	Shale and subordinate thin interbeds of sandstone.	Incompetent. Considerable internal structural thickening. Forms flats of thrust faults and cores folds in Kanayut.	Lower detachment unit.

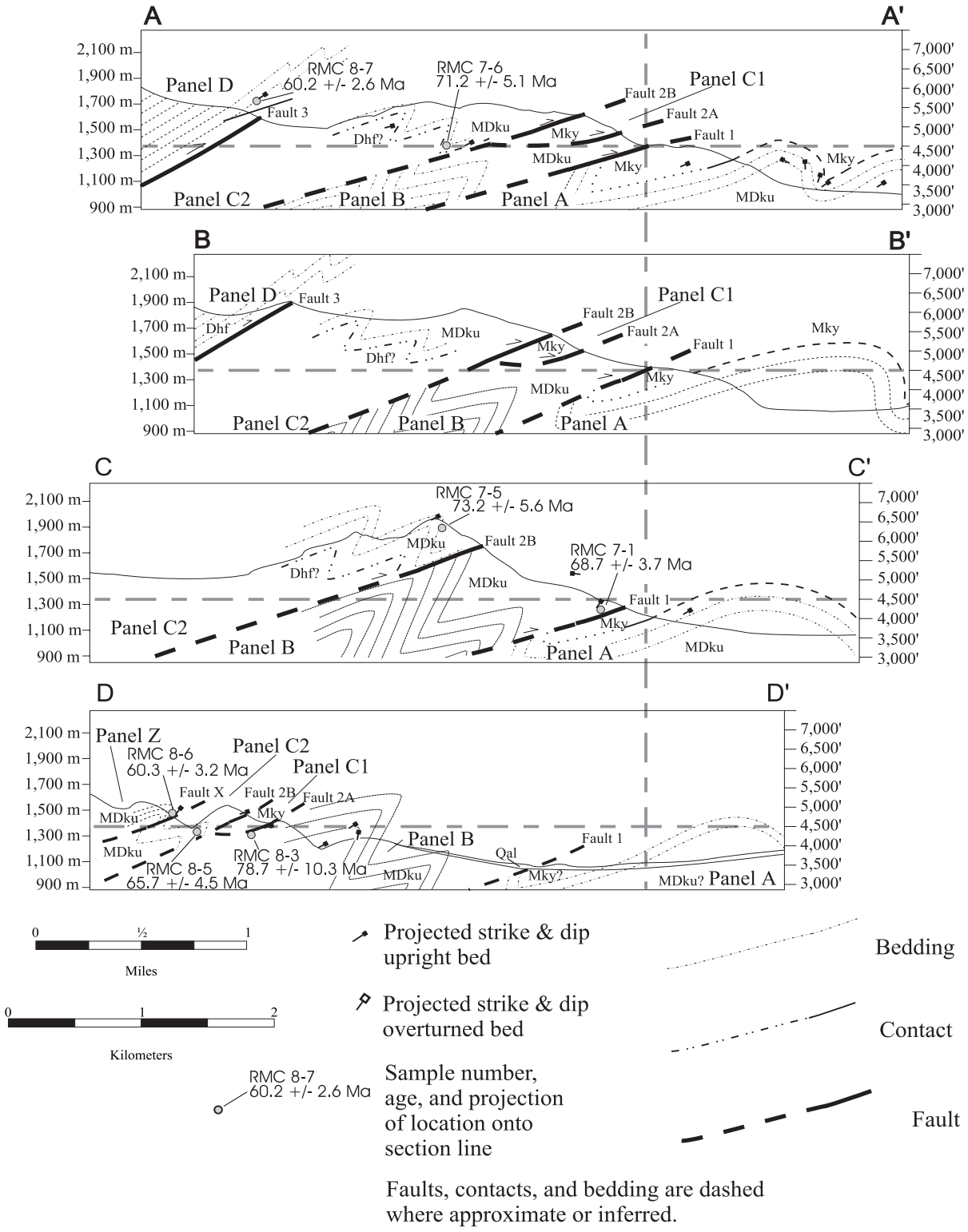

Figure 4. *Cross sections across the Toyuk thrust zone, including locations and ages of cooling apatite fission-track samples. Sections have been lined up based on the intersection of fault 1 and the 4,500 ft elevation mark.*

folds (Boyer and Elliott, 1982; Mitra, 1986; Mitra and Boyer, 1986).

An alternative interpretation of the same structural geometry would be an imbricate fan (fig. 6A). The primary difference between a duplex and an imbricate fan is the presence or absence of a roof thrust. An imbricate fan consists of thrusts that branch upward from a common floor, while a duplex consists of thrusts that link a floor thrust with a roof thrust (Boyer and Elliott, 1982; McClay, 1992). It is difficult to distinguish between the two in areas where the roof thrust has been eroded, but the restricted range of stratigraphic section contained in each panel and the evidence for flats in Hunt Fork and Kayak both locally and regionally support the duplex interpretation. Furthermore, carbonate rocks of the Lisburne Group, exposed in an erosional remnant to the northwest of the field area, are folded disharmonically with respect to the underlying Kanayut. This relationship supports the interpretation of a roof thrust in the intervening Kayak Shale (fig. 2).

MODELS FOR THE DISPLACEMENT OF THE TOYUK THRUST ZONE

Each of the panels within the study area exposes Kanayut Conglomerate and/or Kayak Shale, with the exception of panel D (figs. 3, 4). This topographically and

Table 2. *Summary of fault-bounded panels within the field area*

Panel	Thickness	Upper contact	Lower contact	Stratigraphic units (see table 1)
A	>200 m	Fault 1	Not exposed	MDks and Mky
B	300–400 m in the eastern half of field area; 600–800 m in the western half.	Fault 2A or 2B	Fault 1	MDku
C1	100–150 m	Fault 2B	Fault 2A	Mky
C2	500 m	Fault 3 and Fault X	Fault 2B	MDke(?), Dns(?), and Dhf(?)
D	>400 m	Not exposed	Fault 3	Dhf
Z	>200 m	Not exposed	Fault X	MDku

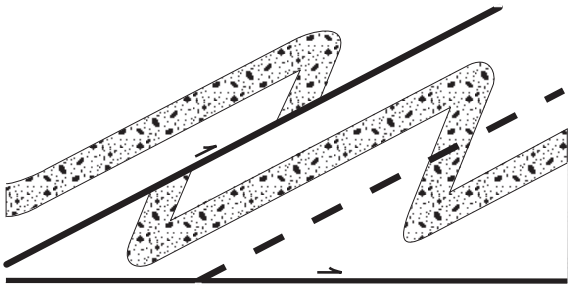

Figure 5 (left). *Thrust truncation of detachment folds. Folds in competent conglomerate are cored by incompetent shale. Further shortening allows thrust faults to breach the forelimbs of the anticlines and to displace the folded package over the synclines.*

Figure 6 (below). *Imbricate fan versus duplex. (A) An imbricate fan consists of thrust faults which branch upward from a single basal thrust. (B) A duplex consists of stacked panels of fault-bounded rocks. A duplex must have both a floor and a roof thrust, as well as thrusts linking the two. Pattern fills do not designate bedding.*

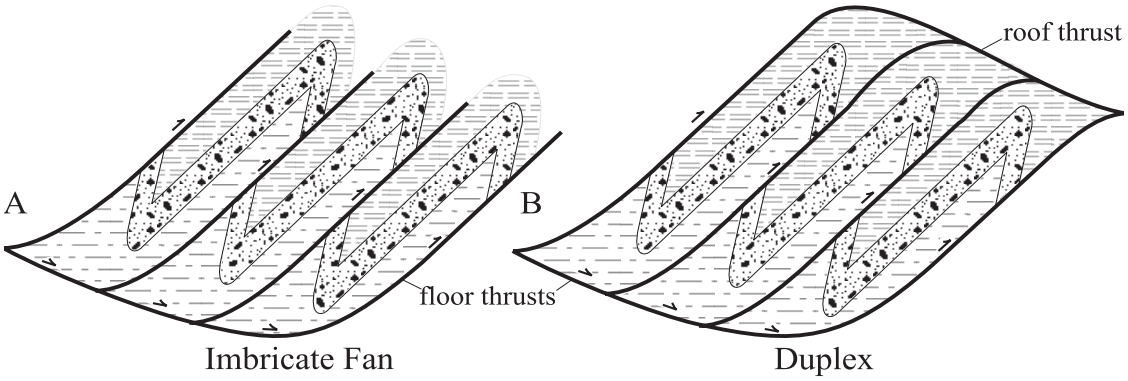

structurally highest panel exposes only Hunt Fork Shale, the oldest stratigraphic unit of the area. However, Hunt Fork is present in the hanging walls of the other faults up-plunge to the east of the area (Brosgé and others, 1979a; Wallace and others, 1997). The Toyuk thrust zone has previously been interpreted as a major large-displacement fault (Moore and others, 1997). The duplex interpretation proposed above does not *require* a large displacement, although it still allows for large displacement. Multiple faults within a duplex may bring underlying units such as Hunt Fork into contact with overlying units such as Kanayut with fairly little displacement on any one fault, although the cumulative structural relief across the duplex may be large.

Two end-member models with different implications for displacement are consistent with the observations of this study and the duplex interpretation (fig. 7). In both models, a duplex in the Kanayut Conglomerate is bounded below by a floor thrust in Hunt Fork. The difference between the models is in the amount of displacement on the highest and hindmost fault in the duplex. The exact position and character of the change between the northern and southern facies of the Kanayut are unknown, so two versions of each model were constructed to explore the consequences for displacement of the different thicknesses of each facies. One version uses a thickness measured in the northern facies (~2,600 m), and the other uses a thickness determined for the southern facies (~1,000 m) (Moore and others, 1989).

These models were based on cross section C–C' (fig. 4) for several reasons. It is the section where panel B is thickest and has the best constrained boundaries. It is relatively near a small exposure of probable Hunt Fork Shale in panel C2 (fig. 3 or see plate 1, Chmielowski, 1998) that provides a constraint on the location of the top of that unit within the panel. Panel C1 is absent in that area, which simplifies the model by requiring only a single fault to be considered between panels B and C2.

Panels A and C2 are the best constrained. Panel A has a well defined contact between the Kanayut Conglomerate and the overlying Kayak Shale, and so approximate thicknesses for each facies of the Kanayut were projected downward from that contact. Folds were projected upward and downward to match the axial surfaces and bedding attitudes observed in the cross section. The elevation of the probable Hunt Fork/Kanayut contact in panel C2 was used as the baseline from which to project the thicknesses of overlying Kanayut. For the sake of simplicity, the Noatak Sandstone was combined with the Kanayut in these models. Since the location of contacts in panel B is less constrained, it is taken to have a displacement intermediate between that of panels A and C2. Panel D is the least constrained of the panels; the main difference in the two models is in the displacement of this panel on fault 3. Model one shows similar displacements on each of the thrusts so that fault 3 simply serves as another linking thrust in the duplex (fig. 7, top). Model two shows a much larger displacement on fault 3 so that panel D forms the roof of the duplex (fig. 7, bottom).

Since no truncated footwall synclines are exposed in the field area, their locations were approximated on the models by assuming that only the folds exposed at the surface plus a truncated trailing syncline were present (as in fig. 5). Similarly, a leading truncated anticline was inferred if one wasn't exposed in the panel. The inferred folds were placed such that their geometry matched other folds in the area, and were located to give the minimum possible displacement on each fault.

Both models are partially restored in figure 8. Movement along the faults was removed by restoring each panel to the point where the bedding contacts matched across the faults. This restoration attempts to restore each fold to its pre-faulted configuration. The restorations are only approximate because some faulting likely was contemporaneous with the folding in both cut and uncut folds. However, this restoration is still useful to determine the minimum displacements necessary along each fault.

The minimum displacement on each fault is given in table 3. These estimates are based on the amount of fault movement necessary to restore the bedding contacts across the faults. These numbers are approximate because the truncated footwall synclines in each panel are inferred and the truncated hanging-wall anticlines do not expose their upper contacts. In model two there are no constraints upon which to base the estimates for displacement for fault 3. Therefore I have used a "greater than" symbol to indicate that the value is not calculable at this time.

Table 3. *Estimates of minimum displacement on the faults of the Toyuk thrust zone*[a]

	A Northern facies	**B Southern facies**
Fault 1	500 m	625 m
Fault 2	800 m	750 m
Fault 3		
Model 1	450 m	1,000 m
Fault 3		
Model 2	≥6,300 m[b]	≥4,000 m[b]

[a]These values were obtained by comparison of the partially restored versions (fig. 8) with the unrestored models (fig. 7).

[b]No constraints are known upon which to base estimates for displacement on fault 3 in model 2, except that they must exceed the minimum values in model 1. The values given here are based on figure 7, which shows displacement if panel D overlaps faults 1 and 2.

MODEL ONE

All of the faults in this model show minimum displacements (table 3). The southward increase in structural relief within the duplex is greater than the increase in elevation of the erosion surface. Consequently, the erosion surface cuts down-section to the south, and panel D is the only one that exposes a significant amount of Hunt Fork Shale at the surface (fig. 7, top). The minimum displacements for this model are much less than previously published estimates for the Toyuk thrust zone (Moore and others, 1997) because the model considers only the displacement needed to account for the current configuration via a duplex of thrust-truncated detachment folds.

MODEL TWO

Model two differs from model one only in the amount of displacement assumed on the southernmost and structurally highest fault, fault 3 (fig. 7, table 3). Displacement on this fault must be greater than the minimum assumed in model one but otherwise is unconstrained since the hanging-wall cutoff of the Hunt Fork/Kanayut contact has been eroded. For this model, fault 3 is assumed to have sufficient displacement to place panel D over the exposed positions of faults 1 and 2 (fig. 7, bottom). Thus, panel D forms the roof of the duplex, with the roof thrust located between Hunt Fork in the hanging wall and Kayak in the footwall. This assumption yields a much greater displacement for fault 3 than for the other (linking) thrusts in model two or any of the thrusts in model one (table 3).

STRATIGRAPHIC BEST-GUESS VERSION OF THE MODELS

Many more versions of the models are possible to represent different positions and widths of facies change across the Toyuk thrust zone in the study area, but the available data aren't sufficient to determine which of these models is correct. However, the fact that the three members of the Kanayut can be identified and mapped as far south as fault 3 just south of the field area (Wallace, unpublished mapping) suggests that these rocks belong to the northern facies and that the facies change lies somewhere at or to the south of fault 3, but north of exposures of the southern facies at Atigun Pass. This suggests the interpretation that the Toyuk thrust zone formed at the facies change (Wallace and others, 1997; Chmielowski, 1998), with the southernmost fault in the duplex being localized at the facies change and additional horses forming within the northern facies in the footwall of this fault. Another version of the models is presented to illustrate this best guess as to the relation between the facies change and the thrust zone (fig. 9). This version is simply a composite of the versions presented in figures 7 and 8 in which an abrupt thickness change is assumed just below fault 3 so that the northern facies is shown in the horses below and forward of fault 3, and the southern facies is shown above fault 3. Thus, the estimated displacements reported in table 3 that would apply to this version are for the southern facies for fault 3 and for the northern facies for faults 1 and 2. In this interpretation, the hindmost fault that is localized at the facies change might also be expected to be the fault with the greatest displacement. Although this cannot be determined within the study area, it is consistent with an estimated minimum displacement of 5 km on the probable continuation of fault 3 south of the study area (Wallace and others, 1997).

APATITE FISSION-TRACK ANALYSIS

METHODOLOGY AND THERMOCHRONOLOGY

To constrain the unroofing history of the Toyuk thrust zone and to relate its activity to regional Brooks Range tectonics, apatite fission-track (AFT) data were gathered from seven outcrop samples collected across a broad range in elevation from four different fault panels (figs. 3, 4).

Fission tracks in apatite grains preserve a record of the thermal history of the host rock below temperatures of ~110°C. Thus, they are ideal for determining the timing of denudation in response to uplift of upper crustal rocks (Naeser, 1979). The length reduction of confined tracks leads to the reduction of fission track age, and the length distribution of the confined tracks in apatite directly reflects its thermal history subsequent to the last time it cooled below ~110°C (Gleadow and others, 1986; Green and others, 1989). In this study, the AFT data have been interpreted using the system response (Green and others, 1989) based on an empirical kinetic description of laboratory annealing data in Durango apatite (Laslett and others, 1987). Thermal history interpretations are based on a quantitative treatment of annealing achieved by forward modeling (Green and others, 1989) of track shortening and age evolution through likely thermal histories for an apatite composition equal to that of Durango apatite (0.4 weight percent chlorine [Cl]).

The annealing behavior of fission tracks in apatite is sensitive to apatite chemistry, particularly to the ratio of chlorine to fluorine (Green and others, 1986; O'Sullivan and Parrish, 1995), so the Cl content of individual grains dated in three representative samples from different fault panels (RMC7-6, RMC7-1, RMC8-6) was determined by microprobe analysis. The results indicate that all 75 grains were F-apatite with Cl concentrations ranging between ~0.0 and 0.4 weight percent Cl, thus there is no evidence of major compositional variation among the different apatite grains. These Cl concentrations are less than or

A: If the northern facies of the Kanayut (2,600 m thick) is present in the field area.

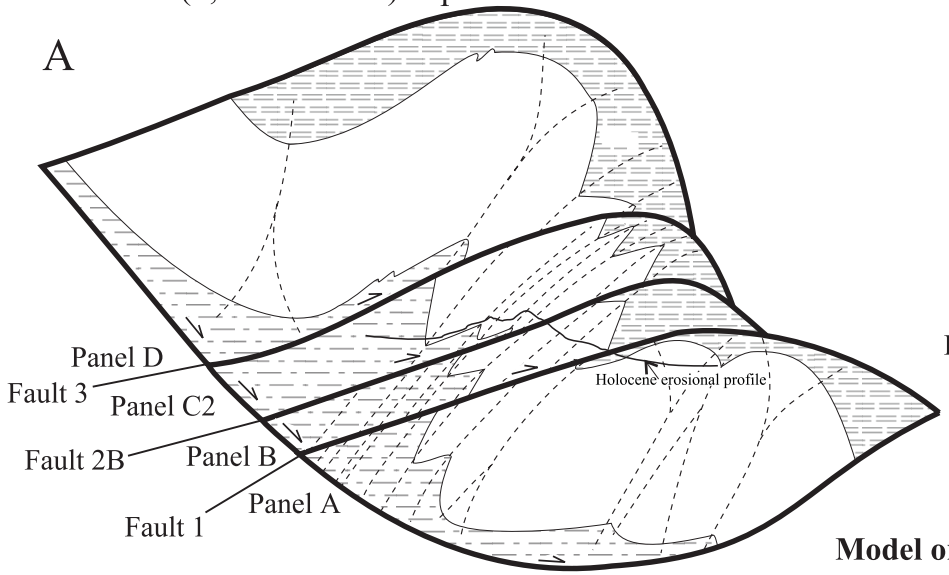

B: If the southern facies of the Kanayut (1,000 m thick) is present in the field area.

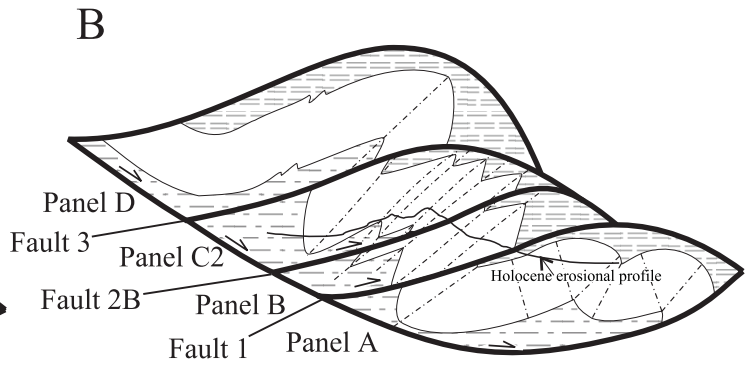

Model one: All of the faults show a similar amount of displacement.

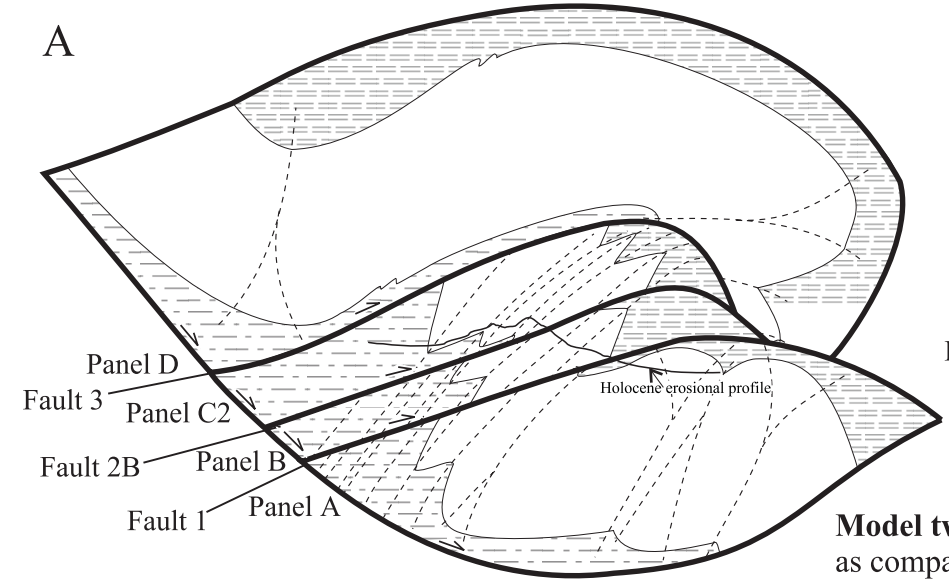

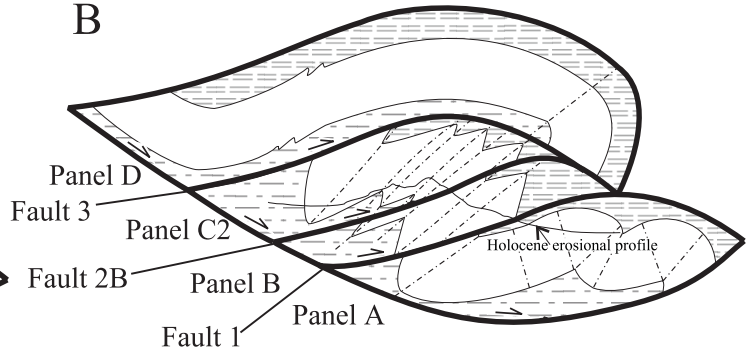

Model two: There is a much greater amount of displacement on fault 3 as compared to the other faults.

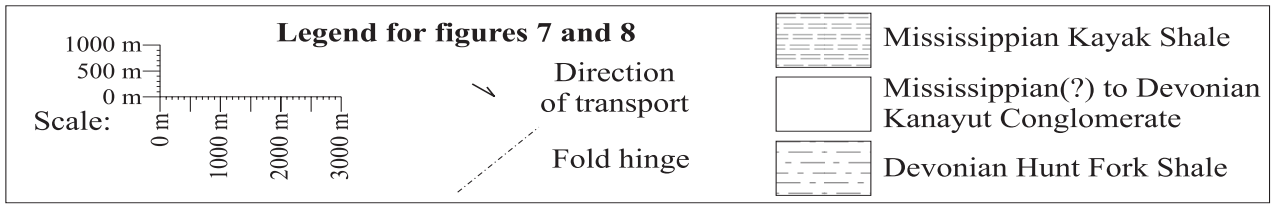

A: If the northern facies of the Kanayut (2,600 m thick) is present in the field area.

B: If the southern facies of the Kanayut (1,000 m thick) is present in the field area.

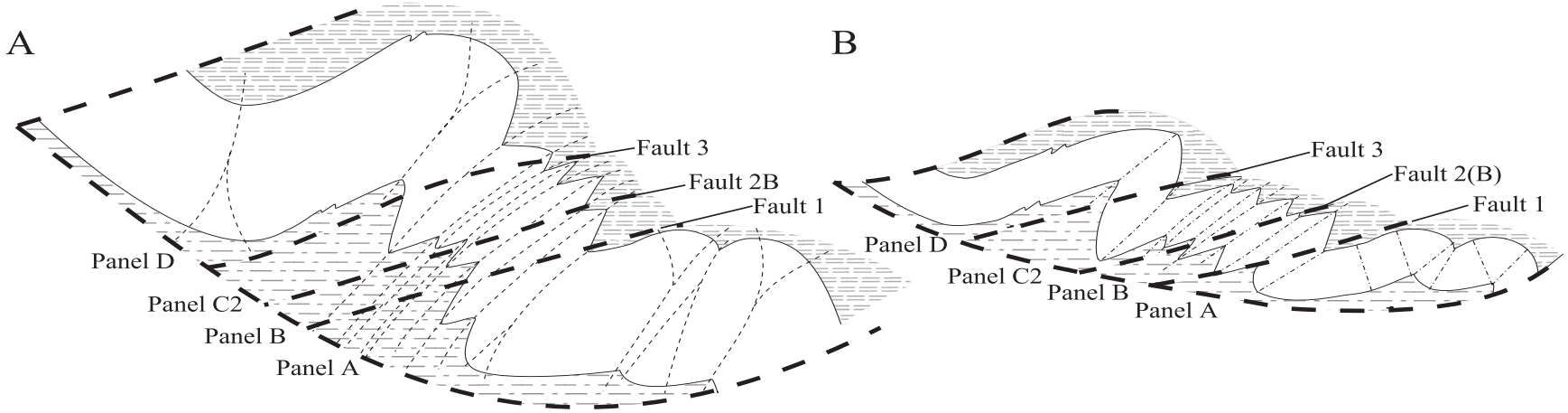

Partially restored sections: Fault displacement is restored to show fold shortening only. In actuality this configuration likely never existed, as some folding probably occurred after the faulting began.

Figure 7 (page 22). *Models for thrust displacement. Model one has a similar displacement on all faults. Model two has a much greater displacement on fault 3. Each model has two versions, one with thicknesses appropriate to the northern facies of the Kanayut, one for the southern facies.*

Figure 8 (above). *Partially restored sections: Fault displacement is restored to show fold shortening only. In actuality this configuration likely never existed, as some folding probably occurred after the faulting began. Each model has two versions, one with thicknesses appropriate to the northern facies of the Kanayut, one for the southern facies. All three members of the Kanayut Conglomerate as well as the Noatak Sandstone are included in MDku. Dhf is the Hunt Fork Shale, and Mky is the Kayak Shale. Pattern fills do not designate bedding.*

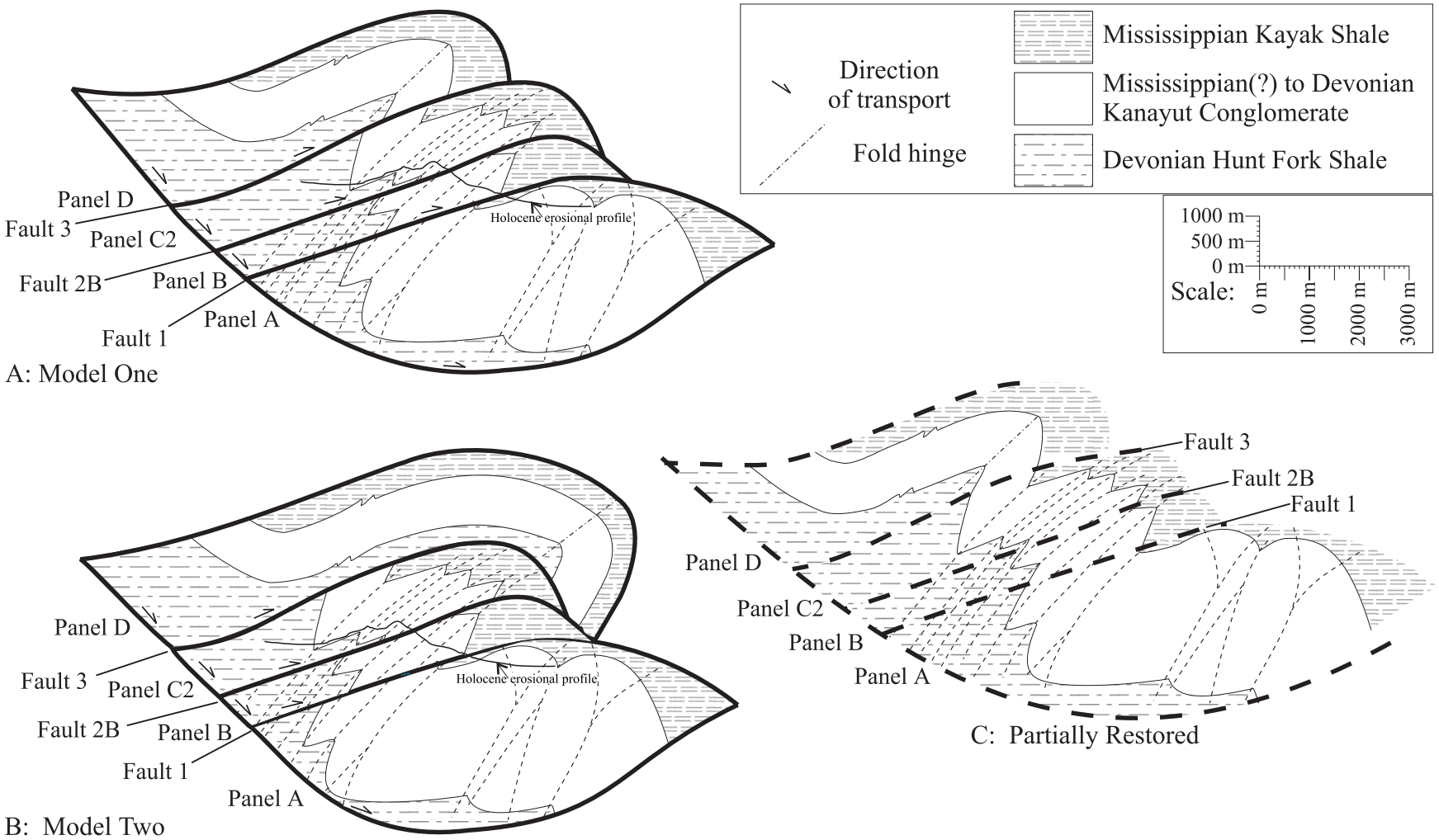

Figure 9. *Stratigraphic best-guess version of the models. Comparison of model one (A) and model two (B) and the partially restored section (C) for each if it is assumed that fault 3 is the border between the thicker northern facies of the Kanayut and the thinner southern facies. This version is intermediate between the two end-member versions of the models presented in figures 7 and 8.*

equal to that for Durango apatite (0.4 weight percent Cl), so paleotemperatures estimated by applying the Laslett and others (1987) model for track annealing are interpreted to be maximum values. Gallagher (1995) automated the modeling procedure to give a forward modeling approach that combines a Monte-Carlo simulation of numerous possible thermal histories with statistical testing of the outcome against the observed fission-track measurements. A genetic algorithm is also used to provide rapid convergence to an acceptable fit. The absolute paleotemperature estimates quoted in this paper have an uncertainty of ±10°C (Green and others, 1989).

RESULTS AND INTERPRETATIONS

Sample information and results are presented in table 4, while the complete results are presented in Appendix B of Chmielowski (1998). In figure 4, the ages are shown on the cross sections to put them into geological context, and in table 4 the samples are grouped according to the nearest cross-section line to illustrate the changes in age with elevation across different parts of the area. The AFT ages of these samples range between 60 ± 3 and 79 ± 10 Ma and the mean track lengths range between 13.4 ± 0.1 µm and 14.4 ± 0.1 µm with standard deviations between 1.1 and 1.6 µm (all uncertainties presented below are ±1s unless otherwise stated).

All AFT ages were much younger than the Devonian to Mississippian depositional ages of the rocks, which indicates a reduction in grain ages in response to thermal annealing since the rocks were deposited. Furthermore, the long mean track lengths (most >13.8 µm) and narrow track length distributions (most standard deviations <1.3 µm) indicate that these samples cooled rapidly from temperatures >~110°C to temperatures <~50–60°C at the time given by the AFT age for each sample. This is particularly true for sample RMC8-7 with a mean length of ~14.4 µm and a standard deviation of ~1.1 µm. Therefore, these results record a major episode of rapid cooling during the Paleocene at ~60 Ma. This age of cooling is consistent with the 60 ± 4 Ma age for a series of samples collected east of the Dalton Highway near the range front (O'Sullivan and others, 1997).

The results from two of the samples (RMC8-3, RMC7-6), however, show slightly shorter mean track lengths and broader track-length distributions (table 4). Modeling of these results using the forward modeling approach described by Gallagher (1995) indicates an earlier episode of cooling from temperatures >~110°C to temperatures in the range of ~80–90°C prior to the later episode of cooling to temperatures <~50–60°C at ~60 Ma. The best-fit model for timing of this earlier event suggests cooling at some time between ~90–110 Ma. The timing of this event also fits well with the previous results by O'Sullivan and others (1997), who suggested that a major episode of cooling/denudation occurred at ~100 ± 5 Ma in the region around Atigun Pass.

Therefore, we believe that the AFT data indicate that the rocks within the Toyuk thrust zone have undergone two major episodes of relatively rapid cooling from elevated paleotemperatures: an initial period of cooling in the mid-Cretaceous at ~100 Ma, after which some samples remained at elevated paleotemperatures between ~80 and 90°C, followed by a later Paleocene cooling at ~60 Ma (fig. 10). Of the two episodes of cooling, the Paleocene event is better constrained as the samples with the best data yield the youngest ages. Evidence for the earlier cooling event is reflected in a few of the samples (RMC8-3, RMC7-6) by the range of single-grain ages, including some bimodal distributions, and the broader track-length distributions (Appendix B of Chmielowski, 1998). The data indicate that these samples resided for some period

Table 4. *Fission track data sorted by physical location of samples collected*[a]

Nearest Cross Section	Sample Number	Fault Panel	Elevation	Unit	Pooled Age (Ma)[b]	Central Age (Ma)[c]	Mean Track Length (µm)	Standard Deviation (µm)
A–A'	RMC8-7	D	5,800 ft	Dhf	60.2 ± 2.6	60.2 ± 3.0	14.35 ± 0.11	1.13
A–A'	RMC7-6	C2	4,600 ft	Dns?	71.2 ± 5.1	71.8 ± 14.07	13.81 ± 0.16	1.61
C–C'	RMC7-5	C2	5,700 ft	MDke?	73.2 ± 5.6	73.2 ± 5.5	13.43 ± 0.11	1.09
C–C'	RMC7-1	B	4,100 ft	MDku	68.7 ± 3.7	68.7 ± 3.6	13.97 ± 0.13	1.29
D–D'	RMC8-6	Z	4,500 ft	MDku	60.3 ± 3.2	60.2 ± 3.8	13.86 ± 0.15	1.51
D–D'	RMC8-5	C2	4,250 ft	MDke?	65.7 ± 4.5	65.7 ± 4.4	13.35 ± 0.13	1.29
D–D'	RMC8-3	B	4,000 ft	MDku	71.6 ± 6.7	78.7 ± 10.3	13.92 ± 0.15	1.49

[a]Note changes in age as elevation changes along each section line. All analyses by Paul O'Sullivan, La Trobe University, Australia. For more detail see the full fission track report in Appendix B of Chmielowski (1998). See O'Sullivan and others (1997) for a more complete explanation.
[b]Pooled age is the best estimate of age for samples in which all grains represent a single age population.
[c]Central age is a better estimate where this is not the case.

of time at paleotemperatures high enough to reset some grain ages but not high enough to reset all grain ages. The samples with the youngest ages (RMC8-6, RMC8-7) seem to have been the most thoroughly overprinted (higher paleotemperatures) prior to the Paleocene cooling.

The mechanism of the mid-Cretaceous cooling episode is unknown based on data from the study area alone. O'Sullivan and others (1997) proposed that cooling at this time was the result of kilometer-scale denudation associated with active thrust faulting and folding within the core of the Brooks Range at the end of the initial period of major shortening in the main axis of the range, although they also mention the alternative possibility of unroofing by regional extension. These new results do not constrain the mechanism any further, but indicate that, whatever the mechanism, the rocks must have cooled to paleotemperatures of ~90–80°C during that time to start accumulating fission tracks in the apatite grains.

The Paleocene cooling episode, on the other hand, is most likely to be the result of more deeply buried rocks being thrust into higher structural levels within the study area. As shown in figure 4, the samples from panels D and Z gave the youngest AFT ages. In detail, the results from these particular samples record only the Paleocene event and indicate that they must have cooled from temperatures >~110°C to temperatures <~50–60°C at ~60 Ma. However, the results from samples collected from the lower thrust panels C-2 and B suggest that they record both episodes of cooling. Therefore, samples with the most precise and youngest (Paleocene) AFT ages are juxtaposed across thrust faults over samples with older, less precise AFT ages (fig. 4). This relationship indicates that those samples that are now structurally highest were located at greater depths (higher paleotemperatures) before thrusting than samples now located in structurally lower panels (fig. 4). This evidence supports Paleocene activity for both fault X, which is shown elsewhere to be an out-of-sequence fault (Wallace and others, 1997), and fault 3, which is the highest potentially in-sequence fault and also happens to have the largest probable displacement.

Previous work in the central Brooks Range has identified 60 Ma cooling/denudation ages primarily in the range-front region (Blythe and others, 1996; O'Sullivan, 1996; O'Sullivan and others, 1997), as well as locally within internal parts of the orogen (Murphy and others, 1994; O'Sullivan and others, 1998b). However, as samples collected for these previous studies came from areas either south or north of the Toyuk thrust zone, those studies did not find any evidence to suggest Paleocene activity in the zone. In apparent contrast, the results from this study, which was the first study to sample rocks from within the fault zone itself, indicate that the Toyuk thrust system was indeed active—and perhaps even formed—during the 60 Ma event. Furthermore, the thrust zone is located ~25 km south of the range front, which suggests

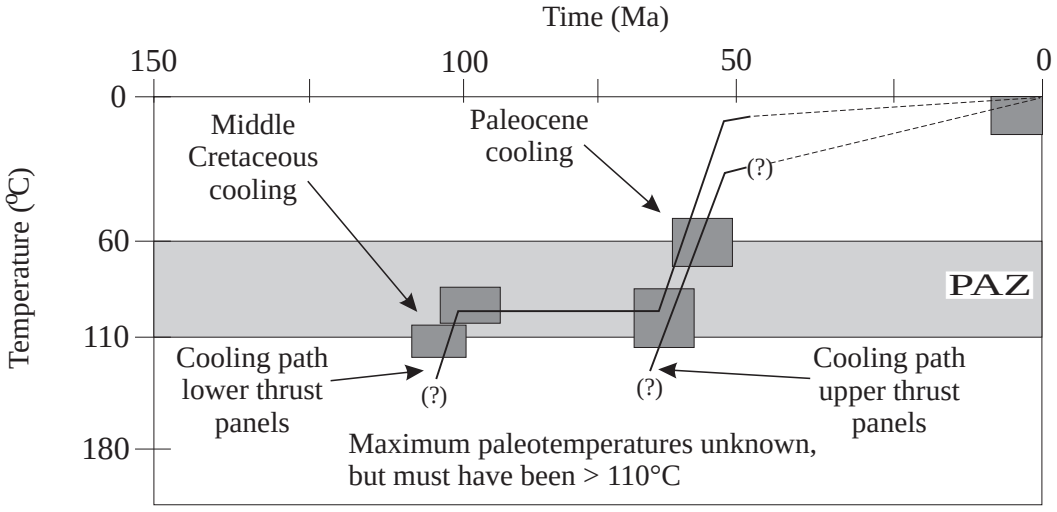

Figure 10. *Proposed cooling histories below ~110°C for the samples analyzed from the Toyuk thrust zone. Apatite fission track (AFT) data record two episodes of cooling, at ~100 Ma and ~60 Ma. Results from samples from the highest thrust panels record only Paleocene cooling/denudation, whereas results from samples from the lower thrust panels record both cooling events. PAZ refers to the partial annealing zone for apatite, the temperature range within which AFT ages are significantly reduced (for more explanation see Gleadow and others, 1986). See text for further details.*

that structural thickening occurred within the orogenic wedge, rather than solely at its base and leading edge. Thus, the fission-track results indicate that at least some faulting occurred in the Toyuk thrust zone at ~60 Ma in a location hindward of the position of the deformation front both during the ~60 Ma event and during earlier thrusting events. Deformation internal to the wedge at ~60 Ma represents a departure from a simple forward-propagating thrust sequence as the older orogenic wedge continued its growth during the ~60 Ma event. Models for orogenic wedges predict such apparently "out of sequence" activity within wedges (Platt, 1986; Dahlen and Suppe, 1988; Hardy and others, 1998), but such activity is difficult to document.

CONCLUSIONS

This study supports the conclusion that the structural geometry and evolution of the area has been strongly influenced by its mechanical stratigraphy. The alternation of incompetent and competent units allowed the formation of detachment folds, which were then truncated by thrust faults, and ultimately led to the formation of a duplex of thrust-truncated detachment folds. The duplex geometry in this interpretation contrasts with other published duplex geometries (Boyer and Elliott, 1982; Mitra, 1986; Mitra and Boyer, 1986) that limit folding within a duplex to fault-bend folding or, rarely, fault-propagation folding. However, this is not the first study to suggest duplexes of thrust-truncated detachment folds (Homza, 1992; Morley, 1994). This study addresses a particular example of this type of duplex, but such structures are widespread in the northern Brooks Range (Wallace, 1993; Wallace and others, 1997) and likely exist in fold-and-thrust mountain ranges worldwide.

Two end-member models presented in this study to account for the exposure of the various units at the surface differ only in their interpretation of the structurally highest fault, fault 3. In model one, fault 3 is a linking fault within the duplex, and the roof has been eroded in this area. In model two, fault 3 is the roof of the duplex. Neither version requires a large displacement on the linking faults of the duplex. Further study of the Toyuk thrust zone along strike is required to determine which model better represents the area. Locating both hanging-wall and footwall cutoffs across a fault would allow the actual displacement on that fault to be determined. Locating remnants of the duplex roof would allow further control. If the rocks overlying the roof repeat the same stratigraphic section as that exposed in the duplex (as in model two), this would support a larger displacement along the fault (fig. 11A), and the exposed length of the roof across strike would provide a measure of its minimum displacement. However, if the rocks overlying the roof consist of younger units than exposed within the duplex, it would support the smaller-displacement model (fig. 11B). Different versions of these models can be visualized depending on the location and character of the facies change in the Kanayut Conglomerate between the thicker northern facies and the thinner southern facies (fig. 7). The most likely possibility is that the southernmost fault in the duplex was localized at the facies change and additional horses formed within the northern facies in the footwall of this fault.

Regardless of the details of the structural geometry, an important conclusion is that the Toyuk thrust zone in the study area is not a single fault, but a series of thrusts that, along strike, place Hunt Fork Shale over Kanayut Conglomerate. Within the study area, the southernmost fault is the fault that separates extensive Hunt Fork to the

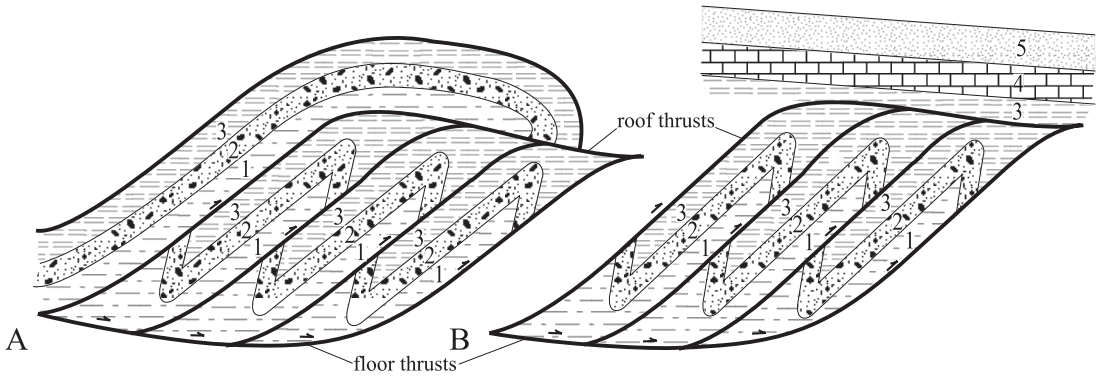

Figure 11. *Duplex roofs. (A) Older-over-younger. The stratigraphy of the duplex repeats above the roof. (B) Younger-over-older. The normal stratigraphic succession continues undisturbed above the duplex. Pattern fills do not designate bedding.*

south from extensive Kanayut to the north, and hence would be identified regionally as "the Toyuk thrust" (fig. 2). This also is the fault most likely to separate the two facies of the Kanayut and to have the largest displacement. However, along strike to the east of the Dalton Highway (fig. 2), Hunt Fork is separated from Kanayut by a different fault, a deeper-level exposure of one of the smaller-displacement faults to the north. Thus, it should not be assumed regionally that the fault that forms the local boundary between Hunt Fork and Kanayut is necessarily either a large-displacement fault or the fault that marks the facies change within the Kanayut. Instead, the Toyuk thrust zone should be viewed as a complex zone of multiple thrusts that likely formed at or near the facies change in Kanayut and may have significant displacement, although the amount and distribution of displacement likely varies along the length of the zone.

The apatite fission-track data from this study indicate Paleocene displacement of at least the structurally highest and hindmost thrusts. Previous studies in the central Brooks Range (Blythe and others, 1996; O'Sullivan, 1996; O'Sullivan and others, 1997) documented Paleocene cooling at the range front, some 25 km to the north, but not along the Toyuk thrust. Other studies have documented apparent out-of-sequence deformation at the range-front (Mull and others, 1997), breaching thrusts within the Endicott Mountains allochthon (Wallace and others, 1997), and Paleocene cooling in more internal parts of the orogen (Murphy and others, 1994; O'Sullivan and others, 1998b). These observations suggest that deformation has occurred within the orogenic wedge, at least in part during Paleocene time, but they do not identify the time at which specific structures were active. This study shows that specific faults were displaced during Paleocene time far hindward of the front both of the already existing orogenic wedge, and the wedge that was active in Paleocene time. Such internal deformation of a wedge to attain critical shape is predicted by orogenic wedge models (Platt, 1986; Dahlen and Suppe, 1988; Hardy and others, 1998). Detailed geochronology was necessary in this case to determine that such internal deformation occurred, and structural style or relative structural sequence were not sufficient in themselves to determine the age of that deformation.

ACKNOWLEDGMENTS

This work was made possible with funding by the industry sponsors of the Tectonics and Sedimentation Research Group at the University of Alaska Fairbanks and a grant from the Geological Society of America. Support for the AFT sample irradiations at the HIFAR reactor at Lucas Heights, Australia, was supplied through an Australian Institute of Nuclear Science and Engineering grant to the La Trobe University Fission-Track Research Group. We also thank Charles G. Mull and Thomas Moore for their reviews of this manuscript.

REFERENCES

Blythe, A.E., Bird, J.M., and Omar, G.I., 1996, Deformation history of the central Brooks Range, Alaska: Results from fission-track and 40Ar/39Ar analyses: Tectonics, v. 15, no. 2, p. 440–455.

Boyer, S.E., and Elliott, David, 1982, Thrust systems: American Association of Petroleum Geologists Bulletin, v. 66, no. 9, p. 1196–1230.

Brosgé, W.P., Reiser, H.N., Dutro, J.T., Jr., and Detterman, R.L., 1979a, Bedrock geologic map of the Philip Smith Mountains quadrangle, Alaska: U.S. Geological Survey Miscellaneous Field Studies Map 897B, 2 sheets, scale 1:250,000.

Brosgé, W.P., Reiser, H.N., Dutro, J.T., Jr., and Nilsen, T.H., 1979b, Geologic map of Devonian rocks in parts of the Chandler Lake and Killik River quadrangles, Alaska: U.S. Geological Survey Open-File Report 79-1224, 1 sheet, scale 1:200,000.

Chmielowski, R.M., 1998, Structural geometry and evolution of the Toyuk Thrust Zone, Brooks Range, Alaska. Unpublished Master's Thesis: University of Alaska, Fairbanks, 92 p., 2 plates, scale 1:25,000.

Dahlen, F.A., and Suppe, John, 1988, Mechanics, growth, and erosion of mountain belts, *in* Clark, S.P., Jr., Burchfiel, B.C., and Suppe, John, eds., Processes in continental lithospheric deformation: Geological Society of America Special Paper 218, p. 161–178.

Gallagher, Kerry, 1995, Evolving temperature histories from apatite fission-track data: Earth and Planetary Science Letters, v. 136, nos. 3–4, p. 421–435.

Gleadow, A.J.W., Duddy, I.R., Green, P.F., and Lovering, J.F., 1986, Confined fission track lengths in apatite; A diagnostic tool for thermal history analysis: Contributions to Mineralogy and Petrology, v. 94, no. 4, p. 405–415.

Grantz, Arthur, Moore, T.E., and Roeske, S.M., 1991, A-3; Gulf of Alaska to Arctic Ocean: Boulder, Colorado, Geological Society of America Centennial Continent/ Ocean Transect no. 15, 72 p., 3 sheets, scale 1:500,000.

Green, P.F., Duddy, I.R., Gleadow, A.J.W., Tingate, P.R., and Laslett, G.M., 1986, Thermal annealing of fission tracks in apatite; 1, A qualitative description: Chemical Geology; Isotope Geoscience Section, v. 59, no. 4, p. 237–253.

Green, P.F., Duddy, I.R., Laslett, G.M., Hegarty, K.A., Gleadow, A.J.W., and Lovering, J.F., 1989, Thermal annealing of fission tracks in apatite; 4, Quantitative modeling techniques and extension to geological

timescales: Chemical Geology; Isotope Geoscience Section, v. 79, no. 2, p. 155–182.

Hardy, Stuart, Duncan, Chris, Masek, Jeff, and Brown, Dennis, 1998, Minimum work, fault activity and the growth of critical wedges in fold and thrust belts: Basin Research, v. 10, p. 365–373.

Homza, T.X., 1992, A detachment fold-truncation duplex southwest of Bathtub Ridge-northeastern Brooks Range, Alaska: Fairbanks, Alaska, Unpublished M.S. thesis, University of Alaska Fairbanks, 335 p., 10 sheets.

Homza, T.X., and Wallace, W.K., 1991, Thrust-truncated detachment folds and duplex evolution southwest of Bathtub Ridge, northeastern Brooks Range, Alaska: Geological Society of America Abstracts with Programs, v. 23, no. 2, p. 35.

———1997, Detachment folds with fixed hinges and variable detachment depth, northeastern Brooks Range, Alaska, *in* Anastasio, D.J., Ersley, E.A., Fisher, D.M., and Evans, J.P., eds., Special issue, fault-related folding: Journal of Structural Geology, v. 19, nos. 3–4 , p. 337–354.

Jamison, W.R., 1987, Geometric analysis of fold development in overthrust terranes: Journal of Structural Geology, v. 9, no. 2, p. 207–219.

Jones, D.L., Silberling, N.J., Coney, P.J., and Plafker, George, 1987, Lithotectonic terrane map of Alaska (west of the 141st meridian): U.S. Geological Survey Miscellaneous Field Studies Map 1874-A, scale 1:2,500,000.

Kelley, J.S., 1990, Generalized geologic map of the Chandler Lake quadrangle, north-central Alaska: U.S. Geological Survey Miscellaneous Field Studies Map 2144-A, 19 p., 1 sheet, scale 1:250,000.

Kelley, J.S., and Brosgé, W.P., 1995, Geologic framework of a transect of the central Brooks Range; regional relations and an alternative to the Endicott Mountains allochthon: American Association of Petroleum Geologists Bulletin, v. 79, no. 8, p. 1087–1116.

Laslett, G.M., Green, P.F., Duddy, I.R., and Gleadow, A.J.W., 1987, Thermal annealing of fission tracks in apatite; 2, A quantitative analysis: Chemical Geology, Isotope Geoscience Section, v. 65, no. 1, p. 1–13.

Liu, Shumin, and Dixon, J.M., 1995, Localization of duplex thrust-ramps by buckling: analog and numerical modeling, Journal of Structural Geology: v. 17, no. 6, p. 875–886.

Mayfield, C.F., Tailleur, I.L., and Ellersieck, Inyo, 1988, Stratigraphy, structure, and palinspastic synthesis of the western Brooks Range, northwestern Alaska, *in* Gryc, George, ed., Geology and exploration of the National Petroleum Reserve in Alaska, 1974 to 1982: U.S. Geological Survey Professional Paper 1399, p. 143–186.

McClay, K.R., 1992, Glossary of thrust tectonics terms, *in* McClay, K. R., ed., Thrust Tectonics: Chapman and Hall, London, p. 419–433.

Mitra, Gautam, and Boyer, S.E., 1986, Energy balance and deformation mechanisms of duplexes, *in* Platt, J.P., Coward, M.P., Deramond, J., and Hossack, J., eds., Thrusting and deformation: Journal of Structural Geology, v. 8, no. 3–4, p. 291–304.

Mitra, Shankar, 1986, Duplex structures and imbricate thrust systems; geometry, structural position, and hydrocarbon potential: American Association of Petroleum Geologists Bulletin, v. 70, no. 9, p. 1087–1112.

———1990, Fault-propagation folds: geometry, kinematic evolution, and hydrocarbon traps: American Association of Petroleum Geologists Bulletin, v. 74, no. 6, p. 921–945.

Moore, T.E., Nilsen, T.H., and Brosgé W.P., 1989, Sedimentology of the Kanayut Conglomerate, *in* Mull, C.G., and Adams, K.E., eds., Dalton Highway, Yukon River to Prudhoe Bay, Alaska, bedrock geology of the eastern Koyukuk Basin, central Brooks Range, and east-central Arctic Slope: Fairbanks, Alaska, Division of Geological & Geophysical Surveys, Guidebook 7, v. 2, p. 219–252.

Moore, T.E., Wallace, W.K., Bird, K.J., Karl, S.M., Mull, C.G., Dillon, J.T., 1994a, Geology of northern Alaska, *in* Plafker, George, and Berg, H.C., eds., The geology of Alaska: The Geology of North America, Geological Society of America, Boulder, Colorado, v. G1, p. 49–140.

Moore, T.E., Wallace, W.K., Mull, C.G., Karl, S.M., and Bird, K.J., 1994b, Generalized geologic map and sections for northern Alaska, *in* Plafker, George, and Berg, H.C., eds., The geology of Alaska: The Geology of North America, Geological Society of America, Boulder, Colorado, v. G1, 1 sheet, scale 1:2,500,000.

Moore, T.E., Wallace, W.K., Mull, C.G., Adams, K.E., Plafker, George, & Nokleberg, W.J., 1997, Crustal implications of bedrock geology along the Trans-Alaska Crustal Transect (TACT) in the Brooks Range, northern Alaska: Journal of Geophysical Research, v. 102, no. B9, p. 20,645–20,684.

Morley, C.K., 1994, Fold-generated imbricates: examples from the Caledonides of southern Norway: Journal of Structural Geology, v. 16, no. 5, p. 619–631.

Mull, C.G., 1982, The tectonic evolution and structural style of the Brooks Range, Alaska; An illustrated summary, *in* Powers, R.B., ed., Geological Studies of the Cordilleran Thrust Belt: Rocky Mountain Association of Geologists, Denver, Colorado, v. 1, p. 1–45.

———1989, Summary of structural style and history of Brooks Range deformation, *in* Mull, C.G., and Adams, K.E., eds., Dalton Highway, Yukon River to Prudhoe Bay, Alaska; Bedrock geology of the

eastern Koyukuk basin, central Brooks Range, and eastcentral Arctic Slope: Alaska Division of Geological & Geophysical Surveys Guidebook 7, v. 1, p. 47–56.

Mull, C.G., and Adams, K.E., eds., 1989, Dalton Highway, Yukon River to Prudhoe Bay, Alaska, Bedrock Geology of the Eastern Koyukuk Basin, Central Brooks Range, and East Central Arctic Slope: Alaska Division of Geological & Geophysical Surveys, Guidebook 7, 2 vols., 327 p.

Mull, C.G., Adams, K.E., and Dillon, J.T., 1989, Stratigraphy and structure of the Doonerak fenster and Endicott Mountains allochthon, central Brooks Range, Alaska, *in* in Mull, C.G., and Adams, K.E., editors, Dalton Highway, Yukon River to Prudhoe Bay, Alaska: Bedrock Geology of the eastern Koyukuk basin, central Brooks Range, and east-central Arctic Slope: Alaska Division of Geological & Geophysical Surveys, Guidebook 7, v. 2, p. 203-217.

Mull, C.G., Glenn, R.K., and Adams, K.E., 1997, Tectonic evolution of the central Brooks Range mountain front; Evidence from the Atigun Gorge region, *in* Plafker, George, and Mooney, W.D., eds., The Trans-Alaska Crustal Transect (TACT) across Arctic Alaska: Journal of Geophysical Research, v. 102, no. B9, p. 20,749–20,772.

Mull, C.G., Moore, T.E., Harris, E.E., and Tailleur, I.L., 1994, Geologic map of the Killik River quadrangle, central Brooks Range, Alaska: U.S. Geological Survey Open-File report 94-679, 1 sheet, scale 1:125,000.

Mull, C.G., Roeder, D.H., Tailleur, I.L., Pessel, G.H., Grantz, Arthur, and May, S.D., 1987, Geologic sections and maps across Brooks Range and Arctic Slope to Beaufort Sea: Geological Society of America Map and Chart Series MC-28S, 1 sheet, scale 1:500,000.

Murphy, J.M., O'Sullivan, P.B., and Gleadow, A.J.W., 1994, Apatite fission track evidence of episodic Early Cretaceous to late Tertiary cooling and uplift, central Brooks Range, Alaska, in Thurston, D.K., and Fujita, Kazuya, eds., 1992 Proceedings International Conference on Arctic Margins: U.S. Minerals Management Service Outer Continental Shelf Study 94-0040, p. 257–262.

Naeser, C.W., 1979, Fission track dating and geologic annealing of fission tracks, *in* Jaeger, E., and Hunziker, J.C., eds., Lectures in Isotope Geology: New York, Springer-Verlag, p. 154–169

Oldow, J.S., Seidensticker, C.M., Phelps, J.C., Julian, F.E., Gottschalk, R.R., Boler, K.W., Handschy, J.W., and Ave Lallemant, H.G., 1987, Balanced cross sections through the central Brooks Range and North Slope, Arctic Alaska: Tulsa, Oklahoma, American Association of Petroleum Geologists, 19 p., scale 1:200,000.

O'Sullivan, P.B., 1996, Late Mesozoic and Cenozoic thermotectonic evolution of the Colville Basin, North Slope, Alaska, *in* Johnsson, M.J., and Howell, D.G., eds., Thermal evolution of sedimentary basins in Alaska: U.S. Geological Survey Bulletin 2142, p. 45–79.

O'Sullivan, P.B., and Parrish, R.R., 1995, The importance of apatite composition and single-grain ages when interpreting fission track data from plutonic rocks; a case study from the Coast Ranges, British Columbia: Earth and Planetary Science Letters, v. 132, p. 213–224.

O'Sullivan, P.B., Kohn, B.P., and Mitchell, M.M., 1998a, Phanerozoic reactivation along a fundamental Proterozoic crustal fault, the Darling River Lineament, Australia: constraints from apatite fission track thermochronology: Earth and Planetary Science Letters, v. 164, no. 3–4, p. 451–465.

O'Sullivan, P.B., Moore, T.E., and Murphy, J.M., 1998b, Tertiary uplift of the Mt. Doonerak antiform, central Brooks Range, Alaska; apatite fission-track evidence from the Trans-Alaska Crustal Transect, *in* Oldow, J.S., and Avé Lallemant, H.G., eds., Architecture of the central Brooks Range fold and thrust belt, Arctic Alaska: Geological Society of America Special Paper 324, p. 179–193.

O'Sullivan, P.B., Murphy, J.M., and Blythe, A.E., 1997, Late Mesozoic and Cenozoic thermotectonic evolution of the central Brooks Range and adjacent North Slope foreland basin, Alaska; Including fission-track results from the Trans-Alaska Crustal Transect (TACT), in Plafker, George, and Mooney, W.D., eds., The Trans-Alaska Crustal Transect (TACT) across Arctic Alaska,: Journal of Geophysical Research, v. 102, no. B9, p. 20,821–20,845.

Platt, J.P., 1986, Dynamics of orogenic wedges and the uplift of high-pressure metamorphic rocks: Geological Society of America Bulletin, v. 97, p. 1037–1053.

Poblet, Josep, and McClay, Ken, 1996, Geometry and kinematics of single-layer detachment folds: American Association of Petroleum Geologists Bulletin, v. 80, no. 7, p. 1085–1109.

Porter, S.C., 1966, Stratigraphy and deformation of Paleozoic section at Anaktuvuk Pass, central Brooks Range, Alaska: American Association of Petroleum Geologists Bulletin, v. 50, no. 5, p. 952–980.

Silberling, N.J., Jones, D.L., Monger, J.W.H., Coney, P.J., Berg, H.C., and Plafker, George, 1994, Lithotectonic terrane map of Alaska and adjacent parts of Canada, *in* Plafker, George, and Berg, H.C., eds., The geology of Alaska, The Geology of North America: Boulder, Colorado, Geological Society of America, v. G1, 1 sheet, scale 1:2,500,000.

Suppe, John, 1983, Geometry and kinematics of fault-bend folding: American Journal of Science, v. 283, no. 7, p. 684–721.

Suppe, John, and Medwedeff, D.A., 1990, Geometry and kinematics of fault-propagation folding, *in* Jordan, Peter, Noack, Thomas, Schmid, Stefan, and Bernoulli, Daniel, eds., The Hans Laubscher volume: Eclogae Geologicae Helvetiae, v. 83, no. 3, p. 409–454.

Wallace, W.K., 1993, Detachment folds and a passive-roof duplex: Examples from the northeastern Brooks Range, Alaska, *in* Solie, D.N., and Tannian, Fran, eds., Short Notes on Alaskan Geology 1993: Alaska Division of Geological & Geophysical Surveys Professional Report 113, p. 81–99.

Wallace, W.K., and Homza, T.X., 1996, Thrust-truncated detachment folds and their distinction from fault-propagation folds; Examples from the Brooks Range: Geological Society of America Abstracts with programs, v. 28, no. 7, p. A-239.

Wallace, W.K., and Homza, T.X., 1997, Differences between fault-propagation folds and detachment folds and their subsurface implications: Annual Meeting Abstracts, American Association of Petroleum Geologists and Society of Economic Paleontologists and Mineralogists, v. 6, p. A122.

Wallace, W.K., Moore, T.E., and Plafker, George, 1997, Multistory duplexes with forward dipping roofs, north central Brooks Range Alaska, in Plafker, George, and Mooney, W.D., eds., The Trans-Alaska Crustal Transect (TACT) across Arctic Alaska: Journal of Geophysical Research, v. 102, no. B9, p. 20,773–20,796.

BOREHOLE BREAKOUTS AND IMPLICATIONS FOR REGIONAL *IN SITU* STRESS PATTERNS OF THE NORTHEASTERN NORTH SLOPE, ALASKA

Catherine L. Hanks,[1] Melissa Parker,[1] and Emily B. Jemison[1]

ABSTRACT

Significant variations exist in the orientation of present-day horizontal *in situ* stresses in the North Slope of northeastern Alaska. *In situ* horizontal stress orientations based on borehole breakouts in 30 wells north and west of the Arctic National Wildlife Refuge (ANWR) exhibit two different patterns. Maximum horizontal stress orientations (S_{hmax}) generally are perpendicular to the deformation front in wells immediately north of the northeastern Brooks Range fold-and-thrust belt. S_{hmax} orientations range from north-northeast trending offshore of northern ANWR to northwest trending near the Dalton Highway. *In situ* stresses in this region are probably due to active compression related to the fold-and-thrust belt. In contrast, borehole breakout orientations in wells on or near the Barrow arch that are more distal to the thrust front are more variable and commonly have bimodal orientations. These data can be interpreted to represent S_{hmax} orientations that are northwest and northeast trending. These orientations may reflect *in situ* stresses resulting from either extension along the northern Alaska continental margin, complex interactions between extension along the Barrow arch and stresses generated by thrusting from the south, or local stress perturbations on the Barrow arch associated with complex local fault patterns.

INTRODUCTION

In situ stresses can play a significant role in hydrocarbon exploration and production. Low differential stresses in the foreland basin of a fold-and-thrust belt can be an important factor in developing and maintaining an open fracture network in rocks forward of the growing thrust belt (for example, Lorenz and others, 1991). These fractures in turn can be influential in controlling fluid movement through the foreland basin and can enhance reservoir characteristics in potential reservoir rocks. *In situ* stresses also influence fluid flow in producing reservoirs by controlling the direction of fracture and fault permeability. Determining the direction of the *in situ* stress can therefore provide a predictive tool for evaluating both the fluid movement within a basin and the development of fracture porosity and permeability in potential and producing reservoir rocks, as well as aid in the development of production strategies.

The importance of understanding the distribution of *in situ* stresses on the North Slope of Alaska has been highlighted by recent work on the Carboniferous reservoir interval of the Lisburne field of the North Slope of Alaska, which suggests that production from the field is controlled in part by fractures held open by present-day *in situ* horizontal stresses (Hanks and others, 1997). Production strategies therefore would be greatly aided by a better understanding of the *in situ* stress regime of the North Slope. However, the present-day regional *in situ* stress distribution and orientation in northern Alaska is poorly constrained and/or documented. The objective of this study is to: (1) document the regional distribution and orientation of present-day *in situ* horizontal stresses in the subsurface of northeastern Alaska; and (2) develop a predictive model or models that might explain the observed regional stress regime.

MEASURING *IN SITU* STRESSES IN SEDIMENTARY BASINS

A variety of methods exist to measure the orientation and magnitude of *in situ* stresses, with varying degrees of reliability. The technique used often is governed by what data are available. The two most common and widely used techniques to measure the orientation of *in situ* stresses are borehole breakouts and earthquake focal mechanisms (for example, Zoback, 1992; Bell and others, 1995), with the former most widely used in sedimentary basins. Borehole breakouts were first used as an indicator of *in situ* horizontal stress by Bell and Gough (1979) and Hottman and others (1979), and have subsequently been used in both local and regional stress studies around the world (for example, Zoback and Zoback, 1991). Breakouts are intervals in wells that have undergone preferential caving or spalling due to differential horizontal stress, such that the diameter of the borehole becomes elongated parallel to the least horizontal stress. The shape and orientation of the borehole elongation can be measured with a variety of downhole tools, the most common being the four-arm dipmeter tool. These measurements are routinely done on most exploratory wells; consequently data for measuring *in situ* horizontal

[1]Department of Geology & Geophysics, University of Alaska Fairbanks, P.O. Box 755780, Fairbanks, Alaska 99775-5780.
Email for Catherine Hanks: chanks@dino.gi.alaska.edu

stress are widely available. The technique for deriving the orientation of *in situ* stress orientations from borehole breakouts is summarized in several publications (for example, Bell and Gough, 1979; Bell, 1990; and Bell and others, 1995).

REGIONAL SETTING

The Brooks Range is the northernmost part of the Rocky Mountain fold-and-thrust belt (fig. 1). The majority of shortening in the fold-and-thrust belt occurred in Late Jurassic to Early Cretaceous time when a wide, south-facing late Paleozoic to early Mesozoic passive continental margin collapsed in response to the collision of an intraoceanic arc (Mayfield and others, 1988; Moore and others, 1994). The Colville basin formed in advance of, and was filled with sediment shed from, the growing fold-and-thrust belt (Mull, 1985; Molenaar and others, 1987; Bird and Molenaar, 1987).

Shortly after the main phase of compressional collapse of the continental margin, rifting led to formation of the oceanic Canada basin to the north (present geographic coordinates) in Early Cretaceous time (Grantz and May, 1983; Moore and others, 1994). This continental breakup resulted in separation of the Brooks Range and North Slope from the continent to the north and formation of the present northern continental margin of Alaska. This new continental margin is at an oblique angle to the Brooks Range orogen (fig. 1).

Subsequent shortening has progressed to different extents along the strike of the range and its foreland basin, and consequently has involved different parts of both the earlier south-facing passive continental margin and the new north-facing continental margin. In the western Brooks Range, the thrust front is far south of the present northern continental margin, the Colville basin is wide and, to the north, undeformed by thrust deformation; in the northeastern Brooks Range, the thrust front has overridden the later-rifted continental margin, resulting in a very narrow and deformed foreland basin.

STATE OF KNOWLEDGE REGARDING *IN SITU* STRESSES IN NORTHERN ALASKA

Although the majority of shortening associated with the Brooks Range is Mesozoic in age, the pattern of active seismicity in northern Alaska and northwestern Canada indicates that the northeastern part of the Brooks Range and Colville basin is seismically active (fig. 2; Basham and others, 1977; Biswas and Gedney, 1979). This contrasts with the remainder of northern Alaska, which is seismically quiet (Estabrook and others, 1988). Active seismicity outlines the northeastern Brooks Range in Alaska and Canada, and defines an arcuate thrust front that connects the older part of the Brooks Range to the west and the Canadian Cordillera to the south (Moore and others, 1985). The nature of the boundaries of this deforming belt remain uncertain; only two focal mechanisms are available (Estabrook and others, 1988; Fujita and others, 1983, 1990) from the central part of the Beaufort Sea, both suggesting strike-slip mechanisms. However, the orientations of the faults on which these earthquakes occurred are not known. The location of this seismically active zone corresponds to the limit of folded and thrust-faulted Colville basin sediments observed in the subsurface (fig. 1). The young and probably active nature of this thrust front is also supported by young uplift ages in the range front of the northeastern Brooks Range and in related parts of the central Brooks Range (for example, O'Sullivan and others, 1993 and 1997).

The driving mechanism for this deformation is unclear. Directional indicators of the regional *in situ* stress pattern, such as borehole breakouts and earthquake focal mechanisms, have been summarized for all of Alaska by Estabrook and Jacob (1991). The overall pattern is one of north-south oriented compressive stresses in the southern part of Alaska, orthogonal to the convergent Pacific/North American plate boundary. The orientation of the maximum horizontal *in situ* stress diverges to the north, becoming progressively more east-west towards northwestern Alaska, and rotating to a more northeasterly orientation in northwestern Canada. Estabrook and Jacob (1991) attributed this fanning of the *in situ* stress regime in northern Alaska to the 'indentor effect' caused by collision of the Yakutat block with southern Alaska.

RESULTS OF THIS STUDY

PROCEDURE

The four-arm dipmeter tool is one of the oldest and most widely used downhole tools for measuring the orientation of planar features in the rocks as well as the shape and orientation of the borehole. The tool consists of electrodes located on four orthogonal pads pressed against the borehole wall by hydraulically activated caliper arms. The electrodes measure the resistivity of the rock adjacent to the borehole as the tool is drawn up the hole. Besides the resistivity traces themselves, the uncomputed log shows the orientation of one of the pads relative to true north and the amount of extension or contraction of the pads as the tool rotates up the hole. This provides a means of locating and measuring the orientation of a borehole elongation. If a borehole elongation is encountered as the tool rotates up the hole, one set of pads will extend into the wider part of the borehole, causing the tool to stop rotating as it is drawn up the hole.

Wide zones in the borehole can be due to a variety of different factors. The four most common borehole

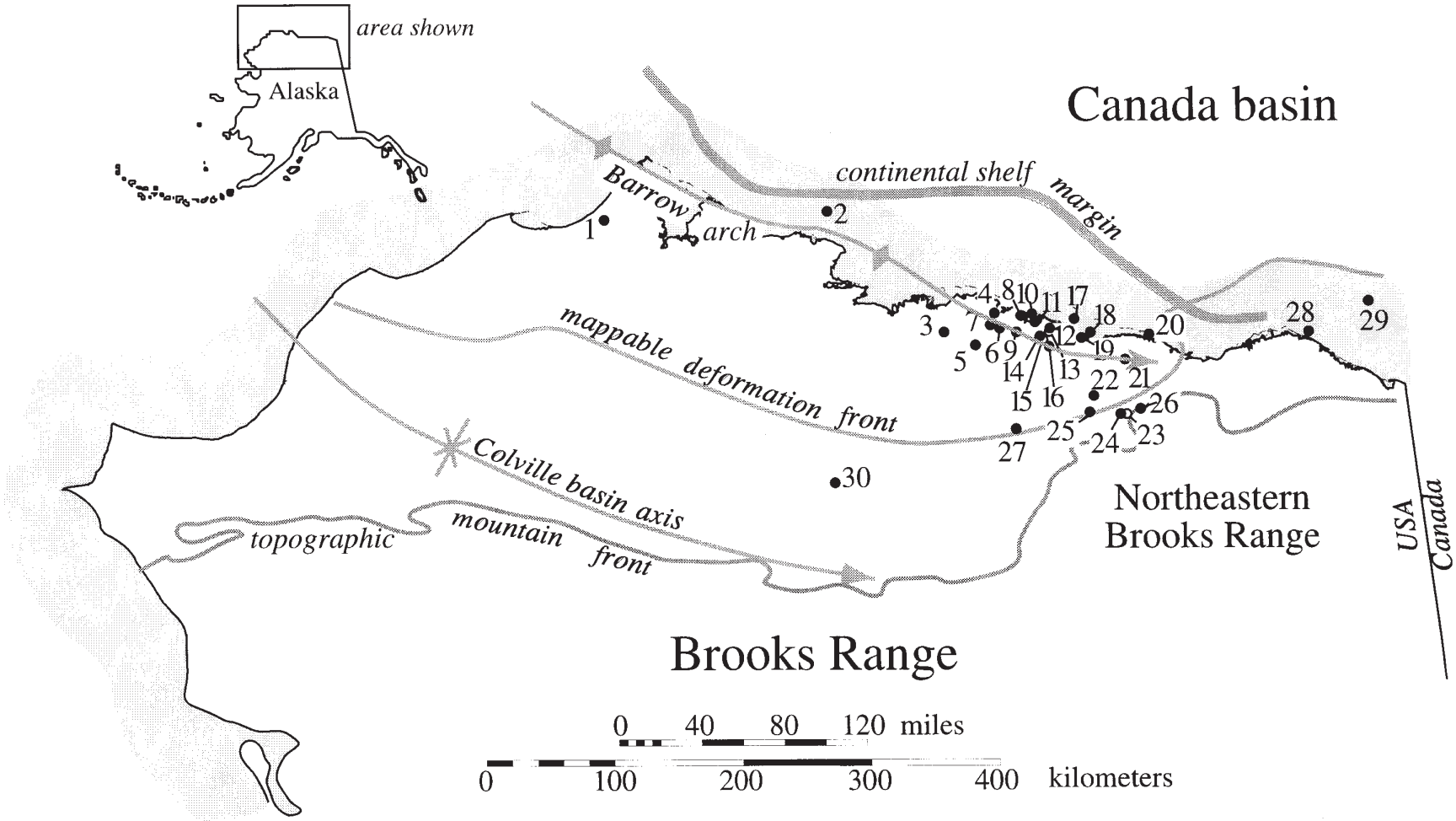

Figure 1. *Regional map of northern Alaska showing major structural features and locations of wells used in this study. Wells are identified in table 1.*

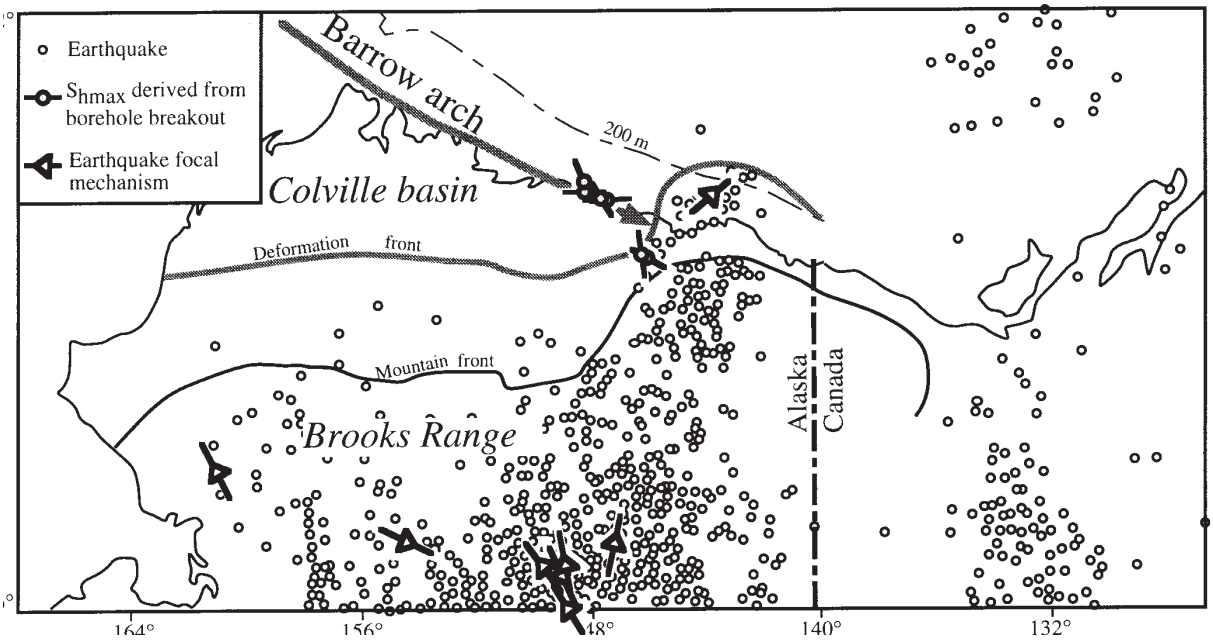

Figure 2. *Map showing the regional stress indicators and pattern of active seismicity of northern Alaska (1968–1978) and northwestern Canada (1962–1974). This map also illustrates the paucity of stress orientation data from northern Alaska. Regional stress indicators in northeastern Alaska consist of two earthquake focal mechanisms and breakouts in ~12 wells, with the majority of the wells clustered in one area on the Barrow arch. There is no information on the orientation of* in situ *stresses from the central or western part of the Colville basin or North Slope. Modified from Basham and others (1977), Biswas and Gedney (1979), and Estabrook and Jacob (1991).*

geometries include in-gauge hole, breakout, washout, and key seating (fig. 3; Plumb and Hickman, 1985; Bell and others, 1995). In order for a wide zone to be identified as a 'breakout,' it must meet certain criteria, including:

- the tool rotation stops in the zone of the breakout;
- the difference between the two sets of pads is greater than 0.6 cm (0.24 inches);
- the smaller of the two caliper readings is close to the bit size, or if greater than the bit size, should exhibit less variation than the larger caliper reading;
- the vertical extent of the zone of borehole elongation is greater than 30 cm (11.8 inches); and
- the direction of the zone of elongation should not coincide with the azimuth of the high side of the borehole when the hole deviates from vertical (that is, keyseating or breakouts due to vertical stresses on a deviated hole [John Lorenz, written commun., 1999]).

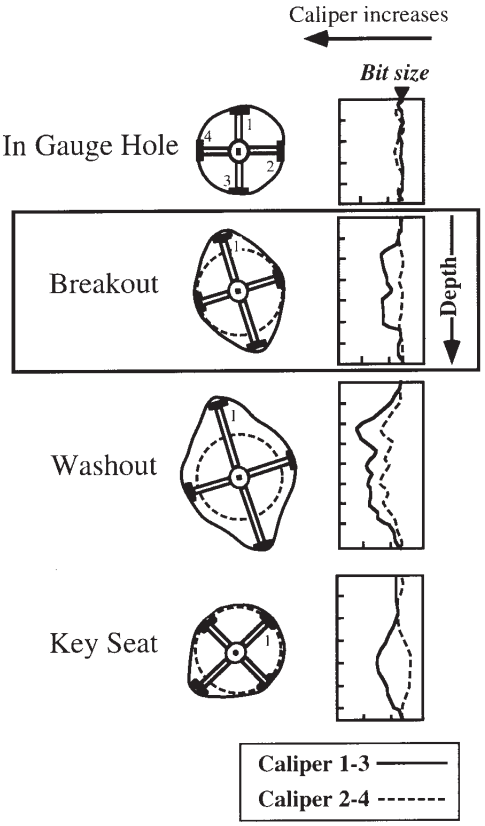

Figure 3 (right). *Four common borehole geometries and their corresponding caliper separations. Modified from Plumb and Hickman (1985).*

In this study, determination that conditions 1, 2, 3, and 4 were met was by visual inspection while analyzing the well logs. Condition 3 guarantees that a washout will not be mistaken for a breakout. Condition 5 precludes either a keyseat or a breakout due to vertical stresses from being mistaken as a breakout due to *in situ* horizontal stresses, and was assessed both by inspection and by plotting the orientation of the breakouts versus the trajectory in individual wells. If a borehole elongation was parallel (±10°) to the azimuth of the high side of the borehole, it was discarded. Wells with breakouts then were classified using the World Stress Map (WSM) quality classification criteria (table 2; Zoback, 1992).

RESULTS

Four-arm uncomputed dipmeter logs from over 60 wells were examined for borehole breakouts. Only 30 wells had measurable breakouts (fig. 1, table 1). Of these, 16 wells had a sufficient number and consistency of breakouts that the wells could be classified as A, B, or C quality according to the WSM criteria (table 2). The breakout orientation in the A, B, and C quality wells could

Table 1. *Wells used in this study. Table includes the number of breakouts observed in each well, the total length of breakouts, the World Stress Map (WSM) classification (table 2) and whether the breakout distribution was bimodal or unimodal.*

Map no.	Well Name	No. of Breakouts	Total Breakout Length(m)	Orientation	St. Dev	WSM Class
1	ARCO Brontosaurus	1	9	2	0	E
2	ARCO Ocs 0267(Fireweed) 1	1	7	30	0	E
3	ARCO W Sak 25590 15	1	41	63	40.9	D
4	ARCO Beechy Pt 1	9	78	173	79	C
5	ARCO Kru W Sak 26	1	88	62.5	0	D
6	ARCO Se Eileen State 1	1	16	153	0	D
7	ARCO Highland State	1	49	153	0	D
8	ARCO Prudhoe Bay Unit Term A	9	571	336	23.3	B
9	BP Put River St 1	2	170	151	11.2	D
10	ARCO Gull Island State 1	8	205	325 47	109.9 (BI)	B
11	ARCO E Bay St 1	3	119	41.7	9.2	D
12	ARCO Delta St 2	3	170	320	18.5	D
13	ARCO Delta St 1	3	88	173	16.0	D
14	ARCO Lake St 1	5	172	42	61.7	C
15	BP Sag Delta 31-10-16	2	71	134	0	D
16	Mobil Kadler 15-9-16	5	108	146	37.7	C
17	Chevron Karluk 1	2	137	78.7	8.0	D
18	ARCO West Mikkelsen Unit 2	6	164	325 40	233.3 (BI)	B
19	ARCO W Mikkelsen St 1	8	491	62 160	39.7 (BI)	B
20	Exxon Alaska St A 1	6	646	69	18.7	B
21	Unocal E De K Leffingwell 1	9	900	177	24.0	B
22	Texaco West Kavik 1	5	683	152	7.1	C
23	Pan Am Kavik 1	1	58	73	0	D
24	ARCO Kavik Unit 2	9	242	313	65.1	B
25	ARCO Gyr 1	7	188	57 325	167.1 (BI)	B
26	Exxon Canning River Unit B 1	8	326	117	5.6	B
27	ARCO Nora Federal 1	11	798	133	4.8	A
28	Tenneco Ocs 0943(Aurora) 1	13	345	181	8.9	A
29	Amoco Ocs 0917(Belcher) 1	2	50	83	2.5	D
30	ARCO Big Bend 1	8	281	31	82.9	B

Table 2. *World Stress Map (WSM) classification criteria for borehole breakouts used to rank the quality of data in this study. From Zoback (1992).*

A	≥10 distinct breakouts in a single well with s.d. ≤12° and/or combined breakout length >300 m
	Average of breakouts in ≥2 adjacent wells with combined length >300 m and s.d. ≤12°
B	≥6 distinct breakout zones in a single well with s.d. ≤20° and/or combined length >100 m
C	≥4 distinct breakouts with s.d. <25° and/or combined length >30 m
D	<4 consistently oriented breakouts or <30 m combined length in a single well
	Breakouts in a single well with s.d. ≥25°
E	Wells in which no reliable breakouts detected.
	Extreme scatter of orientations, no significant mean determined (>40°)

then be used with some degree of confidence to evaluate the *in situ* stress orientation at that location.

Rose diagrams of the breakout orientations in these 16 wells are shown in figure 4. The orientation of the inferred maximum *in situ* horizontal stress (S_{hmax}) direction (corresponding to the perpendicular to the orientation of the long axis of the breakout) is also illustrated on the regional map in figure 5. The orientation of the short axes of breakouts in each well versus the depth of each breakout and the stratigraphic unit (where known) is shown in figure 6.

DISCUSSION

Borehole breakout data acquired during this study suggest that there are at least two local *in situ* stress patterns in the eastern part of the North Slope of Alaska. S_{hmax} in wells adjacent to the mappable deformation front is generally oriented north-northwest, perpendicular to the thrust front. In contrast, S_{hmax} in wells along the Barrow arch have both north-northwest and northeast orientations, sometimes in one well. The following section will discuss these two stress patterns in more detail.

There is no clear relationship between breakouts and gross stratigraphic interval (fig. 6). Breakouts occur in both the Cretaceous and younger clastic Brookian sequence and the Mississippian to Lower Cretaceous mixed clastic and carbonate rocks of the Ellesmerian sequence. There does appear to be a relationship between breakouts and depth, however. Breakout orientation becomes significantly more consistent at depths below 4,000 ft (subsea) as seen in wells 24, 25, 8, and 20 (fig. 6), and is probably a function of the magnitude of S_{hmax} versus the amount of overburden. This suggests that S_{hmax} may not be reliably derived from shallow (<4,000 ft deep) breakouts.

THRUST FRONT WELLS

In wells drilled adjacent to the thrust front, S_{hmax} is generally oriented north-northwest, perpendicular to the active thrust front of the northeastern Brooks Range (fig. 5). Wells that exhibit this stress pattern include nos. 22, 24, 26, 27, 28 (table 1, figs. 1, 3, 4, 6). Out of the nine wells examined in this study that were located near the thrust front, seven (78 percent) were ranked as having either A, B, or C quality breakouts (table 1). The only wells in the study that were ranked as 'A' quality, nos. 27 (ARCO Nora Federal #1) and 28 (Tenneco Aurora #1) both fall into this group. Breakout orientations in the thrust front wells are consistent regardless of stratigraphic interval and at all depths below ~4,000 ft (subsea). This all implies (although doesn't necessarily prove) that the *in situ* stress signal in this area is fairly strong. The close correspondence between the direction of maximum *in situ* stresses and the active thrust front suggests that the stress pattern in this part of northeastern Alaska is strongly influenced by the thrust front.

Two wells west of the main cluster of range front wells, nos. 25 (ARCO Gyr #1) and 30 (ARCO Big Bend #1), are immediately adjacent to the thrust front and have strong breakout signals, but exhibit anomalous breakout directions. The S_{hmax} orientation inferred from breakout orientations in ARCO Big Bend #1 trends northeast. This well is located where the northern limit of active seismicity in the northeastern Brooks Range trends southwest into the central Brooks Range (fig. 2). The northeast trend of S_{hmax} in this region may reflect a change in the *in situ* stress regime from north-northwest-oriented compression at the deformation front of the northeastern Brooks Range to a more transpressive regime at the deformation front of the central Brooks Range.

The second anomalous range-front well, ARCO Gyr #1, shows a bimodal breakout distribution (fig. 4). This breakout distribution may reflect low overall *in situ* stress magnitudes in the vicinity of that well and/or the influence of local structures. However, if the breakouts from depths <4,000 ft (fig. 6) in this well are assumed to be anomalous and eliminated, the inferred S_{hmax} direction becomes unimodal and in the same general direction as ARCO Big Bend #1. This would imply that the change in orientation of S_{hmax} seen in ARCO Big Bend #1 may be regional in scope.

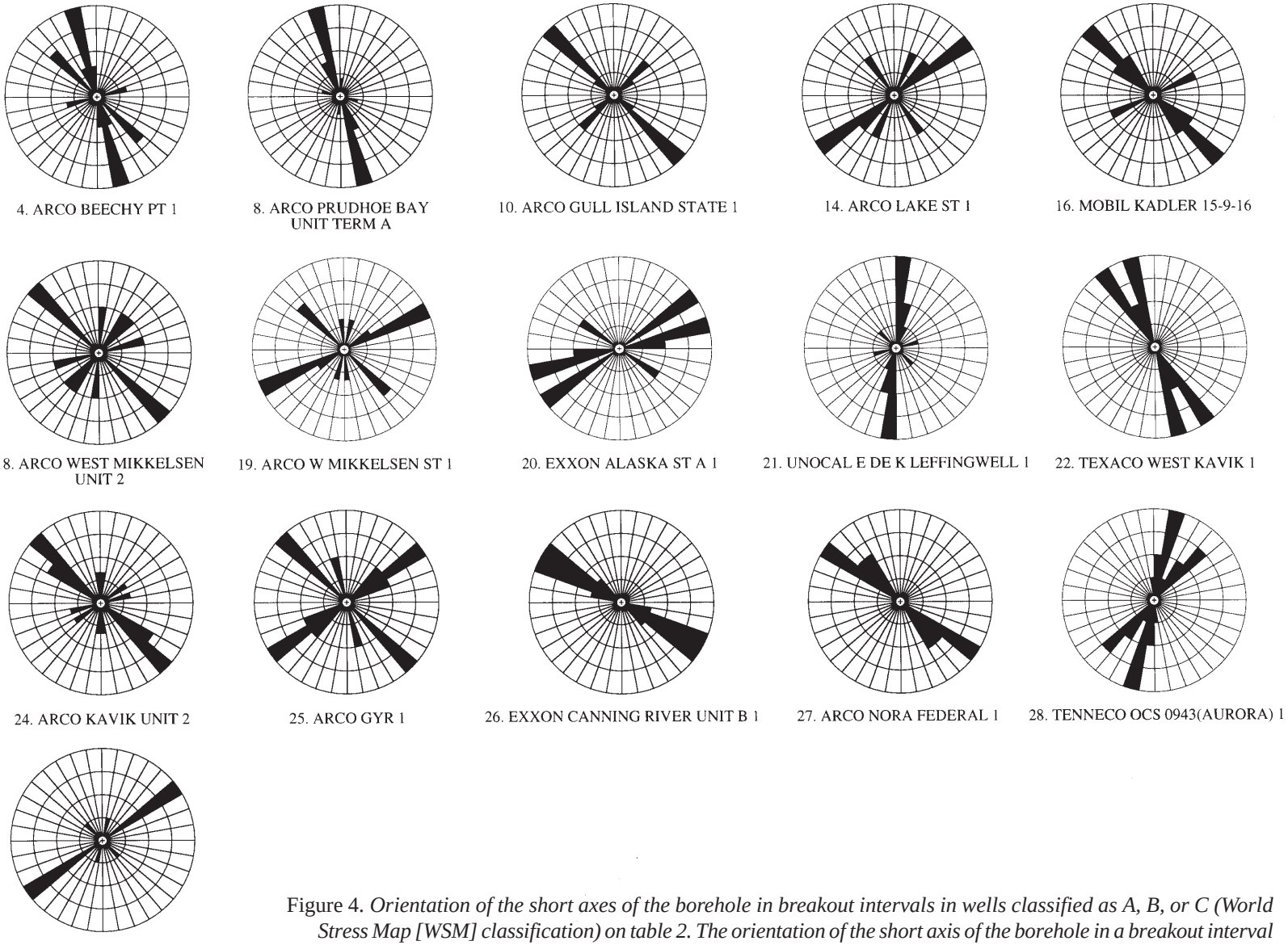

Figure 4. *Orientation of the short axes of the borehole in breakout intervals in wells classified as A, B, or C (World Stress Map [WSM] classification) on table 2. The orientation of the short axis of the borehole in a breakout interval can be interpreted to be parallel to the maximum* in situ *horizontal stress (S_{hmax}).*

BARROW ARCH WELLS

A significantly different stress pattern is localized on and adjacent to the eastern end of the Barrow arch (figs. 4 and 5). Of the 21 wells examined along the Barrow arch in this study, only nine (43 percent) are ranked as A, B, or C class (table 1). The relatively low percentage of wells with a strong to moderately strong breakout signal could be interpreted to reflect a relatively low *in situ* horizontal stress signal.

The breakout pattern seen in this area is exemplified by wells 14, 18, 19, and 20 (figs. 4, 5, and 6). At first glance, S_{hmax} orientations in these wells show a bimodal distribution. However, one well (#20, Exxon Alaska State 1) becomes unimodal with depth (albeit still an anomalous orientation), and a second (#14, ARCO Lake State 1) has few breakouts below 5,000 ft, leaving only two wells (16 and 19) with true bimodal breakout distributions.

Other wells located nearby along the axis of the Barrow arch, including nos. 4, 8, 10, 16, and possibly 21, are unimodal. Most, but not all, have breakout orientations similar to those seen in the deformation front wells further south (fig. 4).

This mixing of bimodal and unimodal breakout patterns in wells along the Barrow arch is not typical of passive margins, and could be interpreted in a variety of ways:

- Faults could be influencing the *in situ* stress patterns in nearby wells (for example, Mount and Suppe, 1987; Evans, 1989; Castillo and Zoback, 1994), causing permutations in a regime where the overall horizontal maximum stress is oriented north-northwest;
- The distance from the active thrust front may have resulted in a lower value of S_{hmax}, causing the maximum and minimum *in situ* stresses in this area to be close to one another in value. This could result in borehole breakouts parallel to both directions (for example, Castillo and Zoback, 1994), both in individual wells, and between nearby wells;
- The Barrow arch could represent a totally different, possibly extensional, stress regime than the compressional stress regime further to the south adjacent to the thrust front. In an extensional regime the maximum stress is vertical, and the minimum and intermediate stresses are both horizontal, leading to a situation in which the horizontal stresses could be close in value and breakouts could occur in both orientations; and
- The pattern of *in situ* stresses seen on the Barrow arch is a result of compressive stresses set up by the thrust front interacting with the basement high.

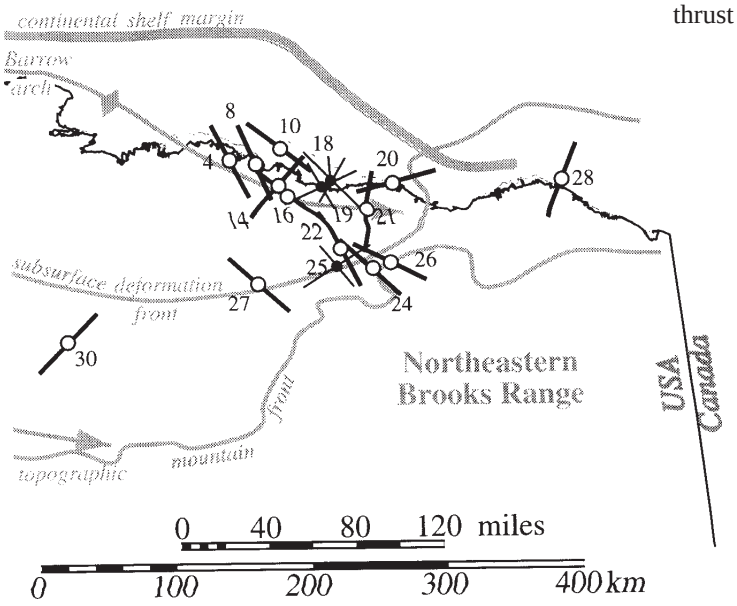

Figure 5 (above). *Enlarged eastern portion of northern Alaska map shown in figure 1. This map of northeastern Alaska shows orientations of S_{hmax} as interpreted from the borehole breakout data in wells classified as A, B, or C (fig. 3; table 1). S_{hmax} direction in wells with a single consistent breakout orientation is shown in heavy lines; thin black lines indicate the orientation of S_{hmax} in wells with a consistent bimodal breakout distribution. Wells are numbered and identified as in table 1.*

Figure 6 (right). *The orientation of the short dimension of breakouts in each well versus the depth of each breakout and the stratigraphic unit (where known). S_{hmax} is inferred to be parallel to the short dimension of the breakout. Brookian sequence rocks consist of Lower Cretaceous and younger clastic rocks; Ellesmerian sequence rocks consist of Mississippian through Jurassic clastic and carbonate rocks. Note that limited vertical distribution of breakouts in some wells is probably due to limited data availability. Stratigraphic information was not available for all wells.*

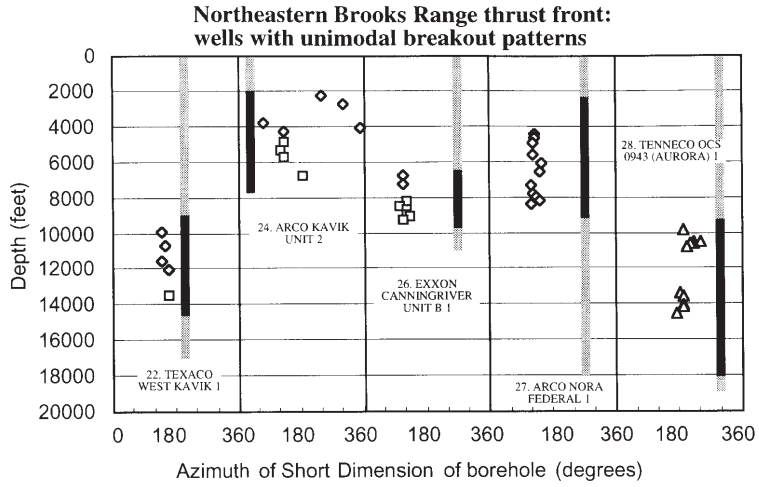

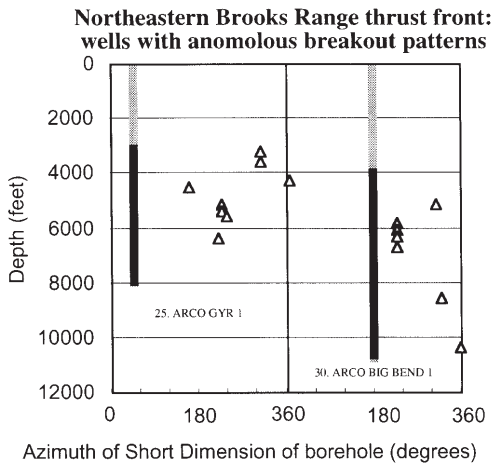

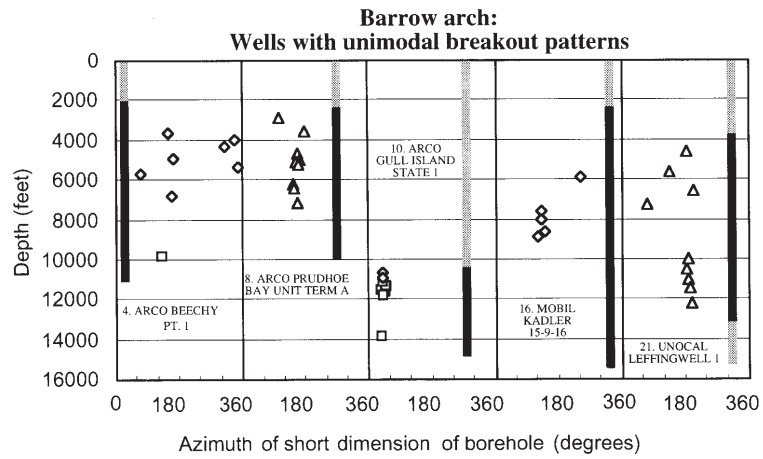

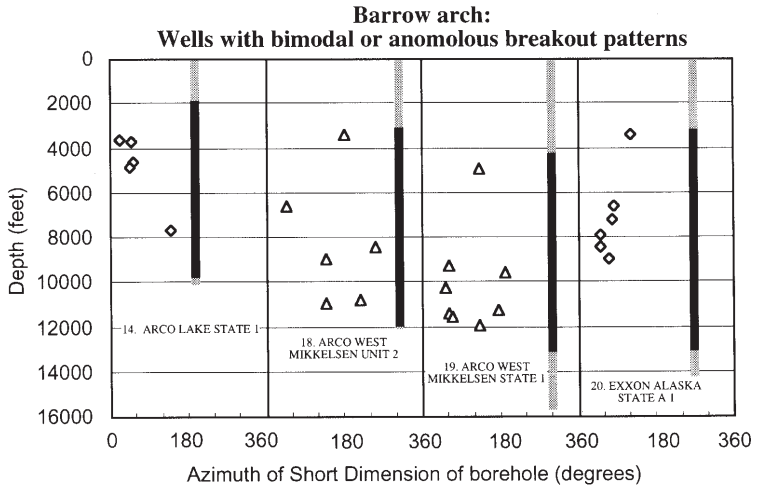

◇ BROOKIAN SEQUENCE ROCKS
△ STRATIGRAPHIC DATA UNAVAILABLE
▒ DRILLED INTERVAL
□ ELLESMERIAN SEQUENCE ROCKS
▬ LOG DATA AVAILABLE IN THIS STUDY

CONCLUSIONS

Borehole breakouts in wells from the eastern North Slope of Alaska can be interpreted to reflect the present-day *in situ* horizontal stress regime of northeastern Alaska. Borehole breakouts in this region occur throughout the Late Paleozoic and younger section. Breakout orientations are most consistent, however, at depths >4,000 ft (subsea).

There are two main patterns in the orientation of present-day S_{hmax} in the subsurface of northeastern Alaska. S_{hmax} orientations generally are perpendicular to the deformation front in wells immediately north of the northeastern Brooks Range fold-and-thrust belt, suggesting that S_{hmax} in this region is probably due to active compression related to the fold-and-thrust belt. In contrast, wells on or near the Barrow arch are more distal to the thrust front. Inferred S_{hmax} orientations in this region are more variable, sometimes bimodal, in distribution, and generally are northwest and northeast trending.

The variable orientations in S_{hmax} along the Barrow arch may be due to either (1) extension along the northern Alaska continental margin, (2) complex interactions between extension along the Barrow arch and stresses generated by thrusting from the south, (3) local stress perturbations on the Barrow arch associated with complex local fault patterns, or (4) a combination of all four factors.

ACKNOWLEDGMENTS

We would like to thank the National Science Foundation for their support of the Geophysical Institute Summer Intern Program, which provided support for M. Parker and E. Jemison. Logs were provided by ARCO Alaska, Inc., BP Exploration, and Chevron. Additional support was provided by industry sponsors of the Tectonics and Sedimentation Research Group, including ARCO Alaska, Inc., BP Exploration, Chevron, Phillips, Petrofina, and Union Texas. We also wish to thank the reviewers who kindly provided their comments on this paper, including Wes Wallace, John Lorenz, and Richard Fox.

REFERENCES

Basham, P.W., Forsyth, D.A., and Wetmiller, R.J., 1977, The seismicity of northern Canada: Canadian Journal of Earth Sciences, v. 14, no. 7, p. 1,646–1,667.

Bell, J.S., 1990, Investigating stress regimes in sedimentary basins using information from oil industry wireline logs and drilling records, *in* Hurst, A. Lovell, M.A., and Morton, A.C., eds., Geological applications of wireline logs: Geological Society Special Publications, v. 48, p. 305–325.

Bell, J.S., and Gough, D.I., 1979, Northeast-southwest compressive stress in Alberta: Evidence from oil wells: Earth and Planetary Science Letters, v. 45, no. 2, p. 475–482.

Bell, J.S., Lorenz, J.C., Aguilera, R., and McLellan, P.J., 1995, Fractured reservoirs—Their recognition, evaluation and production; course notes: Canadian Society of Petroleum Geologists & Canadian Well Logging Society.

Bird, K.J., and Molenaar, C.M., 1987, Stratigraphy: *in* Bird, K.J., and Magoon, L.B., eds., Petroleum geology of the northern part of the Arctic National Wildlife Refuge, northeastern Alaska: U.S. Geological Survey Bulletin 1778, p. 37–59.

Biswas, N.N., and Gedney, L., 1979, Seismotectonic studies of northern and western Alaska: National Oceanic and Atmospheric Administration Report, 50 p.

Castillo, D.A., and Zoback, M.D., 1994, Systematic variations in stress state in the southern San Joaquin Valley; inferences based on well-bore data and contemporary seismicity: American Association of Petroleum Geologists Bulletin, v. 78, no. 8, p. 1,257–1,275.

Estabrook, C.H., and Jacob, K.H., 1991, Stress indicators in Alaska, *in* Slemmons, D.B., Engdahl, E.R., Zoback, M.D., and Blackwell, D.D., eds., Neotectonics of North America; The Geology of North America, Decade Map Vol. 1: Boulder, Colorado, Geological Society of America, p. 387–399.

Estabrook, C.H., Stone, D.B., and Davies, J.N., 1988, Seismotectonics of northern Alaska: Journal of Geophysical Research, v. 93, no. B10, p. 12,026–12,040.

Evans, K.F., 1989, Appalachian stress study 3, Regional scale stress variations and their relation to structure and contemporary tectonics: Journal of Geophysical Research, v. 94, no. 12B, p. 17,619–17,645.

Fujita, Kazuya, Cook, D.B., and Coley, M.J., 1983, Tectonics of the western Beaufort and Chukchi Seas: American Geophysical Union, 1983 spring meeting, EOS Transactions, American Geophysical Union, v. 64, no. 18, p. 263.

Fujita, Kazuya, Cook, D.B., Hasegawa, H.S., Forsyth, David, and Wetmiller, R.J., 1990, Seismicity and focal mechanisms of the Arctic region and the North American plate boundary in Asia, *in* Grantz, Arthur, Johnson, L., and Sweeney, J.F., eds., The Arctic Ocean region, The Geology of North America, v. L, p. 79–100.

Grantz, Arthur, and May, S.D., 1983, Rifting history and structural development of the continental margin north of Alaska, *in* Watkins, J.S., and Drake, C.L., eds., Studies in continental margin geology: American Association of Petroleum Geologists Memoir 34, p. 77–100.

Hanks, C.L., Lorenz, John, Teufel, L.W., and Krumhardt, A.P., 1997, Lithologic and structural controls on natural fracture distribution and behavior within the Lisburne Group, northeastern Brooks Range and North Slope subsurface, Alaska: American Association of Petroleum Geologists Bulletin, v. 81, no. 10, p. 1,700–1,720.

Hottman, C.E., Smith, J.H., and Purcell, W.R., 1979, Relationship among earth stresses, pore pressure and drilling problems, offshore Gulf of Alaska: Journal of Petroleum Technology, v. 31, no. 11, p. 1,477–1,484.

Lorenz, J.C., Teufel, L.W., and Warpinski, N.R., 1991, Regional fractures 1: A mechanism for the formation of regional fractures at depth in flay-lying reservoirs: American Association of Petroleum Geologists Bulletin, v. 75, no. 11, p. 1,714–1,737.

Mayfield, C.F., Tailleur, I.L., and Ellersieck, Inyo, 1988, Stratigraphy, structure, and palinspastic synthesis of the western Brooks Range, northwestern Alaska, *in* Gryc, George ed., Geology and exploration of the National Petroleum Reserve in Alaska, 1974 to 1982: U.S. Geological Survey Professional Paper 1399, p. 143–186.

Molenaar, C.M., Bird, K.J., and Kirk, A.R., 1987, Cretaceous and Tertiary stratigraphy of northeastern Alaska, *in* Tailleur, I.L., and Weimer, Paul, eds., Alaskan North Slope geology, field trip guidebook: Pacific section, SEPM and Alaska Geological Society, Book 50, p. 513–528.

Moore, T.E., Wallace, W. K., Bird, K.J., Karl, S.M., Mull, C.G., and Dillon, J.T., 1994, Geology of northern Alaska, *in* Plafker, George, and Berg, H.C., eds., The Geology of Alaska, the Geology of North America: Boulder, Colorado, Geological Society of America, v. G-1, p. 49–140.

Moore, T.E., Whitney, J.W., and Wallace, W.K., 1985, Cenozoic north-vergent tectonism in northeastern Alaska; indentor tectonics in Alaska?: EOS Transactions, American Geophysical Union, v. 66, no. 46, p. 862.

Mount , V.S., and Suppe, John, 1987, State of stress near the San Andreas fault; implications for wrench tectonics: Geology, v. 15, no. 12, pp. 1,143–1,146.

Mull, C.G., 1985, Cretaceous tectonics, depositional cycles, and the Nanushuk Group, Brooks Range and Arctic Slope, Alaska, *in* Huffman, A.C., Jr., ed., Geology of the Nanushuk Group and related rocks, North Slope, Alaska: U. S. Geological Survey Bulletin 1614, p. 7–36.

O'Sullivan, P.B., Green, P.F., Bergman, S.C., Decker, John, Duddy, I.R., Gleadow, J.W., and Turner, D.L., 1993, Multiple phases of Tertiary uplift and erosion in the Arctic National Wildlife Refuge, Alaska, revealed by apatite fission track analysis: American Association of Petroleum Geologists Bulletin, v. 77, no. 3, p. 359–385.

O'Sullivan, P.B., Murphy, J.M., and Blythe, A.E., 1997, Late Mesozoic and Cenozoic thermotectonic evolution of the central Brooks Range and adjacent North Slope foreland basin, Alaska; including fission track results from the Trans-Alaska Crustal Transect (TACT): Journal of Geophysical Research, v. 102, no. B9, pp. 20,821–20,845.

Plumb, R.A., and Hickman, S.H., 1985, Stress-induced borehole elongation; a comparison between the four-arm dipmeter and the borehole televiewer in the Auburn geothermal well: Journal of Geophysical Research, v. 90, B7, p. 5,513–5,521.

Zoback, M.L., 1992, First- and second-order patterns of stress in the lithosphere; The World Stress Map Project, *in* Zoback, M.L., leader, The World Stress Map Project: Journal of Geophysical Research, v. 97, no. B8, p. 11,703–11,728.

Zoback, M.D., and Zoback, M.L., 1991, Tectonic stress field of North America and relative plate motions, *in* Slemmons, D.B., Engdahl, E.R., Zoback, M.D., and Blackwell, D.D., eds., Neotectonics of North America, The Geology of North America, Decade Map Vol. 1: Boulder, Colorado, Geological Society of America, p. 339–366.

MEASURED SECTION AND INTERPRETATION OF THE TINGMERKPUK SANDSTONE (NEOCOMIAN), NORTHWESTERN DELONG MOUNTAINS, WESTERN ARCTIC SLOPE, ALASKA

David L. LePain,[1] Karen E. Adams,[2] and Charles G. Mull[1]

INTRODUCTION

The State of Alaska Division of Geological & Geophysical Surveys (DGGS) has conducted geological field studies in the northwestern DeLong Mountains since 1993 as part of an assessment of the hydrocarbon potential of the Colville Basin in the western Arctic Slope (fig. 1). This assessment has included detailed geologic mapping at a scale of 1:63,360, analysis of field samples for organic geochemistry and thermal history, biostratigraphy, petrography, apatite fission track cooling and uplift history, and stratigraphic studies of selected stratigraphic units such as the Tingmerkpuk sandstone.

This report summarizes stratigraphic studies carried out during the 1998 field season on exposures of the Tingmerkpuk sandstone on the northwest side of Tingmerkpuk Mountain, and at an outcrop near the head of Eagle Creek (fig. 1). The purpose of this work was to conduct a scintillometer survey through the Tingmerkpuk Mountain section previously measured by R.K. Crowder and K.E. Adams in 1993 (Crowder and others, 1994), and T.N. Nilsen, T.E. Moore, and M.D. Myers in 1996 (Nilsen, 1996). The scintillometer survey (not included here) was conducted to provide a pseudo-gamma ray log that could be used for correlating the outcrop stratigraphy with subsurface stratigraphy to the north and northeast. The section was remeasured so that the scintillometer readings could be accurately tied to the measured section. Owing to the disparate interpretations of the depositional environments presented by Crowder and others (1994) and Nilsen (1996), the section was redescribed in detail while conducting the scintillometer survey.

Previous work on the Tingmerkpuk sandstone along with our description and interpretation of the unit are summarized in the following sections of this report. Due to limited outcrop and subsurface control and the complex fold and thrust history of the area, it is difficult to reconstruct Neocomian paleogeography of the western Arctic. At its present location the Tingmerkpuk sandstone is nearly 350 km south of the Barrow arch, placing it several hundred kilometers south of other known Neocomian shelf sandstones of similar provenance. In an effort to help focus future stratigraphic work in the area, we conclude with some speculative suggestions regarding the Neocomian paleogeography of the western Arctic.

PREVIOUS WORK

Crane and Wiggins (1976) introduced the informal name Tingmerkpuk sandstone for Lower Cretaceous quartzose rocks exposed in the Brooks Range foothills of the DeLong Mountains. The unit was dated as Valanginian age, based on microfossils. One of the best exposures of these rocks is on the north side of Tingmerkpuk Mountain, which serves as the type section for the Tingmerkpuk sandstone (fig. 2).

Detailed mapping of the Tingmerkpuk outcrop belt at a scale of 1:63,360 by Mull, Reifenstuhl, and Harris (in preparation) has documented two parallel facies belts within the Tingmerkpuk. The northern facies belt, which contains the type section on Tingmerkpuk Mountain, consists of ~130 m of interbedded fine- to very fine-grained quartzose sandstone and black clay shale. The southern facies belt, which is superimposed over the northern belt by thrust faulting, consists of a generally finer grained, more thinly bedded, section of quartzose sandstone, siltstone, and interbedded clay shale. Owing to generally poor exposures of this muddier facies of the Tingmerkpuk, the thickness of the southern facies belt has not been measured but is estimated to be about the same thickness as the unit in the northern facies belt.

Mickey and others (1995) assigned a Valanginian age to the base of the Tingmerkpuk sandstone based on the macrofossil *Buchia sublaevis* and an abundant palynomorph flora, and a Hauterivian to Barremian age to the top of the Tingmerkpuk based on palynomorphs. This indicates that the Lower Cretaceous unconformity (LCu) horizon is contained somewhere within the Tingmerkpuk sandstone. The underlying Kingak Shale ranges up into the Valanginian (Mickey and others, 1995).

Petrographic studies by Reifenstuhl (1997) show that the Tingmerkpuk sandstones can be characterized as compositionally mature very fine- to medium-grained quartz arenite.

[1]Alaska Division of Geological & Geophysical Surveys, 794 University Ave., Suite 200, Fairbanks Alaska 99709-3645.
Email for David L. LePain: Dave_LePain@dnr.state.ak.us
[2]U.S. Geological Survey, 345 Middlefield Rd., Menlo Park, California 94025

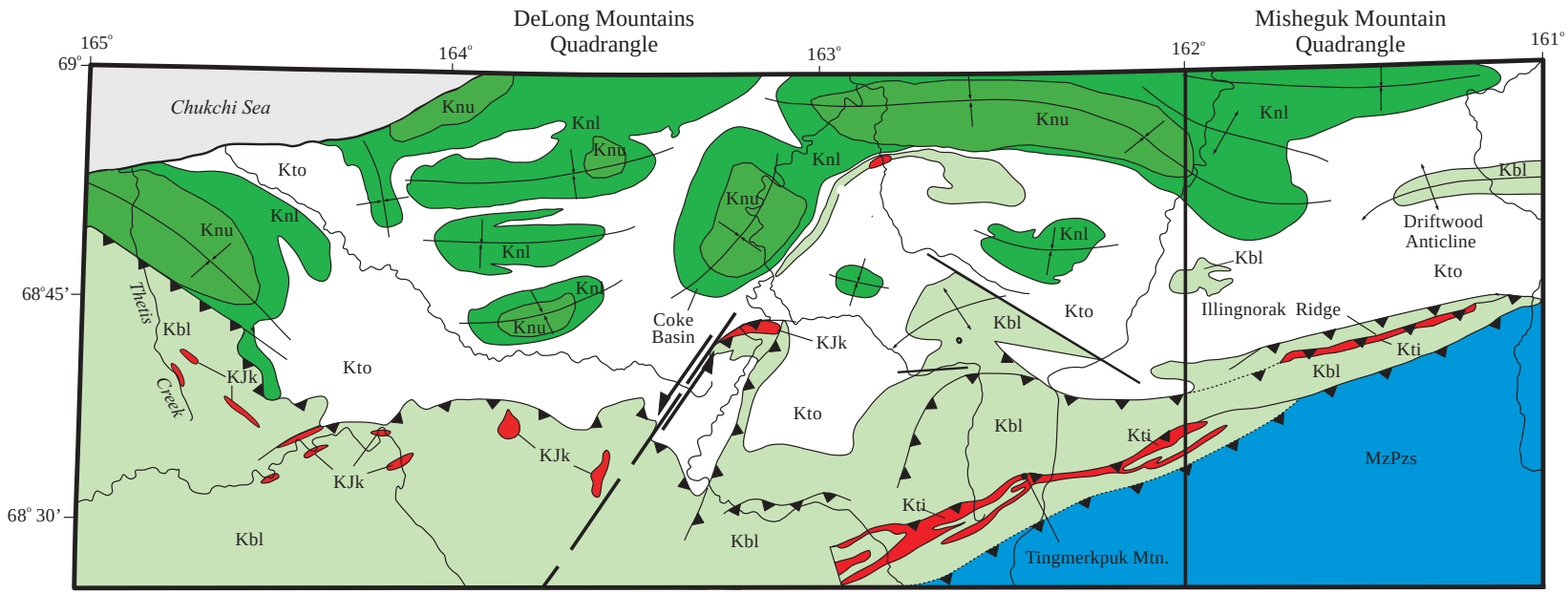

Knl / Knu	Nanushuk Group (Albian - Cenomanian) deltaic deposits
Kto	Torok Shale (Albian) pro delta shale
Kbl	Lower Brookian (Aptian - Barremian?) shale and graywacke turbidites
Kti / KJk	Tingmerkpuk sandstone and Kingak Shale (Neocomian - Upper Jurassic)
MzPzs	Mesozoic and Paleozoic sedimentary rocks undifferentiated

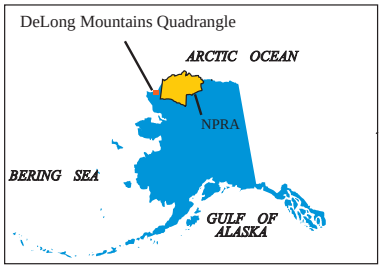

0 5 10 Mi
0 8 16 Km

Geochemical studies of Triassic to Cretaceous shales in the northwestern DeLong Mountains indicate that the clay shales interbedded with the Tingmerkpuk sandstones, the underlying Kingak Shale, and the overlying Lower Brookian shale contain up to 1.8 percent total organic carbon (TOC) (Mull, 1995). Although thermally overmature where sampled, these units contain sufficient organic material to have been fair hydrocarbon source rocks.

Crowder and others (1994) measured 131 m of Tingmerkpuk sandstone conformably overlying the Kingak Shale on Tingmerkpuk Mountain. In this study, the Tingmerkpuk sandstone was interpreted as a conformable succession that records episodic, highly fluidized turbidity currents that, over time, built a series of progradational outer fan lobes. This interpretation was based on the presence of complete Bouma sequences, conspicuous dewatering features, convolute lamination, graded bedding, sole markings, amalgamated beds, and parasequence stacking patterns. The interpretation placed the Tingmerkpuk sandstone off the shelf in a basinal setting and fits the conventional paleogeographic model for Beaufortian sandstones (that is, shallow water shelf and associated sandstones deposited along the Barrow arch and a deeper water basin toward the south; sandstones were assumed to be derived from a northern source terrane). In this model, the Tingmerkpuk sandstone is interpreted as a deeper water (lowstand fan) deposit that is coeval with shallow-marine Neocomian sandstones along the Barrow arch, such as the Kuparuk River Formation and Kemik Sandstone. Interestingly, Schenk and Bird (1992) speculated that the Tingmerkpuk sandstone represents a lowstand fan derived from the Tunalik shelf region.

Due to some uncertainty in the nature of the depositional system, T.N. Nilsen (Consultant), T.E. Moore (U.S. Geological Survey), and M.D. Myers (Alaska Division of Oil & Gas) remeasured the type section in 1996. Nilsen (1996) interpreted the Tingmerkpuk as the depositional record of repeated storm events in a mid- to outer-shelf setting. This interpretation is based on the presence of hummocky and swaley cross stratification, symmetrical wave ripple bedforms, wave ripple and wave-modified current ripple cross lamination, trace fossils typical of shelf settings, and the general absence of Bouma sequences and other features characteristic of turbidites. Paleocurrent indicators and hummocks overturned toward the east in

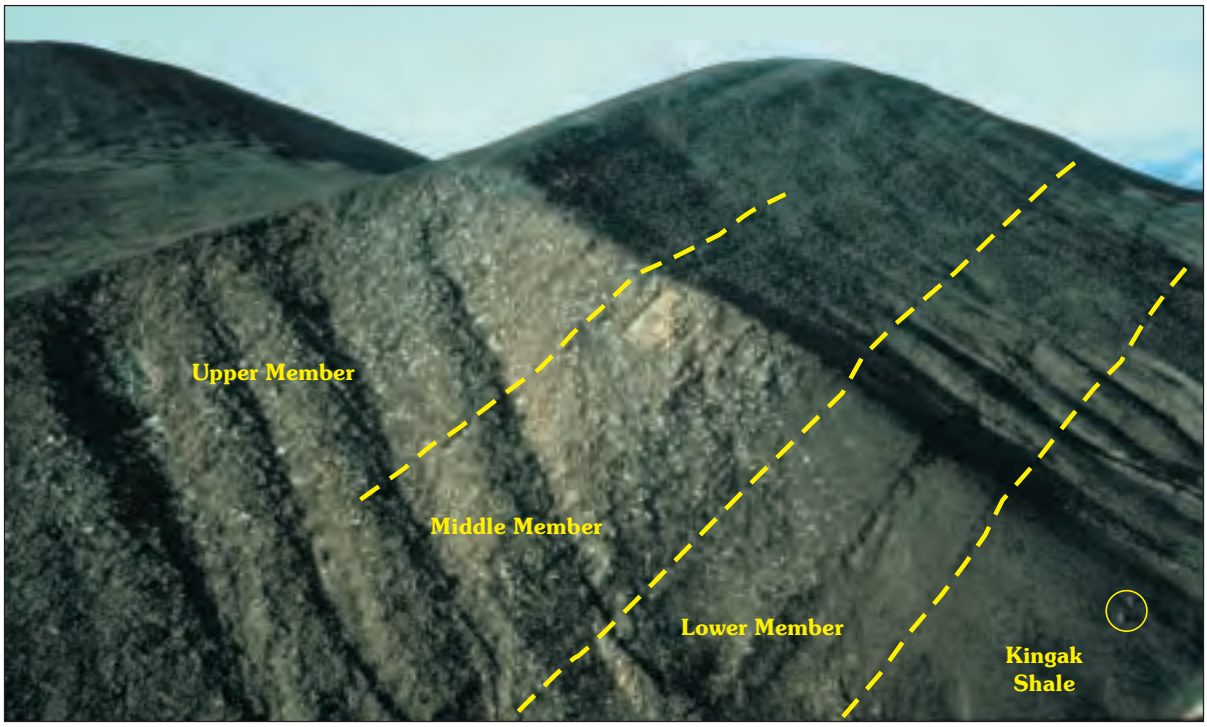

Figure 1 (left). *Generalized geologic map of the northwest DeLong Mountains, western Brooks Range, Alaska. Modified from Reifenstuhl (1997).*

Figure 2. *View toward the northwest showing the type section of the Tingmerkpuk sandstone on the north flank of Tingmerkpuk Mountain. Geologist in the lower right corner of the photo (in circle) is standing near the base of the lower member. The prominent beds in the center of the photo belong to the middle member. The rubble-covered interval near the top of the slope is the upper member. Photo by Gil Mull.*

convolute laminated beds suggest the dominant direction of storm movement was eastward, along the trend of the outcrop belt (Nilsen, 1996).

Nilsen's interpretation does not fit well into the existing paleogeographic model for Beaufortian sandstones. If the Tingmerkpuk was derived from a northern source, either associated with or located north of the Barrow arch, then the shelf upon which the Tingmerkpuk was deposited was at least 350 km wide. This is a conservative estimate that does not account for north-vergent thrusting that displaced the Tingmerkpuk sandstone northward an unknown distance. Further, low-angle south-dipping clinoforms in the Kingak Shale are clearly visible on seismic lines from the NPRA. These reflectors indicate a ramp-like or low-angle slope that deepened from the Barrow arch southward during Late Jurassic to Early Cretaceous time.

Although biostratigraphic data indicate that the time equivalent of the LCu occurs within the Tingmerkpuk sandstone, neither group found stratigraphic evidence for the unconformity. Crowder and others (1994) interpreted the contact between the Tingmerkpuk sandstone and the underlying Kingak Shale as the correlative conformity to the LCu.

REGIONAL STRATIGRAPHY

The Arctic Alaska terrane experienced a 100 m.y. interval of extension that lasted from Early Jurassic to Early Cretaceous (Hubbard and others, 1987). This interval is characterized by an Early Jurassic failed rift episode, and an Early Cretaceous (Valanginian–Hauterivian) successful rift event which led to the opening of the Canada Basin (Grantz and May, 1983; Hubbard and others, 1987). Strata deposited during this interval include the Jurassic to Lower Cretaceous (Valanginian) Kingak Shale, various Upper Jurassic to Hauterivian–Barremian sandstone bodies of local extent, and the Hauterivian to Barremian Pebble Shale unit. These rocks are referred to as the Beaufortian plate sequence by Hubbard and others (1987). As in the underlying Ellesmerian sequence (lower Ellesmerian sequence of Grantz and others, 1990), sandstones in the Beaufortian plate sequence are quartzose and were derived from a northern source terrane north of the present day Arctic coast line.

Uplift along the northern margin of the Arctic Alaska terrane associated with Valanginian to Hauterivian rifting created the Barrow arch and led to development of a regional unconformity. This erosional surface, commonly referred to as the Lower Cretaceous unconformity (LCu), is considered the breakup unconformity by Grantz and May (1983). In the subsurface north and northeast of the DeLong Mountains, the LCu is commonly placed at the Valanginian–Hauterivian boundary, but at some locations the surface is probably contained within the Hauterivian. On the south flank of the Barrow arch the LCu truncates rocks as young as the Kingak Shale; the LCu cuts progressively downsection northward toward the crest of the Barrow arch, where rocks as old as late Proterozoic have been truncated.

Numerous discontinuous shallow-marine, quartzose sandstone bodies of Neocomian age are associated with the LCu. These are the sandstone bodies of local extent mentioned above. These sandstones have been recognized from the Aurora-1 well east of Barter Island to the western Arctic Slope and Chukchi Sea. Some of the better known include the Thomson sand, Put River sandstone, the Hauterivian to Barremian Kemik Sandstone (Mull, 1987; Reifenstuhl, 1995), and the Valanginian to Barremian Kuparuk River Formation (Masterson and Paris, 1987). Lesser known sandstone bodies include Valanginian sandstones in the Tunalik well and Neocomian sandstones on the Chukchi Sea east of Point Barrow.

A variety of contact relations with the LCu have been recognized. Some sandstones are truncated by the LCu, others rest on the LCu, and still others are split by the LCu. Four members are recognized in the Kuparuk River Formation. The lower A and B members gradationally overlie the Kingak Shale and are truncated by the LCu; the C and D members overlie the LCu. The Kemik Sandstone is present in discontinuous surface exposures between the Sadlerochit and Echooka rivers in the Arctic National Wildlife Refuge (ANWR) and foothills of the northeastern Brooks Range, and extends into the subsurface west of the Echooka River. South of the Barrow arch, the LCu passes gradually into a correlative conformity. South of the maximum southerly extent of the LCu, Neocomian sandstones rest with apparent conformity above the Kingak Shale. An example of this conformable relation is seen along the Echooka River approximately 20 km southwest of the Kemik #1 well on the northeastern Arctic Slope near ANWR, where the Kingak Shale is gradationally overlain by the Kemik Sandstone. Northeast of this location, the Kemik rests unconformably above older rocks.

The contact between these Neocomian sandstones and the overlying Pebble Shale unit is sharp, but apparently conformable. Where the sandstones are absent, the Pebble Shale unit rests directly on the LCu.

In the northern DeLong Mountains, the Tingmerkpuk sandstone is exposed in thrust sheets along an 80-km-long trend (fig. 1) (Reifenstuhl and others, 1997). Along this trend the Tingmerkpuk consists of a conformable succession of interbedded shale and sandstone (Crowder and others, 1994). The Tingmerkpuk rests with

apparent conformity above the Kingak Shale and is apparently conformably overlain by Brookian strata (fig. 3). Throughout much of its outcrop trend, two distinct facies belts of Tingmerkpuk sandstone have been recognized (Reifenstuhl and others, 1997): the southern belt has been superimposed over the northern belt by north-vergent thrusting. The northern facies belt is characterized by a higher sandstone:shale ratio and coarser grained sandstones, whereas the southern facies belt has a lower sandstone:shale ratio and finer grained, more thinly bedded sandstones. These observations suggest a relatively proximal depositional setting for the northern belt and a more distal setting for the southern belt. Unlike its correlatives in the subsurface and in the northeastern Brooks Range, the Pebble Shale unit is absent and Brookian strata overlie the Tingmerkpuk sandstone with apparent conformity.

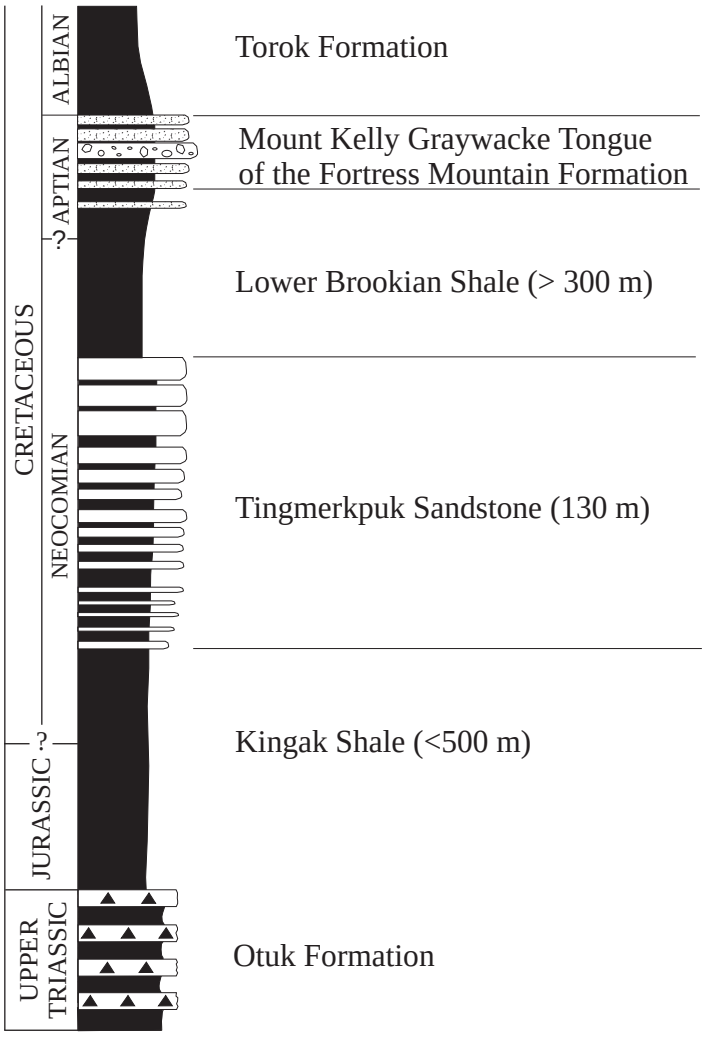

Figure 3. *Generalized stratigraphic column for the northern DeLong Mountains, western Brooks Range, Alaska. No vertical scale is intended.*

STRATIGRAPHY AND SEDIMENTOLOGY OF THE TINGMERKPUK SANDSTONE TYPE SECTION

The type section of the Tingmerkpuk sandstone is located in the northern facies belt on the northern flank of Tingmerkpuk Mountain (figs. 1, 2). It contains a nearly continuous succession of sandstone and shale that lies with apparent conformity (in an exposed contact) upon the underlying Kingak Shale (fig. 4A). A detailed measured section at a scale of 1:30 is available from DGGS (LePain and others, 1999).

The upper 10–15 m of Tingmerkpuk consists largely of rubble crop and the upper contact is a thrust fault. The thrust fault defines the base of a repeated section of uppermost Kingak and Tingmerkpuk sandstone (thrust repeat of the northern facies belt). The type section as we measured it consists of approximately130 m of interbedded sandstone and shale (fig. 4A). Crowder and others (1994) accurately describe the stratigraphic organization of the type section, which they divided into three members. Each member is distinguished by the gross sandstone:shale ratio (increases upward), sandstone bed thickness (average thickness increases upward overall and within members), and the degree of amalgamation in sandstone bedsets (increases upward). Crowder and others (1994) viewed the contact between the Kingak Shale and the Tingmerkpuk sandstone as a sequence boundary.

KINGAK SHALE

The upper 27 m of the Kingak consists of dark gray clay shale to slightly silty clay shale. The Kingak is locally red weathering and includes thin beds of very fine-grained sandstone and small (few centimeters in diameter) ovoid-shaped iron and/or manganese concretions. Overall the sandstone beds increase in number and thickness upsection from a few millimeters near the base of the measured section (27 m below the Tingmerkpuk) to a few centimeters near the contact with the Tingmerkpuk. Superimposed on this overall increase in the sandstone:shale ratio is a cyclic variation in the abundance of sandstone beds that defines meter-scale sandier-

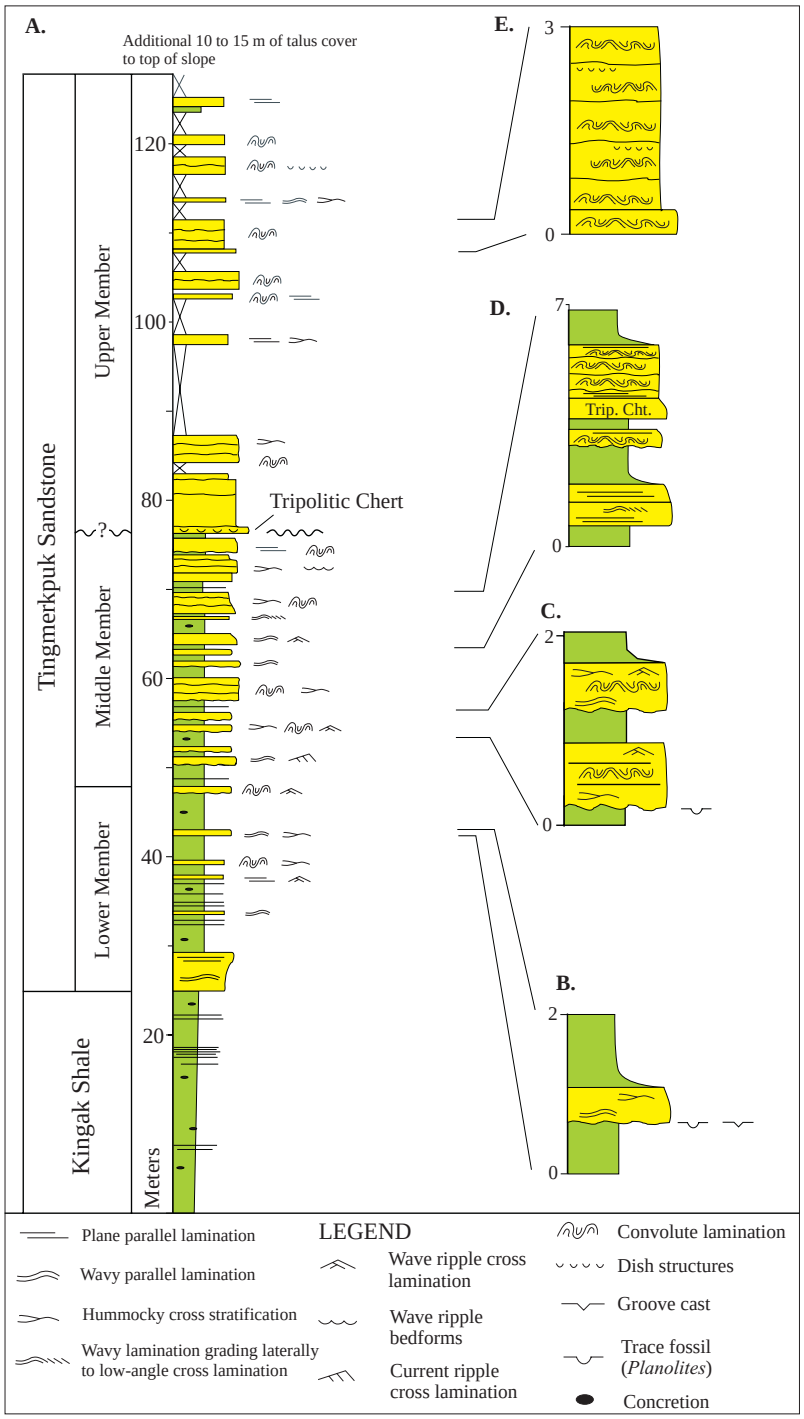

Figure 4. *(A) Simplified measured stratigraphic section through the Tingmerkpuk sandstone at its type section on the northern flank of Tingmerkpuk Mountain. Due to the scale, individual parasequences are not shown. (B) Blowup showing typical event bed in the lower member. (C) Blowup showing two event beds near the base of the middle member; the vertical sequence of sedimentary structures shown is common, but is not the only vertical sequence observed. (D) Blowup showing two bedsets and one solitary bed. Each bedset is composed of at least two amalgamated beds; each bed represents a single depositional event. (E) Blowup showing a thick bedset in the upper member. Convolute lamination is the most common structure in the upper member; other structures observed are shown in figure 4A.*

upward successions (fig. 4A). Sandstone beds typically have sharp basal contacts, are very subtly graded, and are horizontally laminated. In some beds horizontal laminae grade laterally to single sets of ripple cross lamination. Some laminae drape ripple bedforms and pass laterally into foreset laminae. Cross laminae set bounding surfaces are irregular and characterized by complex geometries. The basal portions of laterally adjacent sets of cross laminae are interleaved and one or more laminae commonly drape individual sets. The complex geometry of set bounding surfaces, the geometry of the ripple cross laminae sets, and the common presence of draping laminae, resembles wave ripple cross lamination illustrated by de Raaf and others (1977).

LOWER MEMBER

Description

The contact between the Kingak Shale and the overlying Tingmerkpuk sandstone is sharp and placed at the base of the first prominent sandstone bench on the northwest side of Tingmerkpuk Mountain (fig. 4A). A 10-cm-thick sandstone bed at the base of the bench consists of medium to dark gray, very fine-grained argillaceous sandstone that rests above a sharp erosive contact with the underlying Kingak Shale. This 10-cm-thick bed forms the base of a 4.2-m-thick coarsening upward bedset that comprises the sandstone bench (fig. 4A). The lower member extends from the base of the sandstone bench at 27 m to the top of the first bedset of amalgamated sandstone beds (above the sandstone bench) at 49.5 m.

Above the sandstone bench at 27 m, the lower member consists of interbedded slightly silty dark gray to black shale and very fine to fine grained quartzose sandstone. The lower member is shale dominated and has a sandstone:shale ratio less than 0.5. The shales include thin (less than 2 cm) bentonite beds and ovoid-shaped iron and manganese (?) concretions. Most sandstone beds are very fine grained, medium gray to red-brown weathering, and are medium to light gray on fresh surfaces. Sandstone beds range from less than 1 cm to approximately 0.5 m thick. The thinner beds are characterized by sharp upper and lower contacts, whereas the thicker beds have sharp basal and gradational upper contacts with enclosing shale. The amalgamated beds at the top of the member have undulatory basal contacts.

Horizontal trace fossils similar to *Planolites* and linear tool marks are abundant on the undersides of many sandstone beds (fig. 5A). Horizontal trace fossils range from a few millimeters wide to robust forms up to 1 cm wide; horizontal trace fossils are preserved in semi-relief, usually have a meandering plan form, and rarely branch. Tool marks range from small, faintly visible (fig. 5A), discontinuous linear features to discontinuous groove casts up to 2 cm wide and several centimeters long. Discrete vertical burrows were not observed, but circular burrows up to 1.5 cm in diameter are present on the undersides of some sandstone beds (*Planolites?*), where they are preserved in cross section parallel to bed surfaces. Rare pieces of sandstone float with casts of the pelecypod *Buchia sublaevis* were observed. Some casts included iridescent shell material.

The suite of sedimentary structures recognized in the sandstone beds include: (1) plane-parallel lamination (less than 1 cm thick) (figs. 5B, 5C); (2) low amplitude (less than 2 to 3 cm) wavy, parallel lamination (fig. 5B); (3) small-scale hummocky cross stratification (HCS) with wavelengths from 20 cm to approximately 50 cm and amplitudes from a few centimeters to approximately 8 cm (figs. 5C, 5D, 5E); (4) wave or wave-modified current ripple cross-lamination; (5) wave ripple bedforms (fig. 5F); (6) convolute lamination; and (7) parting lineation. Parting lineation was observed in plane-parallel laminated beds. Beds with HCS consist of laminae dipping at low angles (usually less than 10°) relative to truncation surfaces and laminae draping low-relief hummocks. Symmetric versus asymmetric forms of HCS were not distinguished. The undisturbed laminae geometry is difficult to determine in convolute laminated intervals. However, low-angle laminae truncations are common, suggesting hummocky cross stratification. Plane-parallel lamination and wavy lamination are typically the most common structures in the thinner beds; HCS is present, but is not as common. Lateral gradations between plane-parallel lamination, wavy lamination, and hummocky cross stratification are common in many beds. The degree of deformation in convolute laminated intervals typically decreases abruptly upsection and gradationally parallel to bedding. Folds within convolute laminated intervals are commonly overturned toward the east.

Several meter-scale sandier-upward parasequences have been recognized in the lower member. Each parasequence is characterized by a gradual increase in the number and thickness of sandstone beds upsection. The stratigraphic organization of the lower member is similar to the organization of the uppermost Kingak Shale, except that in the latter the sandstone:shale ratio and average thickness of the sandstone beds are much less. If not for the bedset between 27 and 31.2 m, which is markedly different from any of the sandstones observed in the Kingak, the lower member would simply grade downsection into the Kingak Shale. The low sandstone:shale ratio and absence of sand-on-sand contacts (amalgamation surfaces) suggest an aggradational stacking pattern for the lower member.

Figure 5. *Sedimentary structures in sandstones from the lower member. (A) Trace fossils preserved on the underside of a sand bed in the lower member. Some traces resemble* Planolites. *Low-relief tool marks are also visible. (B) Plane-parallel lamination and low-relief wavy lamination in a sandstone bed from the lower member. The underside of this bed contains* Planolites *traces. A low-relief hummock grades upward to plane-parallel lamination immediately above the geologist's finger. (C) Plane-parallel lamination, low-relief wavy lamination, and possible hummocky cross-stratification (HCS) in a sandstone bed from the lower member. Plane-parallel laminae are visible in the lower left corner of the bed, which is overlain by a low-relief convex upward hummock; laminae in the hummock downlap on plane-parallel laminae. The hummock grades upward to low-relief wavy laminae which, in turn, grade upward to plane-parallel laminae. (D) Small-scale (wavelengths range from 15 to 25 cm) HCS in a sandstone bed from the lower member. HCS grades upward to plane-parallel laminated sandstone. (E) Small-scale HCS in sandstone bed from the lower member. (F) Wave ripple bedform preserved on the surface of a sandstone bed in the lower member.*

MIDDLE MEMBER

Description

The middle member extends from 49.5 m to 77.2 m, consists of interbedded shale and sandstone, and is distinguished from the lower member by a higher sandstone:shale ratio (greater than 3), greater average sandstone bed thickness, and the presence of amalgamated sandstone beds. The latter two criteria are the most important for separating the lower and upper members. The stratigraphic organization recognized in the middle member can be viewed as the continuation of a vertical trend (that is, increasing sandstone upsection) that started in the uppermost Kingak Shale.

The shales are slightly silty, with only minor "clean" clay shale intervals, and include common iron and manganese (?) concretions, and minor thin (less than 1 cm) beds of pale yellow weathering bentonite. Most sandstones are very fine- to fine-grained, weather light gray to light tan-brown, and are light colored on fresh surfaces. Sandstone beds range from less than 1 cm to greater than 1 m thick. The thinner sandstone beds have sharp contacts with the enclosing shales. Thicker beds that are enclosed in shale have sharp, erosive lower contacts and gradational upper contacts. Bedsets of amalgamated sandstone beds are common and occur throughout the member. The basal surface of most thinner sandstone beds is flat, whereas most thicker beds have undulatory bases. Trace fossils and sole marks similar to those described in the lower member are common.

Trace quantities of glauconite are visible on fresh surfaces of many sandstone beds. Notably, granule-sized clasts of tripolitic (leached) chert are present at the base of the sandstone bed at 68.5 m. The granules are floating within a "matrix" of sand-sized grains. This is the lowest stratigraphic occurrence of visible tripolitic chert recognized thus far in the Tingmerkpuk type section. The reader is referred to Reifenstuhl and others (1997) for a detailed discussion of the petrography of the Tingmerkpuk sandstone.

The suite of sedimentary structures recognized in sandstone beds include: (1) plane-parallel lamination ranging from a few millimeters to 2 cm thick (figs. 6A, 6B), (2) low amplitude (from less than 2 to 3 cm) wavy parallel lamination, (3) small-scale HCS with wavelengths from a 20 cm to approximately 50 cm, and amplitudes from a few centimeters to approximately 8 cm, (4) wave ripple cross lamination, (5) wave-modified current ripple cross lamination (fig. 6C), (6) wave ripple bedforms with wavelengths from 10 to 25 cm and amplitudes to 4 cm, (7) convolute lamination (figs. 6A, 6B), and (8) parting lineation (fig. 6C). Wave ripple bedforms (symmetric to slightly asymmetric profiles) are present in float and on the surface of some sandstone beds. Convolute lamination is more abundant in the middle member than in the lower member. Parting lineation was only observed in plane-parallel laminated beds. Small shale ripups were noted in a sandstone bed at 72.1 m. Plane-parallel lamination, wavy lamination, and convolute lamination are the most common sedimentary structures (figs. 6A, 6B). A number of different vertical sequences have been recognized in sandstone beds of the middle member; however, hummocky cross stratification and wavy parallel lamination is most commonly present near the base of beds and usually grades upsection to convolute lamination or wave ripple cross lamination.

Owing to the higher sandstone:shale ratio and greater average sandstone bed thickness, individual parasequences are less obvious in the middle member than in the lower member. The relatively uniform interbedding of sandstone and shale defines an aggradational stacking pattern for the middle member; the appearance of amalgamated beds near the top of the member indicates a decrease in accommodation space relative to the lower member.

UPPER MEMBER

Description

The upper member extends from 77.2 m to the top of the section at 140 m. Approximately 50 percent of the thickness of the upper member is sandstone talus and minor shale fragments. The exposed 50 percent consists of very fine- to fine-grained quartzose sandstone, minor medium grained sandstone, and minor black to dark gray, slightly silty shale. The upper member is distinguished from the middle member by the increase in bed thickness, the "cleaner" appearance of the sandstones, and the apparent reduced thickness of interbedded shale. Sandstones are light tan to tan-brown weathering and light tan on fresh surfaces (fig. 6E). Visible basal bed contacts are sharp and flat over the scale of the outcrop; both gradational and sharp upper bed contacts have been observed. Bedding in the sandstones is faint to invisible and, where visible, ranges from 0.5 m to more than 1 m thick. Where internal structures are visible, plane-parallel lamination is most common (fig. 6F). No trace fossils or sole marks were observed on the undersides of sandstone beds.

Glauconite is visible in trace quantities on fresh surfaces in many sandstone beds. Sand- to granule-size tripolitic chert grains were observed in the lowermost bed (77.2 m) of the member (figs. 4A, 6E). This bed represents the uppermost of two occurrences of megascopic tripolitic chert in the Tingmerkpuk type section. The reader is referred to Reifenstuhl and others (1997) for a detailed discussion of the petrography of the Tingmerkpuk sandstone.

Figure 6A. *Convolute laminated bed in the middle member. Convolute laminated interval is abruptly overlain by plane-parallel laminated sandstones; the convolute laminated interval is underlain abruptly by sandstone with small-scale HCS. Determining whether this succession is a bedset of amalgamated beds or a single bed deposited during one event is difficult; the lack of evidence for erosion along the surfaces bounding the convolute laminated interval suggests that the succession records a single depositional event.*

Figure 6B. *Convolute laminated interval abruptly overlain by a plane-parallel laminated sandstone in the middle member. The convolute laminae grade upward to incipient convolute laminae which, in turn, are abruptly overlain by plane-parallel laminae. This bed is interpreted as the product of a single depositional event.*

Figure 6C. *Wave ripple or wave-modified (combined flow) cross lamination in a sandstone bed from the middle member. The foreset laminae are bounded by plane-parallel laminated sandstones. Foreset laminae overlie an erosional surface characterized by complex geometry; foreset laminae are grouped in bundles that are bounded by complexly shaped surfaces. The ripple cross lamination resembles wave-generated cross lamination shown by de Raaf and others (1977).*

Figure 6. *Sedimentary structures in sandstones from the middle and upper members.*

Figure 6D. *Parting lineation on the underside of a sandstone bed in the middle member. Parting lineation indicates high energy conditions, equivalent to the upper flow-regime in unidirectional flows.*

Figure 6E. *Light colored "clean" sandstone at the base of the upper member. Note the rubbly character of the exposure. Geologist is examining the tripolitic chert-bearing bed at the base of the member.*

Figure 6F. *Light colored "clean" sandstones with wavy lamination in the upper member. Wavy laminae grade upward to plane-parallel lamination.*

Figure 6G. *Convolute laminated sandstone beds in the upper member.*

The suite of sedimentary structures recognized in sandstones include plane-parallel lamination (0.5 cm to 2 cm thick), wavy parallel lamination, small-scale HCS (similar size range as recognized lower in section), convolute lamination, and dish structures. Apparently structureless sandstones are also present in the upper member. Convolute lamination is the most common sedimentary structure recognized in the upper member, and the structure is ubiquitous in many beds (fig. 6G). No recurring vertical sequence of sedimentary structures has been recognized.

Abundant amalgamated beds, relatively uniform grain size in sandstones, and the lack of exposed shales preclude identification of individual parasequences. The ubiquitous presence of amalgamated sandstone beds indicates a significant reduction in accommodation relative to the lower and middle members. The contact between the upper and middle members is interpreted as a sequence boundary.

STRATIGRAPHY OF THE SOUTHERN FACIES BELT OF THE TINGMERKPUK SANDSTONE

The southern facies belt can be traced for a number of kilometers along strike (fig. 1). Brief reconnaissance of this belt was conducted at a location 3 km south-southwest of Tingmerkpuk Mountain. Owing to relatively poor exposures, no sections of the Tingmerkpuk in this belt have been measured, but its thickness and stratigraphic organization appears to be comparable to the Tingmerkpuk in the northern belt. Petrographic study of the Tingmerkpuk in the southern facies belt shows no significant difference in framework grain composition relative to the northern facies belt (Reifenstuhl and others, 1997). Megascopic tripolitic chert was not observed at exposures of the Tingmerkpuk in the southern facies belt.

Exposures of the southern facies belt of the Tingmerkpuk sandstone are present on the slope

immediately southwest of a northwest-flowing tributary to Eagle Creek. Bedding is nearly vertical to slightly overturned toward the south. Tundra covered shale intervals are interrupted by resistant sandstone bedsets ranging from less than 1 m to 2 m thick. The dominant sedimentary structures are plane-parallel lamination, low-relief wavy lamination, and convolute lamination. Most wavy laminae are not perfectly parallel, but do not intersect. The most common vertical sequence observed in individual bedsets is plane-parallel lamination and low-relief wavy lamination near the base that grades upsection to convolute lamination. Members have not been identified in the Tingmerkpuk at this location, but sandier-upward successions are apparent.

INTERPRETATION OF THE TINGMERKPUK SANDSTONE AT TINGMERKPUK MOUNTAIN

LOWER MEMBER INTERPRETATION

Thin sharp-based sandstone beds in the lower member record episodic, high-energy events that transported coarse-grained sediment into a mud-dominated depositional setting. The low sandstone:shale ratio indicates that low energy conditions prevailed and high energy events were relatively infrequent. During low energy conditions, clay- and fine silt-sized particles settled out of suspension to build the relatively thick interbedded mudstone successions. Hummocky cross stratification, wave ripple bedforms and cross lamination, and wave-modified current ripple cross lamination suggest deposition from oscillatory, or oscillatory-dominant combined flows that operated between fair-weather and the storm wave base associated with powerful storms. The presence of thick interbedded mudstone successions indicates that the sediment-water interface was only occasionally affected by wave activity.

Some of the storm-generated flows were able to scour into the muddy substrate as indicated by the *Planolites* burrows preserved in semi-relief on the undersides of many sandstone beds. In tiered trace fossil assemblages, *Planolites* usually occupies a shallow tier below, but close to, the sea floor (Bromley, 1996). *Planolites* is associated with well-oxygenated to slightly dyoxic sediment pore waters (Bottjer and others, 1986). Rare circular burrows, preserved on the undersides of some sandstone beds, may represent escape structures produced shortly after the beds were emplaced. Linear groove marks preserved on the undersides of many sandstone beds indicate that flows were strong enough to transport objects up to 2 cm wide.

Plane-parallel lamination is the most common sedimentary structure in the lower member. Plane-parallel lamination may develop from several different types of flows, including unidirectional currents under upper-flow regime conditions (Simons and others, 1965; Harms and others, 1982), strong oscillatory flows (Arnott and Southard, 1990), and from oscillatory-dominant combined flows (Arnott and Southard, 1990). Lateral gradations observed within individual beds range from plane-parallel lamination to wavy lamination and HCS; these structures and the presence of wave-modified current-ripple cross lamination near the tops of some of these beds suggests deposition from oscillatory-dominant combined flows. Laboratory flume studies show that plane-parallel laminae result from the superposition of weak unidirectional currents on strong oscillatory flows (Arnott and Southard, 1990). The presence of parting lineation in plane-parallel laminated sandstone beds attests to deposition from high-energy flows and is commonly associated with storm-generated sandstone beds (Leckie and Krystinik, 1989; Cheel, 1990).

Subtle size grading recognized in many of the plane-parallel laminated beds suggests the presence of sand-sized material in suspension above the sea floor. Graded bedding has been observed near the base of many storm-generated beds (for example, Aigner, 1985; Dott and Bourgeois, 1982; Kreisa, 1981; and Walker and others, 1983) and, in distal settings, may comprise the entire thickness of storm beds. Some graded plane-parallel laminated beds recognized in the lower member resemble graded rhythmites described by Dott and Bourgeois (1982) and Myrow (1992).

The origin of the wavy lamination is unclear. Arnott (1987, cited in Arnott and Southard, 1990), de Raaf and others (1977), and Kreisa (1981) describe gently undulating parallel-laminated sandstones that resemble the low-amplitude wavy lamination in the lower member. In flume studies of oscillatory and combined flows, Arnott and Southard (1990) noted that purely oscillatory bedforms were quickly planed off forming a gently undulating bed after a relatively weak unidirectional current was superposed on a strong oscillatory flow. Based on observations from their flume studies, Arnott and Southard (1990) suggested a combined flow origin for the gently undulating parallel lamination observed in the stratigraphic record. The wavy parallel lamination in the lower member may have a similar origin. Alternatively, the wavy parallel lamination in the Tingmerkpuk may record deposition from clouds of suspended sediment under strong oscillatory flows resulting in vertical accretion of the wavy bedform with little or no horizontal translation. In either case, if the bedform responsible for the wavy parallel lamination in the Tingmerkpuk consisted of three-dimensional hummocks, it may be genetically related to HCS. Lateral gradation from wavy lamination to plane-parallel lamination, and from wavy lamination

to hummocky cross stratification (middle and upper members) strongly suggests a genetic connection between these structures. Lateral gradations between structures indicate spatial variations in the flow strength and the concentration of suspended sediment near the sea bottom.

Convolute laminated beds may have formed shortly after deposition and possibly during the event responsible for deposition of the bed. The relatively consistent direction of eastward asymmetry observed in the convolute laminated intervals suggests that either the storm-generated currents exerted enough frictional drag on the bed surface to cause overturning in the direction of the dominant bottom current (Nilsen, 1996), or that the sand beds were deposited on a surface that sloped toward the east. We prefer the former possibility.

The gradational tops of many of the thicker sandstone beds indicate gradually waning flow strength and suspension fallout. Gradational upper contacts may also have been accentuated by the activities of burrowing organisms. As mentioned in the description for this member, discrete burrows were not observed within sandstone beds. This may reflect complete bioturbation of the uppermost portion of sand beds in the months to years following deposition.

All of the HCS observed in the Tingmerkpuk sandstone ranges from a few decimeters to 5 dm in wavelength, and as such would be classified as "small-scale." Small-scale HCS recognized in the Tingmerkpuk sandstone warrants further discussion. Campbell (1966) described the wavelength of HCS (his truncated wave ripple lamination) as ranging from a few decimeters to several meters. Most recent literature on shelf storm deposits list a lower wavelength limit of approximately 0.5 m for HCS (Harms, 1979; Mount, 1982; Myrow, 1992; and Walker, 1984). However, Cheel and Leckie (1993) point out that there is no physical basis for the 0.5 m lower size limit on the wavelength of HCS. Dott and Bourgeois (1982) and Brenchley and others (1986) describe examples of small-scale HCS interpreted to record deposition from strong oscillatory flows associated with storms in marine shelf settings. Higgs (1991 and 1998) describes small-scale HCS from the Carboniferous Bude Formation in southwest England, which he interprets as a storm-influenced lacustrine shelf deposit. Although the lacustrine setting of the Bude Formation is fundamentally different than the Tingmerkpuk's marine setting, like the Tingmerkpuk, controversy surrounds its interpretation as many workers consider it to be a lacustrine turbidite succession (Burne, 1995; Burne, 1998; Melvin, 1986).

Prave and Duke (1990) described decimeter-scale HCS associated with turbidites in Upper Cretaceous strata in the Basque Pyrenees. They interpreted the HCS as a form of antidune stratification that developed under standing waves formed at the boundary of a denser, thinner underflow and an overlying, less dense layer in a basinal setting. Prave and Duke (1990) suggest that small-scale hummocky cross stratification is multi-genetic and not indicative of a specific depositional environment or hydrodynamic condition.

The geometry of the HCS observed in the lower member is similar in every aspect to examples of larger-scale HCS reported in the literature (for example, Dott and Bourgeois, 1982; Harms, 1979; and Walker and others, 1983), which suggests a similar origin—deposition and reworking from powerful storm-generated oscillatory flows. The association of hummocky cross stratification and wave ripple cross lamination in sandstones from the lower member strongly suggests a storm origin and indicates deposition above storm wave base. This association makes a standing wave antidune origin unlikely.

We speculate that the small size of the hummocky cross stratification in the Tingmerkpuk is the result of deposition at water depths near storm wave base, in a subsiding outer-shelf setting. If the bedform responsible for HCS is correctly classified as an orbital ripple, then the bedform wavelength is related to the near bottom orbital diameter of the associated waves. This implies that at the exact depth that storm waves first begin to interact with the sea floor, the near-bottom orbital diameter is zero. At depths close to but less than storm wave base, the near-bottom orbital diameter is small and resulting bedforms have small wavelengths. A paleohydraulic analysis of HCS by Duke and Leckie (1986) supports this reasoning. From their analysis Duke and Leckie (1986) concluded that hummocky cross stratification forms under oscillatory-dominant flow from three-dimensional orbital ripples with wavelengths approximately equal to the near-bottom orbital diameter.

In marine shelf settings we do not believe that HCS is genetically related to orbital ripples. Clifton (1976) originally introduced the term orbital ripple and stated that they are associated with short period waves typically encountered in relatively protected shallow-water settings. For waves to entrain fine sand at water depths typically encountered in middle-to outer-shelf settings, long period waves similar to those encountered on shelves facing deep oceans are required. Bedforms associated with long period waves, referred to as anorbital ripples by Clifton (1976), have wavelengths that are unrelated to the near-bottom orbital diameter of the waves.

Regardless of the correct classification of the HCS bedform (orbital or anorbital), it seems reasonable to assume that for a given size surface wave, the mean

wavelength of oscillatory bedforms will decrease as water depth increases. If this assumption is correct, small-scale HCS should be generated near mean storm wave base and the scale of HCS should gradually increase with a gradual decrease in water depth, at least to within the wavelength range commonly observed in ancient shelf successions (0.5m to a few meters wavelength). In many ancient middle-to outer-shelf settings, mean storm wave base was probably situated above the sea floor (as it is in most Modern settings). Consequently, in these settings only waves associated with the most intense storms were able to entrain fine sand-sized sediment. Wave base associated with the most intense storms would be slightly deeper than mean storm wave base. The preserved recurrence interval for these intense storms may have been greater than 1,000 years (see Walker, 1985, p. 294). By analogy, the typical tempestite bed in the Tingmerkpuk may represent the 1,000-year or 2,000-year storm event, and may record deposition slightly below mean storm wave base.

Based on the analysis presented above and paleobathymetry (outer neritic to bathyal) estimates from foraminifera recovered from the base of the Tingmerkpuk and the uppermost beds of the Kingak Shale (Mickey and others, 1995), we infer an outer-shelf setting for the lower member. Thick intervening silty shales and the progressive thickening of sandstone beds at the top of successively higher members defines an aggradational to slightly progradational stacking pattern.

Similar depositional processes are inferred for the upper 27 m of the underlying Kingak Shale. The depositional setting was likely deeper and less storm-disturbed than that recorded in the lower member of the Tingmerkpuk sandstone. Another possibility is that the uppermost Kingak reflects deposition lateral to the lower member (lateral facies change) in a middle-to outer-shelf setting, and is not a proximal to distal relation.

MIDDLE MEMBER INTERPRETATION

The suite of sedimentary structures recognized in the middle member is similar to that observed in the lower member and is similarly interpreted as the record of storm-influenced sedimentation. The scale of hummocky cross stratification in the middle member appears similar to that observed in the lower member, which is inferred to have formed near, but above, storm wave base. If the organization of the middle member reflects a shoaling trend, HCS with wavelengths more typically observed in shelf settings (0.5 m and larger) would be expected. However, convolute lamination is more abundant in the middle member than in the lower member, which could obscure an increase in the wavelength of HCS.

The appearance of amalgamated beds suggests that storm events impacting this part of the shelf were more frequent. The change in stratigraphic organization from the lower to the middle member suggests a decrease in accommodation, and a corresponding increase in the progradation rate.

UPPER MEMBER INTERPRETATION

The suite of sedimentary structures recognized in the upper member is similar to that recognized in the lower two members, and is similarly interpreted. Thick amalgamated intervals in the upper member and the apparent lack of interbedded shales are suggestive of deposition under conditions of significantly reduced accommodation. The mature quartzose sandstones with convolute lamination and dish structures attest to rapid deposition of individual beds. There are three possible explanations for the apparent lack of mudstone: (1) background energy levels were too high for fine-grained material to settle out of suspension; (2) deposition occurred well above storm wave base, and episodic high energy storm flows were frequent and removed most mudstone; or (3) mudstones are present, but are covered by sandstone talus. Abundant amalgamation surfaces, the ubiquitous presence of "clean" sandstones, and the presence of at least one mudstone interval (at 123.7 m) suggests a combination of the second and third explanations.

INTERPRETATION OF THE TINGMERKPUK SANDSTONE IN THE SOUTHERN FACIES BELT

Individual sandstone beds represent episodic events. Unlike the section at Tingmerkpuk Mountain, wave-formed and wave-modified structures were not observed at the site visited in the southern facies belt. This may reflect the fact that the section was not examined in detail, or it may reflect a more distal depositional setting that was below storm wave base. The latter case seems more likely and by analogy with the northern facies belt, the event beds at this location likely record deposition from storm-generated flows below storm wave base. Two types of storm-generated flows can potentially transport sand on shelves in water depths below storm wave base: (1) geostrophic currents (Swift, 1985) and (2) turbidity currents (Walker, 1984; Myrow and Southard, 1996). At present it is not possible to distinguish between these two flow types in the southern facies belt.

DISCUSSION

The inferred outer-shelf depositional setting for the Tingmerkpuk sandstone is based on the presence of HCS, wave ripple cross lamination, wave-modified current ripple cross lamination, and wave ripple bedforms. Although these features are not the most

common sedimentary structures recognized in the type section, their significance far outweighs their abundance. These structures are wave-formed or, at least wave-modified, and indicate deposition above storm wave base. The depth of storm wave base is dependent on the overall wave climate in a particular basin. Wave climate is influenced by many factors, including the shape, size, and depth of the basin, as well as the basin's paleolatitude and the size and location of surrounding land masses. Storm waves capable of moving fine-grained sand have been reported in water depths greater than 200 m on the Oregon coast (Komar and others, 1972). Bathymetry estimates from foraminifera recovered from the uppermost beds of the Kingak and basal Tingmerkpuk (Mickey and others, 1995) suggest deposition in water at least 100 m deep. This is consistent with deposition in an outer-shelf setting. As mentioned previously, mean storm wave base was likely above the sea floor along the Tingmerkpuk trend and only the most intense storms (1,000+-year events) were recorded in the succession.

The overall organization of the Tingmerkpuk sandstone is regressive, suggesting basinward progradation of the depositional system. If our reasoning regarding the wavelength of hummocky cross stratification preserved in the Tingmerkpuk is correct, and if the Tingmerkpuk records gradually shoaling conditions, then a progressive increase upsection in the average wavelength of HCS should be recorded. We hypothesize that the wavelength increases upsection to within the range typically observed in shallow-marine storm deposits (0.5 m to 2 m). This hypothesis should be tested in future work on the Tingmerkpuk.

The significance of the tripolitic chert in the sandstone bed at 68.5 m and at the base of the upper member (bed at 77.2 m) is unknown. Tripolitic chert is abundant in the Ivishak Formation, immediately below the LCu along the Barrow arch; is present but less abundant in the Ivishak Formation south of the Barrow arch; and is also present in the Kemik Sandstone overlying the LCu (Mull, 1987). The appearance of megascopic tripolitic chert in the Tingmerkpuk may be related in some way to development of the LCu and erosion of chert-bearing older lithologic units (Ivishak Formation and Lisburne Group). Interestingly, the two occurrences of tripolitic chert recognized in the Tingmerkpuk are located at, and just below, the base of the upper member. The base of the upper member corresponds to a significant change in stratigraphic organization characterized by "clean" sandstone and thick, amalgamated bedsets. These bedsets are either convolute laminated or appear structureless. Common dish and pillar structures in these beds suggest extensive dewatering. We interpret the abrupt appearance of megascopic tripolitic chert in granule- and pebble-bearing coarse-grained sandstone at the base of the upper member to mark an intraformational unconformity (sequence boundary). The distance from the Barrow arch (rift shoulder) suggests that this unconformity is unrelated to the LCu (C. Paris, oral commun.).

SPECULATION ON NEOCOMIAN PALEOGEOGRAPHY

The present location of Tingmerkpuk sandstone outcrops in the western DeLong Mountains is 350 km south of the Barrow arch. With only one exception, the inferred depositional setting for these sand bodies ranges from marginal- to shallow-marine environments on the south flank of the Barrow arch. The single exception is a thin 0.5-m- to 2-m-thick bed of quartzose sandstone referred to as the Kemik Sandstone member of the Kongakut Formation that is extensively exposed in the western Bathtub Ridge area in the eastern Brooks Range (Camber and Mull, 1987; Mull, unpublished field data, 1985). Based on composition and stratigraphic position, this Kemik bed is considered a deep-water equivalent of the Kemik Sandstone, which is exposed from the Echooka River to Ignek Valley in the northeastern Brooks Range.

The paleogeographic implications of an outer-shelf interpretation for the Tingmerkpuk sandstone are difficult to reconcile if the source terrane was the Barrow arch or some landmass north of the arch. For the Barrow arch to have been the source, sand would have had to travel at least 350 km across a broad shallow-marine shelf and intervening slope and basinal area to the depositional site. This estimate does not account for the shortening recorded by thrust faults mapped along the Tingmerkpuk outcrop belt. In fact, the location of the Tingmerkpuk so far from the inferred source along the Barrow arch is probably one of the factors that initially led Crowder and others (1994) to suggest deposition in a basinal setting. We view the Barrow arch as an unlikely source for the Tingmerkpuk sandstone.

A northern source located south of the Barrow arch would significantly reduce the distance from the source terrane to the depositional site. Schenk and Bird (1992) show a paleogeographic reconstruction of the North Slope and Barrow arch at the maximum development of the LCu during Valanginian–Hauterivian time. In their reconstruction, a broad lowland coastal plain and narrow shelf are shown on the south flank of the Barrow arch. If this lowland area served as a source for terrigenous clastic sediment, then the distance between the source area and the depositional site in the DeLong Mountains would be significantly less (possibly less than 250 km). In fact, Schenk and Bird (1992) suggested a source for the Tingmerkpuk sandstone in the vicinity of the Tunalik

well. The LCu has been recognized in the Tunalik well, where the surface truncates Neocomian sandstones. If the Tingmerkpuk was derived from erosion of older Neocomian sandstones in the Tunalik area, a mechanism is necessary to bypass the intervening slope and basinal areas. We view the Tunalik area as an unlikely source for the Tingmerkpuk sandstone. Careful petrographic comparison of sandstones from the Tingmerkpuk outcrop belt and the Tunalik well may shed light on this possibility.

Alternatively, several workers have suggested a western or northwestern source for late Paleozoic and Lower Cretaceous clastics in the western Arctic. Grantz and May (1988) suggested that the Chukchi platform may have been an additional source terrane for Ellesmerian clastics, and Molenaar (1988) suggested a possible northwestern source for the Tingmerkpuk sandstone. The seemingly anomalous presence of a Neocomian (Beaufortian) sandstone in the western DeLong Mountains, distal from the Barrow arch, lends support to the possibility of a source terrane on the Chukchi platform. Like the two previous models, a mechanism is necessary to bypass the intervening Hanna trough.

A third possibility is that the Tingmerkpuk sandstone was derived from a southern source in the Brooks Range. Coeval strata in the Okpikruak Formation south and southeast of the Tingmerkpuk thrust sheets include only sandstones and conglomerates that are highly lithic. On petrographic grounds, a southern source appears unlikely.

A fourth possibility is that the Tingmerkpuk sandstone was derived from an unrecognized paleotopographic high in what is now the southern Colville basin. If such a high exists, it is probably now buried beneath the thrust sheets of the western Brooks Range. The underlying Kingak Shale rests unconformably on the Triassic Otuk Formation, is less than 350 m thick, and is no older than Valanginian. The thickness and age of the Kingak in this area suggest deposition on a paleotopographic high – perhaps on an uplifted fault block. Quartzose sandstone of the Tingmerkpuk may have been derived from this paleotopographic high.

East-directed paleocurrent indicators in the Tingmerkpuk suggest a fifth possibility – that sands were derived from an unrecognized western source located east of the Hanna trough. If this source terrane existed, it was subsequently removed from the area, possibly along a strike-slip fault. This possibility is not incompatible with derivation from a local paleotopographic high and the Tingmerkpuk outcrop belt could represent a remnant of a once larger block.

ACKNOWLEDGMENTS

We thank Kirk Sherwood and Mark Myers for their reviews of this manuscript.

REFERENCES

Aigner, Thomas, 1985, Storm Depositional Systems—dynamic stratigraphy in modern and ancient shallow-marine sequences, *in* Friedman, G.M., Neugebauer, H.J., and Seilacher, Adolf, eds., Lecture notes in earth sciences: Berlin, Springer-Verlag, 174 p.

Arnott, R.W., and Southard, J.B., 1990, Exploratory flow-duct experiments on combined-flow bed configurations, and some implications for interpreting storm-event stratification: Journal of Sedimentary Petrology, v. 60, no. 2, p. 211–219.

Bottjer, D.J., Arthur, M.A., Dean, W.E., Hattin, D.E., and Savrda, C.E., 1986, Rhythmic bedding produced in Cretaceous pelagic carbonate environments—sensitive recorders of climatic cycles, *in* Arthur, MA., and Garrison, R.E., eds., Special section—Milankovitch cycles through geologic time: Paleoceanography, v. 1, no. 4, p. 467–481.

Brenchley, P.J., Romano, Michael, and Gutierrez-Marco, J.C., 1986, Proximal and distal hummocky cross-stratified facies on a wide Ordovician shelf in Iberia, *in* Knight, R.J., and McLean, J.R., eds., Shelf sands and sandstones: Canadian Society of Petroleum Geologists, Memoir 11, p. 241–255.

Bromley, R.G., 1996, Trace fossils—biology, taphonomy and applications (second edition): London, Chapman & Hall, 361 p.

Burne, R.V., 1995, The return of "The Fan That Never Was"—Westphalian turbidite systems in the Variscan Culm basin—Bude Formation (southwest England), *in* Plint, A.G., ed., Sedimentary facies analysis—A tribute to the research and teaching of Harold G. Reading: International Association of Sedimentologists, Special Publication 22, p. 101–135.

Higgs, Roger, Reading, H.G., and Burne, R.V., 1998, Return of "The Fan That Never Was" —Westphalian turbidite systems in the Variscan Culm basin— Bude Formation (southwest England)—discussion and reply: Sedimentology, v. 45, no. 5, p. 961–975.

Camber, W.R., and Mull, C.G., 1987, Stratigraphy and depositional environment of Lower Cretaceous strata, western Bathtub Ridge, northeastern Brooks Range, Alaska: Geological Society of America, Abstracts with Programs, v. 19, no. 6, p. 364.

Campbell, C.V., 1966, Truncated wave-ripple laminae: Journal of Sedimentary Petrology, v. 36, no. 3, p. 825–828.

Cheel, R.J., 1991, Grain fabric in hummocky cross-stratified storm beds—genetic implications: Journal of Sedimentary Petrology, v. 61, no. 1, p. 102–110.

Cheel, R.J., and Leckie, D.A., 1993, Hummocky cross-stratification: Sedimentology Review, p. 103–122.

Clifton, H.E., 1976, Wave-formed sedimentary structures—a conceptual model, *in* Davis, R.A., and Ethington, R.L., eds., Beach and nearshore marine sedimentation: Tulsa, Oklahoma, Society of Economic Paleontologists and Mineralogists Special Publication 24, p. 126–148.

Crane, R.C., and Wiggins, V.D., 1976, Ipewick Formation, significant Jurassic-Neocomian map unit in northern Brooks Range foldbelt: American Association of Petroleum Geologists Bulletin, v. 60, no. 12, p. 2177.

Crowder, R.K., Adams, K.E., and Mull, C.G., 1994, Measured stratigraphic section of the Tingmerkpuk sandstone (Neocomian), western NPRA, Alaska: Division of Geological & Geophysical Surveys Public-Data File 94-29, 8 p., 1 sheet.

Dott, R.H., Jr., and Bourgeois, Joanne, 1982, Hummocky stratification; significance of its variable bedding sequences: Geological Society of America Bulletin, v. 93, no. 8, p. 663–680.

Duke, W.L., and Leckie, D.A., 1986, Origin of hummocky cross-stratification, part 2, paleo-hydraulic analysis indicates formation by orbital ripples within the wave-formed flat-bed field, *in* Knight, R.J., and McLean, J.R., eds., Shelf sands and sandstones: Calgary, Canadian Society of Petroleum Geologists Memoir 11, p. 339.

Grantz, Arthur, and May, S.D., 1982, Rifting history and structural development of the continental margin north of Alaska, *in* Watkins, J.S., and Drake, C.L., eds., Studies in Continental Margin Geology: American Association of Petroleum Geologists Memoir 34, p. 77–100.

Grantz, Arthur, and May, S.D., 1988, Regional geology and petroleum potential of the United States Chukchi shelf north of Point Hope, in Gryc, George, ed., Geology and exploration of the National Petroleum Reserve in Alaska, 1974 to 1982: U.S. Geological Survey Professional Paper 1399, p. 209–229.

Grantz, Arthur, May, S.D., and Hart, P.E., 1990, Geology of the Arctic Continental Margin of Alaska, *in* Grantz, Arthur, Johnson, L., and Sweeney, J.F, eds., The Arctic Ocean region—The geology of North America, v. L: Boulder, Colorado, Geological Society of America, p. 257–288.

Harms, J.C., 1979, Primary sedimentary structures: Annual Review of Earth and Planetary Sciences, v. 7, p. 227–248.

Harms, J.C., Southard, J.B., and Walker, R.G., 1982, Structures and sequences in clastic rocks: Tulsa, Oklahoma, Society of Economic Paleontologists and Mineralogists, SEPM Short Course Notes no. 9, variously paginated.

Higgs, Roger, 1991, The Bude Formation (Lower Westphalian), SW England: siliciclastic shelf sedimentation in a large equatorial lake: Sedimentology, v. 38, p. 445-469.

Higgs, Roger, 1998, Return of "The Fan That Never Was"—Westphalian turbidite systems in the Variscan Culm basin—Bude Formation (southwest England): Sedimentology, v. 45, no. 5, p. 961–975.

Hubbard, R.J., Edrich, S.P., and Rattey, R.P., 1987, Geologic evolution and hydrocarbon habitat of the "Arctic Alaska microplate," *in* Tailleur, I.L., and Weimer, Paul, eds., Alaskan North Slope geology: Bakersfield, Pacific Section, Society of Economic Paleontologists and Mineralogists, v. 50, p. 797–830.

Komar, P.D., Neudeck, R.H., and Kulm, L.D., 1972, Observations and significance of deep-water oscillatory ripple marks on the Oregon Continental Shelf, *in* Swift, D.P.J., Duane, D.B., and Pilkey, O.H., eds., Shelf sediment transport—process and pattern: Stroudsburg, Pennsylvania, Dowden, Hutchinson & Ross, p. 601–619.

Kreisa, R.D., 1981, Storm-generated sedimentary structures in subtidal marine facies with examples from the Middle and Upper Ordovician of southwestern Virginia: Journal of Sedimentary Petrology, v. 51, no. 3, p. 823–848.

Leckie, D.A., and Krystinik, L.F., 1989, Is there evidence for geostrophic currents preserved in the sedimentary record of inner to middle-shelf deposits?: Journal of Sedimentary Petrology, v. 59, no. 5, p. 862–870.

Masterson, W.D., and Paris, C.E., 1987, Depositional history and reservoir description of the Kuparuk River Formation, North Slope, Alaska, *in* Tailleur, I.L., and Weimer, Paul, eds., Alaskan North Slope geology: Bakersfield, Pacific Section, Society of Economic Paleontologists and Mineralogists, Field Trip Guidebook 50, p. 95–107.

Melvin, John, 1986, Upper Carboniferous fine-grained turbiditic sandstones from southwest England: a model for growth in an ancient, delta-fed subsea fan: Journal of Sedimentary Petrology, v. 56, no. 1, p. 19–34.

Mickey, M.B., Haga, Hideyo, and Mull, C.G., 1995, Paleontologic data; Tingmerkpuk sandstone and related units, northwestern DeLong Mountains, Brooks Range, Alaska: Division of Geological & Geophysical Surveys Public-Data File 95-31, 44 p.

Molenaar, C.M., 1988, Depositional history and seismic stratigraphy of Lower Cretaceous rocks in the National Petroleum Reserve in Alaska and adjacent areas, *in* Gryc, George, ed., Geology and exploration of the National Petroleum Reserve in Alaska, 1974 to

1982: U.S. Geological Survey Professional Paper 1399, p. 593–621.

Mount, J.F., 1982, Storm-surge-ebb origin of hummocky cross-stratified units of the Andrews Mountain Member, Campito Formation (Lower Cambrian), White-Inyo Mountains, eastern California: Journal of Sedimentary Petrology, v. 52, no. 3, p. 941–958.

Mull, C.G., 1987, Kemik Sandstone, Arctic National Wildlife Refuge, Northeastern Alaska, *in* Tailleur, I.L., and Weimer, Paul, eds., Alaskan North Slope Geology: Bakersfield, Pacific Section, Society of Economic Paleontologists and Mineralogists, Field Trip Guidebook 50, p. 405–431.

Mull, C.G., 1995, Preliminary evaluation of the hydrocarbon source rock potential of the Tingmerkpuk sandstone (Neocomian) and related rocks, northwestern DeLong Mountains, Brooks Range, Alaska: Division of Geological & Geophysical Surveys Public-Data File 95-30, 22 p.

Myrow, P.M., 1992, Bypass-zone tempestite facies model and proximality trends for an ancient muddy shoreline and shelf: Journal of Sedimentary Petrology, v. 62, no. 1, p. 99–115.

Myrow, P.M., and Southard, J.B., 1996, Tempestite deposition: Journal of Sedimentary Research, v. 66, no. 5, p. 875–887.

Posamentier, H.W., Jervey, M.T., and Vail, P.R., 1988, Eustatic controls on clastic deposition I—Conceptual framework, *in* Wilgus, C.K., Hastings, B.S., Ross, C.A., Posamentier, H.W., Van Wagoner, John, Kendall, C.G.St.C., eds., Sea-level changes—An integrated approach: Society of Economic Paleontologists and Mineralogists Special Publication 42, p. 109–124.

Prave, A.R., and Duke, W.L., 1990, Small-scale hummocky cross-stratification in turbidites—a form of antidune stratification: Sedimentology, v. 37, no. 3, p. 531–539.

de Raaf, J.F.M., Boersma, J.R., and van Gelder, A., 1977, Wave-generated structures and sequences from a shallow marine succession, Lower Carboniferous, County Cork, Ireland: Sedimentology, v. 24, no. 4, p. 451–483.

Reifenstuhl, R.R., 1995, Lithofacies, petrology, and petrophysics of the Kemik Sandstone (Lower Cretaceous), eastern Arctic Slope, Alaska, *in* Combellick, R.A., and Tannian, Fran, eds., Short notes on Alaska geology 1995: Fairbanks, Alaska, Division of Geological & Geophysical Surveys Professional Report 117, p. 53–67.

Reifenstuhl, R.R., Mull, C.G., and Wilson, M.D., 1997, Petrography of the Tingmerkpuk sandstone (Neocomian), northwestern Brooks Range, Alaska—a preliminary study, *in* Clough, J.G., and Larson, Frank, eds., Short notes on Alaska geology 1997: Division of Geological & Geophysical Surveys Professional Report 118, p. 111–124.

Schenk, C.J., and Bird, K.J., 1992, Depositional sequences in Lower Cretaceous rocks, Atigun syncline and Slope Mountain areas, Alaskan North Slope, *in* Dusel-Bacon, Cynthia, and Till, A.B., eds., Geologic Studies in Alaska by the U.S. Geological Survey, 1992: Washington, U.S. Geological Survey Bulletin 2068, p. 48–58.

Simons, D.B., Richardson, E.V., and Nordin, C.F., Jr., 1965, Sedimentary structures generated by flow in alluvial channels, *in* Middleton, G.V., ed., Primary sedimentary structures and their hydrodynamic interpretation—a symposium: Tulsa, Oklahoma, Society of Economic Paleontologists and Mineralogists, Special Publication, p. 34–52.

Swift, D.J.P., 1985, Response of the shelf floor to flow, *in* Tillman, R.W., Swift, D.J.P., and Walker, R.G., eds., Shelf sands and sandstone reservoirs: Tulsa, Oklahoma, Society of Economic Paleontologists and Mineralogists, Short Course 13, p. 135–241.

Van Wagoner, J.C., Mitchum, R.M., Campion, K.M., and Rahmanian, V.D., 1990, Siliciclastic sequence stratigraphy in well logs, cores, and outcrops—Concepts for high-resolution correlation of time and facies: American Association of Petroleum Geologists, Methods in Exploration Series, no. 7, 55 p.

Van Wagoner, J.C., 1995, Overview of sequence stratigraphy of foreland basin deposits—Terminology, summary of papers, and glossary of sequence stratigraphy, *in* Van Wagoner, J.C., and Bertram, G.T., eds., Sequence stratigraphy of foreland basin deposits—outcrops and subsurface examples from the Cretaceous of North America: American Association of Petroleum Geologists Memoir 64, p. ix–xxi.

Walker, R.G., 1985, Geological evidence for storm transportation and deposition on ancient shelves, *in* Tillman, R.W., Swift, D.J.P., and Walker, R.G., eds., Shelf sands and sandstone reservoirs: Tulsa, Oklahoma, Society of Economic Paleontologists and Mineralogists, Short Course 13, p. 243-302.

Walker, R.G., 1984, Shelf and shallow marine sands, *in* Walker, R.G., ed., Facies models (second edition), Geoscience Canada, p. 141–170.

Walker, R.G., Duke, W.L., Leckie, D.A., Dott, R.H., Jr., and Bourgeois, Joanne, 1983, Hummocky stratification—significance of its variable bedding sequences—discussion and reply: Geological Society of America Bulletin, v. 94, no. 10, p. 1245–1251.

STRATIGRAPHIC ARCHITECTURE OF THE UPPER JURASSIC–LOWER CRETACEOUS NUTZOTIN MOUNTAINS SEQUENCE, NUTZOTIN AND MENTASTA MOUNTAINS, ALASKA

Jeffrey D. Manuszak[1] and Kenneth D. Ridgway[1]

ABSTRACT

The Nutzotin Mountains sequence is a 2,000-m-thick sequence of predominantly siliciclastic deposits that filled the Upper Jurassic to Lower Cretaceous Nutzotin basin. The Nutzotin basin is part of a series of deformed sedimentary basins located between rocks representing the Mesozoic continental margin of western North America and rocks representing an assemblage of allochthonous terranes that were accreted to the continental margin. Twenty-one measured stratigraphic sections define three facies associations that we use to develop a stratigraphic framework for the Nutzotin basin. The stratigraphically lowest facies association (FA1) consists of a basal conglomerate with outsized limestone clasts capped by a thick sequence of black shale with minor red, calcareous mudstone and conglomerate. Outsized limestone clasts of FA1 are on the order of tens of meters in diameter. Paleoflow indicators from FA1 are to the northwest. The next facies association (FA2) forms the bulk of the sequence, and consists of interbedded siltstone and shale with subordinate amounts of channelized pebble conglomerate and sandstone. Greenstone, limestone, granite, and chert clasts are common in conglomerates of FA2. Paleoflow indicators from FA2 are to the east and northeast. The stratigraphically highest facies association (FA3) consists of fossiliferous mudstones that grade upward into an overlying volcanic sequence.

Stratigraphic correlation of the three facies associations throughout the Nutzotin basin shows the following general trends. FA1 is best developed along the southern margin of the Nutzotin basin. FA2 is the most widespread facies association and is especially well developed along the axis of the basin. FA3 is restricted to the southeastern margin of the basin and appears to be closely related to the overlying Chisana volcanic strata. We interpret the stratigraphic architecture defined for the Nutzotin basin to represent a basin configuration in which local coarse-grained submarine fan systems (FA1) prograded northward transverse to the axis of the basin. A large axial submarine fan system (FA2) transported mainly sand and mud eastward and filled a large part of the basin. FA3 represents the final stages of sedimentary deposition in the Nutzotin basin before the onset of widespread Chisana volcanism. This facies association was probably deposited on a shallow muddy shelf, rich in marine invertebrates, that flanked the growing Chisana volcanic arc in the southeastern corner of the Nutzotin basin.

INTRODUCTION

The accretion of allochthonous terranes to the Mesozoic continental margin of western North America was an important process in the growth of the North American continent (Coney and others, 1980; Burchfiel and others, 1992; Plafker and Berg, 1994; Nokleberg and others, 1994). Sedimentary basins that form coeval with accretionary events commonly contain a detailed record of accretionary processes (Lundberg and Dorsey, 1988; McClelland and others, 1992). For example, the discontinuous belt of Jurassic–Cretaceous sedimentary basins exposed from Washington to Alaska (fig. 1) records the collision, uplift, and denudation of allochthonous terranes with the North American margin (Rubin and Saleeby, 1991; McClelland and others, 1992; Cohen and others, 1995; Kapp and Gehrels, 1998). Unfortunately, most of the basinal strata within this belt are highly metamorphosed and structurally complex, thus the original depositional setting and structural configuration of the basins are unclear. The Nutzotin basin, one of the northernmost basins in the belt (fig. 1), however, has undergone only minor metamorphism (Berg and others, 1972; Richter, 1976; Kozinski, 1985). The deposits of the Nutzotin basin consist of at least 2 km of rhythmically bedded mudstone, siltstone, sandstone, conglomerate, and impure limestone (Berg and others, 1972) deposited in a submarine fan deposystem (Kozinski, 1985; Manuszak and others, 1998).

Our report is the first detailed stratigraphic analysis of the entire Nutzotin Mountains sequence. We present stratigraphic data from 21 measured sections throughout the Nutzotin and Mentasta mountains (fig. 2), which we use to develop a more complete basin-wide stratigraphic architecture. Development of a stratigraphic framework for the relatively undeformed Nutzotin Mountains sequence will provide a better understanding of the original basin configuration. Additionally it will serve as a template for analysis of correlative sedimentary basins (fig. 1) where the stratigraphy is more difficult to

[1]Department of Earth & Atmospheric Sciences, Purdue University, West Lafayette, Indiana 47907-1397.
Email for J.D. Manuszak: Manuszak@epicenter.eas.purdue.edu

delineate because of metamorphism and deformation.

GEOLOGIC SETTING

The Nutzotin Mountains sequence outcrops in the Nutzotin and Mentasta mountains of the eastern Alaska Range, southeastern central Alaska (fig. 2). The Denali fault separates the Nutzotin Mountains sequence from the parautochthonous Yukon–Tanana terrane to the north (fig. 2). The Yukon–Tanana terrane represents the dissected continental margin of North America (Richter and Jones 1973b, Hansen, 1990). Rocks of the Yukon–Tanana terrane consist of sparse orthogneiss of Late Proterozoic age; polymetamorphosed and polydeformed quartz-rich schist; pelitic schist; sparse marble of Precambrian, Devonian, and Mississippian age; and orthogneiss, augen gneiss, and intermediate to felsic volcanics of Late Devonian to Early Mississippian age (Plafker and Berg, 1994).

The southern boundary of the Nutzotin Mountains sequence is the Wrangellia member of the Wrangellia composite terrane (fig. 2), an allochthonous island arc with respect to western North America (Jones and others, 1986; Nokleberg and others, 1994; Plafker and Berg, 1994). The stratigraphy of the Wrangellia terrane near the study area includes: Pennsylvanian and Permian marine volcanic rocks of the Tetelna Formation; Lower Pennsylvanian and Lower Permian marine volcanic and sedimentary rocks of the Slana Spur and Station Creek Formations, Permian nonvolcanogenic limestone and argillite of the Eagle Creek and Hasen Creek Formations; Upper Triassic submarine and subaerial basalts and mafic intrusives of the Nikolai Greenstone; and calcareous sedimentary rocks and limestones of the Chitistone, Nizina, and McCarthy limestones (Nokleberg and others, 1994; Richter and Jones, 1973b; Plafker and Berg, 1994). The Nutzotin Mountains sequence lies both depositionally (Berg and others, 1972; Richter and Jones, 1973b) and in fault contact (Manuszak and others, 1998) with the Wrangellia composite terrane.

Depositionally overlying the Nutzotin Mountains sequence is the Chisana Formation (fig. 2) which consists primarily of interlayered andesitic flows and volcaniclastic

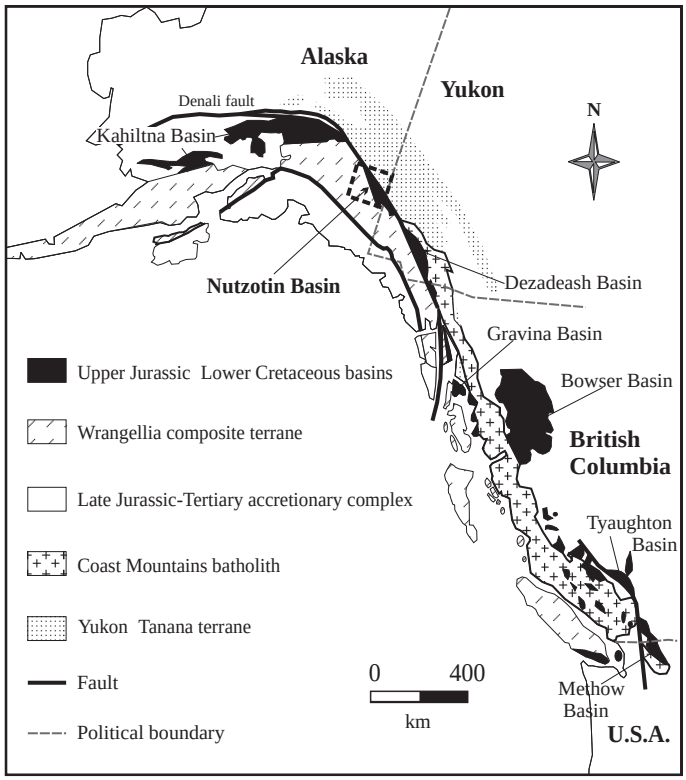

deposits that are up to 3,000 m thick (Berg and others, 1972). Crosscutting relationships with mid-Cretaceous plutons constrain the age of the Chisana Formation to post-Valanginian (Richter and Jones, 1973b). Berg and others (1972) note that the occurrence of the ammonite *Shasticrioceras* is indicative of a Barremian age (Early Cretaceous) for the Chisana Formation. Most of the volcaniclastic strata are interpreted to be deposited by massive submarine lahars and debris flows (Richter and Jones, 1973b). The volcanic flows are of transitional tholeiitic–calc–alkaline affinity (Barker, 1987). Unconformably overlying the Nutzotin Mountains sequence and the Chisana Formation are nonmarine conglomerates, sandstones, shales, and coals (Richter, 1971b; Richter and Jones, 1973). Abundant well-preserved floras suggest a Late Cretaceous age for these deposits (Richter and Jones, 1973).

Within and locally along the southern margin of the Nutzotin Mountains sequence, the Totschunda fault extends in a northwestern direction from Canada to its junction with the Denali fault (fig. 2). Displacement is dominantly dextral slip with offsets of as much as 4 km (Plafker and others, 1977). Initiation of faulting may have begun as late as 200–400 ka based on a slip rate of 1–2 cm/year (Plafker and others, 1977). The Denali fault, which borders the Nutzotin basin to the north, has a much longer history of displacement (Lanphere, 1977; Csejtey and others, 1982). Eisbacher (1976) and Lowey (1998) estimate 300–400 km of right-lateral displacement on the Denali fault based on the interpretation that the Nutzotin Mountains sequence is the offset equivalent of the Dezadeash basin found in northern Canada (fig. 1).

Figure 1 (left). *Generalized tectonic map showing the distribution of Upper Jurassic to Lower Cretaceous basins and surrounding terranes along the western margin of North America (modified from McClelland and others, 1992). The Upper Jurassic to Lower Cretaceous basins (black) include marine clastic strata and volcanic rocks. The Wrangellia composite terrane (diagonal dashed pattern) includes the Peninsular, Alexander, and Wrangellia terranes. The Coast Mountains batholith (cross pattern) includes the Skagit terrane. The Nutzotin basin is located along the Canada–Alaska border in the north-central part of the diagram. Area of geologic map shown on figure 2 is outlined by the dashed rectangle surrounding the Nutzotin basin.*

Figure 2 (below). *Generalized geologic map of the Nutzotin Mountains sequence within the Nabesna Quadrangle. Measured section locations are labeled and correspond to those found on figure 3. Geology is modified from Richter (1976). Scale = 1:250,000.*

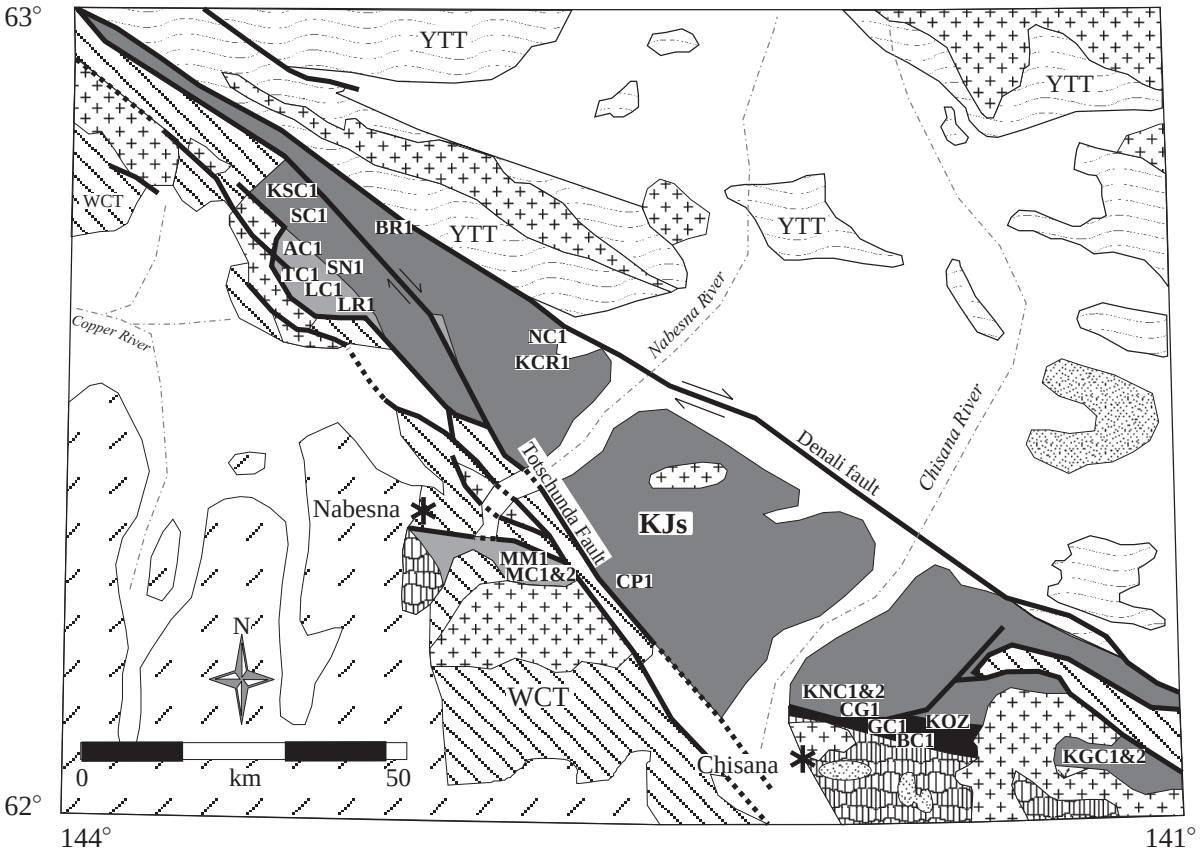

EXPLANATION

- Qa: Quaternary deposits
- QTv: Quaternary/Tertiary volcanic rocks
- Cretaceous Chisana volcanic rocks
- Cretaceous plutonic rocks
- KJs: Nutzotin Mountains sequence
  - Facies Association 1
  - Facies Association 2
  - Facies Association 3
- Tertiary-Cretaceous sandstone and conglomerate
- WCT: Wrangellia composite terrane
- YTT: Yukon-Tanana terrane

- Fault
- Inferred fault
- Contact
- River
- LC1 Location and name of measured section within the Nutzotin Mountains sequence
- Town

PREVIOUS RESEARCH

Previous studies of the Nutzotin Mountains sequence consist primarily of the initial regional geologic mapping (Richter, 1971; Richter and Schmoll, 1973; Richter, 1976 Lowe and others, 1982). These initial investigations divide the Nutzotin Mountains sequence into three mappable units: "upper," "middle," and "lower" (Richter, 1976). We use these divisions as a starting point to construct the stratigraphic framework for the Nutzotin Mountains sequence.

Previous tectonic interpretations for the formation of the Nutzotin basin include: (1) deposition in a rapidly subsiding long-linear-interarc (back-arc) basin within an ancient volcanoplutonic arc (Berg and others, 1972); (2) deposition within a back-arc or intra-arc basin that formed on top of the Wrangellia terrane (Kozinski, 1985); (3) "...sedimentation in large linear basins generally far behind the continental margin" (Richter and Jones, 1973b); and (4) evolution within or proximal to a regional, transtensional, basinal arc complex (McClelland and others, 1992). Our working hypothesis suggests that the Nutzotin basin formed as a flexural foredeep in response to the collision of the Wrangellia composite terrane with the North American continental margin (Manuszak and others, 1998).

FACIES ASSOCIATIONS

We have defined three facies associations (FA1, FA2, and FA3) within the Nutzotin Mountains sequence based on new stratigraphic data and previous work (Berg and others, 1972; Kozinski, 1985; Richter, 1976; and Richter and Jones, 1973b).

FACIES ASSOCIATION 1 (FA1)

The stratigraphically lowest facies association (FA1) is divided into two separate lithofacies. The first unit is a conglomerate with interbedded black shale and gray-green sandstone. The second unit consists of black shale with interbedded red, calcareous mudstone, and subordinate amounts of conglomerate.

CONGLOMERATE AND INTERBEDDED SHALE

The first lithofacies is up to 200 m thick and is best exposed in the MC1, MC2 and MM1 measured sections along the south-central margin of the basin, east of the town of Nabesna (figs. 2 and 3). The lowermost conglomerates in the first lithofacies have the following characteristics: (1) average bed thickness of ~1–1.5 m; (2) channelized geometries; (3) mainly limestone clasts with minor amounts of chert, argillite, and volcanic clasts; (4) both matrix- and clast-supported framework; and (5) average maximum particle size ranging from 6–29 cm. Outsized limestone clasts, exceeding 10 m in diameter (figs. 4A and 4B), are observed in measured section MM1 and south of Nabesna.

Conglomerates in the upper part of the first lithofacies have similar channelized geometries, but more commonly are clast-supported, have smaller average maximum particle sizes (6–8 cm), and contain more interbedded shale and sandstone than the lower conglomerates. The upper conglomerates also contain a wider range of clast types that include tuff, quartz, greenstone, limestone, plutonic rocks, argillite, and chert. Paleocurrent data collected from imbricated clasts within the upper conglomerates indicate northwestward paleoflow (measured section MM1; fig. 3).

The black shale and sandstone found between and commonly interbedded with the upper and lower conglomerates comprise 50 percent of the first lithofacies of FA1. The shale has horizontal laminations, but more commonly no structures are observed because of pervasive fractures. The black shale contains disarticulated bivalves, *Buchia,* in measured section MC2 and carbonaceous plant debris at the top of measured section MM1 (fig. 3). Throughout measured sections MM1, MC1, and MC2, gray-green porphyritic sills and dikes commonly intrude the shale. The interbedded sandstones have bed thicknesses that range from a few centimeters to a meter. Sandstones commonly display normal graded bedding, and isolated pebble- to cobble-sized conglomerate clasts. We interpret the first lithofacies of FA1 to represent proximal sedimentation in a submarine fan system (Manuszak and others, 1998).

BLACK SHALE AND RED, CALCAREOUS MUDSTONE

The second lithofacies of FA1 is at least 300 m thick and found in measured sections AC1, TC1, and LC1 (fig. 3). The strata is best exposed in measured section LC1 located in the northwestern corner of the basin, along the headwaters of Lost Creek (fig. 2). The black

Figure 3 (right). *Simplified and correlated stratigraphic sections from the Nutzotin Mountains sequence. Label at the top of each section corresponds to location on figure 2. Vertical placement of each section based on correlation of facies associations described in the text and direct projection along strike where possible. "??" = uncertain stratigraphic correlation. Horizontal placement of each section is based on its general location in figure 2. Measured section KOZ compiled from Kozinski (1985). Paleocurrent data (arrows) are representative of numerous measurements taken from a series of beds within a particular part of the section and indicate average flow direction. Types of sedimentary structures measured for paleocurrent data are discussed in text.*

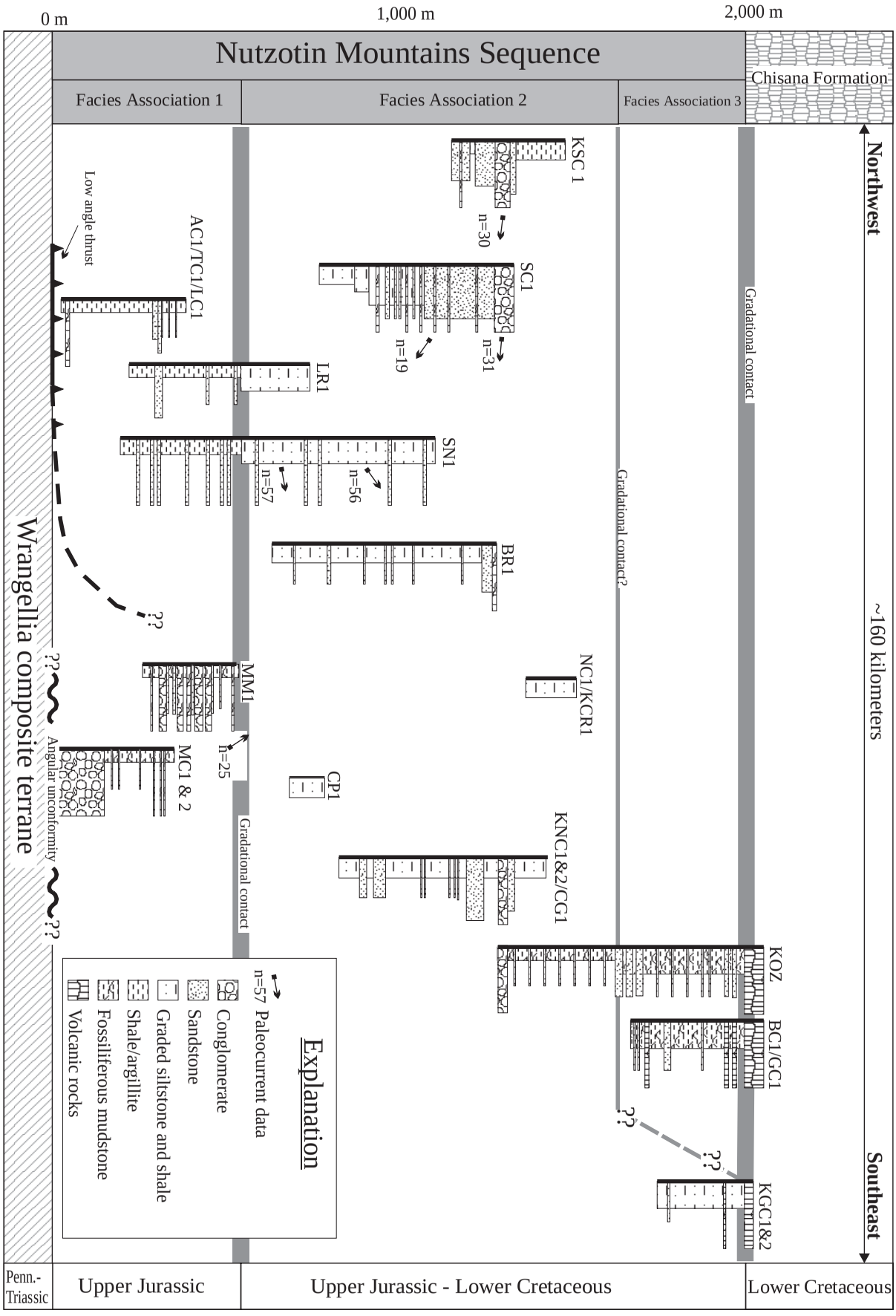
0 m
1,000 m
2,000 m
Nutzotin Mountains Sequence
Facies Association 1
Facies Association 2
Facies Association 3
Chisana Formation
Northwest
Southeast
~160 kilometers
Gradational contact
Gradational contact?
Low angle thrust
KSC 1
n=30
SC1
n=19
n=31
AC1/TC1/LC1
LR1
SN1
n=57
n=56
BR1
??
MM1
n=25
NC1/KCR1
CP1
KNC1&2/CG1
KOZ
BC1/GC1
KGC1&2
??
??
??
??
Angular unconformity
MC1 & 2
Gradational contact
Wrangellia composite terrane
Explanation
n=57 Paleocurrent data
Conglomerate
Sandstone
Graded siltstone and shale
Shale/argillite
Fossiliferous mudstone
Volcanic rocks
Penn.-Triassic
Upper Jurassic
Upper Jurassic - Lower Cretaceous
Lower Cretaceous

shale, which comprises the majority of this facies association, is commonly devoid of primary sedimentary structures and lacks macrofauna (fig. 4C). Faint subhorizontal laminations, however, are observed in a few of the coarser beds. Bioturbation is present throughout the black shale in the form of both horizontal and vertical burrows that are less than a few millimeters in diameter. The red calcareous mudstone beds are up to 30 cm thick (fig. 4C) and commonly display boudinage, lack internal sedimentary structure, and become less common toward the top of the unit. Locally, channelized conglomerates up to 10 m in width and a meter in thickness occur within the thick section of shale. The conglomerates are mostly matrix supported and consist predominantly of limestone clasts. Dikes and sills commonly intrude the shale. We interpret this lithofacies of FA1 to represent distal sedimentation on a submarine fan system.

AGE CONSTRAINT

The two lithofacies of FA1 correlate to map units Ja (Richter and Schmoll, 1973), Jcs (Richter, 1971), and "lower unit" (Richter, 1976). These map units are constrained by paleontologic data to be Late Jurassic (Tithonian–Oxfordian) in age (Richter and Schmoll, 1973; and Richter, 1971; Richter and Jones, 1973b).

FACIES ASSOCIATION 2 (FA2)

FA2 is divided into two lithofacies. The first lithofacies consists of alternating beds of laterally continuous shale, noncalcareous siltstone, and sandstone with subordinate amounts of light gray, calcareous siltstone (fig. 4D). The second lithofacies consists of massively bedded, laterally continuous, green sandstone (fig. 4E), and poorly sorted channelized conglomerate (fig. 4F).

INTERBEDDED SHALE, SILTSTONE, AND SANDSTONE

This lithofacies of FA2 is the most common in the basin. It is over 1,000 m thick and found in measured sections KSC1, SC1, BR1, NC1, KCR1, KNC1, KNC2, CP1, and CG1 (fig. 3). This lithofacies is well exposed throughout the basin, but is best exposed in measured section KCR1 (fig. 3) in the central part of the basin (fig. 2).

The coarser beds are comprised predominantly of medium- to fine-grained sandstone. Sedimentary features include normal grading (fig. 4G); ripple cross-stratification; horizontal stratification; fine, wispy mud laminations; and flute casts. Individual bed thickness ranges from less than a centimeter to half a meter. Rip-up clasts and pebble inclusions are common at the base of the sandstones. Paleocurrent data collected from ripple cross-stratification in the coarser units show flow to the east and northeast (measured section SC1; fig. 3).

The noncalcareous siltstones and shales contain horizontal laminations, horizontal and vertical burrows a few millimeters in width, strictly horizontal burrows up to 2 cm in width, and rip-up clasts. The calcareous siltstones commonly lack sedimentary structures and are highly fractured. The tops of the fine-grained beds are often scoured into and/or form an abrupt contact with the overlying coarser sandstone beds (fig. 4G). Locally, this unit is metamorphosed to argillite. We interpret the shales, siltstones, and sandstones of FA2 to represent sandy, low-density turbidite deposits of an outer submarine fan environment (Manuszak and others, 1998).

CONGLOMERATE AND SANDSTONE

The second lithofacies of FA2 is up to 300 m thick and is laterally continuous and interbedded with the first lithofacies of FA2. This stratum was documented in measured sections KNC1, KNC2, SC1, KSC1, and the top of BR1 (fig. 3). The best exposure of the second lithofacies of FA2 is along Suslota Creek in the northwestern part of the basin (measured section SC1; figs. 2, 3).

The sandstones are structureless, medium- to very coarse-grained, commonly contain pebbles and rip-up clasts, may display flute casts at the base of individual beds, and have an average bed thickness of 0.5–1 m (fig. 4E). The conglomerates are predominantly clast supported and poorly sorted (fig. 4F), but a few beds have matrix support. The clast-supported conglomerates have an average maximum particle size ranging from 5–20 cm, whereas the matrix-supported conglomerates have an average maximum particle size of ~5 cm. Both matrix- and clast-supported conglomerates contain greenstone, limestone, plutonic, and black chert clasts. Paleocurrent data collected from imbricated clasts and ripple stratification show paleoflow predominantly to the east and northeast (measured sections KSC1 and SC1; fig. 3). We interpret this unit of FA2 to represent gravelly and sandy high-density turbidite deposits of proximal and medial portions of a submarine fan environment (Manuszak and others, 1998).

AGE CONSTRAINT

The two units of FA2 correlate to map units Jg (Richter and Jones, 1973), KJms (Richter, 1971), KJg (Richter and Schmoll, 1973), KJs (Lowe and others, 1982; Richter and others, 1973, Richter and others, 1976), KJgc (Richter and Schmoll, 1973), and "middle unit" (Richter, 1976). The Jg and KJs units of Richter and Jones (1973) and Richter and others (1973), respectively, have been constrained with paleontologic data to be Late

Jurassic. The other units are loosely constrained by paleontologic data to be Late Jurassic (Tithonian) to Early Cretaceous (Valanginian) in age (Richter, 1976).

FACIES ASSOCIATION 3 (FA3)

FA3 consists of at least 300 m of fossiliferous mudstone with distinctive fossil-rich horizons (fig. 4H), minor interbedded sandstone, and andesitic flows (measured sections BC1, GC1, and KOZ; fig. 3). FA3 is best exposed at measured section BC1, located along Bonanza Creek, in the southeastern corner of the basin (fig. 2).

The fossiliferous mudstone is commonly poorly exposed, but abundant disarticulated and articulated *Buchia*, a bivalve, are observed. The mudstones also contain dewatering structures, laminations, rip-up clasts, and horizontal and vertical burrows. The distinctive fossil-rich horizons occur as both coquina (figs. 4I, 4J) and *in-situ* deposits of *Buchia*. The in-situ horizons consist of densely clustered articulated bivalve shells that are uniform in length (~4 cm down the long axis of the shell), and form 10–20-cm-thick beds that are laterally continuous at the outcrop scale. The coquina beds consist of fragmented shell hash that is fairly uniform in size. The beds range in thickness from a few centimeters to 0.75 m. Thin, laterally continuous coquina beds are interbedded with the in-situ fossil horizons. Thicker coquina beds range in thickness from 0.25–0.75 m and are channelized over a distance of 5 m. The channelized coquinas are generally structureless, but horizontal stratification was observed in a few channel tops. The channelized coquinas grade upward into fossiliferous mudstone and contain mudstone rip-up clasts up to 30 cm in length (fig. 4J). Internally, the rip-up clasts contain soft sediment deformation. Clasts of tuff, coalified wood fragments, and isolated pebbles are also observed in FA3 (measured section GC1; fig. 3).

The intercalated andesitic flows increase in abundance up-section within FA3. The green sandstones, located lower in FA3, are texturally and compositionally immature, and contain medium to coarse grains of sedimentary and volcanic lithics, shell fragments, feldspar, and quartz. The green sandstones range in thickness from less than a centimeter to 30 cm. We interpret FA3 to represent the last stages of sedimentary deposition in the Nutzotin basin before the onset of Chisana volcanism. This facies association was probably deposited on a muddy, fauna-rich shelf that flanked the embryonic Chisana volcanic arc that was building in the southeastern corner of the basin.

Age constraint

FA3 correlates to map units KJa (Richter and Jones, 1973) and "upper unit" (Richter, 1971). These map units are constrained by paleontologic data to be Late Jurassic (Tithonian) to Early Cretaceous (Valanginian) in age.

STRATIGRAPHIC CORRELATIONS

Twenty-one stratigraphic sections have been simplified and correlated on figure 3 to show our interpretation of the stratigraphic architecture of the Nutzotin Mountains sequence. The stratigraphic position of each measured section is based on correlation of facies associations and direct projection along strike where possible. This type of correlation permits only a rough approximation of the thickness for each facies association. Additional structural mapping and measured sections are required in several areas to allow for a better correlation of stratigraphic data.

AGE RELATIONSHIPS BETWEEN FACIES ASSOCIATIONS

The correlation diagram shown on figure 3 provides a general temporal relationship for the three facies associations. The age range from Oxfordian (Late Jurassic) to Barremian (Early Cretaceous) is based on sparse and poorly preserved species of *Buchia* (Richter, 1976; Richter, 1971; Richter, 1975; Richter and Jones, 1973; Richter and Jones, 1973b; and Berg and others, 1972). The broad and overlapping age ranges of *Buchia* in the Nutzotin basin suggest that, at times, the three facies associations were probably coeval, laterally equivalent lithofacies. Samples collected for palynologic analysis and radiometric age determinations during the 1998 field season will hopefully permit more accurate reconstruction of temporal and spatial relationships.

FACIES ASSOCIATION CONTACTS

Contact between Wrangellia and FA1

We have recognized a potentially basin-wide, low-angle thrust fault that separates much of the Nutzotin Mountains sequence from the underlying Wrangellia composite terrane (Manuszak and others, 1998). This relationship is well exposed in the northwestern Mentasta Mountains at measured sections AC1, TC1, and LC1 (figs. 2, 3). At measured section MC1, near the headwaters of the Nabesna River (fig. 2), the contact between FA1 and Wrangellia is an erosional unconformity (fig. 3). A similar depositional relationship can be seen directly south of Nabesna.

Contact between FA1 and FA2

Measured sections LR1 and SN1 (fig. 3) document a gradational contact between FA1 and FA2 in the northeastern central part of the basin (fig. 2). The gradational contact is characterized by a gradual loss of

Figure 4A. *Outsized limestone clast that is over 15 m in diameter found east of Nabesna at the base of Facies Association 1 (arrows point toward clast). Clast is surrounded by conglomerate and interbedded shale.*

Figure 4B. *Limestone megaclast located south of Nabesna in Facies Association 1. Person (black arrow) is standing on the gray limestone clast. Notice the interbedded shale (white arrow) and limestone conglomerates surrounding the megaclast.*

Figure 4C. *Outcrop of the fine-grained lithofacies of Facies Association 1 displaying interbedded, red calcareous mudstone. Arrow points to 30-cm-long hammer whose head is resting on the top of a calcareous mudstone bed.*

Figure 4D. *Outcrop of rhythmically interbedded siltstones, sandstones, and shales of Facies Association 2. This is the dominant lithofacies of the Nutzotin Mountains sequence. Individual bed thickness within photo ranges from 5 to 20 cm. Bedding is dipping to the left. Arrow points to hammer (30 cm) for scale.*

Figure 4E. *Outcrop of laterally continuous, thick-bedded, tabular, green sandstones of Facies Association 2. Bedding dips to the right in the photograph, which is looking along strike. Hammer for scale.*

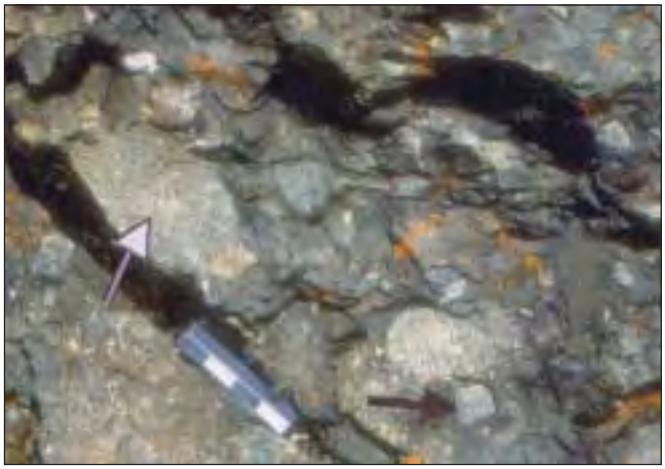

Figure 4F. *Close-up of poorly sorted conglomerate of Facies Association 2. White arrow points to large clast of granodiorite. Black arrow points to a clast of limestone. Scale in upper right is 8 cm long.*

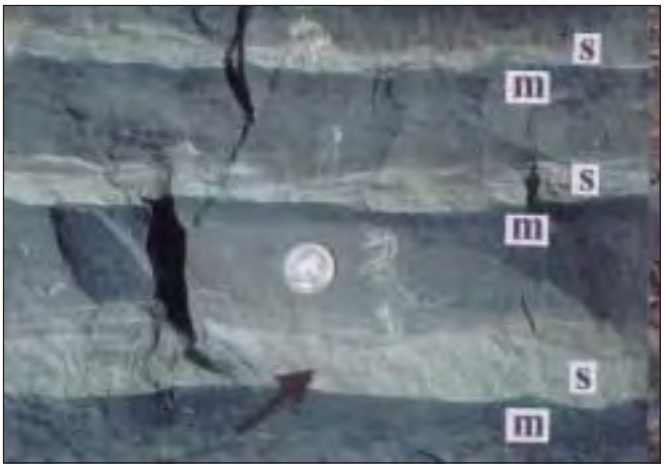

Figure 4G. *Close-up photo of graded beds within Facies Association 2 that show ripple cross-lamination (arrow) within a medium-grained sandstone, and normal grading. Notice sharp contacts of sandstone bases (s), which grade upward into mudstone (m). Coin for scale.*

Figure 4H. *Outcrop of Facies Association 3 showing interbedded sandstone and fossiliferous shale. White arrows point to individual sandstones.*

Figure 4I. *Coquina lithofacies of Facies Association 3 composed of bivalve fragments capped by a laminated grainstone. Coin for scale.*

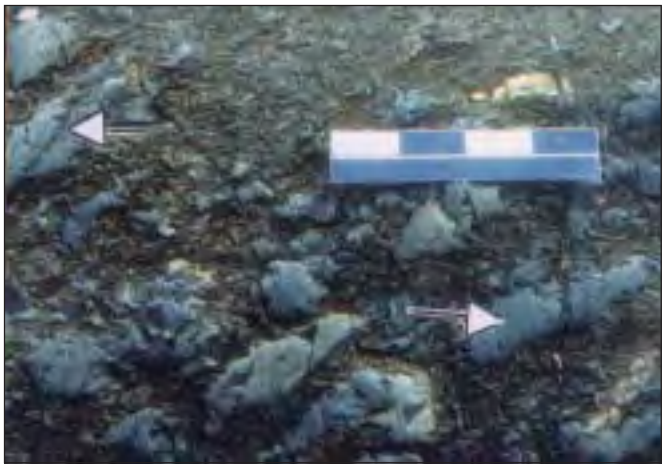

Figure 4J. *Close-up photo of fossil hash and mudstone rip-up clasts within a channel of Facies Association 3. Fossil hash is composed of disarticulated bivalve fragments. Arrows point to individual rip-up clasts. Scale is 8 cm long.*

red calcareous siltstone and a corresponding increase in interbedded noncalcareous siltstone and shale.

CONTACT BETWEEN FA2 AND FA3

Our measured sections from the 1998 field season did not include exposures that record the transition from FA2 to FA3. A previous measured stratigraphic section from the southeastern corner of the basin by Kozinski (1985), however, includes this contact (section KOZ; fig. 3). The gradational contact is marked by a decrease in bed thickness, and increase in grain size (Kozinski, 1985). This contact is exposed along Bonanza Creek, southwest of the town of Chisana (fig. 2).

CONTACT BETWEEN FA2/FA3 AND THE CHISANA FORMATION

Measured sections KOZ and BC1 document a gradational contact between FA3 and the Chisana Formation (fig. 3). The contact is characterized by an upsection increase in intercalated volcanic flows. In the southeastern part of the basin a gradational contact between FA2 and the Chisana Formation exists at measured section KGC1 and KGC2 (figs. 2, 3). The absence of FA3 in this part of the basin, and the gradational contact of both FA2 and FA3 with the Chisana Formation suggest that either FA3 was only deposited locally and pinches out to the southeast, and/or that FA2 and FA3 are spatially related coeval deposits. Continued fieldwork during the 1999 field season will address this specific issue.

IMPLICATIONS OF THE DISTRIBUTION OF FACIES ASSOCIATIONS

Facies Association 1 is restricted to the northwestern and central southern margin of the Nutzotin basin (fig. 2). The northwestern outcrops of Facies Association 1 consist of mudstone with localized lenticular conglomerate channels. FA1 exposed along the central southern basin margin consists of conglomerate containing marine macrofossils, coalified plant remains, and outsized limestone clasts. The lateral relationship between the two areas cannot be established by direct correlation because of the presence of several faults of unknown displacement. The two lithofacies have similar ages (Richter, 1971b; Richter and Jones, 1973); therefore we interpret the south-central outcrops of FA1 to represent proximal deposits of a submarine fan system. Paleocurrent data from these outcrops indicate northwestward sediment transport within the fan system. The finer-grained outcrops of FA1 exposed in the northwestern part of the basin are interpreted as more distal deposits of the same general submarine fan system.

Facies Association 2 is extremely thick (>1,000 m) and is common throughout the entire Nutzotin basin (fig. 2). The bulk of the coarse-grained deposits of Facies Association 2 are concentrated in the northwestern segment of the basin (measured sections SC1 and KSC1; fig. 3). To the southeast along the axis of the basin, there is a decrease in conglomerate and sandstone of FA2 and a corresponding increase in mudstone. The reduction in grain size along the axis of the basin, combined with paleocurrent data that indicate eastward paleoflow, suggest to us that FA2 represents a major axial submarine fan system that was responsible for filling a large part of the Nutzotin basin. Gravelly and sandy high-density turbidite deposits of FA2 from the northwestern part of the basin represent proximal and medial parts of the submarine fan system. Silty and muddy low-density turbidite deposits of the central and southeastern parts of the basin represent the distal parts of the submarine fan system.

Facies Association 3 is restricted to a local area within the southeastern part of the Nutzotin basin (fig. 2). The abundance of in-place and disarticulated fossils, occurrence of coalified plant debris, and channelized coquina beds

indicate a shallower marine environment of deposition than for FA1 and FA2. The upsection increase in intercalated volcanic flows suggests to us that FA3 is closely related to the overlying Chisana Formation. We interpret FA3 to represent the last stages of sedimentary deposition in the Nutzotin basin before the onset of widespread Chisana volcanism. This facies association was probably deposited on a shallow muddy shelf, rich in marine invertebrates, that flanked the growing Chisana volcanic arc in the southeastern corner of the Nutzotin basin.

ACKNOWLEDGMENTS

We thank the Wrangell–St. Elias National Park and Preserve staff, especially Danny Rosenkrans, for their help and support of our field activities. We also thank Don Richter for encouragement and discussions on the Nutzotin Mountains sequence. Brian Lareau and Mike De Persia provided assistance in our field operations. Acknowledgment is made to the donors of the Petroleum Research Fund, administered by the American Chemical Society, for support of this research. Partial support for this research was provided by the Geological Society of America's John T. Dillon grant, American Association of Petroleum Geologist's Fred A. Dix grant, Purdue University's Linda Horn Memorial Scholarship and Andrews Fellowship, Sigma Xi's Alexander Bache Fund, and the Society of Petroleum Engineers. We thank reviewers George Gehrels and Don Richter for improving this manuscript.

REFERENCES

Barker, Fred, 1987, Cretaceous Chisana island arc of Wrangellia, eastern Alaska: Geological Society of America Abstracts with Programs, v. 19, p. 580.

Berg, H.C., Jones D.L., and Richter, D.H., 1972, Gravina–Nutzotin belt—tectonic significance of an upper Mesozoic sedimentary and volcanic sequence in southern and southeastern Alaska: U.S. Geological Survey Professional Paper 800-D, p. D1–D24.

Burchfiel, B.C., Cowan, D.S., and Davis, G.A., 1992, Tectonic overview of the Cordilleran orogen in the western United States, *in* Burchfiel, B.C., Lipman, P.W., and Zoback, M.L., eds, The Geology of North America—The Cordilleran Orogen, Conterminous U.S.: Geological Society of America, v. G-3, p. 407-479.

Cohen, H.A., Hall, C.M., and Lundberg, Neil, 1995, $^{40}Ar/^{39}Ar$ dating of detrital grains constrains the provenance and stratigraphy of the Gravina belt, southeastern Alaska: Journal of Geology, v. 103, p. 327-337.

Coney, P.J., Jones, D.L., and Monger, J.W.H., 1980, Cordilleran suspect terranes: Nature, v. 288, p. 329-333.

Csejtey, B., Jr., Cox, D.P., Evarts, R.C., Stricker, G.D., and Foster, H.L., 1982, The Cenozoic Denali fault system and the accretionary development of southern Alaska: Journal of Geophysical Research, v. 87, p. 3,741-3,754.

Eisbacher, G.H., 1976, Sedimentology of the Dezadeash flysch and its implications for strike-slip faulting along the Denali fault, Yukon Territory and Alaska: Canadian Journal of Earth Sciences, v. 13, p. 1,495-1,513.

Hansen V.L., 1990, Yukon–Tanana terrane: A partial acquittal: Geology, v. 18, p. 365–369.

Jones, D.L., Silberling, N.J., and Coney, P.J., 1986, Collisional tectonics in the Cordillera of western North America: examples from Alaska, *in* Coward, M.P., and Ries, A.C., eds., Collisional Tectonics: London, United Kingdom, Geological Society of London Special Publication, v. 19, p. 367-387.

Kapp, P.A., and Gehrels, G.E., 1998, Detrital zircon constraints on the tectonic evolution of the Gravina belt, southeastern Alaska: Canadian Journal of Earth Sciences, v. 35, p. 253–268.

Kozinski, J., 1985, Sedimentology and tectonic significance of the Nutzotin Mountains sequence, Alaska: Albany, New York, State University of New York at Albany, Master's Thesis, 132 p.

Lanphere, M.A., 1978, Displacement history of the Denali fault system, Alaska and Canada: Canadian Journal of Earth Sciences, v. 15, p. 817–822.

Lundberg, N., and Dorsey, R.J., 1988, Synorogenic sedimentation and subsidence in a Plio-Pleistocene collisional basin, eastern Taiwan. *in* Kleinspehn, K.L., and Paola, C., eds., New Perspectives in Basin Analysis: New York, Springer-Verlag, p. 265–280.

Lowe, P.C., Richter, D.H., Smith, R.L., and Schmoll, H.R., 1982, Geologic map of the Nabesna B-5 quadrangle, Alaska: U.S. Geological Survey Map GQ-1566, 1 sheet, scale 1:63,360.

Lowey, G.W., 1998, A new estimate of the amount of displacement on the Denali fault system based on the occurrence of carbonate megaboulders in the Dezadeash Formation (Jura-Cretaceous), Yukon, and the Nutzotin Mountains Sequence (Jura-Cretaceous), Alaska: Bulletin of Canadian Petroleum Geology, v. 46, p. 379–386.

Manuszak, J.D., Ridgway, K.D., and Lareau, B.L., 1998, Stratigraphic architecture of a collisional basin, Nutzotin Mountains sequence, Alaska Range, south central Alaska: Geological Society of America Abstracts with Programs, v. 30, p. 338.

McClelland, W.C., Gehrels, G.E., and Saleeby, J.B., 1992, Upper Jurassic–Lower Cretaceous basinal strata along the Cordilleran margin: implications for the accretionary history of the Alexander–Wrangellia–Peninsular Terrane: Tectonics, v. 11, p. 823–835.

Nokleberg, W.J., Plafker, George, and Wilson, F.H., 1994, Geology of south-central Alaska, *in* Plafker, George, and Berg, H.C., eds., The Geology of Alaska: The Geology of North America, Geological Society of America, v. G-1, p. 311–366.

Plafker, George, and Berg, H.C., 1994, Overview of the geology and tectonic evolution of Alaska, *in* Plafker, George, and Berg, H.C, eds., The Geology of Alaska: The Geology of North America, Geological Society of America, v. G-1, p. 989–1,021.

Plafker, George, Hudson, T., and Richter, D.H., 1977, Preliminary observations on late Cenozoic displacements along the Totschunda and Denali fault systems: U.S. Geological Survey Circular 751-b, p. B67–B69.

Richter, D.H., 1971, Reconnaissance geologic map and section of the Nabesna A-3 quadrangle, Alaska: U.S. Geological Survey Map I-655, scale 1:63,360.

———1971b, Reconnaissance geologic map and section of the Nabesna B-4 quadrangle, Alaska: U.S. Geological Survey Map I-656, scale 1:63,360.

Richter, D.H., 1975, Reconnaissance geologic map of the Nabesna B-3 quadrangle, Alaska: U.S. Geological Survey Map I-904, scale 1:63,360.

———1976, Geologic map of the Nabesna quadrangle, Alaska: U.S. Geological Survey Map I-932, scale 1:250,000.

Richter, D.H., and Jones, D.L., 1973, Reconnaissance geologic map of the Nabesna A-2 quadrangle, Alaska: U.S. Geological Survey Map I-749, scale 1:63,360.

Richter, D.H., and Jones, D.L., 1973b, Structure and stratigraphy of eastern Alaska Range, Alaska: Tulsa, Oklahoma, American Association of Petroleum Geologists Memoir, v. 19, p. 408–420.

Richter, D.H., Matson, N.A., Jr., and Schmoll, H.R., 1973, Geologic map of the Nabesna A-1 quadrangle, Alaska: U.S. Geological Survey Map I-807, scale 1:63,360.

———1976, Geologic map of the Nabesna C-4 quadrangle, Alaska: U.S. Geological Survey Map GQ-1303, scale 1:63,360.

Richter, D.H., and Schmoll, H.R., 1973, Geologic map of the Nabesna C-5 quadrangle, Alaska: U.S. Geological Survey Map GQ-1062, scale 1:63,360.

Rubin, C.M., and Saleeby, J.B., 1991, The Gravina sequence: Remnants of a mid-Mesozoic oceanic arc in southern Southeast Alaska: Journal of Geophysical Research, v. 96, p. 14,551–14,568.

STRATIGRAPHY, DEPOSITIONAL SYSTEMS, AND AGE OF THE TERTIARY WHITE MOUNTAIN BASIN, DENALI FAULT SYSTEM, SOUTHWESTERN ALASKA[1]

Kenneth D. Ridgway,[2] Jeffrey M. Trop,[2,3] and Arthur R. Sweet[4]

ABSTRACT

The White Mountain strike-slip sedimentary basin is located adjacent to the Farewell segment of the Denali fault system in southwestern Alaska. A detailed stratigraphic section from the basin documents three main lithofacies. The lithofacies, in order of abundance, include (1) granule and pebble conglomerate; (2) massive and trough cross-stratified sandstone; and (3) mudstone. The conglomerates and sandstones contain evidence of stream-flow processes such as clast support, imbrication, crude upward-fining trends, trough cross-stratification, and unimodal paleocurrent indicators. Paleocurrent data indicate that the exposed strata of the White Mountain basin were deposited predominantly by west-flowing fluvial systems. Palynological analyses indicate that deposition in the White Mountain basin occurred during the late Oligocene and possibly into the earliest Miocene. We interpret the White Mountain basin to be time-correlative to other Oligocene strike-slip basins along the eastern and central parts of the Denali fault system such as the McGrath, Talkeetna, Burwash, and Bates Lake basins. Our correlation suggests that the Oligocene was an important time for strike-slip displacement and basin development along much of the ~2,000 km length of the fault system.

INTRODUCTION

The Denali fault system is one of the major fault systems of the northern Cordillera, extending more than 2,000 km from British Columbia to southwestern Alaska (fig. 1; Grantz, 1966; Lanphere, 1978; Dodds, 1995). Although previous studies have demonstrated that strike-slip displacement along the fault system is probably post-Early Cretaceous (Dodds, 1995), a more precise age of displacement is lacking. The amount of offset along the Denali fault system is also controversial, with estimates ranging from 0 to 450 km (see Lowey, 1998, for review). One potential data set that has been underutilized in analyzing the history of the Denali fault system is the Mesozoic and Cenozoic sedimentary basins that outcrop adjacent to the fault system (for example, Eisbacher, 1976; Nokleberg and others, 1985; Cole and others, 1996, 1999; Ridgway and others, 1997; fig. 1). A regional stratigraphic and geochronologic database of all the basins along the fault system has the potential to better define timing of displacement, and to determine if individual basins have been offset by the fault and can serve as markers to calculate fault displacement. This paper presents the first detailed stratigraphic, sedimentologic, and geochronologic data from sedimentary strata that crop out for over 15 km along the Farewell segment of the Denali fault system in southwestern Alaska. These strata are informally named the White Mountain basin (figs. 1, 2).

One catalyst for this study was to test a hypothesis that strata of the White Mountain basin, exposed on the south side of the Denali fault system in southwestern Alaska, are offset equivalents to strata of the lower Cantwell Formation (Late Cretaceous) in the Cantwell basin, exposed on the north side of the Denali fault in the central Alaska Range (fig. 1). Sainsbury (1965) was the first to tentatively interpret the White Mountain basin deposits as time-correlative to the lower Cantwell Formation. His correlation, however, was based solely on lithologic similarities. Our study uses palynological analysis to determine if the White Mountain basin deposits are time-correlative with the lower Cantwell Formation. A recent palynological analysis of the lower Cantwell Formation has shown it to be Late Cretaceous (Ridgway and others, 1997) but a similar analysis has not been reported from strata of the White Mountain basin. Our study also presents a measured stratigraphic section from the White Mountain basin for comparison with the stratigraphy of the Cantwell basin (Trop, 1996; Ridgway and others, 1997). Stratigraphic data were collected to determine if the two basins had similar depositional histories and were possibly offset-equivalents. If the basins are offset-equivalents, about 350 km of dextral displacement would be required along the western part of the Denali fault system, a value similar to estimates of offset along the eastern part of the fault system (Eisbacher, 1976; Plafker and Berg, 1994).

Another previous mapping study (Gilbert, 1981) assigned a Tertiary age to the White Mountain basin deposits because of their lithologic similarity to the

[1]Geological Survey of Canada Contribution No. 1998218.
[2]Department of Earth and Atmospheric Sciences, Purdue University, West Lafayette, IN 47907-1397.
Email for Kenneth D. Ridgway: ridge@omni.cc.purdue.edu
[3]Present address: Department of Geology, Bucknell University, Lewisburg, PA 17837.
[4]Geological Survey of Canada, Calgary, Alberta T2L 2A7, Canada.

Usibelli Group (Wahrhaftig and others, 1969; Wahrhaftig, 1987). The Usibelli Group is exposed north of the central Alaska Range in the Usibelli basin (fig. 1). The Usibelli Group ranges in age from Late Eocene to Miocene, but most of the deposits are Miocene (Wahrhaftig and others, 1969; Leopold and Liu, 1994). At the type section, for example, the entire Usibelli Group (about 585 m) is Miocene (Leopold and Liu, 1994).

This paper presents new geochronologic, sedimentologic, and paleocurrent data from surface exposures of the White Mountain basin. Our analysis allows comparison of timing of deposition in the White Mountain basin to Late Cretaceous development of thrust-top basins (Cantwell basin on fig. 1; Ridgway and others, 1997), Eocene-Oligocene strike-slip basins (Burwash and Bates Lake basins; Ridgway and DeCelles, 1993a, b), and Miocene foreland basins (Usibelli Group; Ridgway and others, 1998, 1999) of southern Alaska and northwestern Canada.

STRATIGRAPHY AND DEPOSITIONAL SYSTEMS

Our stratigraphic and sedimentologic data from the White Mountain basin are from a 440 m detailed measured stratigraphic section (fig. 3) located in the northeastern corner of the basin (fig. 2). The basal contact between deposits of the White Mountain basin and underlying rocks is not exposed, and the top of the section is eroded; therefore the original thickness of the basin fill cannot be determined. The measured section at White Mountain is dominated by three main lithofacies, which are, in order of abundance: (1) granule and pebble conglomerate; (2) massive and trough cross-stratified sandstone; and (3) mudstone.

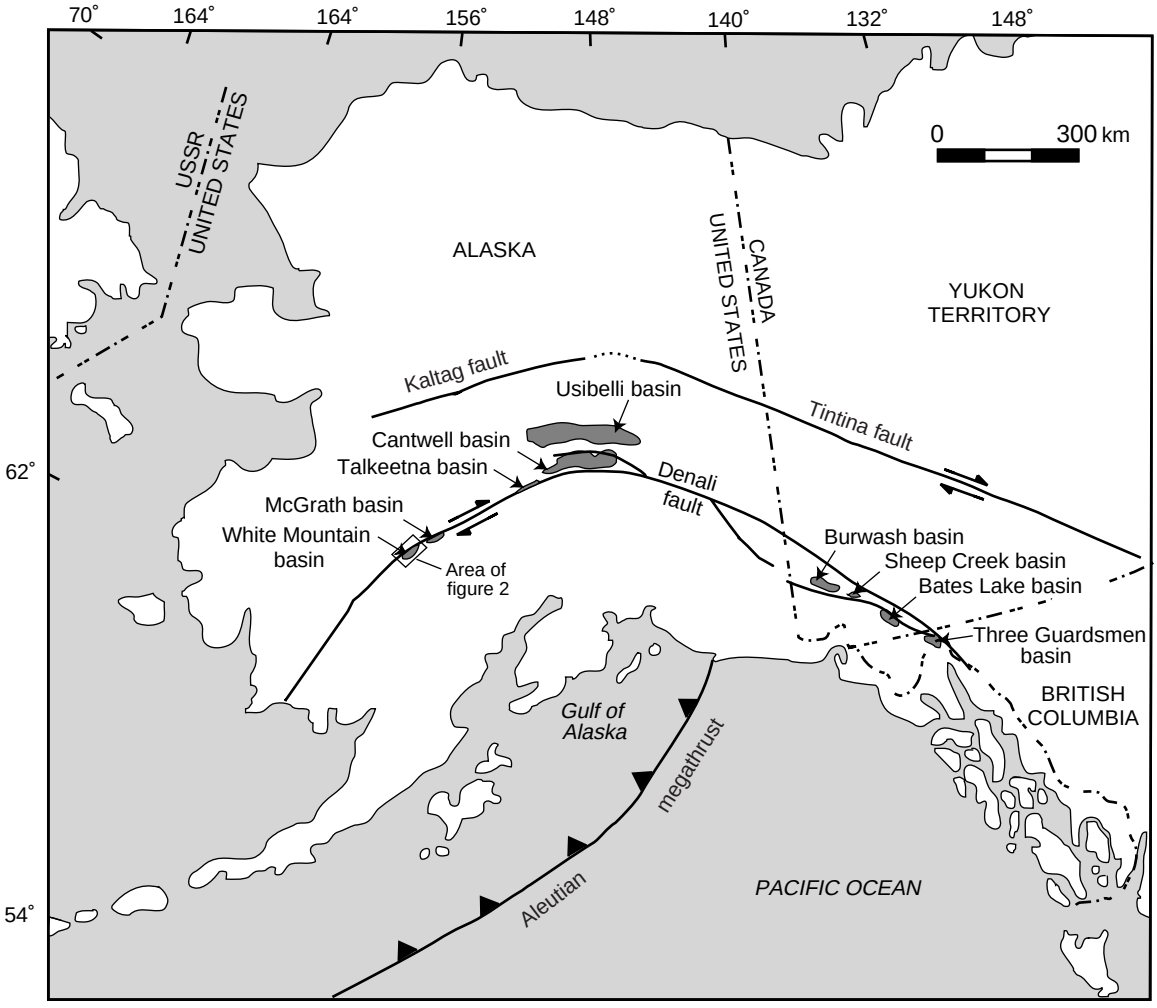

Figure 1. *Map of the Denali fault system in British Columbia, Yukon Territory, and Alaska showing the location of sedimentary basins (dark gray shaded areas). The Sheep Creek and Three Guardsmen strike-slip basins are not discussed in the text, but their locations are shown.*

LITHOFACIES 1 – GRANULE AND PEBBLE CONGLOMERATE

Clast-supported, granule and pebble conglomerate is the dominant lithofacies in the White Mountain basin measured section (figs. 3, 4). Conglomerates are medium- to thick-bedded, are well sorted, and contain rounded clasts (fig. 5A). Average maximum clast size in the conglomerate is 5 cm (figs. 3, 5B). Common clast types in the conglomerates are quartz, argillite, and chert (fig. 3). Lenticular sandstones (less than 50 cm thick) are commonly interbedded within the conglomerates. Where Lithofacies 1 is best exposed in our measured section (for example, 12.5 to 18 m and 34 to 40 m on fig. 3), it consists of upward-fining sequences that have a lower 1- to 4-m-thick conglomerate unit capped by a 0.5- to 1-m-thick massive sandstone. Few sedimentary structures were recognized in Lithofacies 1, but clast imbrication is present. At five different stratigraphic positions in the section, we measured 10 imbricated clasts from a single conglomerate bed to determine paleocurrent direction. The stratigraphic position of these measurements and restored paleocurrent orientations are shown on figure 3. The measurements indicate an overall westward paleoflow.

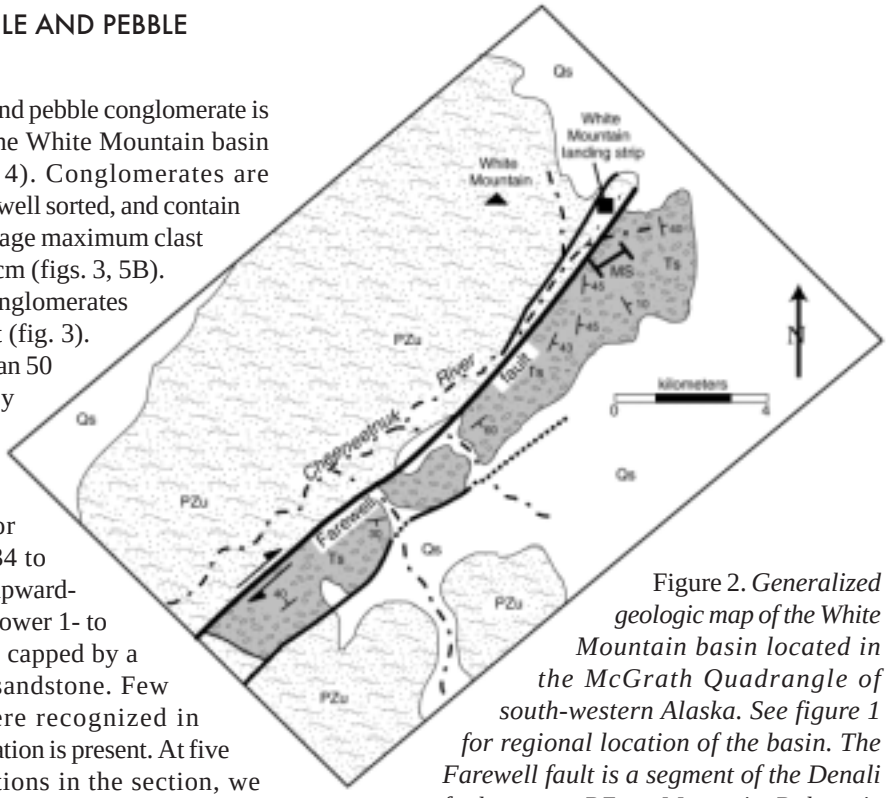

Figure 2. *Generalized geologic map of the White Mountain basin located in the McGrath Quadrangle of south-western Alaska. See figure 1 for regional location of the basin. The Farewell fault is a segment of the Denali fault system. PZu = Mesozoic–Paleozoic rocks of the Farewell terrane and White Mountain sequence (Decker and others, 1994); Ts = sedimentary strata of the White Mountain basin; Qs = Quaternary deposits. MS = location of measured stratigraphic section shown on figure 3. Geology and structural data from Gilbert (1981).*

LITHOFACIES 2 – MASSIVE AND TROUGH CROSS-STRATIFIED SANDSTONE

Lithofacies 2 consists mainly of massive, coarse- to medium-grained sandstone with maximum bed thicknesses of ~6 m. Trough cross-stratification was documented in some units but other sedimentary structures are uncommon. Conglomerate lags and lenses are common in Lithofacies 2.

LITHOFACIES 3 – MUDSTONE

Lithofacies 3 consists of poorly exposed mudstone that was best studied by trenching. Most of the lithofacies consists of alternating thin beds (less than 15 cm) of siltstone and shale. Plant fragments were documented in this lithofacies. Samples for palynological analysis were collected from this lithofacies (table 1).

Table 1. *Type and abundances of pollen and miospores*

Species	Percentage of Sample		
	155 m	330 m	387 m
Gymnosperm pollen			
T/C/T[a]	65.2	83.1	42.0
Bisaccate	6.5	3.1	21.0
Tsuga	3.3	0.8	2.1
Miospores			
Laevigatosporites	11.4	4.6	8.4
Lycopodium	0.0	0.0	0.4
Cyathidites	0.0	0.0	0.4
Angiosperm pollen			
Alnus	8.2	5.8	19.3
Betulacae	3.3	2.3	5.5
Pterocarya	0.0	0.0	0.4
Tricolpate	0.0	0.0	0.4
Total Number of Taxa Counted	**230**	**254**	**238**

[a]T/C/T = Taxodiaceae/Cupressaceae/Taxaceae

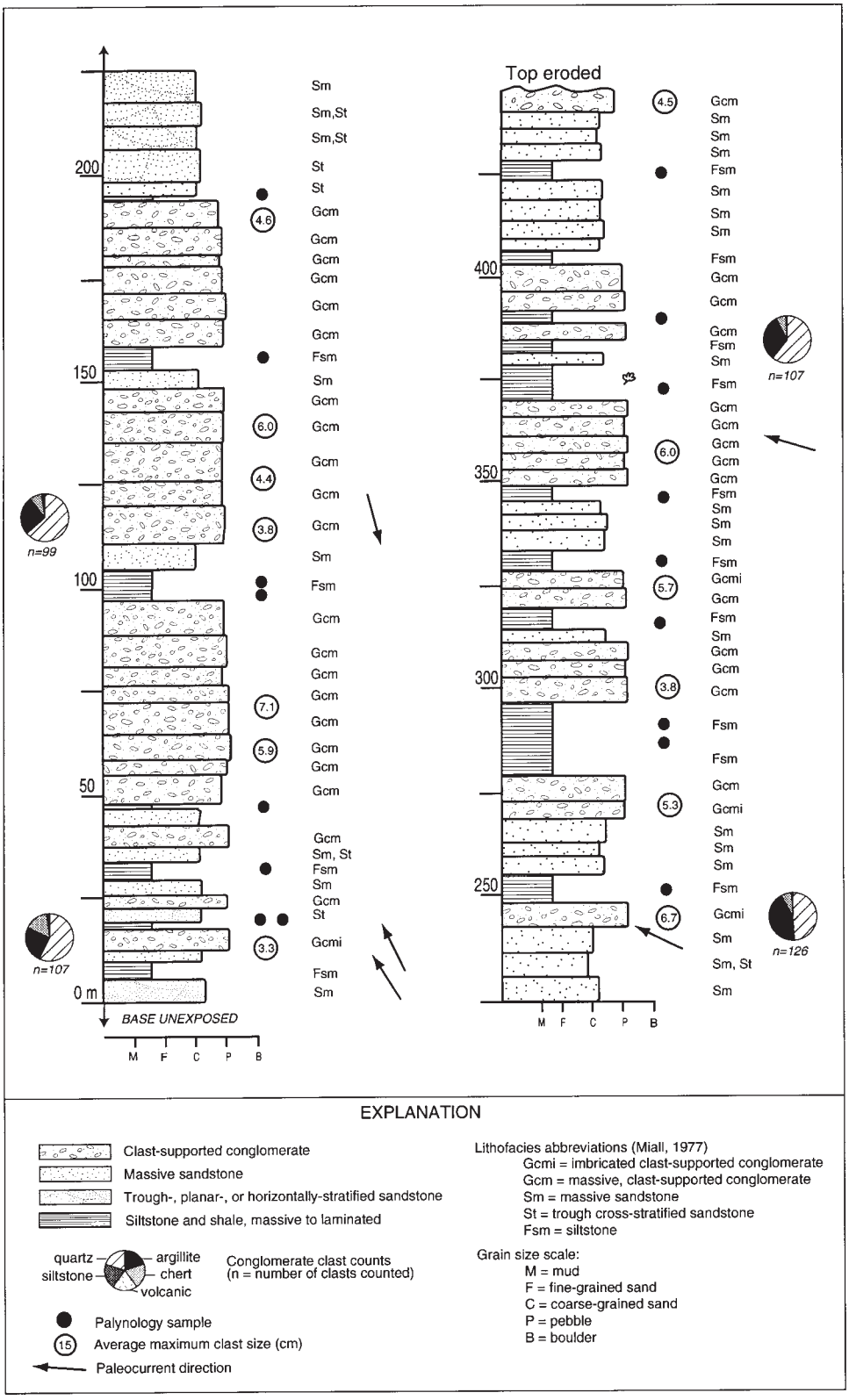

Figure 3. *Measured stratigraphic section of the White Mountain basin showing lithofacies in the northeastern part of the basin. Vertical scale is in meters. Each arrow represents restored paleocurrent direction based on mean measurement of ten imbricated conglomerate clasts. See figure 2 for location of measured section.*

Figure 4. *Typical outcrops of the White Mountain basin. Beds are dipping about 45° southeast (to the left in the photo). Conglomerates and sandstones of Lithofacies 1 and 2 form resistant along-strike ridges. Recessive grassy layers are mudstones of Lithofacies 3. Trace of the Farewell fault is in the large valley between the outcrops and the man. Stratigraphic section shown in figure 3 was measured in this area.*

Figure 5A. *Granule and pebble conglomerate of Lithofacies 1. Lichens cover the lower right part of the outcrop. Hammer is 28 cm long.*

Figure 5B. *Close-up of clast-supported conglomerate of Lithofacies 1. Pen is about 14 cm long.*

DEPOSITIONAL SYSTEMS INTERPRETATION

We interpret the White Mountain basin strata as having been deposited predominantly by fluvial depositional systems. The conglomerates (Lithofacies 1) and sandstones (Lithofacies 2) contain evidence of stream-flow processes including clast support, imbrication, crude upward-fining trends, trough cross-stratification, and fairly unimodal paleocurrent indicators. Lithofacies 1 and 2 appear similar to lithofacies described for modern low-sinuosity stream systems where gravel and sand are transported as bedload and deposited on longitudinal bars and within channels (Rust, 1978; Collinson, 1986). The laterally discontinuous lenses of sandstone within conglomerates of Lithofacies 1 were probably deposited in shallow channels on bar tops and along the flanks of bars during falling-stage and low-stage flows (Miall, 1977).

The mudstones of Lithofacies 3 require low energy depositional processes with a large component of suspension fallout. Suspension fallout within the proposed fluvial deposystem probably occurred mainly in overbank areas where flood water underwent a sudden decrease in velocity or where sediment entered ponded areas within the basin. A fluvial overbank interpretation for Lithofacies 3 is consistent with the presence of plant megafossils, a lack of marine megafossils, and the absence of marine microfossils (checked for during palynological analyses).

AGE

The age of the White Mountain basin deposits has been unclear due to a lack of age data. Previous studies have interpreted the age of the White Mountain strata as Early Cretaceous (Sainsbury, 1965) or Tertiary (Gilbert, 1981) on the basis of regional lithologic correlations. To better constrain the age of the White Mountain basin, palynological analyses were conducted by one of us (ARS) on 17 mudstone samples collected from our measured stratigraphic section. Locations of samples are shown on figure 3. Table 1 shows counts from the three best preserved assemblages recovered from the stratigraphic section (155, 330, and 387 m). Similar palynoflora are present in all 17 of the samples over the entire 440 m of measured section.

Palynological analyses indicate that strata of the White Mountain basin were most likely deposited during the late Oligocene or earliest Miocene. The age interpretation is based on the following arguments. The presence of *Alnus*, *Pterocarya*, and *Tsuga*, of modern aspect, restricts the age to being within the range of Eocene to Miocene or possibly early Pliocene (table 1). The persistent absence of *Pistillipollenites* and a wide range of warm temperate taxa (*Fagus*, *Liquidambar*, *Quercus*, and *Tilia*) further restricts the age to within the range of Oligocene to possibly early Pliocene. The apparent absence of *Parviprojectus* makes it unlikely that the samples are of early Oligocene age. When compared to the late early Miocene Upper Ramparts Canyon organic bed 1 in central Alaska, which is dominated by bisaccates with relatively low Taxodiaceae/Cupressaceae/Taxaceae counts (White and Ager, 1994), our data does not compare well (table 1). Deposition during the late early Miocene is, therefore, unlikely (J.M. White, written commun., 1996). The low diversity and the lack of thermophilous taxa in the White Mountain basin samples (even in the three best preserved assemblages; table 1) eliminate the warm interval within the middle Miocene (White and others, 1997). The lack of herbs (Cyperaceae, *Ambrosia*, Poaceae, other Asteraceae, Polemoniaceae) probably eliminates the late Miocene–Pleistocene (White and others, 1997).

In addition to the constraints stated above, the abundance of *Picea* and *Tsuga*, the dominance of *Alnus* in the angiosperm component, the less frequent presence of *Pterocarya*, and the possibly rare occurrence of *Juglans*, suggest that the late Oligocene or earliest Miocene is the most probable age for the assemblage—a time of relatively cool but moist climate (Wolfe, 1986; J.M. White, written commun., 1996). Similar assemblages are present in the youngest strata of the Oligocene Amphitheatre Formation, Burwash basin, Canada, but they contain *Parviprojectus* (Ridgway and others, 1995). Our preferred age interpretation for the exposed strata of the White Mountain basin, then, is late Oligocene possibly extending into the earliest Miocene.

DISCUSSION

This study shows that the deposits of the White Mountain basin along the Farewell segment of the Denali fault system in southwestern Alaska were deposited by fluvial deposystems during the late Oligocene and possibly into the earliest Miocene. The major fluvial system probably entered the basin from the east and deposited sediment as it flowed westward along the axis of the White Mountain basin. The late Oligocene or earliest Miocene fluvial system may have been part of a regional drainage system that flowed west-southwestward, possibly in part along a trough controlled by the Denali fault system. The same general fluvial system may have deposited sediment in other nonmarine strike-slip basins presently located to the northeast along the Denali fault system, including the McGrath and Talkeetna basins of Dickey (1984) (fig. 1). The McGrath basin, located about 25 km northeast of the White Mountain basin, is characterized by an overall southward paleoflow (Dickey, 1984). Dickey (1984) reports that no palynomorphs were recovered from

samples collected during his study of the McGrath basin, but that unpublished data of ARCO Alaska, Inc. identified Eocene to middle Oligocene pollen in equivalent deposits. The Talkeetna basin was mapped by Reed and Nelson (1980) along the north side of the central part of the Denali fault system (fig. 1). No palynological studies have been published on the Talkeetna basin. Dickey (1984) correlated the Talkeetna basin with the McGrath basin based on similar petrologic characteristics.

We interpret the White Mountain basin to be time-equivalent to Eocene-Oligocene strike-slip basins located along the eastern part of the Denali fault system in the Yukon Territory, Canada, on the basis of similar pollen assemblages (for example, Burwash and Bates Lake basins on fig. 1). For a detailed discussion on the palynology and structural development of strike-slip basins in the Yukon Territory, see Ridgway (1992) and Ridgway and others (1995). Our correlation disagrees with Sainsbury's (1965) correlation of the White Mountain basin with the Late Cretaceous Cantwell basin (fig. 1) and with Gilbert's (1981) correlation of the White Mountain basin with the Usibelli basin (fig. 1). Since Gilbert's (1981) map was published, detailed palynological studies have shown that most of the Usibelli Group was deposited during the middle and late Miocene (Leopold and Liu, 1994; Liu and Leopold, 1994). If the White Mountain basin is time-correlative to strike-slip basins along the eastern and central parts of the Denali fault system, it would suggest that the Oligocene was an important time for strike-slip displacement and basin development along the entire fault system.

Our analysis of the White Mountain basin is limited to one measured section, and much more research needs to be done on this basin and other strike-slip basins along the Denali fault system. Not until all the basins along this fault system are studied will a complete understanding of this ~2,000-km-long tectonic feature be possible. We hope that the data from this study will be a useful starting point for future studies of the White Mountain basin.

ACKNOWLEDGMENTS

This research was funded by grants from the National Science Foundation (EAR-9406078 and EAR-9725587). We thank Robert Blodgett for making us aware of the White Mountain basin, and for advice and airphotos needed to access the area. We also thank James White for useful discussions on the age of the pollen assemblages. Constructive reviews by Warren Nokleberg, Rocky Reifenstuhl, and an anonymous reviewer improved the manuscript.

REFERENCES

Cole, R.B., Ridgway, K.D., Layer, P.W., and Drake, Jeffrey, 1996, Volcanic history, geochronology, and deformation of the upper Cantwell Formation, Denali National Park, Alaska: Early Eocene transition between terrane accretion and strike-slip tectonics: Geological Society of America Abstracts with Programs, v. 28, p. 313.

———1999, Kinematics of basin development during the transition from terrane accretion to strike-slip tectonics, Late Cretaeous–early Tertiary Cantwell Formation, south central Alaska: Tectonics, v. 18, p. 1224-1244.

Collinson, J.D., 1986, Alluvial sediments, *in* Reading, H.G., ed., Sedimentary environments and facies: Oxford, United Kingdom, Blackwell, p. 20-62.

Decker, John, Bergman, S.C., Blodgett, R.B., Box, S.E., Bundtzen, T.K., Clough, J.G., Coonrad, W.L., Gilbert, W.G., Miller, M.L., Murphy, J.M., Robinson, M.S., Wallace, W.K., (1994), Geology of southwestern Alaska, *in* Plafker, George, and Berg, H.C., eds., The Geology of Alaska: Boulder, Colorado, Geological Society of America, The Geology of North America, v. G-1, p. 285-310.

Dickey, D.B., 1984, Cenozoic non-marine sedimentary rocks of the Farewell fault zone, McGrath Quadrangle, Alaska: Sedimentary Geology, v. 38, p. 443-463.

Dodds, C.J., 1995, Denali fault system, *in* Gabrielse, H., and Yorath, C.J., eds., Structural styles, Chapter 17: Geology of the Cordilleran Orogen in Canada: Geological Survey of Canada, no. 4, p. 656-657.

Eisbacher, G.H., 1976, Sedimentology of the Dezadeash flysch and its implications for strike-slip faulting along the Denali fault, Yukon Territory and Alaska: Canadian Journal of Earth Sciences, v. 13, p. 1495-1513.

Gilbert, W.G., 1981, Preliminary geologic map of the Cheeneetnuk River area, Alaska: Alaska Division of Geological & Geophysical Surveys, Alaska Open-File 153, one sheet, scale 1:63,360, 10 p.

Grantz, Arthur, 1966, Strike-slip faults in Alaska (Ph.D. thesis): Stanford University, California, 82 p.

Lanphere, M.A., 1978, Displacement history of the Denali fault system, Alaska and Canada: Canadian Journal of Earth Sciences, v. 15, p. 817-822.

Leopold, E.B., and Liu, Gengwu, 1994, A long pollen sequence of Neogene age, Alaska Range: Quaternary International, v. 22/23, p. 103-140.

Liu, Gengwu, and Leopold, E.B., 1994, Climatic comparison of Miocene pollen flora from northern East-China and south-central Alaska, USA: Palaeogeography, Palaeoclimatology, Palaeoecology, v. 108, p. 217-228.

Lowey, G.W., 1998, A new estimate of the amount of displacement on the Denali fault system based on the occurrence of carbonate megaboulders in the Dezadeash Formation (Jura-Cretaceous), Yukon, and the Nutzotin Mountains sequence (Jura-Cretaceous), Alaska: Bulletin of Canadian Petroleum Geology, v. 46, p. 379-386.

Miall, A.D., 1977, A review of the braided-river depositional environments: Earth Science Reviews, v. 13, p. 1-62.

Nokleberg, W.J., Jones, D.L., and Silberling, N.J., 1985, Origin and tectonic evolution of the Maclaren and Wrangellia terranes, eastern Alaska Range: Geological Society of America Bulletin, v. 96, p. 1251-1270.

Plafker, George, and Berg, H.C., 1994, Overview of the geology and tectonic evolution of Alaska, *in* Plafker, G., and Berg, H.C., eds., The Geology of Alaska: Geological Society of America, The Geology of North America, v. G-1, p. 989-1021.

Reed, B.L., and Nelson, S.W., 1980, Geologic map of the Talkeetna quadrangle, Alaska: U.S. Geological Survey Miscellaneous Investigations Map I-1174A, 15 p., scale 1:250,000.

Ridgway, K.D., 1992, Cenozoic tectonics of the Denali fault system, Saint Elias Mountains, Yukon Territory: Synorogenic sedimentation, basin development, and deformation along a transform fault system (Ph.D. thesis): Rochester, New York, University of Rochester, 508 p.

Ridgway, K.D., and DeCelles, P.G., 1993a, Stream-dominated alluvial-fan and lacustrine depositional systems in Cenozoic strike-slip basins, Denali fault system, Yukon Territory: Sedimentology, v. 40, p. 645-666.

———1993b, Petrology of mid-Cenozoic strike-slip basins in an accretionary orogen, St. Elias Mountains, Yukon Territory, Canada, *in* Johnsson, M.J., and Basu, Abhijit, eds., Processes controlling the composition of clastic sediments: Geological Society of America Special Paper 284, p. 67-89.

Ridgway, K.D., Sweet, A.R., and Cameron, A.R., 1995, Climatically induced floristic changes across the Eocene-Oligocene transition in the northern high latitudes, Yukon Territory, Canada: Geological Society of America Bulletin, v. 107, p. 676-696.

Ridgway, K.D., Trop, J.M., and Sweet, A.R., 1997, Thrust-top basin formation along a suture zone, Cantwell basin, Alaska Range: Implications for development of the Denali fault system: Geological Society of America Bulletin, v. 109, p. 505-523.

Ridgway, K.D., Trop, J.M., Nokleberg, W.J., and Davidson, C.M., 1998, Mesozoic and Cenozoic tectonics of the eastern and central Alaska Range: Progressive basin development and deformation within a suture zone: Geological Society of America Abstracts with Programs, v. 30, p. A-242.

Ridgway, K.D., Trop, J.M., and Jones, D.E., 1999, Petrology and provenance of the Neogene Usibelli Group and Nenana Gravel: Implications for the denudation history of the central Alaska Range: Journal of Sedimentary Research, v. 69, p. 1262-1275.

Rust, B.R., 1978, Depositional models for braided alluvium, *in* Miall, A.D., ed., Fluvial sedimentology: Memoir, Canadian Society of Petroleum Geologists, Calgary, v. 5, p. 605-625.

Sainsbury, C.L., 1965, Previously undescribed Middle(?) Ordovician, Devonian(?), and Cretaceous(?) rocks, White Mountain area, near McGrath, Alaska: U.S. Geological Survey Professional Paper 525-C, p. C91-C95.

Trop, J.M., 1996, Sedimentological, provenance, and structural analysis of the lower Cantwell Formation, Cantwell basin, central Alaska Range: Implications for thrust-top basin development along a suture zone (unpublished M.S. thesis): West Lafayette, Indiana, Purdue University, 222 p.

Wahrhaftig, Clyde, 1987, The Cenozoic section at Suntrana Creek, *in* Hill, M.L., ed., Cordilleran section of the Geological Society of America: Boulder, Colorado, Geological Society of America, Centennial Field Guide, v. 1, p. 445-450.

Wahrhaftig, Clyde, Wolfe, J.A., Leopold, E.B., and Lanphere, M.A., 1969, The Coal-Bearing Group in the Nenana coal field, Alaska: U.S. Geological Survey Bulletin 1274-D, 30 p.

White, J.M., and Ager, T.A., 1994, Palynology, paleoclimatology, and correlation of Middle Miocene beds from the Porcupine River (Locality 90-1), Alaska: Quaternary International, v. 22/23, p. 43-77.

White, J.M., Ager, T.A., Adam, D.P., Leopold, E.B., Liu, Gengwu, Jetté, Helene, and Schweger, C.E., 1997, An 18 million year record of vegetation and climate change in northwestern Canada and Alaska: Tectonic and global climatic correlates: Palaeogeography, Palaeoclimatology, Palaeoecology, v. 130, p. 293-306.

Wolfe, J.A., 1986, Tertiary floras and paleoclimates of the Northern Hemisphere, *in* Broadhead, T.W., ed., Land plants, notes for a short course: San Antonio, Texas, Paleontological Society, p. 182-225.

LATE DEVONIAN (EARLY FRASNIAN) CONODONTS FROM DENALI NATIONAL PARK, ALASKA

Norman M. Savage,[1] Robert B. Blodgett,[2] and Phil F. Brease[3]

INTRODUCTION

A brachiopod-bearing sample, collected in 1980 by Dr. Norman Silberling from dark gray, nodular argillaceous limestone beds in the upper part of an undated and unnamed shale unit in Denali National Park, was processed for conodonts by Savage but yielded only a few broken specimens of general Middle to Late Devonian aspect. New samples were collected in 1994 by Csejtey (Csejtey and others, 1996; Dumoulin and others, 1998), and by Blodgett and Brease from the site (locality 2 herein) and a nearby site (locality 1 herein) at the base of an overlying, unnamed massive limestone unit. These two localities, each yielding conodonts and brachiopods, are located on the north side of a prominent saddle in NE¼ NE¼ sec. 30, T.17 N., R.12 W., Healy B-6 Quadrangle (fig. 1).

At locality 1, the overlying limestone unit is at the base of a prominent, south-facing limestone cliff, about 18.3 m (60 ft) below the ridge crest. Conodonts from the upper limestone unit include *Playfordia* aff. *P. primitiva* (Bischoff and Ziegler, 1957), *Polygnathus* cf. *P. robustus* Klapper and Lane, 1985, *Polygnathus webbi* Stauffer, 1938, *Ancyrodella pristina* Khalymbadzha and Chernysheva, 1970, *Mesotaxis* cf. *M. falsiovalis* Sandberg, Ziegler, and Bultynck, 1989, *Icriodus symmetricus* Branson and Mehl, 1934, and *Mehlina* sp. The interesting feature of the conodont fauna is the abundance of *Playfordia* aff. *P. primitiva*, which is the most common species present. The presence of this species, and *Mesotaxis* cf. *M. falsiovalis*, indicates the *transitans* to *punctata* Zones of Ziegler and Sandberg

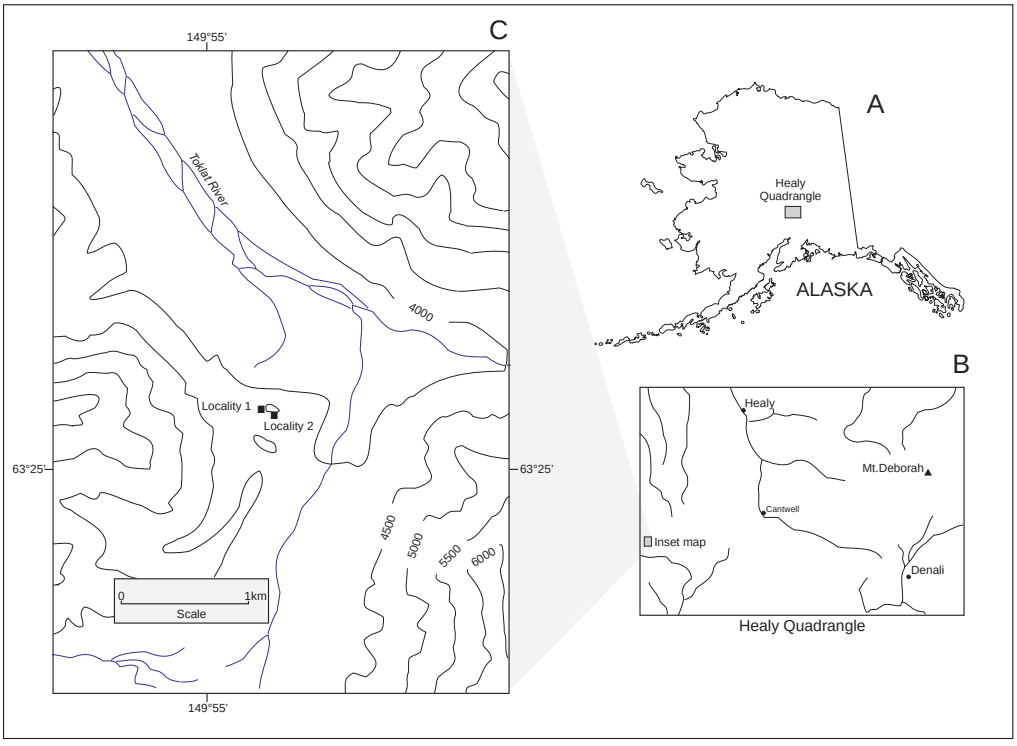

Figure 1. *Locality maps for the Toklat River conodont samples. (A) Location of Healy 1:250,000-scale quadrangle in southcentral Alaska. (B) Location of part of Healy B-6 15-minute quadrangle. (C) Location of sites 1 and 2 near Toklat River.*

[1]Department of Geological Sciences, University of Oregon, Eugene, Oregon 97403.
Email for Norm Savage: nmsavage@oregon.uoregon.edu
[2]Department of Zoology, Oregon State University, Corvallis, Oregon 97331.
[3]Denali National Park, P.O. Box 9, Denali Park, Alaska 99755.

(1990), and an early Frasnian age. Brachiopods include *Hypothyridina* sp., *Variatrypa (Radiatrypa)* sp., *Spinatrypa (Exatrypa)* sp., and *Eleutherokomma* sp. Rugose corals are also common, and include both colonial forms (notably phillipsastreids and undetermined fasciculate types), as well as solitary rugosans. Conodonts from locality 2 were recovered from nodular, argillaceous limestone beds in the uppermost part of the underlying thick unnamed shale unit. These limestone beds represent a thin transitional interval with the overlying unit. Conodonts from these beds include those listed above from the upper unit. Brachiopods from these same beds include *Schizophoria* sp. *Eleutherokomma* sp. and *Ladogioides pax*.

The massive limestone unit and underlying shale unit are widespread in the area and share strong lithologic similarities with similar Frasnian sections recognized near the base of the Mystic sequence of west-central Alaska, notably in the Shellabarger Pass area, Talkeetna C-6 Quadrangle, and in the Lime Hills D-4 Quadrangle (Blodgett and Gilbert, 1992). These close lithologic and faunal ties suggest that the rocks described here form an eastward extension of the Farewell terrane of Decker and others (1994). The areal extent of the Farewell terrane is shown in Blodgett (1998, fig. 2), showing the component subterranes of the Farewell terrane as well as the location of Shellabarger Pass.

The Devonian fossils reported here are of significance in providing badly needed timelines within the weakly metamorphosed sediments exposed along the north side of the central Alaska Range within Denali National Park. Very few Paleozoic age fossil localities were known in this area previously. It is of further interest in terms of biotic diversity, since all Devonian collections from this part of the Park before the 1990s consisted of poorly preserved corals. In addition, the fossils reported here provide important evidence for more correct determination of the stratigraphic framework for this region. The Frasnian age determination and associated brachiopod fauna provide evidence for correlation of these beds with the Mystic sequence (or "subterrane") exposed further to the southwest in the McGrath, Talkeetna, and Lime Hills quadrangles. Prior to this study, rocks from this part of the Park had been assigned to the Dillinger terrane by Jones and others (1981) and later to the Nixon Fork terrane by Mullen and Csejtey (1986) and Csejtey and others (1992). On the basis of our recently acquired fossil data and regional field studies conducted in 1994, we now think the assignment of Dillinger "terrane" is incorrect (it is present and underlies the Mystic strata reported here), and that the assignment of Nixon Fork terrane affinities is also incorrect (no shallow-water carbonate platform equivalent strata of Ordovician–early Middle Devonian age are recognized in the region).

The Mystic subterrane was originally defined by Jones and others (1981) as a separate tectono-stratigraphic entity of full terrane rank. More recently, Decker and others (1994) recognized that the Mystic, as well as the Nixon Fork and Dillinger terranes, were genetically related and all were reduced in rank to subterranes of a larger terrane, termed the Farewell terrane. Gilbert and Bundtzen (1984) considered the Dillinger and Mystic terranes, each of whose type sections were close to one another, to represent a single stratigraphic succession of Paleozoic to Triassic age, preferring to apply the term "sequence" to each. They considered the underlying Dillinger sequence to be a Cambrian to Lower Devonian deep-water succession that is followed depositionally by the Mystic sequence, which consists of laterally variable Devonian to Triassic (?) shallow-water to nonmarine sedimentary rocks and intrusive and extrusive mafic and ultramafic rocks. The close stratigraphic relationship between the Dillinger and Mystic sequences (or subterranes) was supported by stratigraphic studies by Blodgett and Gilbert (1992) to the southwest in the Lime Hills quadrangle.

SYSTEMATIC PALEONTOLOGY

Genus *ANCYRODELLA* Ulrich and Bassler, 1926

ANCYRODELLA PRISTINA Khalymbadzha and Chernysheva, 1970

Figure 2.7

Discussion. The single specimen recovered has an asymmetrical platform outline and few but large nodes.

Material. 1 Pa element from locality 1.

Genus *MEHLINA* Youngquist, 1945

MEHLINA sp.

Figure 2.9

Discussion. These Pa specimens have the lateral profile of *Ozarkodina* but lack the characteristic expanded platform margins and are assigned to *Mehlina*.

Material. 2 Pa elements from locality 2.

Genus *POLYGNATHUS* Hinde, 1879

POLYGNATHUS cf. *P. ROBUSTUS* Klapper and Lane, 1985

Figures 2.5–2.6

Discussion. This specimen differs from typical Pa elements of *P. robustus* in having a convex inner platform margin and smaller anterior denticles on the free blade. It bears some resemblance to *P. ljaschenkoi* Kuzmin, 1995, but has a more convex inner platform margin than that species also.

Material. 1 Pa element from locality 1.

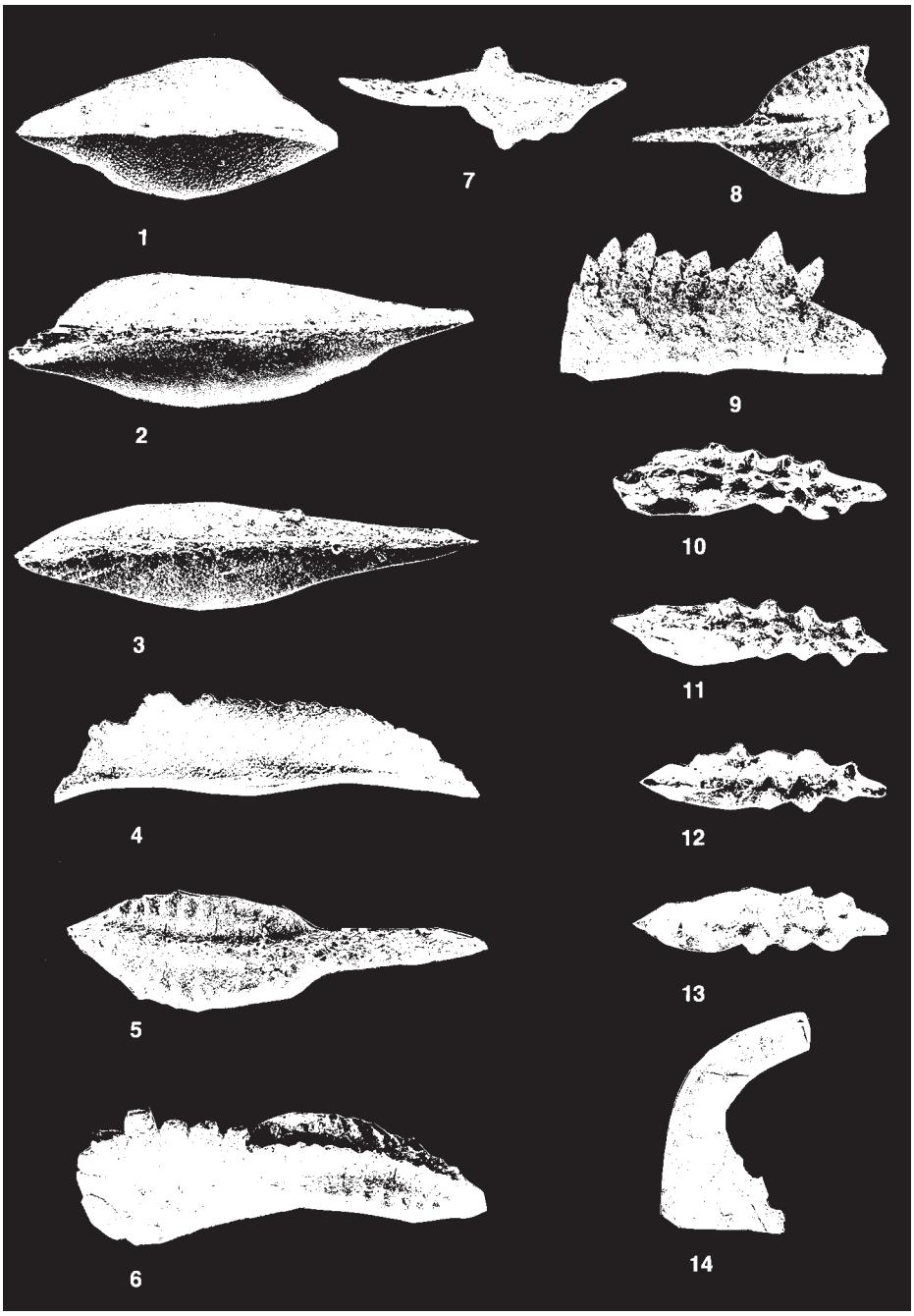

Figure 2. *(1–4),* Playfordia *aff.* P. primitiva *(Bischoff and Ziegler, 1957). (1) Upper view of USNM 481705 from locality 1. (2) Upper view of USNM 481706 from locality 2. (3) Upper view of USNM 481707 from locality 2. (4) Lateral view of USNM 481708 from locality 1, all x 70. (5–6)* Polygnathus *aff.* P. robustus *Klapper and Lane, 1985. Upper and oblique-lateral views of Pa element USNM 471709 from locality 1, x 70. (7)* Ancyrodella pristina *Khalymbadzha and Chernysheva, 1970. Upper view of Pa element USNM 471710 from locality 1, x 70. (8)* Mesotaxis *cf.* M. falsiovalis *Sandberg, Ziegler and Bultynck, 1989. Upper view of broken Pa element USNM 471711 from locality 2, x 70. (9)* Mehlina *sp. lateral view of Pa element USNM 471712 from locality 2, x 70. (10–11)* Icriodus symmetricus *Branson and Mehl, 1934. Upper views of Pa elements USNM 471713-471714, both from locality 1, x 70. (12–13) Possibly juveniles of* Icriodus symmetricus *Branson and Mehl, 1934, or mature specimens of* I. praealternatus *Sandberg, Ziegler, and Dreesen, 1992, both from locality 1, x 70. (14)* Belodella *sp. USNM 471717 from locality 1, x 70.*

Genus *ICRIODUS* Branson and Mehl, 1938
ICRIODUS SYMMETRICUS Branson and Mehl, 1934
Figures 2.10–2.13

Discussion. These Denali specimens are more slender than characteristic specimens of *I. subterminus* Youngquist, 1945, and also differ in having a less expanded posterior platform. They are unlike typical specimens of *I. symmetricus* in having lateral denticles that almost alternate laterally with the median denticles, although Dr. Charles Sandberg (written commun., April 1999), believes that the specimens in Figs 2.10–11 are unquestionably *I. symmetricus*, and those in Figs.2.12–13 look like juveniles of *I. symmetricus* or mature specimens of *I. praealternatus* Sandberg, Ziegler and Dreesen, 1992.

Material. 8 Pa elements; 5 from locality 1, and 3 from locality 2.

Genus *MESOTAXIS* Klapper and Philip, 1972
MESOTAXIS cf. *M. FALSIOVALIS* Sandberg, Ziegler and Bultynck, 1989
Figure 2.8

Discussion. The only specimen is broken but enough is present to suggest the species *Mesotaxis falsiovalis*.

Material. 1 Pa element from locality 2.

Genus *PLAYFORDIA* Glenister and Klapper, 1966
PLAYFORDIA aff. *P. PRIMITIVA* (Bischoff and Ziegler, 1957)
Figures 2.1–2.4

Discussion. The specimens of *Playfordia* aff *P. primitiva* differ from typical members of the species in having less projecting denticles at the posterior end, as pointed out by Dr. Charles Sandberg (written commun., April 1999). The presence of this species, even in its somewhat different form, helps considerably in determining the age of the collections because it is known elsewhere only from the Late *falsiovalis* to *transitans* Zones of Ziegler and Sandberg (1990). Dr. Sandberg has commented (written commun., April 1999) that it has never been reported from the *falsiovalis* Zones. However, the interpretation by the senior author of ongoing work in the Timan Basin, Russia, is that *Playfordia primitiva* occurs there in the Late *falsiovalis* Zone about 2 m (6.5 ft) below the first occurrence of *Palmatolepis transitans*.

Material. 23 Pa elements; 9 from locality 1, and 14 from locality 2.

Genus *BELODELLA* Ethington, 1959
BELODELLA sp.
Figure 2.14

Discussion. The single specimen appears to belong to a *Belodella* apparatus. Devonian species of *Belodella* usually include apparatus elements that bear numerous fine denticles but our small collections do not include any of these elements.

Material. 1 element from locality 1.

ACKNOWLEDGMENTS

We thank Barbara Savage for processing the samples and picking the conodont residues. We also are grateful to Norman Silberling and Wyatt G. Gilbert for bringing the 1980 discovery to our attention. Thanks are also extended to Paul Atkinson for his able assistance in the field. Charles Sandberg and Michael Orchard reviewed the submitted manuscript and provided valuable advice.

REFERENCES

Bischoff, Guenther, and Ziegler, Willi, 1957, Die Conodontenchronologie des Mitteldevons und des tiefsten Oberdevons: Wiesbaden, Germany, Hessisches Landesamt Bodenforschung Abhandlungen, v. 22, 136 p.

Blodgett, R.B., 1998, Emsian (late Early Devonian) fossils indicate a Siberian origin for the Farewell terrane, *in* Clough, J.G. and Larson, Frank, eds., Short Notes on Alaskan Geology 1997: Alaska Division of Geological & Geophysical Surveys Professional Report 118, p. 53–61.

Blodgett, R.B., and Gilbert, W.G., 1992, Upper Devonian shallow-marine siliciclastic strata and associated fauna and flora, Lime Hills D-4 Quadrangle, southwest Alaska, *in* Bradley, D.C., and Dusel-Bacon, Cynthia, eds., Geologic Studies in Alaska by the U.S. Geological Survey, 1991: U.S. Geological Survey Bulletin 2041, p. 106–115.

Branson, E.B., and Mehl, M.G., 1934, Conodont studies no. 3—conodonts from the Grassy Creek Shale of Missouri: University of Missouri Studies, v. 8, no. 3, p. 171–259.

Branson, E.B., and Mehl, M.G., 1938, The conodont genus *Icriodus* and its stratigraphic distribution: Journal of Paleontology, v. 12, no. 2, p. 156–166.

Csejtey, Bela, Jr., Mullen, M.W., Cox, D.P., and Stricker, G.D., 1992, Geology and geochronology of the Healy Quadrangle, south-central Alaska: U.S. Geological Survey Miscellaneous Investigation Series Map I-1961, 63 p., 2 sheets, scale 1:250,000.

Csejtey, Bela, Jr., Wrucke, C.T., Ford, A.B., Mullen, M.W., Dutro, J.T., Jr., Harris, A.G., and Brease, P.F., 1996, Correlation of rock sequences across the Denali fault in south-central Alaska, *in* Moore, T.E. and Dumoulin, J.A., eds., Geologic studies in Alaska by the U.S. Geological Survey, 1994: U.S. Geological Survey Bulletin 2152, p. 149–156.

Decker, John, Bergman, S.C., Blodgett, R.B., Box, S.E., Bundtzen, T.K., Clough, J.G., Conrad, W.L., Gilbert, W.G., Miller, M.L., Murphy, J.M., Robinson, M.S., and Wallace, W.K., 1994, Geology of southwestern Alaska, *in* Plafker, George, and Berg, H.C., eds., The Geology of Alaska: Boulder, Colorado, Geological Society of America, The Geology of North America, v. G-1, p. 285–310.

Dumoulin, J.A., Bradley, D.C., and Harris, A.G., 1998, Sedimentology, conodonts, structure, and regional correlation of Silurian and Devonian metasedimetary rocks in Denali National Park, Alaska, *in* Gray, J.E., and Riehle, J.R., eds., Geologic studies in Alaska by the U.S. Geological Survey, 1996: U.S. Geological Survey Professional Paper 1595, p. 71–98.

Ethington, R.L., 1959, Conodonts of the Ordovician Galena Formation: Journal of Paleontology, v. 33, no. 2, p. 257–292.

Gilbert, W.G., and Bundtzen, T.K., 1984, Stratigraphic relationship between Dillinger and Mystic terranes, western Alaska Range, Alaska: Geological Society of America Abstracts with Programs, v. 16, no. 5, p. 286.

Glenister, B.F., and Klapper, Gilbert, 1966, Upper Devonian conodonts from the Canning Basin, Western Australia: Journal of Paleontology, v. 40, no. 4, p. 777–842.

Hinde, G.J., 1879, On conodonts from the Chazy and Cincinnati group of the Cambro–Silurian, and from the Hamilton and Genesee shale of the Devonian, in Canada and the United States: Quarterly Journal of the Geological Society of London, v. 35, p. 351–369.

Jones, D.L., Silberling, N.J., Berg, H.C., and Plafker, George, 1981, Map showing tectonostratigraphic terranes of Alaska, columnar sections, and summary description of terranes: U.S. Geological Survey Open-File 81-792, 21 p., 2 sheets, scale 1:2,500,000.

Khalymbadzha, V.G., and Chernysheva, N.G., 1970, Conodont genus *Ancyrodella* from Devonian deposits of the Volga-Kamsky area and their stratigraphic significance, *in* Biostratigraphy and paleontology of Paleozoic deposits of the eastern Russian Platform and western pre-Urals [in Russian]: Kazan University, 1, p. 81–103.

Klapper, Gilbert, and Lane, H.R., 1985, Upper Devonian (Frasnian) conodonts of the *Polygnathus* biofacies, N.W.T., Canada: Journal of Paleontology, v. 59, no. 4, p. 904–951.

Klapper, Gilbert, and Philip, G.M., 1972, Familial classification of reconstructed Devonian conodont apparatuses, Symposium on Conodont Taxonomy: Geologica et Palaeontologica, Sonderbuch 1, p. 97–114.

Kuz'min, A.V., 1995, Lower boundary of the Frasnian stage of the Russian Platform: Stratigrafiya, Geologicheskaya Korrelyatsiya [in Russian], v. 3, no. 3, p. 111–120.

Mullen, M.W., and Csejtey, Bela, Jr., 1986, Recognition of a Nixon Fork terrane equivalent in the Healy Quadrangle, *in* Bartsch-Winkler, Susan, and Reed, K.M., eds., Geologic studies in Alaska by the U.S. Geological Survey during 1985: U.S. Geological Survey Circular 978, p. 55–60.

Sandberg, C.A., Ziegler, Willi, and Bultynck, Pierre, 1989, New standard conodont zones and early *Ancyrodella* phylogeny across Middle–Upper Devonian boundary, *in* Walliser, O.H., and Ziegler, Willi, eds., Contributions to Devonian palaeontology and stratigraphy, Part 1, Chinese-German Collaboration; Part 2, Various Devonian topics: Frankfurt, Germany, Courier Forschungsinstitut Senckenberg, v. 110, p. 195–230.

Sandberg, C.A., Ziegler, Willi, Dreesen, Roland, and Butler, J.L., 1992, Conodont biochronology, biofacies, taxonomy, and event stratigraphy around middle Frasnian Lion mudmound (F2h), Frasnes, Belgium: Courier Forschungsinstitut Senckenberg, v. 150, 87 p.

Stauffer, C.R., 1938, Conodonts of the Olentangy Shale: Journal of Paleontology, v. 12, no. 5, p. 411–443.

Ulrich, E.O., and Bassler, R.S., 1926, A classification of the toothlike fossils, conodonts, with descriptions of American Devonian and Mississippian species: Proceedings of the U.S. National Museum, v. 68, 63 p.

Youngquist, W.L., 1945, Upper Devonian conodonts from the Independence Shale(?) of Iowa: Journal of Paleontology, v. 19, no. 4, p. 355–367.

———1947, A new Upper Devonian conodont fauna from Iowa: Journal of Paleontology, v. 21, no. 2, p. 95–112.

Ziegler, Willi, and Sandberg, C.A., 1990, The Late Devonian standard conodont zonation: Courier Forschungsinstitut Senckenberg, v. 121, 115 p.

GEOLOGY AND GOLD MINERALIZATION AT THE DONLIN CREEK PROSPECTS, SOUTHWESTERN ALASKA

David Szumigala,[1] Stan P. Dodd,[2] and Antonio Arribas, Jr.[3]

SUMMARY

The Donlin Creek property in southwestern Alaska is a large gold system with mineralization extending more than 6 mi (9.6 km) in a northeast/southwest direction. The Queen–Lewis–ACMA area in the southern part of the property has the largest gold resource identified to date, with an estimated measured and indicated resource of 5.4 million oz (167.8 tonnes) of gold at a grade of 0.088 oz/ton gold (3.0 g/tonne). Total estimated gold resource at Donlin Creek, including the inferred category, is 11.5 million oz (357.7 tonnes). Mineralization is open to depth and along strike.

Gold mineralization parallels a 5-mi-long (8.2-km-long) Late Cretaceous to early Tertiary bimodal rhyodacitic and mafic dike swarm intruding mid-Cretaceous Kuskokwim Group interbedded graywacke and shale. Intrusive contacts are highly irregular along strike and there are both sill- and dike-like components. Dike morphologies dominate in the northeastern Lewis and Rochelieu areas, whereas igneous sills are dominant in the 400 Area, and the southern Lewis and ACMA areas. Gold mineralization is associated with disseminated sulfides, sulfide veinlets and quartz–carbonate–sulfide veining in sericite-altered igneous rocks and sedimentary rocks. There is a consistent positive correlation between zones of high fault and fracture density, areas of intense sericite alteration, and high gold grades. Alteration (sericite formation) and felsic dike crystallization (biotite formation) ages by $^{40}Ar/^{39}Ar$ dating overlap and are interpreted to indicate that crystallization of the dikes was closely followed by sericite and carbonate alteration accompanied by pyrite–arsenopyrite–gold mineraliza-tion. Stable isotope and fluid inclusion results suggest that fluids responsible for sericite alteration (and at least part of the mineralization) at Donlin Creek formed by mixing of magmatic water and meteoric water. Interpretation of sulfur isotopes suggests that at least some sulfur is derived from clastic sedimentary rocks.

Gold mineralization is structurally controlled and refractory (arsenopyrite-hosted). Higher-grade mineralization occurs at the juxtaposition of favorable lithology (most favorable is rhyodacite, least favorable is shale) and mineralized shear zones/faults (355°–040° trends with moderate to steep, easterly dips). North-trending structures appear to be normal faults having minor displacement (east–west extensional event). Earlier, northwesterly trending thrust faults, occurring along shale beds also have minimal displacements but only minor gold mineralization. Deformation has been minimal since mineralization.

INTRODUCTION

Plutonic-hosted gold deposits have become an important exploration target in Alaska since the discovery and subsequent operation of the five-million-ounce Fort Knox gold deposit. The Fort Knox deposit near Fairbanks remains the best-documented intrusive-hosted gold deposit in Alaska. Other plutonic-hosted gold deposits in Alaska vary dramatically from the Fort Knox model in fundamental aspects such as ore mineralogy and alteration styles (McCoy and others, 1997). Nevertheless, most recent exploration for plutonic-hosted gold deposits in Alaska has focused on the Yukon–Tanana uplands of the eastern Interior. The discovery of the Donlin Creek gold deposit in southwestern Alaska emphasizes that potential for world-class gold deposits in Alaska is not restricted to the Yukon–Tanana uplands.

The Donlin Creek property, in the Kuskokwim Mountains of southwestern Alaska, is approximately 300 mi (480 km) west of Anchorage and 15 mi (20 km) north of the village of Crooked Creek on the Kuskokwim River (fig. 1, inset), the closest navigable waterway. The property is on approximately 42 mi^2 (109 km^2) of privately owned Native land. Calista Corp., a regional Native corporation, has patent to subsurface rights, and The Kuskokwim Corp., a Native village corporation, has patent to surface rights. The project is controlled 100 percent by Placer Dome Inc. under a lease agreement signed with Calista Corp. in March 1995. Calista has the right to earn up to a 15 percent interest in the project upon completion of a positive feasibility study. Locus of exploration activity is in the SE¼ T. 23 N., R. 49 W., Seward Meridian (62°03'N latitude, 158°10'W longitude). The property has a 5,400-ft-long (1,650-m-long) gravel airstrip for access and an 80-person camp on

[1]Alaska Division of Geological & Geophysical Surveys, 794 University Ave., Suite 200, Fairbanks, Alaska 99709-3645.
Email for David J. Szumigala: zoom@dnr.state.ak.us
[2]Consulting Geologist, 3732 Magrath Road, Bellingham, WA 98225.
[3]Placer Dome Exploration, Inc., 240 South Rock Blvd., Suite 117, Reno, NV 89502-2345.

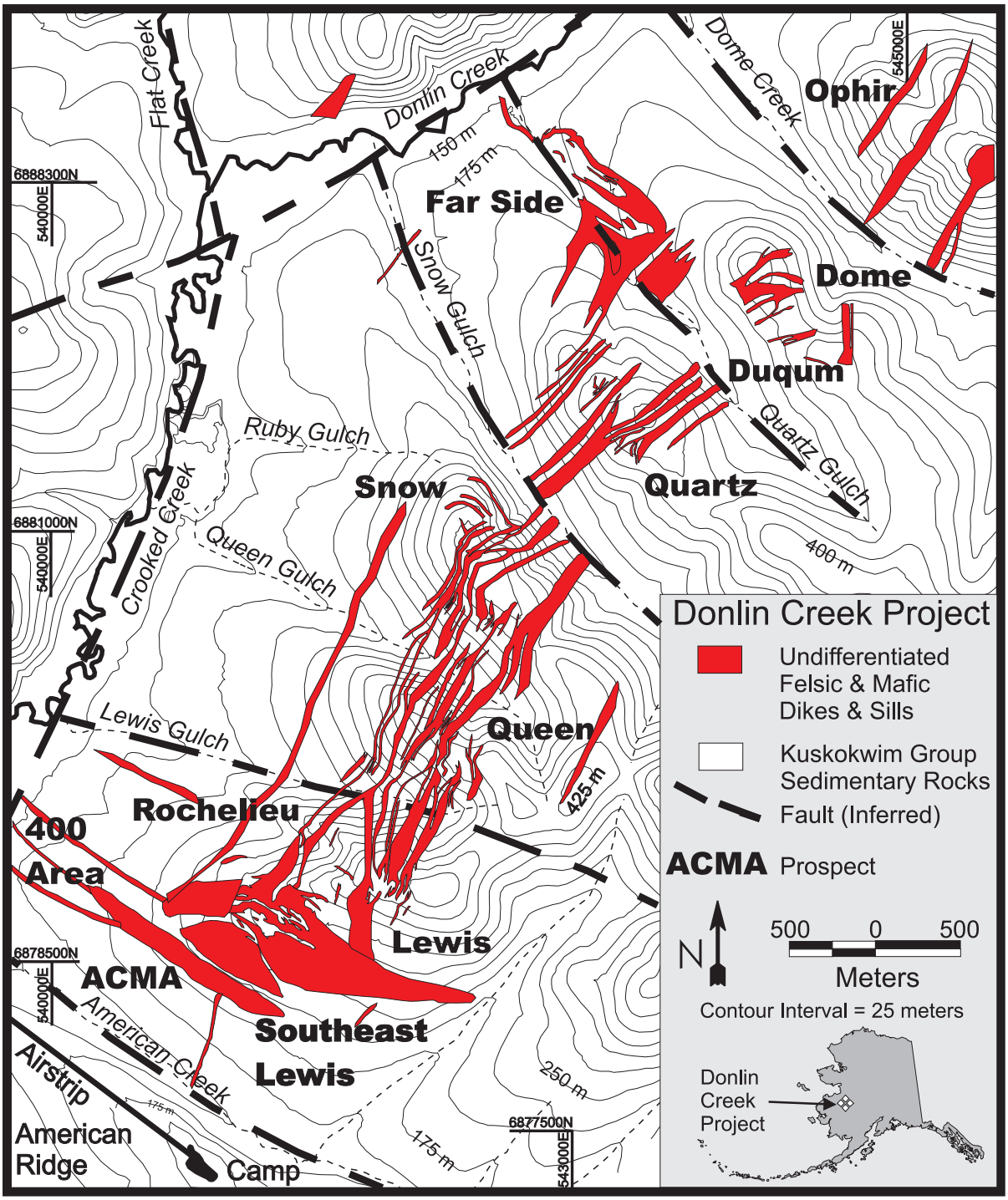

Figure 1. *Simplified geology of the Donlin Creek property and location of gold prospects. Topographic base from aerial survey flown by Aeromap U.S. for Placer Dome Exploration, Inc. Grid marks are Universal Transverse Mercator (UTM) projection 1927 North American datum, zone 4. Geology modified from maps by Western Gold Exploration and Mining Co. and Placer Dome Exploration, Inc. Inset map shows location of the Donlin Creek project in southwestern Alaska.*

American Ridge, immediately south of the exploration area (fig. 1).

The Donlin Creek project is in an area of low topographic relief on the western flank of the Kuskokwim Mountains. Elevations range from 500 to 1,500 ft (150–460 m) above sea level. Ridges are well rounded and ridgetops are typically covered with rubble crop and alpine tundra. Soil solifluction lobes blanket virtually all hillsides; these hillsides are forested with black spruce, tamarack, alder, birch, and larch. Soft muskeg, stunted black spruce forest, and discontinuous permafrost are common at lower elevations in poorly drained areas.

Placer gold was discovered near the Donlin Creek property in 1909 and significant lode exploration at Donlin Creek began in the 1980s. WestGold Exploration and Mining Co. identified eight gold prospects over a 3-mi (5-km) strike length through extensive soil sampling (over 10,000 samples), trenching, and drill programs in 1988 and 1989. These prospects, from north to south, were named Far Side (formerly called Carolyn), Dome, Quartz, Snow, Queen, Rochelieu, Upper Lewis, and Lower Lewis (fig. 1).

Placer Dome began working at Donlin Creek in 1995 and spent approximately $26 million on the Donlin Creek project from 1995 to 1998. Based on WestGold's work, the Lewis–Rochelieu area was deemed the most favorable target for a large bulk tonnage gold deposit and exploration by Placer Dome Exploration Inc. has focused there. Placer Dome's exploration efforts have been largely drill focused, with approximately 39,000 ft (11,900 m) of reverse-circulation drilling and 249,280 ft (76,000 m) of NQ- and HQ-diameter core drilling from 1995 to 1998. Placer Dome also completed 13,850 ft (4,200 m) of excavator and bulldozer trenching, airborne and ground geophysical surveys, and a soil-sampling program. Placer Dome has discovered several additional prospects on the Donlin Creek property, including Duqum, 400 Area, and ACMA (fig. 1). Placer Dome Exploration Inc. is continuing exploration efforts at present.

Extensive core drilling by Placer Dome Exploration Inc. from 1995 through 1998 defined a large gold resource extending from the Queen prospect through the Lewis (formerly Upper Lewis), Rochelieu, Southwest Lewis (formerly Lower Lewis), and Southeast Lewis (formerly Lower Lewis) prospects to the ACMA area. The Queen–Lewis area has the largest gold resource identified at the Donlin Creek property, defined by over 175 core holes with drill spacing varying from 165 to 650 ft (50 to 200 m) centers. Placer Dome announced an estimated measured and indicated resource of 5.4 million oz (167.8 tonnes) of gold contained in 51.7 million tons (57 million tonnes) of gold-bearing material grading 0.088 oz/ton (3 g/tonne) gold, using a 0.06 oz/ton (2 g/tonne) gold cutoff. The total estimated gold resource at Donlin Creek, including the inferred category, increased to 11.5 million oz (357.7 tonnes) with an average grade of 0.085 oz/ton (2.91 g/tonne) gold at a cutoff grade of 0.04 oz/ton (1.5 g/tonne) gold (Placer Dome press release, 2/18/99).

REGIONAL GEOLOGY

The regional geology of southwestern Alaska is summarized in Decker and others (1994), Patton and others (1994), and Szumigala (1993, 1996). Metamorphosed Early Proterozoic sedimentary and plutonic rocks occur as isolated exposures in southwestern Alaska and serve as depositional basement for Paleozoic units of the Ruby, Innoko, and Farewell terranes. The Farewell terrane, a nearly continuous sequence of Paleozoic continental margin rocks over 18,000 ft (5,500 m) thick, underlies much of the southwestern Alaska Range and northern Kuskokwim Mountains and unconformably overlies Early Proterozoic units. The predominantly Upper Cretaceous Kuskokwim Group, a post-accretionary basin-fill flysch sequence, is the most extensively exposed unit in the region and is interpreted to have formed one continuous marine embayment that stitched together most of the terranes of southern and western Alaska by Albian time. The Kuskokwim Group consists largely of interbedded lithofeldspathic sandstone and shale, and in large part rests unconformably on all older rock units. The Kuskokwim Group is at least 7.5 mi (12 km) thick in the region surrounding Donlin Creek and the underlying basement rocks are unknown. Late Cretaceous to early Tertiary plutonic and volcanic rocks intrude and/or overlie all of the younger units.

Two major northeast-trending faults traverse southwestern Alaska, the Denali–Farewell fault system to the south, and the Iditarod–Nixon Fork fault to the north. Latest Cretaceous and Tertiary right-lateral offsets of 56 mi (90 km) to less than 94 mi (150 km) occurred on both faults (Bundtzen and Gilbert, 1983; Miller and Bundtzen, 1988). Numerous high-angle faults are parallel and conjugate to these large faults. Pre-Tertiary rocks have undergone at least two folding phases: open to isoclinal folds with 1–2 mile (2–3 km) amplitudes and northeast-trending axes, and later broad folds with 15 mi (25 km) wavelengths and north-northeast-trending fold axes. Regional structural elements have been modeled by right lateral wrench fault tectonics with accompanying compressional and tensional stresses (Miller and Bundtzen, 1988).

The Kuskokwim Mountains represent one of several latest Cretaceous to earliest Tertiary magmatic belts found in southern and western Alaska. The Kuskokwim Mountains belt consists of calc-alkaline to alkaline basaltic to rhyolitic volcanic fields, isolated calc-alkaline stocks, felsic to mafic dike swarms, and sub-alkaline to

alkaline volcano–plutonic complexes (Moll-Stalcup, 1994). Plutonic rocks of the Kuskokwim Mountains magmatic belt extend over a northeast-trending area of approximately 540 mi by 120 mi (900 km by 200 km). Potassium-Argon (K-Ar) dates from igneous rocks in the Kuskokwim Mountains belt range from 58 to 77 Ma, whereas K-Ar dates for plutonic rocks range from 61 to 73 Ma, with an average age of 69 Ma (Szumigala, 1996, 1993). Geochemical characteristics of the igneous rocks suggest a common arc related petrogenesis for the Kuskokwim igneous centers (Szumigala, 1993). Most plutons of the Kuskokwim Mountains magmatic belt have quartz-monzonitic to monzonitic compositions and are calc-alkaline. Petrographic, magnetic susceptibility, and compositional data for plutonic rocks fit criteria for ilmenite series granitoids and geochemical signatures are compatible with I-type granitoids. Field relationships and limited laboratory measurements indicate the intrusions were emplaced at maximum depths of 0.6 to 2.5 mi (1 to 4 km). On the basis of previous K-Ar dating, mineralization is contemporaneous with plutonism at several localities in the Kuskokwim region (Szumigala, 1993).

PROPERTY GEOLOGY

Graywacke and shale of the Kuskokwim Group occur in subequal proportions at Donlin Creek (fig. 2). Kuskokwim Group rocks generally strike east to northwest (280° to 320°) and dip moderately (40° to 60°) to the south. Graywacke varies from a light gray to dark gray color, from fine-grained sandstone to fine-grained conglomerate, is massively bedded to 40 ft (12 m) thickness and breaks into blocks. Shale and siltstone units have prominent bedding and are good bedding indicators when present in core. Shale and siltstone units are black, carbonaceous, and occasionally contain fine-grained (diagenetic?) pyrite.

A northeast-trending, anastomosing, felsic (rhyodacite) and mafic (alkali basalt/andesite) dike swarm intrudes the Kuskokwim Group sedimentary rocks at Donlin Creek and crops out over approximately 5 mi (8.2 km) of strike length from American Creek to Ophir Creek (figs. 1, 2). In general, igneous units in the Northeast Lewis and Rochelieu areas are dikes with northeast strikes and moderate southeast dips that are clearly discordant to bedding. Igneous units in the Southeast and Southwest Lewis and ACMA areas are mostly sills with northwest strikes and moderate to steep southwest dips. This morphological change is reflected in the bedrock geologic map by the thick mass of rhyodacite present in the southern Lewis area (figs. 1, 2).

In detail, individual rhyodacite body orientations vary greatly. Igneous rocks occur as dikes, sills, and fault-bounded bodies. Igneous units are highly irregular along strike and can have both sill and dike components. Some sills may be thin apophyses to larger dikes. Sills commonly occur below thick shale horizons within the sedimentary rock package. Regional contact relationships between sedimentary and igneous rocks are typically sharp and generally without metamorphic or metasomatic effects. Chilled margins on igneous bodies occasionally occur along all contact types. Individual dikes may be up to 200 ft (60 m) wide, but the average width is 35 to 70 ft (10–20 m). There is no drill evidence that these dikes coalesce into a larger plutonic body within 1,300 ft (400 m) of the surface.

IGNEOUS LITHOLOGIES

Donlin Creek intrusive units comprise a dike swarm; hence, conflicting age relationships are likely. Individual dikes and sills pinch and swell throughout the prospect areas. Igneous units in the Donlin Creek area have been divided into five field categories: aphanitic rhyodacite porphyry (RDA), crystalline rhyodacite (RDX), fine-grained rhyodacite porphyry (RDF), rhyolite (RHY), and mafic dikes (MD).

Rhyodacite porphyry with aphanitic groundmass and porphyritic phenocrysts (RDA) and rhyodacite with medium- to coarse-grained crystalline texture (RDX) are the most common igneous units, representing approximately 80 percent of the dike volume. RDA and RDX can have gradational contacts, probably as textural differences within one dike, but contacts with distinct chilled margins also occur. Overall, the rhyodacite units have similar mineralogy and characteristics. Textures are typical for hypabyssal igneous rocks and vary from porphyritic with very fine-grained matrix ("volcanic") to almost coarse-grained equigranular ("plutonic"). Color varies from light gray to dark blue-gray and phenocrysts compose approximately 50 percent of rock volume. Quartz phenocrysts are subrounded to equant, vary from 0.04 to 0.31 in (1 to 8 mm) diameter and represent 10 to 20 volume percent. Quartz phenocrysts are typically partially to completely resorbed, embayed, and surrounded by sericite. Feldspar phenocrysts range from 0.02 to 0.39 in (0.5 to 10 mm) diameter (average 0.15 to 0.20 in [4–5 mm]) and 5 to 40 rock volume percent. There is a 1:1 to 1:2 ratio between plagioclase and orthoclase. Biotite phenocrysts are similar in size to quartz and feldspar phenocrysts and comprise 2 to 5 volume percent. Trace amounts of rutile, sphene, apatite, titanium oxide, allanite (?) and zircon are present. Red garnet phenocrysts are present in some core samples, but they are extremely rare overall (less than 10 garnets reported in 250,000 feet [76.2 km] of drilling). Graphite spherules up

Figure 2 (right). *Geologic map of the Queen, Rochelieu and Lewis prospects, Donlin Creek property.*

Queen-Lewis Area Geology

Donlin Creek Project Southwest Alaska

rhyodacite
fine rhyodacite porphyry
m *mafic intrusions*
Kuskokwim Group
graywacke
shale
interbedded graywacke & shale
shears & faults
T *thrust fault*

A A' *Cross-section line*

N *Contour Elevations in Meters*

1000 FEET
200 METERS

to 1.1 in (3 cm) in diameter occur locally and indicate a low magmatic oxidation state.

Whole rock analyses of the least altered rhyodacite samples available from drill core are shown in table 1 and plot within the rhyolite and rhyodacite fields (fig. 3). Samples with elevated gold values, high loss-on-ignition values and high normative corundum were eliminated from this data set. The loss of sodium, potassium, and calcium during alteration of feldspar to mica and clay minerals produced major oxide analyses that are strongly peraluminous. Even the least altered samples of igneous rocks from Donlin Creek appear weakly peraluminous due to alteration. It is unclear from the present data whether the original magma was also peraluminous. Most likely, the Donlin Creek igneous rocks have primary metaluminous compositions like Late Cretaceous plutonic rocks throughout the Kuskokwim Mountains (compare Szumigala, 1993). Limited trace-element data in table 1 are similar to data from Kuskokwim plutonic rocks with clear volcanic arc signatures.

Fine-grained rhyodacite porphyry (RDF) occurs as narrow dikes with a fine crystalline matrix and smaller phenocrysts than other rhyodacite units. Extensive drilling indicates that RDF occurs throughout the Lewis and Queen prospects. Maximum apparent thickness in core is 70 ft (22 m). RDF contains 5 percent 0.04–0.08 in (1–2 mm) feldspar phenocrysts and 5 percent 0.04–0.08 in (1–2 mm) quartz phenocrysts, commonly in a flow-banded-like matrix with wispy hairline graphite veinlets. RDF dikes are always strongly altered and no primary minerals for dating have been found. However, RDF dikes fit best in geologic modeling and cross-section building if assumed to be younger than mafic dikes and older than other rhyodacite units.

Rhyolite dikes occur at the northern end of the Donlin Creek property at the Dome and Duqum prospects. The rhyolite appears more siliceous than the rhyodacite units and generally is a light gray to cream color. Quartz phenocrysts have square to slightly rounded shapes that occupy 20 to 25 percent of the rock volume.

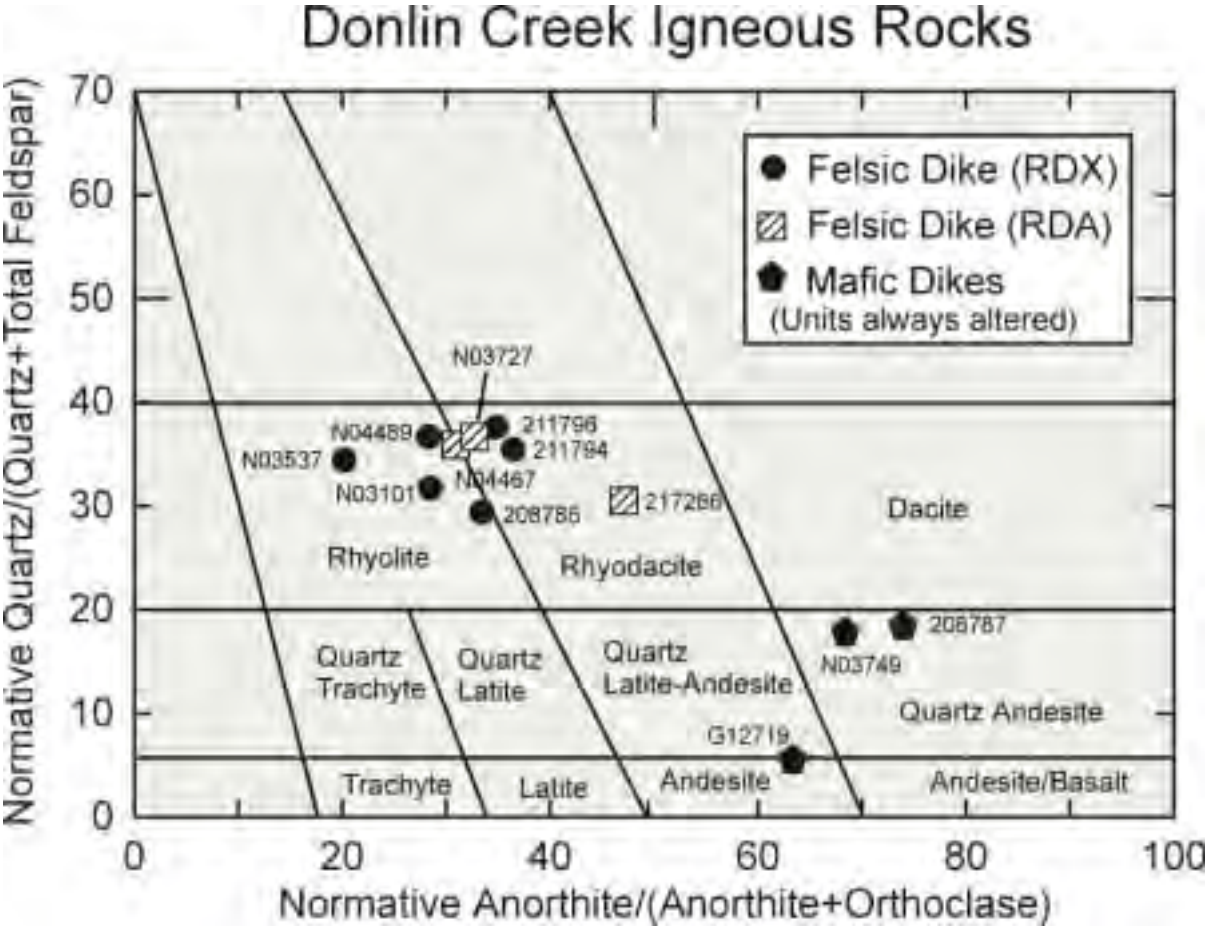

Figure 3. *Compositional plot for Donlin Creek dikes (modified from Streckeisen and LeMaitre, 1979). Dike compositional data shown in table 1.*

Mafic dikes exposed at the surface in the southern part of the Donlin Creek property weather a distinct reddish-brown color with a fine granular texture. Mafic dikes are generally only 5–10 ft (1.5–3.0 m) thick. Sparsely distributed mafic dikes crop out along the runway on American Ridge, beyond the known southern limit of mineralization. Field relationships and $^{40}Ar/^{39}Ar$ dating indicate that mafic dikes are the earliest igneous phase in the Donlin Creek area. Several drill intercepts of fresh mafic dike are biotite-rich (up to 75 percent) and hence lamprophyres. Mafic dikes are generally almost completely altered to carbonate and sericite, with a bleached cream to greenish tan color. A characteristic alteration/oxidation mineral is bright green fuchsite occurring as isolated grains. Petrographic examination shows that mafic dikes contain 2–5 percent opaques (including trace amounts of fine-grained gersdorffite [NiAsS]), 10 percent secondary silica (chalcedony) filling voids, up to 80 percent very fine-grained plagioclase laths (An_{50}), 5 percent possible augite phenocrysts, and highly variable amounts of biotite phenocrysts (10–75 percent) (John McCormack, written commun.). Three relatively unaltered samples of mafic dikes plot in the andesite and quartz andesite fields in figure 3.

RADIOMETRIC DATING

Results from radiometric dating studies on Donlin Creek igneous rocks and alteration are summarized in table 2. Age spectra for the $^{40}Ar/^{39}Ar$ data are shown in figure 4 and separated by rock type.

K-Ar dates for biotite from rhyodacite dikes in the Donlin Creek area range from 65.1 ± 2.0 to 69.5 ± 2.1 Ma (Miller and Bundtzen, 1994). These ages are within the age range for igneous rocks (61 to 73 Ma) of the Kuskokwim Mountains plutonic belt (Szumigala, 1993). Hydrothermal sericite at Donlin Creek has previously been dated at 70.0 ± 0.3 Ma by $^{40}Ar/^{39}Ar$ (Gray and others, 1997, 1992), and 70.9 ± 2.1 Ma by K-Ar (Miller and Bundtzen, 1994), indicating that mineralization is broadly contemporaneous with emplacement of the dike swarm.

Mafic dikes are the oldest igneous rocks in the Donlin Creek area. A mafic dike at the Queen prospect yielded a $^{40}Ar/^{39}Ar$-biotite age of 72.6 ± 0.9 Ma and a whole-rock age of 74.4 ± 0.8 Ma. Biotite from a rhyodacite dike at the Queen prospect yielded a $^{40}Ar/^{39}Ar$-plateau age of 70.3 ± 0.2 Ma. Sericite $^{40}Ar/^{39}Ar$ ages from altered feldspar phenocrysts in rhyodacite dikes from the Queen–Lewis area range from 73.6 ± 0.6 Ma to 67.8 ± 0.3 Ma. Overall, good plateau ages of igneous biotite and sericitized feldspar from rhyodacite dikes yield similar results within analytical error, indicating that alteration (and mineralization?) ages of igneous rocks are indistinguishable from igneous cooling ages.

Sericite from rhyolite dikes at the Dome prospect have the youngest $^{40}Ar/^{39}Ar$ ages (65.1 ± 0.9 Ma and 68.0 ± 1.0 Ma) from the Donlin Creek area. These young ages suggests that mineralization at Dome may be related to a different, younger hydrothermal system than that responsible for gold mineralization at Queen and south Lewis. Alternatively, the Dome rhyolite ages may simply reflect a longer time to cool below the argon blocking temperature for the apparently deeper Dome system.

STRUCTURE

Structural patterns at Donlin Creek are complex and still being deciphered, but several features appear to be important in understanding and predicting mineralization. Structural controls appear to be very important in the deposit's genesis, from ground preparation prior to emplacement of the dike swarm through possible post-mineralization displacements. Core logging with core orientation by the clay impression method and deep trenching programs begun in 1997 were critical in deciphering the structural history.

Major faults in the project area are not exposed, but topographic lineaments and airborne-geophysical data interpretation suggest that modern stream channels follow fault traces. Miller and Bundtzen (1994) mapped northeast-trending Donlin and Crooked creeks as Cretaceous-age splays of the Iditarod–Nixon Fork fault and interpreted a right-lateral motion for these faults. Other drainages (American Creek, Dome Creek, and Snow Gulch) are interpreted to be fault traces based on airphoto lineaments and aeromagnetic patterns (Szumigala, 1997).

Drill core shows numerous shears ranging from microshears to extensive shear zones. The abundance of shears present in drill core is much greater than indicated by previous mapping and figure 2. North-northeast- and northwest-trending faults reflect the dominant structural trends. Many of the igneous/sedimentary contacts observed in core are structural (shears or faults) rather than intrusive.

Multiphase rhyodacitic intrusions are both concordant and discordant to sedimentary rock bedding. Intrusion of these dikes probably occurred during an extensional tectonic phase and may have been controlled by anticlinal structures within the Kuskokwim Group country rocks. Late intrusive phases may have remobilized or dislocated mineralized zones and very minor post-mineralization faulting may have offset both intrusions and mineralization.

Most faults and shear zones appear to be sub-parallel to rhyodacite bodies and have moderate to steep dips. A family of moderately to steeply, east- and west-dipping, normal or oblique-slip faults that strike between 000° and 030° dissects dikes, sills, and sedimentary rocks

Table 1. *Whole-rock analyses of representative, least altered igneous rock types at Donlin Creek*

Rock Type		**RDX**	**RDX**	**RDX**	**RDX**	**RDX**	**RDX**	**RDA**	**RDA**	**RDA**	**MD**	**MD**	**MD**
Sample		**N03101**	**N03537**	**N04489**	**211794**	**211796**	**208786**	**217286**	**N03727**	**N04467**	**208787**	**N03749**	**G12719**
Al_2O_3	%	14.36	13.59	14.25	14.93	14.95	15.55	15.25	14.47	14.20	13.48	9.93	8.91
CaO	%	2.06	1.48	2.16	2.61	2.52	2.49	3.50	2.41	2.18	5.82	5.67	5.64
Cr_2O_3	%	0.01	0.01	0.01	0.00	0.00	0.00	0.00	0.01	0.02	0.03	0.15	0.13
Fe_2O_3	%	0.27	0.21	0.55	0.71	1.14	0.10	0.48	0.27	0.25	0.57	0.36	0.53
FeO	%	2.15	1.57	2.08	2.50	1.88	2.43	3.34	2.66	2.49	5.16	6.46	6.24
K_2O	%	4.19	4.65	4.42	3.63	3.75	3.92	3.13	3.92	3.83	1.44	1.83	1.51
MgO	%	0.62	0.38	0.88	0.93	0.85	0.89	1.10	0.92	0.89	6.64	10.73	13.23
MnO	%	0.04	0.02	0.09	0.08	0.07	0.03	0.08	0.07	0.06	0.10	0.15	0.14
Na_2O	%	3.05	2.94	2.06	2.38	2.26	3.37	2.65	2.17	2.42	2.11	0.43	1.09
P_2O_5	%	0.10	0.09	0.10	0.14	0.15	0.16	0.20	0.15	0.13	0.22	0.26	0.32
SiO_2	%	68.25	70.37	67.14	65.41	66.67	68.73	63.41	65.94	66.03	53.19	47.75	47.27
TiO_2	%	0.28	0.18	0.29	0.36	0.36	0.38	0.54	0.37	0.36	0.90	0.59	0.54
LOI	%	3.43	3.14	4.82	5.44	5.03	1.22	5.98	5.64	5.87	9.01	13.78	12.96
TOTAL		**98.81**	**98.63**	**98.85**	**99.12**	**99.63**	**99.27**	**99.66**	**99.00**	**98.73**	**98.67**	**99.11**	**98.51**

CIPW NORMS

Sample		**N03101**	**N03537**	**N04489**	**211794**	**211796**	**208786**	**217286**	**N03727**	**N04467**	**208787**	**N03749**	**G12719**
Quartz	%	29.250	32.333	33.175	31.456	33.822	26.699	26.864	32.456	32.200	12.378	8.814	2.199
Corundum	%	1.365	1.304	2.541	2.856	3.119	1.652	1.728	2.823	2.608	0.000	0.000	0.000
Orthoclase	%	25.964	28.781	27.783	22.900	23.427	23.627	19.745	24.817	24.380	9.495	12.802	10.447
Albite	%	27.061	26.055	18.540	21.498	20.215	29.083	23.937	19.670	22.057	19.920	4.307	10.798
Anorthite	%	10.031	7.074	10.703	12.846	12.180	11.533	17.141	11.758	10.735	25.727	23.392	17.514
Diopside	%	0.000	0.000	0.000	0.000	0.000	0.000	0.000	0.000	0.000	3.947	6.355	10.241
Hypersthene	%	5.118	3.557	5.579	6.271	4.401	6.144	8.255	6.933	6.570	25.137	41.142	45.835
Magnetite	%	0.410	0.319	0.848	1.099	1.747	0.148	0.743	0.419	0.390	0.922	1.150	0.900
Hematite	%	0.000	0.000	0.000	0.000	0.000	0.000	0.000	0.000	0.000	0.000	0.000	0.000
Ilmenite	%	0.558	0.358	0.586	0.730	0.723	0.736	1.095	0.753	0.736	1.907	1.327	1.201
Apatite	%	0.243	0.218	0.246	0.346	0.367	0.378	0.495	0.372	0.324	0.569	0.713	0.868
SUM	**%**	**100.00**	**100.00**	**100.00**	**100.00**	**100.00**	**100.00**	**100.00**	**100.00**	**100.00**	**100.00**	**100.00**	**100.00**

Trace Element Geochemistry

Sample Number	C %	Ba ppm	Ce ppm	Cs ppm	Co ppm	Cu ppm	Dy ppm	Er ppm	Eu ppm	Gd ppm	Ga ppm	Hf ppm	Ho ppm	La ppm	Pb ppm	Lu ppm	Nd ppm
211794	1.06	1480	--	--	--	--	--	--	--	--	--	--	--	--	--	--	--
211796	0.92	1395	--	--	--	--	--	--	--	--	--	--	--	--	--	--	--
217286	1.04	1920	--	--	--	--	--	--	--	--	--	--	--	--	--	--	--
208786		1505	62.5	3.4	4.5	40	4.6	2.5	1.3	5.7	19	4	0.9	31	30	0.3	26
208787		875	35	5.9	25.5	40	3.2	1.9	1.2	3.9	16	2	0.7	17	<5	0.3	16

Sample Number	Ni ppm	Nb ppm	Pr ppm	Rb ppm	Sm ppm	Sr ppm	Ta ppm	Tb ppm	Th ppm	Tn ppm	U ppm	V ppm	Yb ppm	Y ppm	Zn ppm	Zr ppm
211794	--	10	--	128	--	220	--	--	--	--	--	--	--	18	--	165
211796	--	10	--	134	--	214	--	--	--	--	--	--	--	18	--	153
217286	--	10	--	88	--	282	--	--	--	--	--	--	--	22	--	123
208786	10	16	7.6	104	5.7	332	2.0	0.9	6	0.4	4	25	2.2	23	60	179
208787	75	9	4.5	36	3.9	359	1.0	0.6	3	0.3	2	125	0.5?	15	80	128

Table 2. *$^{40}Ar/^{39}Ar$ and K-Ar dates from the Donlin Creek area, Alaska*[a]

Prospect Area Sample ID	Rock Type	Mineral Dated	Plateau Age (Ma)[b]	Comments
Queen DC96-231C@93.5m	Mafic Dike (MD)	Biotite/ whole rock	none	Mixed phases with relic ages. Coarse fraction.
Queen DC96-231C@93.5m	Mafic Dike (MD)	Biotite	72.6 ± 0.9	Fair plateau. Biotite separate from fine-grained rock matrix.
Queen DC96-231F@93.5m	Mafic Dike (MD)	Whole rock	74.4 ± 0.8	Good plateau. Biotite/whole rock separate from fine-grained matrix.
Queen DC96-240@71m	Rhyodacite (RDX)	Sericite	73.6 ± 0.6	Good plateau, but possible ^{39}Ar recoil loss results in an older age than the "true" age.
Queen DC96-240@288.9m	Rhyodacite (RDA)	Biotite	70.3 ± 0.2	Good plateau.
Southwest Lewis DC96-217@132m	Rhyodacite (RDA)	Sericite	70.5 ± 0.2	Good plateau.
Southwest Lewis DC96-217@35m	Rhyodacite (RDA)	Sericite	70.5 ± 0.3	Good plateau.
Southeast Lewis DC96-261@250.9m	Rhyodacite (RDA)	Sericite	70.9 ± 0.3	Good plateau
Rochelieu DC96-210B@156.5m	Rhyodacite (RDX)	Sericite	67.8 ± 0.3	Bimodal plateau.
Dome DC96-250@131m	Rhyolite (RHY)	Sericite	65.1 + 0.9	Good plateau.
Dome DC96-253@166m	Rhyolite (RHY)	Sericite[c]	68.0 ± 1.0[c]	Mini plateau = 68.6 ± 0.8; agrees with isochron age using only low Ca/K fractions.
Far Side DC96-255@11.3m	Rhyodacite (RDA)	Sericite	68.0 ± 3.1[c]	Isochron ages used due to downstepping plateau.
Lewis Gulch DC96-266@125.3m	Rhyodacite (RDX)	Sericite	72.3 ± 1.4[c]	Downshifting plateau, isochron age agrees well with low Ca/K fractions plateau age.
Snow Gulch USGS1	Rhyodacite	Sericite	70.0 ± 0.3	$^{40}Ar/^{39}Ar$ method. Gray and others (1992).
Snow Gulch USGS2	Rhyodacite	Sericite	69.5 ± 1.1	Isochron-disturbed sample. Gray and others (1997).
West side of Crooked Creek USGS3	Rhyodacite	Biotite	65.1 ± 2.0	K-Ar age, K_2O very low. Miller & Bundtzen (1994).
East side of Dome Creek USGS4	Rhyodacite	Sericite	70.9 ± 2.1	K-Ar age. Miller & Bundtzen (1994).
East side of Dome Creek USGS5	Rhyodacite	Biotite	69.5 ± 2.1	K-Ar age, K_2O very low. Miller & Bundtzen (1994).

[a]Dates via $^{40}Ar/^{39}Ar$ method and analyzed by UAF Geochronology Lab unless noted otherwise, 1 sigma analytical error on ages.
[b]Plateau Age is Best Interpreted Age.
[c]Isochron Age (Ma) = Interpreted Age for more complex or disturbed samples.

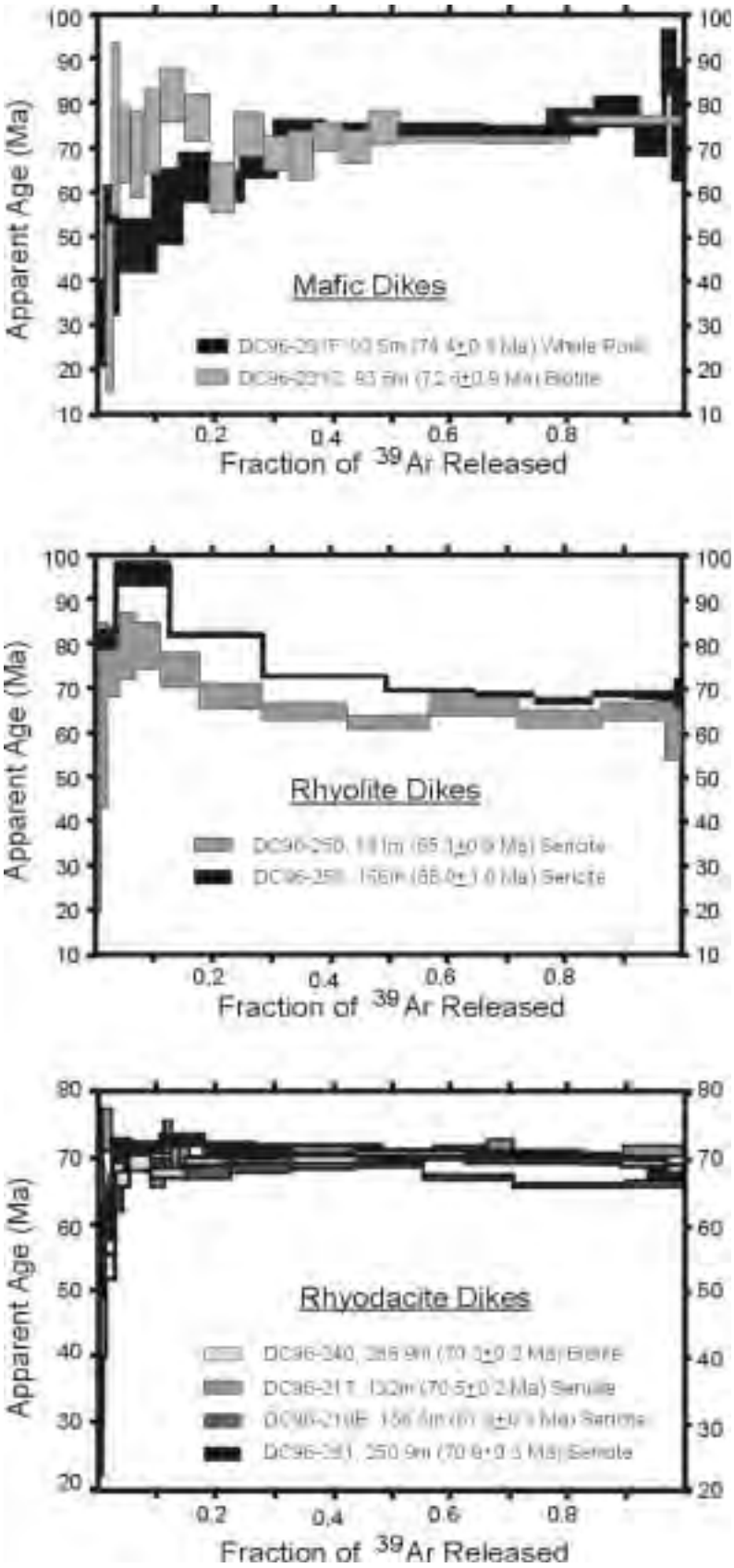

Figure 4. *$^{40}Ar/^{39}Ar$ spectra for sericite and biotite from Donlin Creek igneous rocks. Mafic dike data are slightly erratic, but yield fair plateaus. Rhyolite samples from Dome show a downstepping plateau, with a mini plateau. Biotite and sericite from rhyodacite samples yield good plateaus.*

across the Donlin Creek property (O'Dea, 1997). A well-exposed sequence of Kuskokwim Group sedimentary rocks is present on American Ridge along the airstrip. The sedimentary rocks are cut by a number of north-northeast- to northeast-striking faults, with fault surfaces dipping moderately east or west and characterized by well-developed down-dip slickenside lineations. Several of the faults have broad, open, drag folds developed in their hanging walls (O'Dea, 1997). The absence of cleavage development parallel to the axial planes of these folds and the open geometry of the folds suggest that the folding and faults are a consequence of extensional faulting (O'Dea, 1997).

Fault surfaces in the Lewis trenches are filled with abundant graphite and/or limonite (oxidation of sulfides). Broad zones, up to 7 ft (2 m) wide, of intense micro-fracturing filled with arsenopyrite occur within highly sericitized dikes. Discontinuous, vuggy quartz–carbonate veins occur near fault zones. Quartz–carbonate veins developed in fault wallrocks dip more steeply than the faults and have approximately horizontal fibers. These features are compatible with east-west extension and normal displacement. This north-northeast-trending shear set correlates well with zones of high-grade gold mineralization.

The amount of displacement on any individual fault is less than several feet based on drillhole and trench mapping. Cumulatively, the normal displacement across the fault system in the Lewis area is estimated to be less than 100 ft (30 m) (O'Dea, 1997).

There is widespread evidence from across the Donlin Creek property for a deformational event (D1) that preceded the development of the north-south oriented normal fault system (D2) (O'Dea, 1997). Some important evidence for an early deformational event include:

- Kuskokwim Group strata are tilted and consistently dip shallowly to moderately to the south-southwest. The tilted bedding is cut by north-northeast-striking normal (extensional) faults.
- Kuskokwim Group strata are often imbricated across shallowly south-dipping faults.
- Shale and siltstone strata commonly display zones of bedding-parallel shear and gouge.
- Many igneous units mapped in the trenches display a pervasive shear fracturing that is sub-parallel to layer-parallel shearing in the sedimentary rocks. In many instances, the same tectonic fabric can be traced through bedding and into rhyodacite.
- Consistent overprinting relations indicate that bedding-parallel fabric and faults pre-date steeper oriented northeast-trending fabric and shears. These relations have been observed in exposures from American Ridge to the Queen prospect.

The deformation documented above may have been caused by (1) northward stratigraphic imbrication along south-dipping thrust faults, or (2) rotational tilt block development during north-south extension. A preliminary interpretation of this evidence strongly suggests that the D1 event was a north-directed thrusting event. The development of layer-parallel fabrics within the sedimentary and igneous rocks and the imbrication of strata across south-dipping faults are consistent with thrust fault development (O'Dea, 1997). The intrusive bodies must have been subjected to at least part of the D1 deformation because pervasive shear fracturing in igneous rocks can be traced into layer-parallel shearing in the sedimentary rocks. It is concluded that sills were intruded during the waning of the D1 event because sedimentary rock-igneous rock contacts are not displaced across bedding-parallel D1 faults (O'Dea, 1997).

In summary, structural studies by Placer Dome Exploration Inc. hypothesize two deformation events at Donlin Creek (O'Dea, 1997). The D1 event was compressional with north-directed movement, resulting in imbrication of stratigraphy and layer-parallel fabrics. Low-angle faults dominate this event and shaley units localized most of the movement. Local imbrication of rhyodacite suggests that the D1 event was syn- to post-dike emplacement. The D2 event was an east-west extensional event that fractured all rock units and led to later localization of gold in open fractures. Post-mineralization movement on any given fault or shear plane appears to range from a few inches (centimeters) to less than 10 ft (a few meters).

ALTERATION

Alteration styles are fairly simple at Donlin Creek. All intrusive units are altered and fresh rocks are uncommon. Sericite is the main alteration product replacing both phenocrysts and matrix. Sericite-dominant alteration (sericite $\pm$ illite $\pm$ kaolinite $\pm$ carbonates $\pm$ pyrite) is pervasive, but varies in intensity. Most sericite is a whitish color, but some plagioclase phenocrysts are replaced by light green sericite (montmorillonite?), especially in less altered intrusive rocks. It is unclear whether there was a supergene alteration event at Donlin Creek. Carbonate replaces phenocrysts and rhyodacite matrix.

Pervasive carbonate alteration (mostly dolomitic and ankeritic) is common in all igneous rock units. Quartz–carbonate–sulfide veinlets crosscut clay- and sericite-altered rock, but relative timing between sericite and carbonate alteration has not been determined. However, relative carbonate alteration intensity appears indepen-dent of sericite alteration intensity.

Silicic alteration is weak to absent at Donlin Creek, and confined to weak replacement of porphyry and

graywacke matrix material. Areas of strong pervasive silicic alteration are localized, and present only in rare areas of strong stockwork silica veining.

Altered mafic dikes are bleached to a cream color. Alteration of mafic dikes is dominated by carbonate, with local almost complete carbonate replacement. Carbonate fracture fillings are also very common. Bright green fuchsite (chrome-bearing mica) is a distinctive alteration mineral confined to mafic dikes.

Very fine-grained graphite is pervasive throughout most intrusive rocks as disseminated grains in a volume percentage range of 0.5 to 3 percent and represented by up to 12 percent carbon in chemical analyses (unpublished Placer Dome data). The graphite is thought to be a hydrothermal alteration product, but it is not clear whether graphite is a separate alteration event or part of the sericite and carbonate alteration events. Graphite is common and occurs in open spaces or high porosity areas, often with coarse sericite or as fine, isolated, shred-like fragments, wisps and grains. Graphite content in rhyodacite commonly increases near faults/shears and sedimentary contacts. An increase in graphite, along with an increase in finely disseminated sulfides, imparts a distinct blue-gray color to the typical gray-colored rhyodacite. Coarse graphite clots up to 1.1 in (3 cm) in diameter occasionally occur in rhyodacite units. The genesis of the graphite clots is not clear. It is unlikely that the clots are melted Kuskokwim Group sedimentary rock because rhyolite composition magmas are not hot enough to melt carbon and quartz (major constituents of the sedimentary rocks). The graphite clots may be condensed methane (Rainer Newberry, written commun.). Methane could have formed by decomposition of organic materials in the surrounding sedimentary rocks at depth (essentially a contact metamorphic phenomenon). The rising methane would have cooled, oxidized, and eventually condensed as graphite.

Wall-rock alteration is not megascopically visible in the Kuskokwim Group sedimentary rocks even in close proximity to highly altered intrusive rocks. However, where intrusive sills terminate along strike there is a thin (0.5–3 inch [1.2–8 cm] wide) envelope of black clay or gouge. No contact metamorphic effects were noted in wallrocks except at the Dome and Duqum prospects.

MINERALIZATION

ORE MINERALS

Ore mineralogy at Donlin Creek is dominated by simple sulfide assemblages. The most common ore minerals are pyrite, arsenopyrite, and stibnite. Other ore minerals include marcasite, realgar, orpiment, and limonite, with lesser amounts of native arsenic, native gold, cinnabar, covellite, chalcopyrite, galena, pyrrhotite, malachite, sphalerite, scorodite, molybdenite, stibiconite?, kermesite?, and hematite. Trace amounts of enargite were seen in thin section enclosed in an arsenopyrite grain, and trace amounts of fine-grained gersdorffite were found in mafic dike samples (John McCormack, 1996, unpublished petrographic report for Placer Dome).

Pyrite is common and appears to be the earliest sulfide phase. Pyrite is ubiquitous in the rhyodacite phases and occurs as disseminated grains and as microfracture fillings. Disseminated pyrite is generally absent within the siliciclastic section. Disseminated pyrite in the sedimentary rocks occurs as fine to coarse grains (up to 0.2 in [5 mm] across) preferentially concentrated near igneous contacts. Most, if not all, of the pyrite is believed to be epigenetic in origin. Pyrite is also common in areas of strong quartz–carbonate veining in both igneous and sedimentary rocks. Relative abundance of pyrite is not an indicator of gold grade.

Arsenopyrite is the dominant gold-bearing mineral at Donlin Creek. Arsenopyrite is deposited later than pyrite and commonly replaces pyrite in all cases examined petrographically. Arsenopyrite occurs as fine to very fine grains disseminated in intrusive rocks and as fracture/vein fillings. Fine-grained arsenopyrite is difficult to distinguish from disseminated graphite in hand specimen and visual estimates may vary widely in accuracy. Marcasite is found as coatings on fine- and coarse-grained arsenopyrite.

Native arsenic occurs as dark gray, granular massive to reniform masses and grains commonly associated with stibnite in dolomite veinlets. Stibnite commonly occurs as disseminated grains and masses within carbonate veins and occasionally as interlocking needles up to 0.08 by 1 in (2 mm by 2–3 cm) in size in open spaces within quartz–carbonate veins and on fracture surfaces. Stibnite replaces arsenopyrite in at least some cases and stibnite-dominant mineralization is most common in sedimentary rock-hosted veins.

Sphalerite occurs as rare, scattered grains associated with stibnite in carbonate veins. Galena, tetrahedrite, and sphalerite are found in sedimentary heavy mineral concentrates (Chryssoulis and others, 1996). Realgar and orpiment occur as vein and fracture fillings in late, crosscutting structures ($\pm$ quartz) and locally replace sericite casts of feldspar phenocrysts. Graphite may be deposited last because it typically fills open spaces and fractures, but there is not a clear relationship to other mineralization.

Gold mineralization at Donlin Creek is refractory, with arsenopyrite as the dominant gold-bearing mineral. Geochemical results indicate the affinity of gold with arsenic and antimony. Metallurgical tests indicate that 95–98 percent of the gold in the Lewis area is contained

in arsenopyrite. Fine-grained arsenopyrite (<20 mm diameter) contains 5–10 times more gold than coarse-grained arsenopyrite (Chryssoulis and others, 1996). Visible gold is extremely rare at the Donlin Creek property and has only been found at the Far Side prospect in association with thin quartz veins cutting rhyodacite porphyry. Gold observed in polished thin sections occurs as 1 to 3 mm blebs with no clear paragenetic relationship to other minerals (John McCormack, 1996, unpublished petrographic report for Placer Dome).

MINERALIZATION ZONES

Gold mineralization at Donlin Creek occurs over a remarkable 4-mi-long (6.5-km-long) area with a northeast–southwest trend. Mineralization is open at depth and to the northeast and west. Figure 1 shows 12 prospects, mostly aligned in a northeast-southwest direction along a rhyodacite dike system. Most prospect names refer to the creek immediately north of the ridge on which they occur. From north to south, the prospect names are Far Side (formerly known as Carolyn or Wheetie), Dome, Duqum, Quartz, Snow, Queen, Lewis (further subdivided into Northeast, Southeast, Southwest, Vortex, and Rochelieu areas), 400 Area, and ACMA. The bulk of recent exploration work has been conducted in the Queen, Lewis, and ACMA areas.

Gold mineralization at Donlin Creek is lithologically and structurally controlled. Ore mineralization in igneous rocks is controlled by disseminated arsenopyrite, shear/fracture coatings, and sulfide (pyrite, arsenopyrite, and/or stibnite) ± quartz ± carbonate veinlets. Structurally controlled mineralization typically occurs in the Kuskokwim sedimentary rocks proximal to dike and sill contacts. Quartz–carbonate–sulfide (pyrite, stibnite, and arsenopyrite) veins are the primary mineralized features, but gold mineralization also occurs in thin, discontinuous veinlets and fracture fillings. Veinlets seldom exceed 0.5 in (1 cm) in diameter and most fracture fills are just thin sulfide coats on fracture surfaces. Realgar and orpiment with local high gold values occur as late-stage fracture filling in sediments and intrusive rocks crosscutting other mineralized structures. Realgar and orpiment are locally disseminated in rhyodacite.

Mineralization is open to depth and along strike in the Lewis/Rochelieu area. Figure 5 is a cross-section through the Northeast Lewis and Rochelieu areas. The ore zones are concentrated near rhyodacite bodies, but there is not a one-to-one correlation. Ore zones are offset and discontinuous along portions of their strike length due to faults, shearing, and local rock competency differences. Mineralization occurs in two main structural domains within the Queen to ACMA areas (the main bulk mineable resource). A series of north-northeast-trending dikes and faults with a subordinate northwest fabric occurs in the Northeast Lewis/Rochelieu area whereas north-northeast-trending structures crosscutting northwest-trending dikes, sills, and structures dominate the Southeast and Southwest portions of the Lewis areas and the ACMA area.

In the Rochelieu area, three mineralized zones over a 1,000-ft-wide (300-m-wide) area can be traced for 2,000 ft (600 m) in a northeast direction. The zones are 35 to 70 ft (10–20 m) thick, dip 45°–60° to the southeast and average 0.058 to 0.12 oz/ton (2–4 g/tonne) gold. Mineralized zones are hosted in graywacke, shale, rhyodacite with sheared margins, and a rhyodacite dike.

The Northeast Lewis area contains four mineralized zones controlled by normal faults having minor displacement that can be traced for approximately 1,600 ft (500 m) in a northeast direction. The ore zones vary in strike from 355º to 045º and dips range from vertical to -50°, both to the east and west. The ore zones are similar in thickness to zones described at Rochelieu, with the addition of a zone of variable thickness that is controlled by a low-angle fault subparallel to a rhyodacite/sedimentary rock contact. Factors that apparently controlled gold deposition include the presence of porphyry dikes or thick graywacke units and possibly flexures in structure orientations.

Mineralization at the Queen prospect is associated with northeast-trending rhyodacite dikes and north-northeast-trending faults that dip steeply to the southeast. Igneous lithologies are continuous from Northeast Lewis, and the known mineralization at Queen occurs over a 1,300 ft (400 m) strike length.

The south Lewis area has multiple controls on gold mineralization, with northeast-trending shear zones like those present at the north Lewis and Queen areas, as well as northwest-trending sills and faults. A cross-section of the south Lewis area is shown in figure 6. These multiple controls lead to discontinuous, discrete mineralization zones. Some of the thicker zones of mineralization appear to be southwest dipping. The thickest and highest-grade drill intercepts occur where north-northeast-trending structures intersect northwest-trending sills.

Several gold soil anomalies (>0.5 parts per million gold) occur over a 2.5 mi (4 km) strike length to the west of Lewis ridge in an area without rock exposure. Drilling in this area to the west of the Rochelieu area encountered several igneous bodies as well as several drill intercepts that assayed between 0.088 and 0.15 oz/ton (3–5 g/tonne) gold. Drilling proved that dikes occur west of the main Lewis Ridge and that gold mineralization also occurs within that area.

Rhyodacite bodies were exposed during trenching and excavation of road building materials in the 400 Area. These bodies are southwest of the Lewis area

and approximately 2,600 ft (800 m) from previously known igneous rocks. These rhyodacite bodies have northwest strikes (~300°) and appear to be 30 to 70 ft (10–20 m) thick. Sericite-altered rhyodacite porphyry locally contains up to 0.23 oz/ton (8 g/tonne) gold. Drilling encountered significant gold mineralization hosted in quartz–pyrite–arsenopyrite–carbonate veinlets and local realgar veinlets within altered rhyodacite and immediate wallrocks.

Gold and arsenic have a fairly strong positive correlation, reflecting the occurrence of gold as submicron particles in the crystal lattice of arsenopyrite. Mercury and antimony correlate with gold to a lesser degree. There is a general inverse relationship between gold and sodium. Sodium loss is directly related to an increase in sericite alteration, and geochemical data from the Donlin Creek property indicate that gold values increase with increasing sericite alteration. Based on

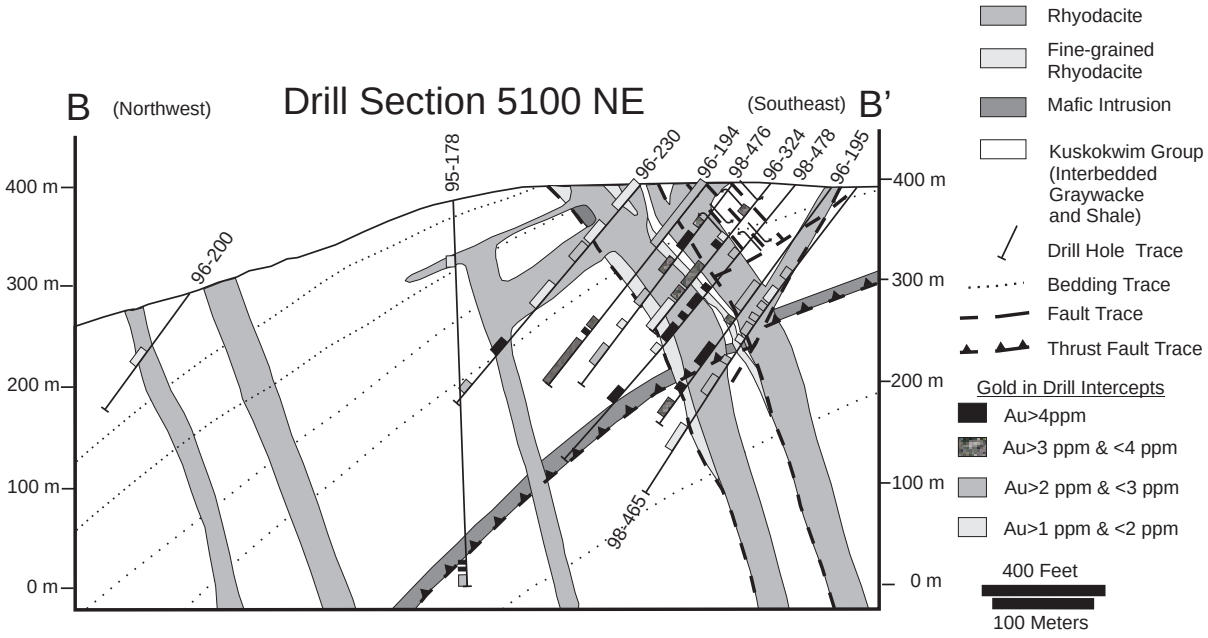

Figure 5. *Geologic cross-section through Lewis and Rochelieu prospects. Note the abundant dikes and high-grade gold intercepts associated with faults in the dikes.*

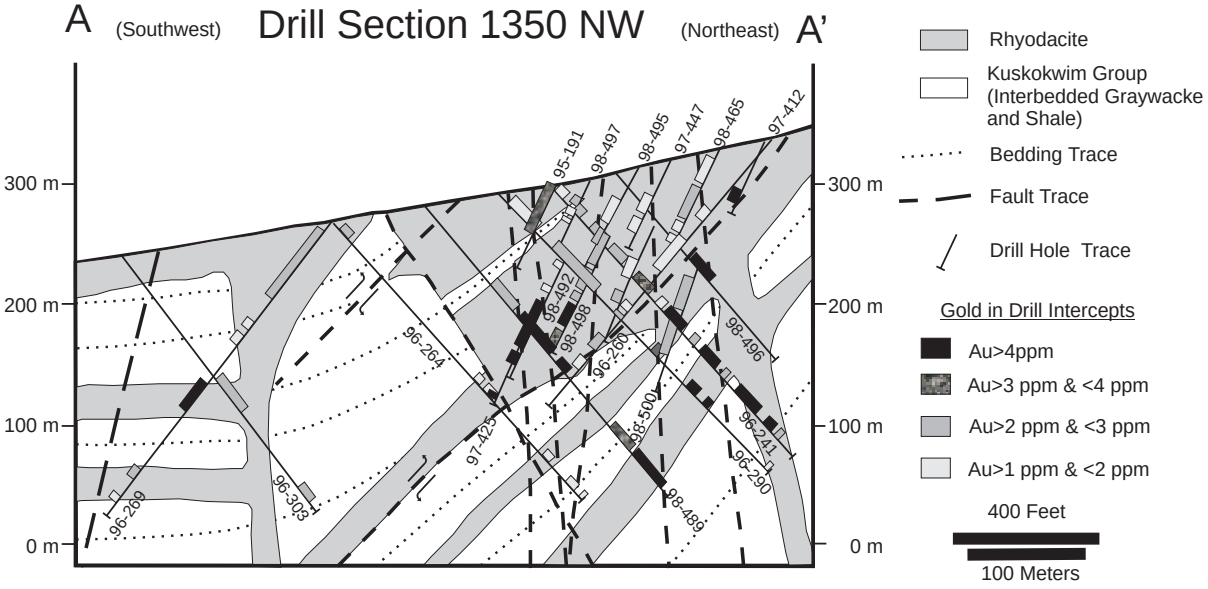

Figure 6. *Geologic cross-section through the Southeast and Southwest Lewis prospects. Note that rhyodacite occurs as both dikes and sills and most high-grade gold intercepts occur within faulted rhyodacite.*

silver:gold ratios and copper:gold ratios, it is inferred that a progressively deeper expression of a hydrothermal system is exposed from south (Lewis area) to north (Dome area).

Gold mineralization (especially ≥0.1 oz/ton [≥ 3 g/tonne] gold) at the Donlin Creek deposit is structurally controlled and, in the northeastern Lewis area, localized within a post-intrusion, small-displacement, normal fault system. Individual faults within this extensional system strike between 000° and 030° and dip predominantly toward the east, reflecting a syn-mineralization east-west extensional event. The majority of mineralization is hosted within an irregular swarm of rhyodacitic and subordinate mafic to intermediate sills and dikes of variable thickness and orientation. Mineralization is hosted, to a lesser degree, within massive graywacke.

Fault orientations commonly change as faults propagate through rock types of varying competence and composition (Ramsay and Huber, 1987). Faults dip more shallowly in incompetent units and steepen abruptly in more competent units. Dilation zones are created around the steeper segments of the faults. At Donlin Creek, dips of the normal faults may change from relatively shallow to relatively steep as the fault propagates from shale to rhyodacite or graywacke. A dilation zone and possible ore shoot may form as a result of this geometry.

Resultant high-grade ore shoots may be localized along these normal faults, where they steepened and dilated as they cut through more competent rock types such as rhyodacite and graywacke. Figure 7 depicts an idealized fault geometry and mineralization pattern. However, the inherent variability of a small-displacement fault system combined with the highly irregular geometries of a dike swarm will create a large degree of variability in the orientation of ore shoots, and likely relatively low degrees of continuity.

A model for structural control of gold mineralization at Donlin Creek is given in figure 7. Competency differences between various rock units are important factors in localization of gold mineralization. The brittle response of igneous rocks and graywacke to stress allows for more fracturing and creation of space for movement of ore fluids. Shale and siltstone tend to act more ductilely under stress and absorb stress by bedding plane movements, restricting the amount of open space for later fluid flow. Shale horizons may have acted more ductilely than the interbedded graywacke and magmatic fluids flowed along shale horizons to produce sills capped by thick shale units.

FLUID INCLUSIONS

A systematic fluid inclusion study at Donlin Creek has not been conducted, but observations have been made on three occasions on separate sets of samples. Results are consistent among sample sets and significant to understanding more about the deposit's origin. Table 3 summarizes observations made during these fluid inclusion studies. Measured vapor phase homogenization temperatures for two-phase, liquid-rich, primary fluid inclusions in vein quartz range from 150° to 260°C (Roberts, 1993; table 3). Crushing tests reveal abundant vapor bubble expansion, indicating a minimum of 0.1 mole percent CO_2 (Roberts, 1993). Porphyry and epithermal attributes (vein textures and various phases within fluid inclusions) were identified (Roberts, 1993), but the fluid inclusions were generally too small for microthermometric work.

Jim Reynolds (Fluid Inc., Denver) conducted preliminary qualitative fluid inclusion work in 1996 for Placer Dome Exploration Inc. Secondary fluid inclusions in igneous quartz phenocrysts are interpreted to broadly record temperature and fluid characteristics associated with hydrothermal fluids responsible for pervasive sericitic alteration. Pervasive sericitic alteration of rhyodacite porphyry at Lewis, Rochelieu and Queen is interpreted to form from dilute fluids in a hydrothermal system with temperatures probably between 200° and 350°C (table 3). Shallow, late quartz ± carbonate ± stibnite ± realgar veinlets, with local associated high gold values, have an inconsistent fluid inclusion population with abundant necking and few reliable primary fluid inclusions, features common in epithermal quartz (Bodnar and others, 1985). No daughter minerals were observed and temperatures of homogenization were estimated at below 200°C.

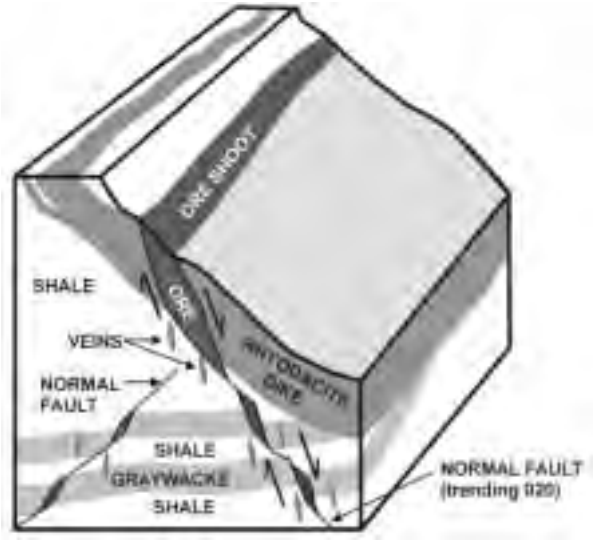

Figure 7. *Model for development of mineralization zones at Donlin Creek. Ore shoots developed in dilation zones along normal faults as the faults steepened in rocks such as rhyodacite and graywacke, which are more competent than the shale units.*

Table 3. *Donlin Creek fluid inclusion data*

Prospect sample no.	Sample description	Texture	%FIs	FI[a] sizes avg/max	FI[a] origin	FI shape	Number of phases	Estimated Temp (°C)	Measured[b] Temp (°C)	Interpretation	Reference[c]
Far Side	*Breccia vein at least 5 cm wide in feldspar–quartz porphyry with vein margin of prismatic quartz (1–2 mm wide). Vein matrix is very fine-grained quartz.*										1
TR-CT1-20m	host wallrock	euhedral quartz "eyes" in dike	2	<1/10	S	irregular–smooth	2 l+v-rich and 3+multi-solid	?			
	fragments in vein	euhedral prismatic quartz with growth zones	20	<3	P	irregular–smooth	2 l-rich	<200	147–196		
	long, thin brecciated shards in breccia vein	plumose-textured quartz	25	<3	S	irregular–smooth	2 l-rich, rare 3+multisolid	<200	220 (270 multi-solid inclusions decrepitate)	hydrothermal fluid from an early, deep? event	
	breccia-vein matrix	euhedral clear quartz (recrystallized?)	<1	<1	P	irregular	2	<200			
	opaque fragment in breccia vein	microcrystalline quartz	?	?	S?	?	?	<160			
Snow	*Breccia vein over 7 cm wide with breccia fragments of stibnite-rich, angular quartz matrix and quartz porphyry.*										1
TR-ST-5m	grains interlocked with anhedral quartz and as cockade texture around porphyry rock fragments	plumose quartz (?after amorphous silica or chalcedony?)	10	10/25	S	smooth	2 l+v-rich and 3+multi-solid	?	216–260 (multi-solid inclusions decrepitate at >300)	early, saline (minimum 23 eq. wt percent NaCl) fluid	
	broken fragments of earlier vein event	anhedral quartz	2	<3	S	irregular	2 l-rich	?	?		
	infilling around breccia fragments	prismatic, euhedral quartz	2	<3	P	irregular–smooth	2 l-rich	~200	153		
Lewis	*Thin (1–2 mm wide), translucent gray quartz vein cutting gray feldspar–quartz porphyry.*										1
TR-LT18-225m	resorbed and broken phenocrysts, FI's along fractures	quartz "eyes" in porphyritic wallrock	10	6/30	PS/S	smooth	2 l+v-rich and rare 3+multi-solid, rare 3-phase CO_2-rich inclusions	?			
		quartz breccia fragments in wallrock	1	<1	PS?	irregular	?	<200			
		prismatic quartz in vein	<1	<1	P	irregular	?	<200			
	FIs along fractures	late, subhedral quartz vein infill	2–20	<3	PS/S	irregular–smooth	2 l-rich	<200			
Lewis	*Highly iron-stained breccia vein over 10 cm wide, with fragments of pale green, feldspar–quartz porphyry and clear to translucent quartz.*							?			1
TR-LT26-146m	resorbed and broken phenocrysts, FIs along fractures	quartz "eyes" in porphyritic wallrock	25	3/15	PS/S	smooth	2 l+v-rich and 3+multi-solid				
	fragments in vein breccia	anhedral, broken quartz crystals	5–15	<3	S	irregular–smooth	2 l-rich and 3-phase solid present	?	~220	formed at 1–3 km depth?	
	matrix of breccia vein	late, euhedral, comb-textured, drusy quartz	<1	<1	P	irregular, & irregular l-v ratios	2 l-rich	<200			
	FIs along fractures	subhedral quartz vug fill	5	<1	S	irregular, & irregular l-v ratios	2 l-rich	<200	93–101		
Rochelieu DC96-210B, 156.5 m	sericite-altered rhyodacite	igneous quartz phenocrysts	scarce	--	S	?	l-rich	275–300		dilute fluids in hydrothermal system	2
Queen DC96-240, 82.9 m	sericite-altered rhyodacite	igneous quartz phenocrysts	scarce	--	S	?	l-rich	275–300		dilute fluids in hydrothermal system	2
Southwest Lewis DC96-260, 148.6 m	sericite-altered rhyodacite	igneous quartz phenocrysts	scarce	--	S	?	l-rich	275–300		dilute fluids in hydrothermal system	2

Prospect sample no.	Sample description	Texture	%FIs	FI[a] sizes avg/max	FI[a] origin	FI shape	Number of phases	Estimated Temp (°C)	Measured[b] Temp (°C)	Interpretation	Reference[c]
Lewis DC96-261, 251 m	sericite-altered rhyodacite	igneous quartz phenocrysts	scarce	--	S	?	l-rich	275–300		dilute fluids in hydrothermal system	2
Southeast Lewis DC96-244, 82.9 m & 92.5 m, DC96-248, 148.6 m	sericite-altered rhyodacite with quartz ± carbonate ± stibnite ± realgar veinlets and high gold grades	abundant necking-down of FIs, few reliable primary FIs	inconsistent			irregular	no daughter minerals	<200		dilute, heated groundwater	2
Dome DC96-250, 131 m	sericite-altered rhyolite	igneous quartz phenocrysts with multiple microfractures	abundant		S		l-rich, v-rich, v-rich w/ hypersaline l	>400–450		formed close to magmatic fluid source	2
Dome DC96-251, 62.5 m	sericite-altered rhyolite with quartz stockworks						l+v-rich	>400–450		formed in zone near (typically above) a magmatic source	2
Dome ?(USGS)	sericite-altered rhyolite with quartz stockworks	low salinity, vapor-rich inclusions with significant CO_2+CH_4					2		350–400	represents early magmatic fluid	3
	sericite-altered rhyolite with quartz stockworks	high salinity, l-rich with 1 or 2 daughter minerals, halite melts above 450°–550°C					2–3		350–400	represents early magmatic fluid	3

[a]FI=fluid inclusion, l=liquid, v=vapor, P=primary, PS=pseudosecondary, S=secondary.
[b]Measured temperature is measured microthermometric homogenization by vapor-phase disappearance and represents the **minimum** estimated trapping temperature.
[c](1) Roberts, 1993, (2) Arribus, written communication, 1996, (3) McCoy and others, 1999.

Sericitized rhyolite with hydrothermal quartz stockwork mineralization from the Dome prospect has vastly different fluid inclusion characteristics. Fluid inclusions are abundant and present along multiple microfractures crosscutting quartz phenocrysts in all directions. Fluid inclusions at the Dome prospect consist of a vapor-rich CO_2-bearing type co-existing with a high-salinity, liquid-rich, halite-bearing type, with liquid–vapor homogenization for both types at 340–380°C (McCoy and others, 1999). Similar fluid inclusions are less common throughout the rest of the Donlin Creek property (preliminary results) and homogenize at 220–300°C. These fluid inclusions are interpreted to be similar to fluid inclusions found in the core zone of porphyry-type deposits. On the basis of observations of porphyry-type deposits, these fluid inclusions would form very close to magmatic fluid sources where both high-temperature hypersaline and vapor-rich inclusions often coexist due to phase separation of a residual aqueous magmatic fluid.

STABLE ISOTOPE STUDIES

Nine sericite samples from sericite-altered feldspar phenocrysts in rhyodacite were collected from across the Donlin Creek property for oxygen and hydrogen isotope analyses (table 4). Figure 8 shows the isotopic composition of calculated hydrothermal fluids responsible for sericite formation and the relationships between those fluids and magmatic and Alaskan Cretaceous–Tertiary meteoric waters. The temperature used for calculation of fractionation factors between water and illite (the main mineral in the sericite collected for analysis) is 300°C on the basis of secondary fluid inclusion observations in igneous quartz phenocrysts from the same samples. Given the higher temperature documented at Dome, water-illite fractionation factors for Dome are plotted at 400°C.

Fluids responsible for sericite alteration (and at least part of the mineralization) at Donlin Creek likely formed by mixing of magmatic water and meteoric water. The mixing trend is evident in figure 8. The largest apparent magmatic component of the stable isotope data is found in samples from the southern Lewis area as well as from Dome. On the basis of the available data, hydrothermal fluids at the Snow prospect are interpreted to have a larger meteoric water component than the south Lewis areas. Fluids from the Queen and Rochelieu prospects are intermediate between the other two groups.

The data are too limited to draw any more conclusions. It is unclear whether the Dome and Lewis prospects are part of the same hydrothermal system or separate systems. No fundamental isotopic differences are apparent between the Dome and Lewis prospects and the calculated hydrothermal fluids and alteration intensities are broadly similar. The geochemical signatures at Donlin Creek are like a classic phyllic zone of a porphyry-type deposit, with some features at the Dome prospect similar to the potassic zone (Zaluski and others, 1994). Further sampling at Donlin Creek within the mineralized system(s) and beyond the system(s) might help to define gradients within the paleo-hydrothermal system as well as the boundaries of one or more systems.

Several oxygen, hydrogen, and sulfur isotope analyses were obtained from samples of stibnite- and pyrite-bearing quartz veins in rhyodacite dikes and

Table 4. *Donlin Creek oxygen and hydrogen isotope compositions of sericite samples and calculated isotope ratios of associated water*

No.	Sample Number	Location	$\delta^{18}O$	δD	$\delta^{18}O_{H2O}$	δD_{H2O}
1	DC96-251@238m	Dome	+ 8.9	- 126	+ 5.4	- 101
2	DC96-250@131m	Dome	+ 4.5	- 144	+ 1.0	- 119
3	Snow (surface)	Snow	+ 5.8	- 151	+ 2.3	- 126
4	DC96-240@71m	Queen	+ 8.3	- 136	+ 4.8	- 111
5	DC96-266@411m	North Lewis	+ 6.6	- 143	+ 3.1	- 118
6	DC96-210B@156.5m	Rochelieu	+ 8.4	- 147	+ 4.9	- 122
7	DC96-204@174.5m	W. of Rochelieu	+ 5.8	- 146	+ 2.3	- 121
8	DC96-261@250.9m	SE Lewis	+ 11.3	- 117	+ 7.8	- 92
9	DC96-238@195m	SW Lewis	+ 12.5	- 106	+ 9.0	- 81
10[c]	USGS, Gray and others (1997)	Snow Gulch	+ 24.9, + 24.5	-181 (d)		

[a]Samples collected by Antonio Arribas, Jr., and analyzed by Geochron Laboratories (Cambridge, Massachusetts), except for #10. Analytical precision reported as better than ± 0.2 per mil ($\delta^{18}O$) and ± 5 per mil (δD).
[b]H_2O calculated for T = 300°C for all samples, except Dome = 400°C. Fractionation factors for sericite (illite/muscovite-water) from Sheppard and Gilg (1996).
[c]$\delta^{18}O$ values for quartz and dickite (d).

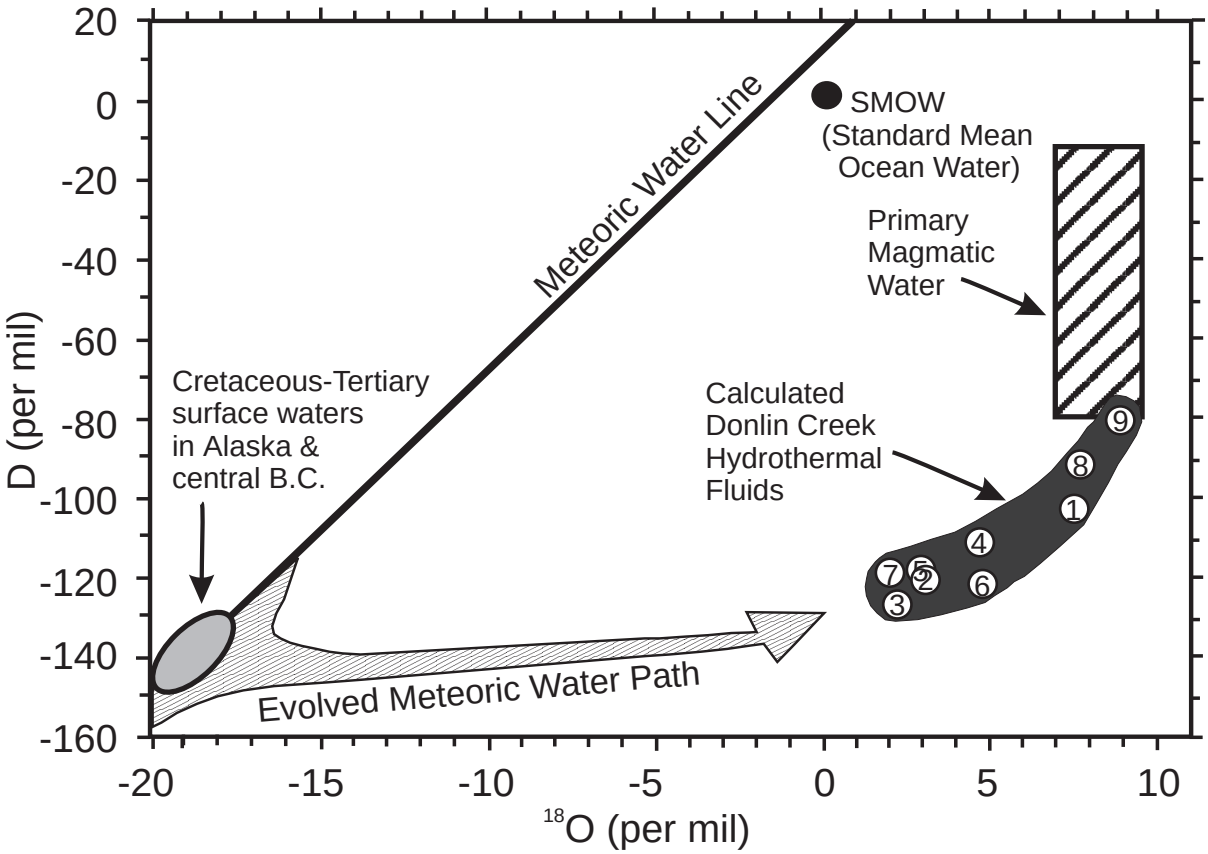

Figure 8. *A δD versus $\delta^{18}O$ plot depicting stable isotope geochemistry of calculated Donlin Creek hydrothermal fluids. Numbers in circles correspond to samples listed in table 4. The stable isotope geochemistry of the Donlin Creek ore fluids can be formed by the interaction of evolved meteoric water with primary magmatic water. Diagram adapted from Taylor (1979) and primary magmatic water is defined somewhat arbitrarily as the calculated water isotopic composition in equilibrium with "normal" igneous rocks or magmas at temperatures greater than or equal to 700°C (Taylor, 1979). Field for Cretaceous–Tertiary surface waters in Alaska and central British Columbia from Zaluski and others (1994).*

graywacke and shale wallrock (Gray and others, 1997; Goldfarb and others, 1990). The heavy oxygen and light hydrogen isotope values are similar to whole rock oxygen isotope results from Kuskokwim Group samples (Gray and others, 1997). The authors concluded that hydrothermal fluids were derived from multiple sources and may be partially derived by the dehydration of surrounding sedimentary rocks. Values of $\delta^{18}O$ from sulfide-bearing quartz veins at Donlin Creek range from 11 to 25 per mil, and the isotopically heaviest values are associated with later, lower temperature sulfide stages (McCoy and others, 1999). The $\delta^{34}S$ values for sulfides from all ore stages are -10 to -20 per mil, with late stibnite values as light as -25 per mil, suggesting that at least some sulfur is derived from clastic sedimentary rocks (McCoy and others, 1999).

Preliminary carbon isotope data from Donlin Creek was obtained from a graphite bleb in rhyodacite porphyry exposed in a Southeast Lewis trench. The graphite had a $\delta^{13}C$ value of -22.8 per mil, similar to a $\delta^{13}C$ value of -21.9 per mil, from a felsic dike with graphite spots in the Sleetmute D-4 Quadrangle (Rich Goldfarb, 1997, written commun.). These carbon isotope values are consistent with reduced carbon (that is, graphite) $\delta^{13}C$ values in igneous rocks, but overlap with values of biogenic carbon (Faure, 1986). The isotope results are inconclusive as to whether the carbon is derived from inorganic or organic sources.

OTHER DONLIN CREEK PROSPECTS

Intrusion/sedimentary rock contact relationships and hydrothermal alteration and mineralization are roughly similar for the ACMA, 400 Area, Rochelieu, Lewis, Queen, Snow, Far Side, and Quartz prospects. The Dome and Duqum prospects share similar characteristics that are different from the above prospects.

FAR SIDE PROSPECT

The Carolyn prospect of WestGold was renamed the Far Side prospect by Placer Dome Exploration. The Far Side prospect is the northernmost prospect on the Donlin Creek property. It is near Quartz Gulch and is off-trend from other prospects. Bedrock exposures are limited to a placer cut in Quartz Gulch and shallow, slumped trenches. The only visible gold seen on the Donlin Creek property is present in quartz veins exposed in trenches and in core at the Far Side prospect. Soil samples collected by WestGold averaged 943 parts per billion gold, with a maximum value of 19.3 parts per million gold. Rhyodacite dikes mapped at the prospect by WestGold have northwest trends, unlike the northeast trend of dikes seen at most Donlin Creek prospects. Drilling by WestGold defined a northeast-trending mineralized zone at least 650 ft (200 m) long and up to 100 ft (30 m) wide, with a calculated gold resource of 38,400 oz (1,194 kg) (Retherford and others, 1989). Placer Dome drilled three core holes on the Far Side prospect during 1996 to test intersecting northwest-trending rhyodacite dikes, north-northeast-trending structures, and coincident strong gold anomalies in soil samples. Spotty, thin, high-grade gold intercepts were encountered in rhyodacite.

WestGold mapped a steeply dipping (approximately 84°) rhyodacite dike 80 ft (25 m) thick and trending 310° azimuth in the immediate lower Far Side area. A 50-ft-thick (15-m-thick) rhyodacite dike with a 40° east plunge occurs south of the above dike. Most mineralization and the only visible gold occur in the southern dike. Other dikes in the southwest portion of the Far Side prospect appear to trend east-west, but the dikes are thin and discontinuous. Sedimentary rocks in this area strike 110° and dip moderately shallowly to the northeast.

Shears noted in trenches and drill logs are semi-pervasive throughout the Far Side prospect. Also, left-lateral offset of the larger, more northerly rhyodacite dike and the dike orientation immediately south suggest an east-west trend to the tectonic fabric of the area. This shearing may have provided a weakened avenue for the smaller porphyry and mafic dikes to follow and could also explain the spotty higher gold values.

SNOW PROSPECT

Soil sampling by WestGold identified an extensive gold soil anomaly (average of 464 parts per billion gold in soils) along the northwest flanks of Snow Ridge (fig. 1). Trenching and shallow reverse-circulation drilling by WestGold in 1989 identified similar geology and mineralization to that found at Queen and Lewis to the southwest. WestGold identified a drill-indicated, kriged resource of 44,000 contained oz (1,368 kg) of gold with an average grade of 0.1 oz/ton (3.59 g/tonne gold) (Retherford and others, 1989). Both rhyodacitic dikes and sills are present and crosscut by north- and northeast-trending mineralized structures. Dikes have northeast trends and southeast dips. Northwest-trending sills containing anomalous gold values crop out to the north. Mineralization appears to be restricted to narrow high-grade structures. The Snow prospect contains the only oxidized ore resource found to date on the Donlin Creek property.

400 AREA PROSPECT

Mineralized rhyodacite at this prospect was discovered in 1996 at several material pits while excavating material for the Lewis Ridge–American Ridge main road and the Lewis Ridge–Snow Gulch road. The 400 Area Prospect straddles these two roads constructed in mostly wetlands without outcrop (fig. 1).

Structurally controlled gold mineralization is found along low-angle, northwest-striking, moderately southwest-dipping sills and bedding plane shears. A complex zone of layer-parallel shearing was intersected in American Creek during drilling. The bedding and structure relationships are consistent with deformational features identified as D1 in the Donlin Creek area. In the 400 Area Prospect, the main mineralized unit is a rhyodacite sill. This sill is proximal to the American Creek fault, and most of the unit is logged as sheared or with abundant mineralized fractures (although it is unresolved if shearing is really from this particular fault). Mineralized veins strike north-northeast with steep dips both to the northwest and southeast. Although veins trend north-northeast, the mineralized package appears to closely follow the sill, probably due to competency contrasts in this area of high shearing. The sill is projected to intersect the surface just north of the American Ridge–Lewis road and, appears to branch down-dip into multiple thin sills to the south, still containing gold values, below the American Creek fault.

Numerous, generally thin (<15 ft [<4.5 m] wide) rhyodacite units found by drilling are not as well constrained as the main 400 Area Prospect sill. Drilling along the American Creek–Snow Gulch road penetrated what appears to be a northwest-trending rhyodacite dike, with a sill-like appendage. High-grade gold mineralization hosted in graywacke in drillhole intercepts is possibly due to a nearby mineralized rhyodacite sill not encountered in drilling. Mafic rocks encountered during drilling in the 400 Area Prospect are mostly thin sills that are generally unmineralized. However, a 65-ft-thick (20-m-thick), well-mineralized mafic dike with a northwest strike and moderate northeast dip was encountered in one drillhole.

AMERICAN CREEK MAGNETIC ANOMALY (ACMA) AREA

The American Creek Magnetic Anomaly (ACMA) area occurs on the south slopes of Lewis Ridge (fig. 1). The ACMA area measures 1 mi by 1,750 ft, or 0.33 mi^2 (1,700 m by 530 m, or 0.9 km^2), with the long axis aligned nearly parallel to American Creek.

Airborne-magnetic data in conjunction with soil sampling data discovered and delineated mineralization in the ACMA area. Drilling in the area intersected sericite-altered rhyodacite porphyry (RDX) with up to 2 percent disseminated graphite. The dominant strike direction of bedding in the ACMA area is 125° with dips to the southwest and northeast. A map based on strike and dip direction of bedding on a hole-per-hole basis suggests an antiformal structure trending 290° or sub-parallel to American Creek. Sills are the dominant igneous style in ACMA and drilling has encountered two thick (in excess of 300 ft [100 m]) south-southwest-dipping sill packages formed by multiple sill-within-sill intrusions. Sills decrease in thickness to the east-southeast. Three dikes (north-northeast trending), up to 80 ft (25 m) thick, were also documented within the ACMA area.

Gold mineralization is associated with north-northeast-trending quartz–arsenopyrite–pyrite veinlets, fracture coatings of realgar, quartz–stibnite veinlets, and local disseminated acicular arsenopyrite hosted mainly within rhyodacite. Gold mineralization is structurally controlled by north-northeast striking structures with moderate southeast dips. The thickest ore zones occur where northerly structures crosscut rhyodacite.

DOME PROSPECT

The Dome prospect is the northeasternmost prospect on the property along the northeast trend of the Donlin Creek dike swarm (fig. 1), on the ridge between Quartz and Dome creeks. WestGold conducted soil sampling and trenching, but never drilled the Dome prospect. Placer Dome Exploration drilled the Dome prospect in 1996 and 1997. Drill targets were in one of the largest untested gold soil anomalies on the Donlin Creek property. Soil anomalies average 270 parts per billion gold, with a high value of 1,541 parts per billion gold (with coincident arsenic and mercury anomalies). Rock chip samples from trenches contained up to 10 parts per million gold.

The geology of the Dome prospect is distinct from most other Donlin Creek prospect areas. Kuskokwim Group sedimentary rocks have been hornfelsed to intermixed biotite hornfels and greenish gray calc-silicate hornfels adjacent to porphyritic rhyodacite and rhyolite. Some of the hornfels may be intermixed volcanoclastic units. The dominant igneous rock is a light gray to cream colored, quartz-eye rhyolite. Secondary biotite (potassic alteration) is present in the rhyolite dike in addition to ubiquitous sericite alteration. Igneous breccias and equigranular granodiorite are also present (observed only in core). Dikes exposed on the surface and in drill core at the Dome prospect do not appear to have enough volume to have hornfelsed the Kuskokwim Group sedimentary rocks. This observation suggests that there may be a more extensive plutonic body at depth.

Copper mineralization in the form of disseminated chalcopyrite and quartz–chalcopyrite veinlets occurs in altered intrusive rock and hornfels and appears correlative with elevated silver values. Disseminated pyrrhotite is common in both igneous and contact metamorphosed sedimentary units. Elevated gold values appear to be associated with disseminated and vein-controlled arsenopyrite and occur over broad zones (McCoy and others, 1999). Gold mineralization is "porphyry style" and hosted in both igneous and metamorphic/sedimentary rock types. Fluid inclusions from quartz veins indicate filling temperatures in excess of 400°C, suggesting a magmatic source for fluids and a porphyry-style setting for mineralization.

Much of the available geologic and geochemical data indicate that Dome prospect gold mineralization is part of the 4-mi-long (6.5-km-long) system extending northward from the Lewis prospect. Based on silver:gold ratios, it can be inferred that a progressively deeper expression of a hydrothermal system is exposed from south (Lewis areas) to north (Dome). Homogenization temperatures from fluid inclusion studies also indicate that the Dome prospect may be the deeper, hotter portion of the Donlin Creek hydrothermal system. Alternatively, it may be indicative of lateral fluid flow with Dome being closer to the hotter part of the hydrothermal system. Nevertheless, other evidence, such as the presence of younger rhyolite dikes and a hornfels aureole, suggests that the Dome prospect may be part of a different hydrothermal system, or a slightly younger, magmatic $\pm$ hydrothermal event has been superimposed on the Lewis–Dome system.

DUQUM PROSPECT

The Duqum prospect is the southwestern extension of the Dome prospect into Quartz Creek. The geology and mineralization styles are similar to the Dome prospect. Auger soil samples from this area contained up to 7 parts per million gold. Coincident gold, arsenic, and mercury soil anomalies and aeromagnetic anomalies in the Duqum area were drill-tested in 1997.

DONLIN CREEK DEPOSIT GEOCHRONOLOGY AND MODEL

Pervasive sericitic alteration occurs within rhyodacite intrusive rocks over a 4.3-mi by 1-mi (7-km by 1.5-km) area. This large area of alteration is evidence that an unusually large magmatic-hydrothermal system was active in the Donlin Creek area. Dike and sill emplacement and alteration are contemporaneous within limits of radiometric dating methods. It is possible that alteration occurred as a magmatic degassing event as the igneous bodies were emplaced near the paleosurface.

The Donlin Creek dikes represent a bimodal (felsic and mafic) assemblage. This assemblage, along with the general orientation of the dikes sub-parallel to north-northeast-trending normal faults, strongly suggests an extensional setting for magma emplacement. The morphology of igneous rocks at Donlin Creek as a dike swarm instead of the much more common Kuskokwim volcanoplutonic complex also suggests a relationship between extension and magmatism at Donlin Creek (R.J. Newberry, written commun., 1999).

Despite intrinsic mineralization variability, a positive one-to-one correlation has been established between fault density, alteration intensity, gold tenor, and intrusive rock thickness. Specifically, the thicker the intrusive body, the greater the fault density. The greater the fault density, the higher and more consistent the grade, and the more intense the alteration. It appears that the thickest intrusions are cut by the largest number of faults, resulting in the widest ore zones and most intense alteration zones.

Age dating, crosscutting relationships, and mappable features present in core and trenches suggest the following geologic and metallogenic chronology at Donlin Creek:

1. Deposition of Kuskokwim Group sediments in an elongate basin formed by wrench fault tectonics and lithification of these sediments during the mid-Cretaceous.
2. Lithification of the Kuskokwim Group rocks was followed by a major deformation event characterized by northward stratigraphic imbrication along south-dipping thrust faults.
3. Emplacement of intermediate to mafic dikes and sills (oldest), fine-grained rhyodacitic porphyry dikes, and rhyodacitic dikes and sills (youngest) in the Late Cretaceous/Early Tertiary, near the end of the major deformation event. Rhyolite dikes in the Dome area may be part of this igneous event or a slightly later, separate igneous event. Dikes likely followed structures subparallel to the regional grain.
4. Crystallization of rhyodacitic rocks was closely followed by sericite and carbonate alteration accompanied by pyrite–arsenopyrite–gold mineralization. Mineralization occurred almost contemporaneously with emplacement of the intrusions as a magmatic-hydrothermal system concentrated gold within a volatile-rich magma. The hydrothermal system led to pervasive sericite alteration of the intrusions and deposition of gold–arsenic mineralization.
5. East-west extension and development of north-trending normal faults occurred during and after emplacement of the intrusive units.
6. Mixed magmatic and meteoric fluids remobilized and deposited gold accompanied by graphite and arsenopyrite in shears.
7. The latest mineralization event deposited gold + stibnite + realgar + native arsenic $\pm$ quartz $\pm$ carbonate in open spaces within igneous and sedimentary rocks.
8. Faulting occurred throughout the deposit history, but significant post-mineralization faulting is not recognized in the Lewis area of the Donlin Creek property.

ACKNOWLEDGMENTS

The authors are grateful to Placer Dome Exploration Inc. for permission to publish this paper. The data presented in this paper are the result of many people from Placer Dome, Calista Corporation, and The Kuskokwim Corporation working together on the Donlin Creek project. Thanks are especially extended to Rich Moses, Darren O'Brien, and David Barnett for insightful discussions and careful analysis of the plethora of data generated during exploration efforts at Donlin Creek. Placer Dome Exploration's research group provided gold resource calculations. All of the geologists who logged drill core over the years at Donlin Creek are thanked for their consistently detailed observations. Roland Bartch and Mark O'Dea of Steffen, Robertson and Kirsten provided critical structural observations and interpretations. Thanks also are due to Rainer Newberry and Melanie Werdon for their technical reviews that significantly improved the final version of this paper.

REFERENCES

Bodnar, R.J., Reynolds, T.J., and Kuehn, C.A., 1985, Fluid inclusion systematics in epithermal systems, *in* Berger, B.R., and Bethke, P.M., eds., Geology and geochemistry of epithermal systems: Reviews in Economic Geology, v. 2, p. 73–97.

Bundtzen, T.K., and Gilbert, W.G., 1983, Outline of geology and mineral resources of upper Kuskokwim region, Alaska, *in* Proceedings of the 1982 symposium

on western Alaska geology and resource potential: Journal of Alaska Geological Society, v. 3, p. 101–117.

Chryssoulis, Stephen, Kafritsa, Gina, and Wong, Clarissa, 1996, Deportment of gold in the Donlin Creek ores: unpublished Advanced Mineral Technology Laboratory (London, ON, Canada) report 96/11, 34 p.

Decker, John, Bergman, S.C., Blodgett, R.B., Box, S.E., Bundtzen, T.K., Clough, J.G., Coonrad, W.L., Gilbert, W.G., Miller, M.L., Murphy, J.M., Robinson, M.S., and Wallace, W.K., 1994, Geology of Southwestern Alaska, *in* Plafker, George, and Berg, H.C., eds., The Geology of Alaska, The Geology of North America: Boulder, Colorado, Geological Society of America, v. G-1, p. 285–310.

Faure, Gunter, 1986, *Principles of Isotope Geology:* New York, John Wiley and Sons, 589 p., ISBN 0-471-86412-9.

Goldfarb, R.J., Gray, J.E., Pickthorn, W.J., Gent, C.A., and Cieutat, B.A., 1990, Stable isotope systematics of epithermal mercury–antimony mineralization, southwestern Alaska, *in* Goldfarb, R.J., Nash, J.T., and Stoeser, J.W., eds., Geochemical Studies in Alaska by the U.S. Geological Survey, 1989: U.S. Geological Survey Bulletin 1950, p. E1–E9.

Gray, J.E., Gent, C.A., Snee, L.W., and Wilson, F.H., 1997, Epithermal mercury–antimony and gold-bearing vein lodes of southwestern Alaska, *in* Goldfarb, R.J, and Miller, L.D., eds., Mineral Deposits of Alaska: Economic Geology Monograph 9, p. 287–305.

Gray, J.E., Goldfarb, R.J., Snee, L.W., and Gent, C.A., 1992, Geochemical and temporal conditions for the formation of mercury–antimony deposits, southwestern Alaska: Geological Society of America Abstracts with Programs, v. 24, no. 5, p. 28.

McCoy, D.T., Dodd, S.P., Arribas, Jr., Antonio, Miller, M.L. Goldfarb, R.J., and Szumigala, D.J., 1999, Geology and geochemistry of the Donlin Creek gold deposit, southwestern Alaska (abs): GSA Cordilleran Section Centennial, Geological Society of America Abstracts with Programs, v. 31, no. 6, p. A-78.

McCoy, D.T., Newberry, R.J, Layer, P.W., DiMarchi, J.J., Bakke, A.A., Masterman, J.S., and Minehane, D.L., 1997, Plutonic-related gold deposits of Interior Alaska, *in* Goldfarb, R.J, and Miller, L.D., eds., Mineral Deposits of Alaska: Economic Geology Monograph 9, p. 191–241.

Miller, M.L., and Bundtzen, T.K., 1994, Generalized geologic map of the Iditarod quadrangle, Alaska, showing potassium–argon, major-oxide, trace-element, fossil, paleocurrent, and archaeological sample localities: U.S. Geological Survey Miscellaneous Field Studies Map 2219-A, 48 p., 1 sheet, scale 1:250,000.

Miller, M.L., and Bundtzen, T.K., 1988, Right-lateral offset solution for the Iditarod–Nixon Fork fault, western Alaska, *in* Galloway, J.P., and Hamilton, T.D., eds., Geologic Studies in Alaska by the U.S. Geological Survey during 1987: U.S. Geological Survey Circular 1016, p. 99–103.

Moll-Stalcup, E.J., 1994, Latest Cretaceous and Cenozoic magmatism in mainland Alaska, *in* Plafker, George, and Berg, H.C., eds., The Geology of Alaska, The Geology of North America: Boulder, Colorado, Geological Society of America, v. G-1, p. 589–620.

Newberry, R.J., McCoy, D.T., and Brew, D.A., 1995, Plutonic-hosted gold ores in Alaska; igneous vs. metamorphic origins, in Ishihara, Shunso, and Czamanske, G.K., eds., Proceedings of the Sapporo international conference on mineral resources of the Northwest Pacific Rim, Shigen Chishitsu: Resource Geology Special Issue No. 18, p. 57–100.

O'Dea, M., 1997, Structural controls on gold mineralization at the Donlin Creek deposit, southwest Alaska: unpublished Etheridge Henley Williams Geoscience Consultants report, 59 p., 22 figs., 19 trench maps, 3 sheets.

Patton, W.W., Jr., Box, S.E., Moll-Stalcup, E.J., and Miller, T.P., 1994, Geology of west-central Alaska, *in* Plafker, George, and Berg, H.C., eds., The Geology of Alaska, the Geology of North America: Boulder, Colorado, Geological Society of America, v. G-1, p. 241–269.

Ramsay, J.G., and Huber, M.I., 1987, *The techniques of modern structural geology, Volume 2, Folds and fractures*: London, U.K, Academic Press Ltd., 462 p. ISBN: 0-12-576902-4.

Retherford, R.M., Graff, P., and Hinderman, T.K., 1989, Donlin Creek project (Alaska) 1989 exploration program final report: unpublished Western Gold Exploration and Mining Company Ltd. report, 186 p., 7 appendices, 52 sheets, various scales.

Roberts, Paul, 1993, Report on trench mapping and sampling, Donlin Creek Project: unpublished Teck Exploration Ltd. report, 37 p., 4 sheets.

Sheppard, S.M.F., and Gilg, H.A., 1996, Stable isotope geochemistry of clay minerals; the story of sloppy, sticky, lumpy and tough: Clay Minerals, v. 31, no. 1, p. 1–24.

Streckeisen, A.B., and LeMaitre, R.W.L., 1979, A chemical approximation to the modal QAPF classification of the igneous rocks: Neues Jahrbuch für Mineralogie Abhandlungen., v. 136, no. 2, p. 169–206.

Szumigala, David J. 1997, Donlin Creek Project—1996 summary report of exploration activities: unpublished Placer Dome Exploration Inc. report, 2 vols., 5 sheets, 114 p.

Szumigala, D.J., 1996, Gold mineralization related to Cretaceous–Tertiary magmatism in west-central Alaska—A geochemical model and prospecting guide for the Kuskokwim region, *in* Coyner, A.R., and Fahey, P.L., eds., Geology and ore deposits of the American Cordillera: Reno, Nevada, Geological Society of Nevada Symposium Proceedings, p. 1317–1340.

Szumigala, D.J., 1993, Gold mineralization related to Cretaceous–Tertiary magmatism in the Kuskokwim Mountains of west-central and southwestern Alaska: University of California, Los Angeles, Ph.D. dissertation, 301 p.

Taylor, H.P., Jr., 1979, Oxygen and hydrogen isotopes in hydrothermal mineral deposits, *in* Barnes, H.L., ed., Geochemistry of hydrothermal ore deposits: New York, John Wiley & Sons, 798 p., ISBN 0-471-05056-3.

Zaluski, Gerard, Nesbitt, Bruce, and Muehlenbachs, Karlis, 1994, Hydrothermal alteration and stable isotope systematics of the Babine porphyry Cu deposits, British Columbia—implications for fluid evolution of porphyry systems: Economic Geology, v. 89, no. 7, p. 1518–1541.

PRELIMINARY $^{40}AR/^{39}AR$ AGES FROM TWO UNITS IN THE USIBELLI GROUP, HEALY, ALASKA: NEW LIGHT ON SOME OLD PROBLEMS

Don M. Triplehorn,[1] Jeff Drake,[2] Paul W. Layer[1,2]

ABSTRACT

Single-crystal $^{40}Ar/^{39}Ar$ ages from the Usibelli Group, Healy, Alaska, illustrate the problems and power of using radiometric ages to date sedimentary sequences. For an ash in the Grubstake Formation, at the top of the Usibelli Group, a mineral age of 6.7 ± 0.1 Ma is significantly younger than previous K–Ar (and new $^{40}Ar/^{39}Ar$) ages of glass from the same samples. This new age is consistent with stratigraphic controls on the age of the Grubstake Formation. It also better constrains the first stirrings of uplift in the central Alaska Range and is consistent with other age information on uplift. In addition, our data imply that, in some instances, volcanic glass is not an accurate recorder of the age of eruption and can incorporate excess argon that is difficult to detect. For a tonstein near the top of coal bed #6 in the Middle Miocene Suntrana Formation, sanidine and plagioclase single crystals give ages of ~35 Ma, which are clearly too old based on extensive stratigraphic control. The unit that we dated appears to be an air-fall tuff, and it was our expectation that the age of the minerals would reflect the age of deposition of this stratigraphic marker. At this time, neither the origin of these xenocrystic minerals nor the reasons our ages exceed the expected ages by ~20 million years are known. Finally, the similarity of ages and possible relation between our ash unit and the Sugar Loaf volcanics, which have a K-Ar age of 32–34 Ma, are interesting. As a further complication, it seems likely that Sugar Loaf should be much younger than 30+ Ma; first because it overlies sediments identified as Healy Creek Formation, and second because a volcanic landform probably could not survive that long in this setting. Further work is needed to resolve this enigma.

INTRODUCTION

The exposures of the Usibelli Group from the Nenana Coal Field near Healy, Alaska, are well-preserved records of Tertiary deposition. Numerous coal units, interspersed in a clastic sedimentary sequence, have been interpreted to record changes in climate in the region (Leopold and Liu, 1994; Wolfe, 1994). Although the sequence has abundant fossil control, there are few absolute age determinations from ash layers. Our purpose is to report new radiometric ages for the Grubstake and Suntrana formations of the Usibelli Group. The geology of the Healy area was summarized by Wahrhaftig and others (1969) to accompany publication of eight 15-minute geologic quadrangles. Figure 1 shows the location and figure 2 the stratigraphic column for the Usibelli Group at Suntrana on Healy Creek.

The following description of the geologic setting and significance of the Suntrana Creek locality (fig. 1) is largely taken from Wahrhaftig (1987). After the last major fall of sea level at the end of the Cretaceous, much of interior Alaska probably was a broad fluvial plain of low to moderate relief. After a long interval of subaerial exposure, large areas of slow subsidence developed in which alluvial, lacustrine, and swamp deposits accumulated. During much of Miocene, and perhaps Oligocene, time rivers flowed southward on an extensive fluvial plain, across the site of the (then non-existent) Alaska Range toward the Gulf of Alaska. Near the end of Miocene time the Alaska Range began to rise across this drainage, damming it and creating one or more lakes that ultimately spilled northwestward to form the present Tanana River system. The Nenana Gravel overlies the Usibelli Group and represents an alluvial apron developed on the north side of the Alaska Range as it rose in Pliocene time (Ager and others, 1994, discuss evidence for Pliocene age of the Nenana Gravel).

The record for much of the Cenozoic geologic history of a large part of interior Alaska is contained in these rocks. Unfortunately, that record is based on limited data. Age assignments are mainly derived from correlations with floral assemblages elsewhere in Alaska or on the West Coast of the conterminous United States; these in turn are dated by sparse and sometimes questionable radiometric ages, usually from distant localities (see fig. 3, regional stratigraphic section). Our new data add some points of increased certainty but mostly raise new questions, suggest new implications, and provide guidance for future research.

ANALYTICAL METHODS

For $^{40}Ar/^{39}Ar$ analysis, samples were sieved and washed in deionized water, and biotite, feldspar, and

[1]Department of Geology and Geophysics, University of Alaska Fairbanks, Fairbanks AK 99775-5780.
[2]Geophysical Institute, University of Alaska Fairbanks, Fairbanks, AK 99775-7320.
Email for Paul W. Layer: player@dino.gi.alaska.edu

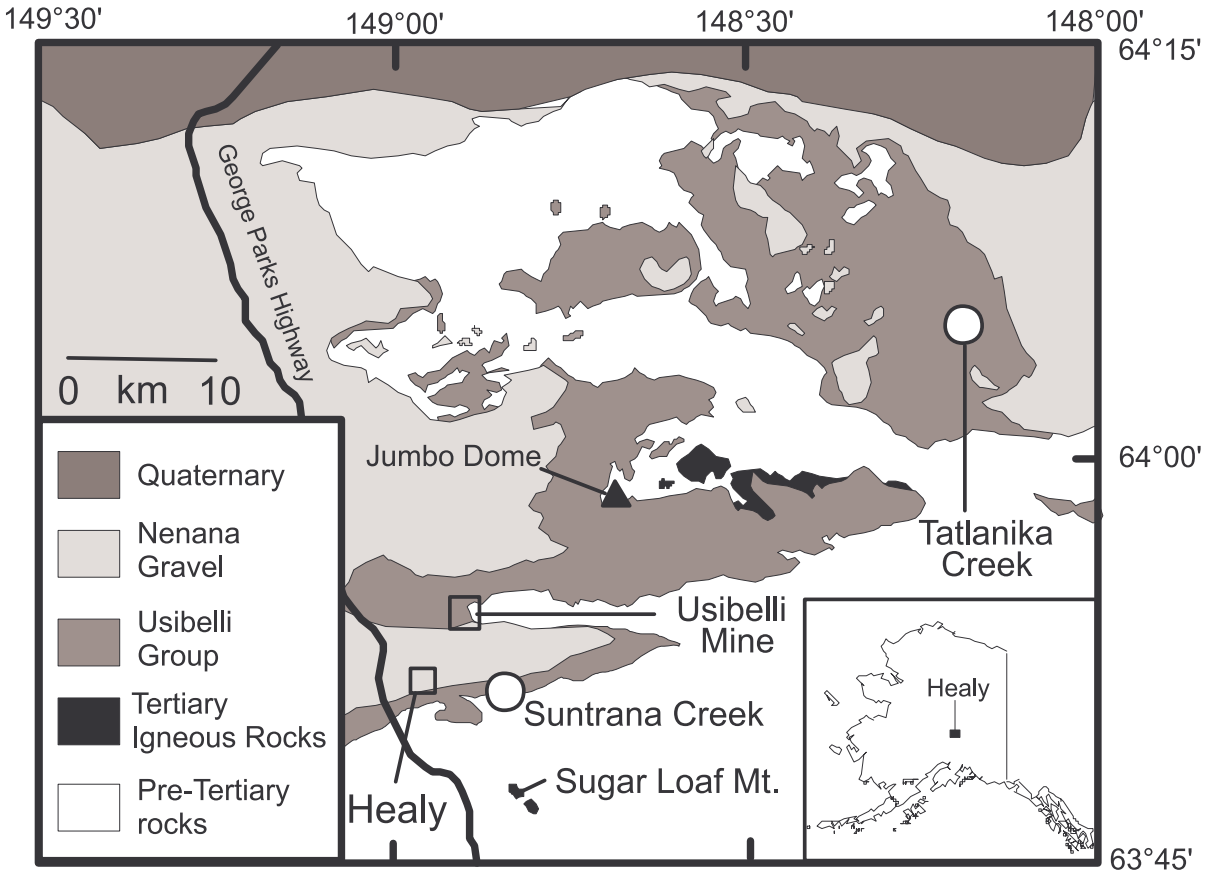

Figure 1. *Generalized geologic map of the Healy area, central Alaska, modified from Wahrhaftig and others (1994). Circles show the ash sample locations from the Suntrana and Tatlanika creeks of the Usibelli Group. The town of Healy and the Usibelli Coal Mine are also shown. Jumbo Dome, a Quaternary volcano and a prominent geographic feature of the region, is denoted by the triangle.*

hornblende crystals were hand-picked from both ash layers. In addition, clean glass shards without visible phenocrysts were selected from the Grubstake ash. The samples were wrapped in aluminum foil and arranged in one of two levels, labeled top and bottom, within aluminum cans of 1 in (2.5 cm) diameter and 1.8 in (4.5 cm) height. Samples of biotite standard Bern-4B, with an age of 17.25 Ma (C. Hall, oral commun., 1990), were used to monitor the neutron flux. The samples were irradiated for 2 megawatt hours in position 5c of the uranium-enriched research reactor of McMaster University in Hamilton, Ontario, Canada.

Upon their return from the reactor, subsamples (5–100 crystals) of the original samples and separates as well as monitors were loaded into 1/16 inch (2 mm) diameter holes in a copper tray that was then loaded in an ultra-high vacuum extraction line. The monitors were fused, and samples either fused or step-heated using a 6-watt argon-ion laser using the technique described in York and others (1981) and Layer and others (1987). Argon purification was achieved using a liquid nitrogen cold trap and a SAES Zr-Al getter at 400°C. The samples were then analyzed in a VG-3600 mass spectrometer at the Geophysical Institute, University of Alaska Fairbanks. The argon isotopes measured were corrected for system blank and mass discrimination, as well as calcium, potassium, and chlorine interference reactions following procedures outlined in McDougall and Harrison (1988). Where possible, a plateau age was determined from three or more consecutive fractions whose ages are within 2 sigma of each other and total more than 50 percent of gas release. Figure 4 shows selected spectra while table 1 gives a summary of all the $^{40}Ar/^{39}Ar$ results, with all ages quoted to the ±1 sigma level and calculated using the constants of Steiger and Jäger (1977).

VOLCANIC ASH IN THE BASAL GRUBSTAKE FORMATION

Wahrhaftig and others (1969, p. D24) described two beds of fine white vitric ash, about 13 ft and 24 ft thick,

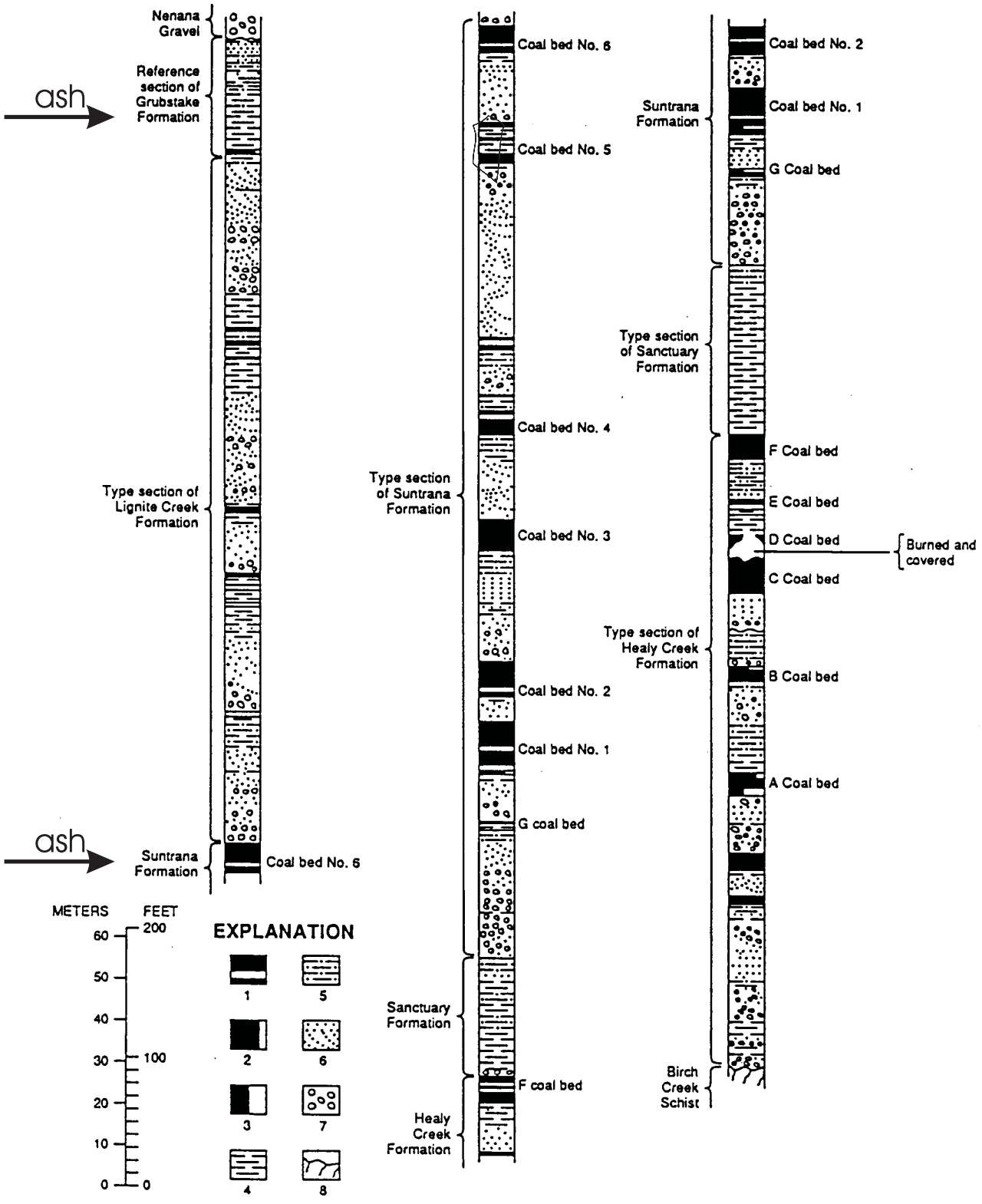

Figure 2. *Type section of the Usibelli Group at Suntrana from Wahrhaftig and others (1994). (1) Coal, showing bone and clay partings; (2) bony coal; (3) bone; (4) claystone and shale; (5) siltstone; (6) sandstone, in part cross bedded; (7) pebbles and conglomerate; and (8) schist (unconformity at top). Stratigraphic locations of ash layers dated in this study are shown by arrows.*

in the lower part of the Grubstake Formation on the east bank of Tatlanika Creek between the mouths of Roosevelt and Hearst creeks (see their fig. 6 for a geologic map and specific location). Leopold and Liu (1994, p. 115) note at least 23 ft (7 m) of Grubstake formation below the ashes, and show it on their measured section (p. 120) as a basal conglomerate overlain by sand and then shale. The lower ash lies directly on a paleosol developed on the shale, and includes a fossil forest bed at the base with leaves, cones, roots, stumps, (Wahrhaftig and others, 1969, p. D24) and even coalified trunks standing in growth position that extend 15–20 ft (4.5–6.0 m) into the ash. Jack Wolfe identified the megaflora from this outcrop (Wahrhaftig and others, 1969) and Leopold and Liu (1994) studied the pollen. They consider the Grubstake flora to be Late Miocene in age.

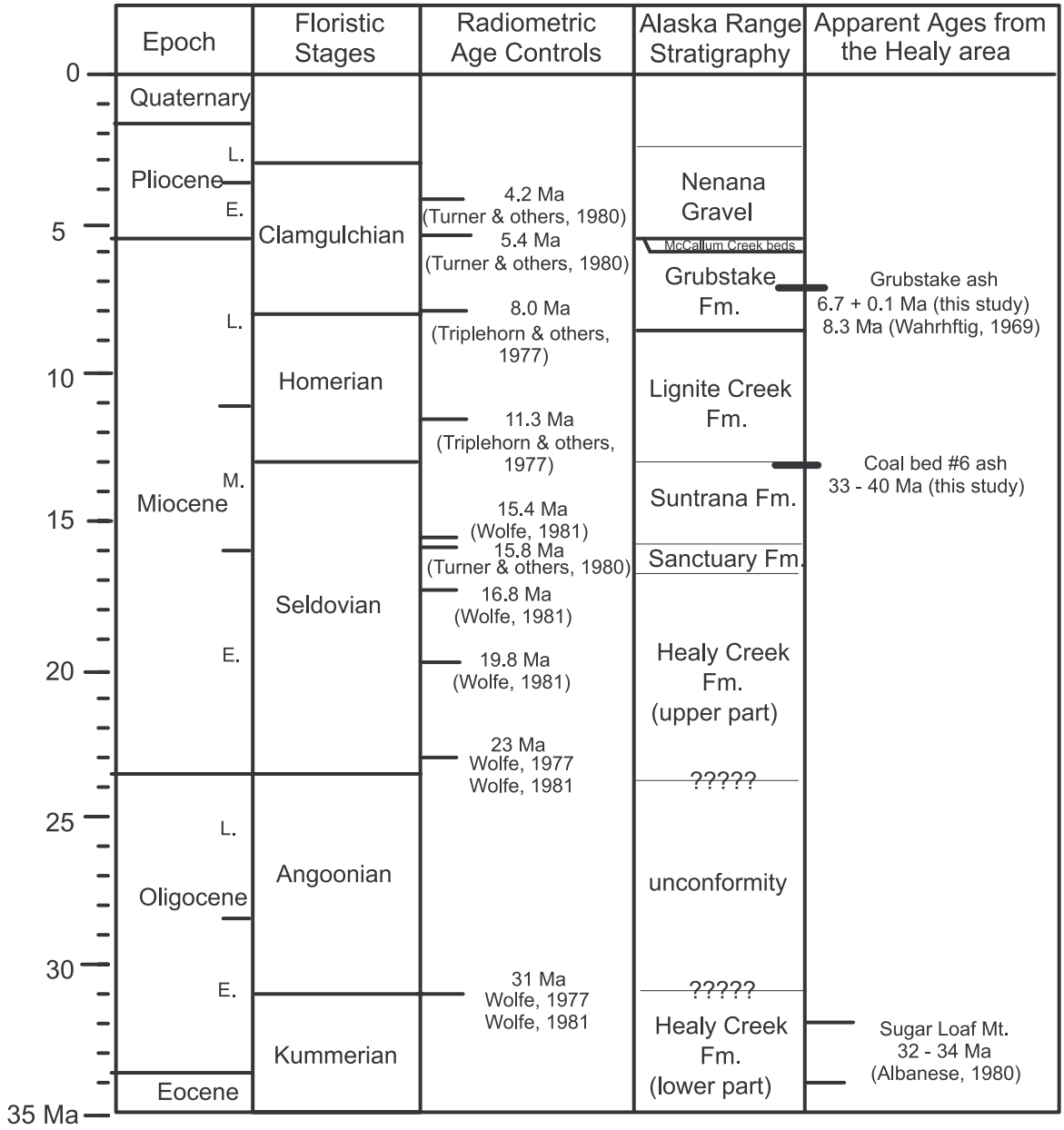

Figure 3. *Stratigraphic correlation diagram adapted from Ager and others (1994) showing the floristic stages and the radiometric age constraints established from the Cook Inlet and Pacific Northwest. The Alaska Range formations are from Wahrhaftig and others (1969) and have been correlated to the floristic stages. Ages obtained from the Healy area are also shown. Note that the ages for the Grubstake formation are stratigraphically consistent with the floristic ages, while that from coal bed #6 in the Suntrana formation is not.*

Wahrhaftig's sample for radiometric dating apparently came from the basal part of the lower ash, which includes the forest bed that lies directly on the paleosol. Our dated sample is from this same layer and from essentially the same location. The basal part of the upper ash contained biotite and plagioclase that appeared datable, but this was not attempted.

RADIOMETRIC DATES

Wahrhaftig and others (1969) reported a conventional K-Ar age for glass of 8.1 ± 0.4 Ma, recently revised to 8.3 ± 0.4 Ma (Wahrhaftig, 1987) using the new decay constants. They also reported an age of 57.3 ± 2.3 Ma for a biotite concentrate (with 10 percent chlorite), and an age of 54.4 ± 2.2 Ma for a muscovite concentrate (50 percent muscovite, with plagioclase, sanidine, quartz, and glass). The mica concentrates are both clearly too old based on the age of the flora and disagreement with the age of the glass and may represent incorporation of older, inherited grains in the ash.

Our ash sample contained four components for radiometric analysis: glass, biotite, plagioclase, and

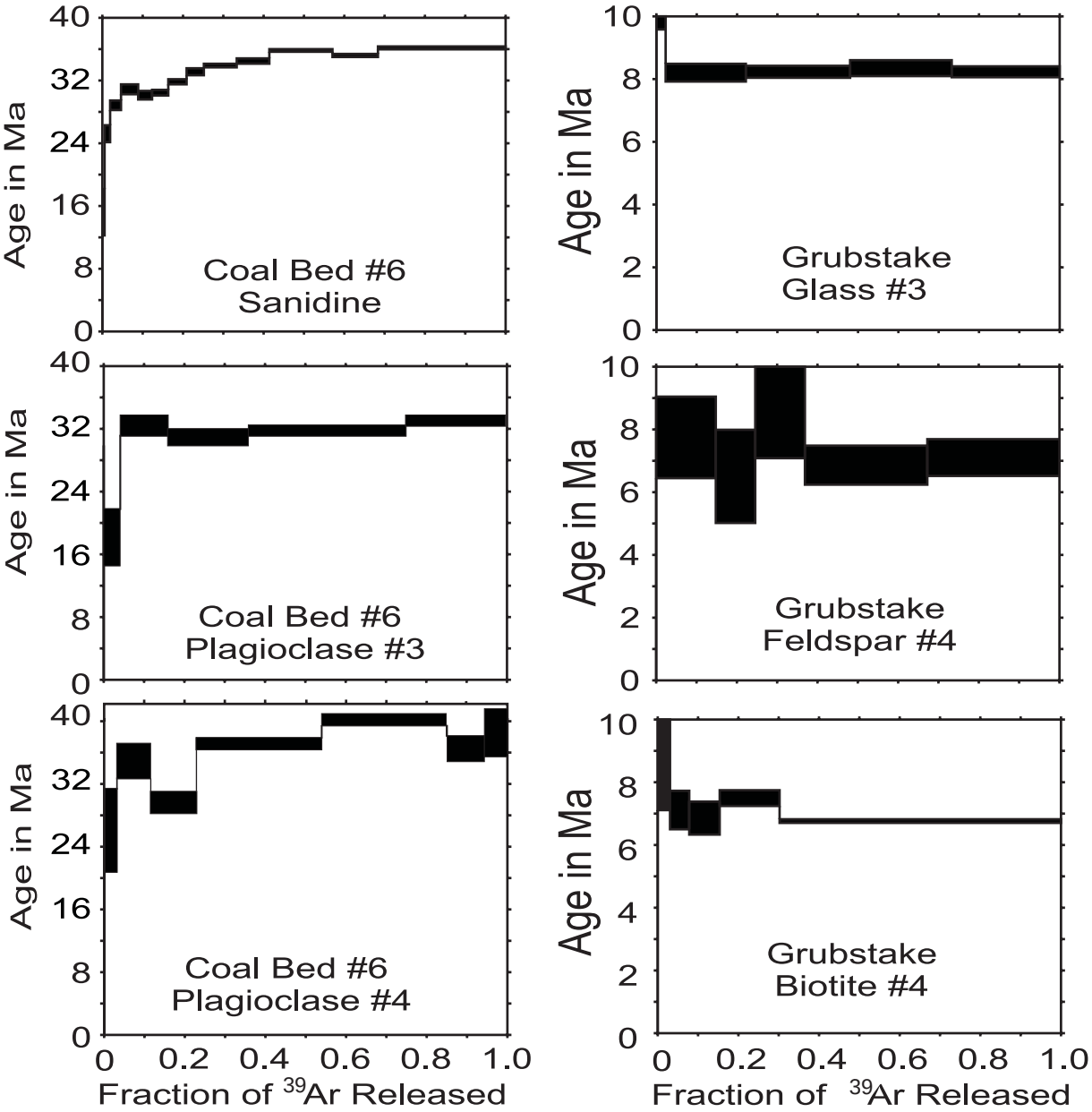

Figure 4. *$^{40}Ar/^{39}Ar$ age spectra of representative samples from coal bed #6 at Suntrana Creek and the Grubstake ash at Tatlanika Creek. See table 1 for interpreted ages.*

hornblende. Analyses on four glass subsamples (one step-heat, three fusions) yielded an $^{40}Ar/^{39}Ar$ average age of 8.3 ± 0.1 Ma, essentially identical to the age obtained by Wahrhaftig (1987). However biotite, plagioclase, and hornblende gave consistent and significantly younger $^{40}Ar/^{39}Ar$ ages, with interpreted ages of 6.4 ± 0.6 to 6.7 ± 0.1 Ma (see table 1). We did not see any evidence of minerals with ages older than 50 Ma and cannot explain the observation of Wahrhaftig (1987), however we do see evidence of excess Ar in some step-heating analyses (fig. 4). The remarkable concordance between feldspar, biotite, and hornblende ages and the presence of excess Ar in some samples may imply that the glass age that we and Wahrhaftig obtained was influenced by excess Ar and that the younger age of the three minerals more accurately reflects the depositional age of this ash. Either age is consistent with the paleobotanical age cited above (fig. 3). However, we prefer a weighted mean age of 6.7 ± 0.1 Ma for the ten mineral subsamples as the age of the Grubstake ash.

Table 1. *Summary of $^{40}Ar/^{39}Ar$ ages from the Healy area*[a]

Mineral	Integrated age or fusion age (Ma)	Plateau (p) or isochron (i) age (Ma)	Comments
		GRUBSTAKE ASH AT TATLANIKA CREEK	
Feldspar #1	**7.6 ± 0.2**	fused	
Feldspar #2	**6.9 ± 0.6**	fused	
Feldspar #3	6.9 ± 0.1	**6.5 ± 0.1 (p)**	3 fraction plateau, 72% of release.
Feldspar #4	7.2 ± 0.4	7.0 ± 0.4 (p)	2 fraction plateau, 63% of release.
		6.6 ± 1.5 (i)	$^{40}Ar/^{36}Ar_i$ = 644 ± 859
Biotite #1	6.6 ± 0.1	**6.6 ± 0.1**	Good plateau includes all fractions.
Biotite #2	**6.6 ± 0.2**	fused	
Biotite #3	**6.8 ± 0.1**	fused	
Biotite #4	7.0 ± 0.1	6.9 ± 0.1 (p)	Most of plateau in last fraction
		6.7± 0.1 (i)	(6.8 ± 0.1 Ma) $^{40}Ar/^{36}Ar_i$ = 303 ± 4
Hornblende #1	**11.1 ± 3.5**	fused	
Hornblende #2	**6.4 ± 0.6**	fused	
Glass #1	**8.2 ± 0.1**	fused	
Glass #2	**8.3 ± 0.1**	fused	
Glass #3	8.4 ± 0.1	**8.3 ± 0.1 (p)**	Good plateau, slight excess??
			Isochron age = 8.2 ± 0.1 $^{40}Ar/^{36}Ar_i$=302 ± 6
Glass #4	**8.4 ± 0.2**	fused	
		COAL BED #6 AT SUNTRANA CREEK	
Plagioclase #1	**33.6 ± 1.0**		Ca/K = 7.6
Plagioclase #2	**37.8 ± 0.3**		Ca/K = 3.3
Plagioclase #3	32.8 ± 0.5	**33.4 ± 0.5 (p)**	Ca/K = 4.5 U shape – 18 Ma reset
Plagioclase #4	38.3 ± 0.6	**39.8 ± 0.6 (p)**	Ca/K = 3.6 ragged – 26 Ma reset
Plagioclase #5	33.3 ± 1.7	**33.3 ± 1.7 (p)**	Ca/K = not determined 2 step – loss?
Sanidine	34.0 ± 0.2	**35.7 ± 0.2 (p)**	Ca/K = 0.04, 15 Ma reset
Hornblende #1	44.1 ± 33.5		25 grains, not precise
Hornblende #2	-0.3 ± 0.9		50 grains, no radiogenic Ar
Hornblende #3	**7.5 ± 1.7**		100 grains
Hornblende #4	-30.5 ± 226.5		No radiogenic Ar
Hornblende #5	-0.4 ± 0.5		No radiogenic Ar
Hornblende #6	51.5 ± 10.3	none	Step heat, not precise

[a]Ages calculated using the constants of Steiger and Jäger (1977) and using the standard MMhb-1 with an age of 513.9 Ma. Best interpreted ages for each sample are shown in bold.

RELATIONSHIP TO OTHER LOCALITIES

About 30 ft (9 m) above the base of the Grubstake formation at its reference section on Suntrana Creek there is a soft white layer 5–6 ft (1.5–1.8 m) thick. This is very likely equivalent to one or both of the volcanic ashes on Tatlanika Creek. Such a correlation is supported by the Wahrhaftig and others (1969) report that glass from Suntrana Creek has an index of refraction identical to that of glass from Tatlanika Creek.

The exact location of the volcano is unknown, but based on thickness and relative coarseness of the ash it probably was near the Tatlanika Creek sample locality, which is 37 mi (60 km) northeast of the Suntrana Creek locality. Absence of air-fall material at Suntrana suggests that during the volcanic eruptions, winds did not carry ash southwest from the volcano. Note that this was prior to or at the beginning of the Alaska Range uplift; hence wind patterns could have been much different from the present, bearing in mind that winds are inherently variable and average patterns may not be significant for short-term events. Note also that prior to uplift of the Alaska Range, drainage was generally to the south or southwest over a broad fluvial plain covering a large part of the Interior and south to the Cook Inlet area. Wahrhaftig and others (1969) interpreted the Grubstake Formation at Suntrana as, in part, a lake deposit, possibly related to first stirrings of Alaska Range uplift that ponded south-flowing streams. If so, streams would have been flowing into the lake from the north, transporting Tatlanika ash from areas somewhere west or north of the volcano. The age of the water-borne ash at Suntrana Creek should be the same as the air-fall ash at Tatlanika because erosion and transport would have occurred immediately after the eruption. Therefore, the ash was deposited almost simultaneously on a forested land surface and in a lake. This implies a shoreline somewhere between the Suntrana and Tatlanika localities. Our radiometric age of 6.7 Ma constrains the timing of this "first stirrings" of uplift to be younger than was implied by the 8.3 Ma age of Wahrhaftig (1987). Our age is consistent with estimates of the onset of uplift of ~5.4 Ma (Ager and others, 1994) based on the McCallum Creek age from the eastern Alaska Range, and ~6 Ma based on apatite fission track ages from Denali (Fitzgerald and others, 1993).

The senior author examined the Suntrana Creek section carefully with the intent of obtaining a radiometric age. However, the soft material contains almost no minerals larger than 62 microns (very fine sand) that appear to be primary volcanic phenocrysts. Moreover, none of the soft, glass-rich material seems to be of air-fall origin. It occurs in varve-like units about ½ in (1 cm) thick, soft and white at the bottom, grading up into dark gray, finer-grained and denser clay at the top. Diatoms are sparsely present in the white, chalky material, suggesting relatively slow rates of deposition. Tiny burrows filled with chalky material from the overlying unit commonly penetrate the dark upper layer. These units are interpreted as seasonal, possibly annual, deposits of ash washed into the Grubstake lake from surrounding watersheds. The darker, finer-grained upper part of each couplet, based on the varve-like appearance, may be a winter layer of the finest suspended material, slowly deposited after freeze-up of streams and an ice cover on the lake.

Wolfe (1994, p. 212) states that the Grubstake leaf assemblage "clearly represents coniferous forest, which is consistent with the radiometric age that indicates a probably latest Homerian or early Clamgulchian age." This reference is to age of the glass cited by Wahrhaftig and others (1969); it also includes, as shown in figure 3, a radiometric age of about 8 Ma for the Homerian–Clamgulchian boundary at Kachemak Bay. Based on his analysis of foliar physiognomy, Wolfe (1994, p. 211) suggests a mean annual temperature of about 3°C for Clamgulchian time. Such a temperature implies strong development of seasonal ice on lakes, which is supported by the varve-like character expressed by the ash-rich layers in the lakebeds at Suntrana Creek. The presence of seasonal ice is also suggested by the common occurrence here of scattered, out-sized sand grains and pebbles up to at least ½ inch (1 cm) in diameter; these are most likely dropstones transported by floating ice during breakup. T. Ager (oral commun., 1999) points out that Clamgulchian time is now thought to span perhaps from about 3 Ma to 8 Ma and that over such a long period the climate probably varied considerably and thus the climate estimates of Wolfe (1994) may apply to only part of the lower Clamgulchian. This does not negate the argument here for seasonal ice in this locality at about 6.7 Ma.

The radiometric age for the volcanic ash in the Grubstake Formation will provide an approximate age for insect wings recently found by the senior author a few feet below the base of the ash-rich, chalky layers on Suntrana Creek. These sparse fossils have the size and general appearance of mosquito wings—not very impressive, but of some interest because they are apparently the only insect fossils reported for the entire Tertiary of interior Alaska. A small collection of the wings has been sent to David Grimaldi, American Museum of Natural History, New York, for identification.

Our radiometric ages from the Tatlanika locality also provide a possible connection to the Canyon Village lakebeds locality on the Porcupine River, described by Kunk and others (1994). They report a slightly reworked

tephra layer ranging from 1/16 to 2 in (0.2–5 cm) thick, consisting primarily of slightly devitrified glass mixed with silt from the enclosing sediments. $^{40}Ar/^{39}Ar$ ages for plagioclase from one locality and biotite from two localities all agree with one another, within the limits of analytical precision. Their best estimate of the age of the tephra is the mean age of these results, 6.57 ± 0.02 Ma (late Late Miocene). This is very close to our preferred age range of 6.7 ± 0.1 Ma for the Tatlanika Creek ash, and suggests that they might be the same ash. Further evidence is required to support this correlation and a direct comparison of samples is planned, including mineralogy, glass morphology, and microprobe chemistry of individual components.

SUNTRANA FORMATION, COAL BED #6 TONSTEIN

A kaolinitic clay layer (tonstein) occurs at a number of localities at or near the top of coal bed #6, the uppermost unit of the Suntrana Formation. This is an altered volcanic ash, and contains a variety of primary phenocrysts, including quartz, plagioclase, and amphibole. At Suntrana Creek it is absent on the east side of the creek and about 1 in (2.5 cm) thick at the top of the coal on the west side. It is approximately this same thickness about 1 mi (1.6 km) west along the haul road toward Usibelli Coal Mine on Lignite Creek, but is overlain by several inches of coal. In the active coal mine on and south of Lignite Creek this tonstein has different amounts of coal above it, ranging up to at least 4 ft (1.2 m). In all of these places the coal is overlain by sand or gravel in erosional contact with the coal; thus variable amounts of the coal have been eroded during deposition of the overlying stream sediments, down to and including the tonstein. So far this is the only volcanic ash that has been found in the Healy area that contains minerals large enough and in sufficient quantity for radiometric dating. There are perhaps several dozen other tonsteins within coal beds around Healy, but they are mostly very thin (¼ in [0.6 cm] or less) and without volcanic phenocrysts in the sand-size range.

AGE OF THE SUNTRANA FORMATION BASED ON PALEOBOTANY

The flora of the Suntrana Formation is poorly known, in part because relatively few samples have been examined. Wahrhaftig and others (1969) indicate that poor induration limited the collection of entire leaves, necessary for identification. In 1992 Tom Ager, USGS, Denver, with the senior author, collected leaves from the lower part of the Suntrana Formation about 6 mi (10 km) from the mouth of Lignite Creek; these have been identified by Jack Wolfe (Leopold and Liu, 1994, p. 126).

Leopold and Liu (1994) reported on a long pollen sequence from Coal Creek, a south tributary of Healy Creek that enters Coal Creek 9 mi (14 km) east from its junction with the Nenana River. It should be noted that this is about 6 mi (10 km) from the type locality of the Suntrana Formation on Suntrana Creek and that the formation increases in thickness from about 764 ft (233 m) at Suntrana Creek to about 1,312 ft (400 m) at Coal Creek (Leopold and Liu, 1994, p. 106).

The Suntrana Formation flora is correlated with the Middle Miocene Seldovian floristic stage of the Cook Inlet area (Wolfe and Tanai, 1980), based mainly on radiometric ages in the Lower 48 (Wolfe, 1981). Turner and others (1980) have one K-Ar age for plagioclase of about 16 Ma from the Seldovian floral stage on the Chuitna River not far from its mouth on the north side of Cook Inlet.

RADIOMETRIC DATES

The significance of the phenocryst-bearing tonstein in coal bed #6 was recognized in 1977, as it is just below the contact between the Suntrana Formation and the overlying Lignite Creek Formation and thus is an important lithostratigraphic boundary. Don Turner, University of Alaska, Fairbanks, performed conventional K-Ar analyses of plagioclase concentrates collected by the senior author at Usibelli Coal Mine south of the mouth of Lignite Creek and on the north side of Lignite Creek about 9.5 mi (15 km) east of the mouth. The former yielded an age of 35.5 ± 1.4 Ma and the latter 27.0 ± 1.1 Ma, a span covering much of the Oligocene and clearly much older than the expected Miocene age based on the Seldovian flora (Wahrhaftig and others, 1969).

We collected an additional sample from an active face at the Suntrana mine, in the NE¼ sec. 5, T. 11 S., R. 7 W., just south of Lignite Creek (the locality has since been reclaimed and is no longer available). An $^{40}Ar/^{39}Ar$ analysis of a small sanidine separate yielded an age of about 32 Ma, again older than the age of the Seldovian flora and consistent with the earlier K–Ar ages. Plagioclase plateau ages range from about 40 to 33 Ma, and both the plagioclase and the sanidine show evidence of Ar loss. This loss, as seen in the first fractions of gas release (fig. 4), is fairly consistent from sample to sample and can be explained by single-loss diffusion modeling. Loss ages ranging from about 15 to 20 Ma are more consistent with the inferred stratigraphic age of this sample.

Hornblende ages and Ca/K ratios were highly variable. Multigrain samples with Ca/K ratios greater than 20 have ages of 44 and 51 Ma, while two samples with lower Ca/K ratios have ages of 0 Ma and one has an age of 7.5 ± 1.7 Ma. Based on the inconsistency of the

data and the low radiogenic content of most samples, we do not ascribe any geologic significance to the hornblende ages.

DISCUSSION OF THE COAL BED #6 RADIOMETRIC AGES

As shown in figure 3, radiometric ages from elsewhere in Alaska provide a reasonably consistent framework for the ages of the Tertiary floristic stages of Alaska. White and Ager (1994, p.57) interpret the Seldovian stage to range in age from about 20 to 13–14 Ma, that is, Lower and Middle Miocene. Correlations in figure 3 are from Ager and others (1994) and show the Suntrana Formation as lower Middle Miocene. Leopold and Liu (1994; fig. 5, p.126) compare the Wolfe and Tanai (1980) interpretation of an upper Middle Miocene age with their interpretation (fig. 13, p.129) of an upper Lower to lower Middle Miocene age for the Suntrana Formation. In any case, our age of greater than 30 Ma is substantially older than the expected age of somewhere between about 11 Ma and 17 Ma. At this time we cannot explain this discrepancy. Either the feldspars in the ash layer are older than the depositional age or, less likely, the correlation of the Suntrana formation with other Cook Inlet Seldovian units is incorrect. If the former is true, this would imply that either the eruption that deposited this ash entrained a substantial amount of old material and no younger material was preserved, or the unit is not an air-fall ash deposit, but rather represents reworking and redeposition of an older unit. However, substantial reworking of sediments is unlikely in a coal swamp.

THE RELATIONSHIP BETWEEN THE SUGAR LOAF VOLCANICS AND THE USIBELLI GROUP

Sugar Loaf Mountain, which outcrops about 5 mi (8 km) south of the Suntrana exposure, is predominantly rhyolites interpreted in a cross section by Wahrhaftig (1970) as a viscous plug dome. Albanese (1980) provided whole-rock K-Ar ages for Sugar Loaf Mountain rhyolites of about 32–34 Ma, consistent with our feldspar ages from coal bed #6. Although the volcanics lie predominantly on the Paleozoic Birch Creek Schist, Wahrhaftig (1970) reports that that there are some strata interpreted to be (presumably) "upper" Healy Creek Formation (Seldovian) between the rhyolite and the underlying schist. As we observed in the Suntrana formation, either the stratigraphic ages of the units are incorrect, or the radiometric ages are too old.

Note that Wahrhaftig's interpretation (1970, cross-section B-B') is that Sugar Loaf Mountain is an eroded remnant of a volcanic landform. Apparently he thought that it had erupted essentially onto the present land surface after the Tertiary sediments, almost 2,000 ft (600 m) thick just 6 mi (10 km) to the north, had been stripped off of the resistant schist during uplift of the Alaska Range. The small patch of Healy Formation below the volcanics might be a problem in this interpretation, as discussed below. In any case, the implication is that the volcano erupted after the Tertiary coal-bearing sediments had been eroded, and thus that the volcano is younger, possibly much younger, than the ~8 Ma age (Wahrhaftig and others, 1969) determined for the top of the coal-bearing sediments.

If the volcano is more than 30 Ma old, serious questions arise. If the volcano erupted before most of the coal-bearing sediments were deposited, could it have been preserved by quick burial under Tertiary sediments and then re-exposed by the present erosional episode? This seems unlikely for several reasons, including the presence of a small patch (erosional remnant or first accumulation?) of underlying coal-bearing sediment, and the lack of rhyolite clasts in the nearby Tertiary sediments.

Wahrhaftig (1970) mapped the sediments below the volcanics as "upper" Healy Creek Formation. We have no information on the nature of these sediments, and assume that this correlation was based on lithology and stratigraphic position, that is, in depositional contact with the underlying basement. Such basal coal-bearing strata have been assigned to the Healy Creek Formation over a wide area, from the Sushana River on the west to Jarvis Creek to the east, a distance of 125 mi (200 km) (Wahrhaftig and others, 1969, p. D7-D8). This implies a widespread, low-lying erosion surface that subsided to receive initial Tertiary sediments of about the same lithology over a large area. No time relationship is implied, and if these basal strata span a significant time range, the effect would be to lengthen the temporal range of the Healy Formation. This is in fact suggested by the occurrence of Healy Formation at Rex Creek and California Creek that has a distinctly different (lower Healy Creek) floral assemblage compared to other (upper Healy Creek) strata in the Nenana Coal Field. See Leopold and Liu (1994, p. 106) for a discussion of this issue. They conclude that there must be a major unconformity separating lower Oligocene strata from probably Lower Miocene sediments. This could amount to 14 Ma to 20 Ma. The point here is that the basal Tertiary sediments in interior Alaska may have been deposited over a considerable span of time, and assignment to the Healy Creek Formation may be just a matter of convenience due to a lack of information.

If the volcano is older than 30 Ma, the sediments under the rhyolite may be part of this "lower" Healy Creek Formation. If so, the relationship to the formation on Healy Creek, only about 5 mi (8 km) to the north, is

in question. It appears that the only information on the floral assemblage on Healy Creek (Wahrhaftig and others, 1969) did not include parts of the formation below the type locality at Suntrana Creek. Thus it is possible that some "lower" Healy Creek Formation is present along Healy Creek, but this would require a 14–20 Ma unconformity within the formation. If the coal-bearing sediments under the Sugar Loaf volcanics are found to have an "upper" Healy Creek flora, this would suggest that the radiometric ages for the volcanics are far too old.

Overall there are inconsistencies involving the ages of the volcanics, the underlying Healy Creek Formation, and the Healy Creek Formation on nearby Healy Creek that cannot be resolved without further information.

CONCLUSIONS

Radiometric dating of stratigraphic sections provides badly needed absolute time constraints and allows for correlation between geographic regions. Volcanic ash layers in sedimentary sequences are obvious targets for radiometric dating. However, as the examples here illustrate, dating these sequences is not always straightforward and what might be applicable for one ash might not work for another.

For the Grubstake ash, the previously accepted age of 8.3 Ma based on K-Ar dating of glass and confirmed by $^{40}Ar/^{39}Ar$ dating of the same glass, is probably in error due to the presence of excess argon in the glass. Minerals from this ash give a consistent age of 6.7 Ma, which we prefer as representing the depositional age of this ash and better defining the lower part of the Grubstake Formation and the first stirrings of uplift in the central Alaska Range.

For the ash in coal bed #6 of the Middle Miocene Suntrana Formation, the radiometric ages from plagioclase and sanidine minerals is about 35 Ma. This age is clearly too old based on stratigraphic correlation with Cook Inlet stratigraphy and implies a complicated geologic history for the minerals in the ash layer. The age spectra from this ash do not exhibit indications of excess Ar, but rather have evidence of Middle Miocene Ar loss. Thus, the minerals in the coal bed #6 ash layer either were inherited from older eruptions during a Middle Miocene eruption, or the ash is a reworked and redeposited older ash unit. There are compelling arguments against each of these hypotheses.

Related to the problems associated with the coal bed #6 ash is the age of the Sugar Loaf rhyolite. The similarity of the ages between the feldspars in the coal bed #6 ash and the Sugar Loaf volcanics suggests a relationship between the two. If the 32–34 Ma K-Ar ages of Albanese (1980) are correct, the sediments under the rhyolites probably are part of the Oligocene "lower" Healy Creek Formation. If so, the lowest part of the Healy Creek Formation nearby on Healy Creek is likely the same age. However, there is no information on the age of this part of the section, and the presence of Oligocene sediments would require a major unconformity within the Healy Creek Formation which is otherwise considered Miocene. There is no reason to suspect that the K-Ar ages are incorrect, nor is there any reason to question identification of these sediments as Healy Creek Formation. Further analytical work and fieldwork are needed to resolve this paradox.

ACKNOWLEDGMENTS

This work was supported through funding to the geochronology laboratory from the Geophysical Institute. We wish to think Evan Thoms for collecting the sample at Tatlanika Creek. Gary Stricker and Tom Ager provided thorough and helpful reviews that improved the manuscript.

REFERENCES

Ager, T.A., Matthews, J.V., Jr., and Yeend, W.E., 1994, Pliocene terrace gravels of the ancestral Yukon River near Circle, Alaska: palynology, paleobotany, paleoenvironmental reconstruction and regional correlation, *in* Ager, T.A., White, J.M., and Matthews, J.V., Jr., eds., Tertiary Quaternary boundaries: Quaternary International, v. 22–23, p. 185–206.

Albanese, M.D., 1980, The geology of three extrusive bodies in the central Alaska Range: University of Alaska Fairbanks, M.S. thesis (unpub.), 104 p.

Fitzgerald, P.G., Stump, Edmund and Redfield, T.F., 1993, Late Cenozoic uplift of Denali and its relation to relative plate motion and fault morphology: Science, v. 259, no. 5094, p. 497–499.

Kunk, M.J., Rieck, H.J., Fouch, T.D. and Carter, L.D., 1994, $^{40}Ar/^{39}Ar$ age constraints on Neogene sedimentary beds, upper Ramparts, Half-way Pillar and Canyon Village sites, Porcupine River, east-central Alaska, *in* Ager, T.A., White, J.M., and Matthews, J.V., Jr., eds., Tertiary Quaternary boundaries: Quaternary International, v. 22–23, p.31–42.

Layer, P.W., Hall, C.M. and York, Derek, 1987, The derivation of $^{40}Ar/^{39}Ar$ age spectra of single grains of hornblende and biotite by laser step-heating, Geophysical Research Letters, v. 14, no. 7, p. 757–760.

Leopold, E.B. and Liu, Gengwu, 1994, A long pollen sequence of Neogene age, Alaska Range, *in* Ager, T.A., White, J.M., and Matthews, J.V., Jr., eds., Tertiary Quaternary boundaries: Quaternary International, v. 22–23, p. 103–140.

McDougall, Ian, and Harrison, T.M., 1988, Geochronology and thermochronology by the $^{40}Ar/^{39}Ar$ method: New York, Oxford University Press, Monographs on Geology and Geophysics, v. 9, 212 p.

Steiger, R.H. and Jäger, Emily, 1977, Subcommission on geochronology: Convention on the use of decay constants in geo- and cosmochronology: Earth and Planetary Science Letters, v. 36, no. 3, p. 359–362.

Triplehorn, D.M., Turner, D.L and Naeser, C.W., 1977, K-Ar and fission-track dating of ash partings in coal beds from the Kenai Peninsula, Alaska—a revised age for the Homerian Stage–Clamgulchian Stage – boundary: Geological Society of America Bulletin, v. 88, no. 8, p. 1156–1160.

Turner, D.L., Triplehorn, D.M., Naeser, C.W. and Wolfe, J.A., 1980, Radiometric dating of ash partings in Alaskan coal beds and upper Tertiary paleobotanical stages: Geology, v. 8, no. 2, p. 92–96.

Wahrhaftig, Clyde, 1970, Geologic map of the Healy D-4 quadrangle, Alaska: U.S. Geological Survey Geologic Quadrangle Map GQ-806, scale 1:63,360.

———1987, The Cenozoic section at Suntrana, Alaska, *in* Hill, M.L., ed., Cordilleran Section of the Geological Society of America, Centennial field guide, vol. 1, p. 445–450.

Wahrhaftig, Clyde, Bartsch-Winkler, Susan, and Stricker, G.D., 1994, Coal in Alaska, *in* Plafker, George, and Berg, H.C., eds., The Geology of Alaska, The Geology of North America: Boulder, Colorado, Geological Society of America, v. G-1, p. 937 – 978.

Wahrhaftig, Clyde, Wolfe, J.A., Leopold, E.B., and Lanphere, M.A., 1969, The coal-bearing group in the Nenana Coal Field, Alaska: U.S. Geological Survey Bulletin 1274-D, p. D1–D30.

White, J.M. and Ager, T.A., 1994, Palynology, paleoclimatology and correlation of Middle Miocene beds from Porcupine River (Locality 90-1), Alaska, *in* Ager, T.A., White, J.M., and Matthews, J.V., Jr., eds.,Tertiary Quaternary boundaries: Quaternary International, v. 22–23, p. 43–77.

Wolfe, J.A.,1977, Paleogene Floras from the Gulf of Alaska Region. U.S. Geological Survey Professional Paper 997, 108 p.

———1981, A chronologic framework for Cenozoic megafossil floras of northwestern North America and its relation to marine geochronology, *in* Armentrout, J.M., ed., Pacific Northwest Cenozoic biostratigraphy: Geological Society of America Special Paper 184, p. 39–47.

Wolfe, J.A., 1994, An analysis of Neogene climates in Beringia, in Cronin, T.M., Ogasawara, K., and Wolfe, J.A., eds., Cenozoic climate and paleogeographic changes in the Pacific region: Palaeogeography, Paleoclimatology, Palaeoecology, v.108, no. 3–4, p. 207–216.

Wolfe, J.A. and Tanai, T., 1980, The Miocene Seldovia Point flora from the Kenai Group, Alaska: U.S. Geological Survey Professional Paper 1105, 52 p.

York, Derek, Hall, C.M., Yanase, Yotaro, Hanes, J.A. and Kenyon, W.J., 1981, $^{40}Ar/^{39}Ar$ dating of terrestrial minerals with a continuous laser, Geophysical Research Letters, v. 8, no. 11, p. 1136–1138.

SEDIMENTOLOGY AND PROVENANCE OF THE PALEOCENE–EOCENE ARKOSE RIDGE FORMATION, COOK INLET–MATANUSKA VALLEY FOREARC BASIN, SOUTHERN ALASKA

Jeffrey M. Trop[1, 2] and Kenneth D. Ridgway[1]

ABSTRACT

The Paleocene–Eocene Arkose Ridge Formation consists of 1,600+ m of sedimentary and volcanic strata that were deposited along the arcward margin of the Cook Inlet–Matanuska Valley forearc basin, southern Alaska. This study reports new petrologic and sedimentologic data from the Arkose Ridge Formation that are used to interpret the provenance, depositional systems, and paleogeography of the forearc basin during the early Cenozoic. Light mineral provenance studies, conglomerate clast counts, and paleocurrent indicators suggest that detritus was derived from local source terranes exposed north of the Castle Mountain fault system. Arkose Ridge Formation sandstones are enriched in quartz and feldspar ($\%Q_{23}F_{67}L_{10}$; $\%Qm_{21}F_{68}Lt_{11}$) and can be divided into a lower petrofacies rich in metamorphic detritus ($\%Lv_{7}Ls_{0}Lm_{93}$) and an upper petrofacies rich in volcanic detritus ($\%Lv_{70}Ls_{0}Lm_{30}$). Initially, metamorphic-rich detritus was eroded from the plutonic roots of a remnant early Mesozoic magmatic arc, whereas during the later stages of sedimentation erosion of an active Cenozoic magmatic arc provided detritus rich in volcanic lithic fragments. Sedimentological analysis of the Arkose Ridge Formation reveals a progressive upsection change in sedimentary deposystems from gravelly, alluvial fans to sandy, braided streams to tidally influenced, sinuous streams. A relative rise in sea level during the Late Paleocene to Middle Eocene resulted in northward onlap of tidally influenced deposystems towards the basin margin and increased preservation of fine-grained sediment adjacent to the magmatic arc. Interbedded lava flows indicate relative proximity to active volcanic centers during deposition of the Arkose Ridge Formation.

INTRODUCTION

The general sedimentologic model for forearc basins predicts a gradual evolution from deep-marine, through shallow-marine, to nonmarine deposystems with progressive infilling of the basin (Ingersoll, 1979; Dickinson, 1995). Numerous past studies have examined the sedimentology and petrofacies of ancient marine depositional systems in forearc basins (for example, Ingersoll, 1979; Heller and Dickinson, 1985; Busby-Spera, 1986; Morris and Busby-Spera, 1988; Morris and others, 1989). In contrast, few sedimentological studies have been reported from ancient nonmarine deposits of forearc basins (exceptions: Kuenzi and others, 1979; Vessel and Davies, 1981; Fulford and Busby, 1993). The Cook Inlet–Matanuska Valley forearc basin in southern Alaska (fig. 1) contains thick sequences of well exposed nonmarine strata and thus provides a unique opportunity to better understand nonmarine sedimentation in forearc basins. This paper examines the Arkose Ridge Formation, a 1,600+-m-thick sequence of Paleocene–Eocene sedimentary and volcanic strata deposited along the arcward (northern) margin of the Cook Inlet–Matanuska Valley forearc basin. The main goals of this paper are to describe the sedimentology and petrofacies of the Arkose Ridge Formation in order to reconstruct the evolution of depositional systems, sediment source terranes, and paleogeography of the arcward margin of the forearc basin during the early Cenozoic. In addition to its contributions toward a better general understanding of forearc basin systems, this study may be useful to persons evaluating Cenozoic deposits in the upper Cook Inlet and lower Matanuska Valley for potential oil and gas reservoirs (Oil and Gas Journal, 1998).

GEOLOGIC SETTING

The Cook Inlet–Matanuska Valley forearc basin, a northeastern continuation of the Aleutian forearc basin, is bounded on the southeast by Mesozoic meta-sedimentary rocks of the Chugach subduction complex and on the northwest by late Mesozoic–Cenozoic igneous rocks of the Alaska Peninsula–Aleutian magmatic arc as well as early Mesozoic igneous, metamorphic, and sedimentary rocks of the Talkeetna magmatic arc (figs. 1, 2; Magoon and others, 1976; Csejtey and others, 1978; Winkler, 1992). The northeastern part of the forearc basin has been uplifted and exposed (Matanuska Valley/Talkeetna Mountains) whereas the southwestern part of the basin (Cook Inlet) is still subsiding (figs. 1, 2; Fisher and Magoon, 1978). The forearc basin strata disconformably overlie early

[1]Department of Earth and Atmospheric Sciences, 1397 Civil Engineering Building, Purdue University, West Lafayette, IN 47907-1397. Email for Jeffrey Trop: jtrop@bucknell.edu
[2]Present address: Department of Geology, Bucknell University, Lewisburg, PA 17837.

Mesozoic sedimentary, igneous, and metamorphic rocks of the Talkeetna magmatic arc, an allochthonous andesitic island arc assemblage that formed at low paleolatitudes, was translated northward, and accreted to southern Alaska during the late Mesozoic and early Cenozoic (Plafker and Berg, 1994). The forearc basin fill consists of 1,000–4,000 m of Cretaceous marine strata and 3,000–7,000 m of mostly nonmarine Tertiary strata (fig. 3; Kirschner and Lyon, 1973; Winkler, 1992). Volcanic and plutonic rocks exposed along the northern margin of the basin record late Mesozoic–Cenozoic arc magmatism in response to northward- to northwestward-directed subduction of the Farallon, Kula, and Pacific oceanic plates (Engebretson and others, 1983; Plafker and Berg, 1994). The Border Ranges fault system, a Mesozoic thrust fault (MacKevett and Plafker, 1974) with localized Cenozoic dextral displacement (Pavlis and Crouse, 1989), separates the forearc basin from the Chugach subduction complex (figs. 1, 2; Plafker and others, 1977). Along the arcward margin of the forearc basin are northeast-trending high-angle reverse faults, including the Castle Mountain fault, which experienced Eocene–Oligocene dextral strike-slip displacement and Neogene dip-slip displacement (figs. 1, 2; Grantz, 1966; Fuchs, 1980; Little, 1990).

The Paleocene–Eocene Arkose Ridge Formation, the focus of this study, has a maximum preserved thickness of 1,600+ m and consists mostly of conglomerate and sandstone with subordinate mudstone, coal, tuff, and lava flows (Martin and Katz, 1912; Silberman and Grantz, 1984). Exposed in a narrow, discontinuous outcrop belt 100 km long and 5–10 km wide, outcrops of the Arkose Ridge Formation are confined to the north side of the east–west trending Castle Mountain fault system in the Talkeetna Mountains (fig. 2; Winkler, 1992). The base of the Arkose Ridge Formation unconformably overlies pre-Cretaceous igneous and metamorphic rocks of the allochthonous Wrangellia

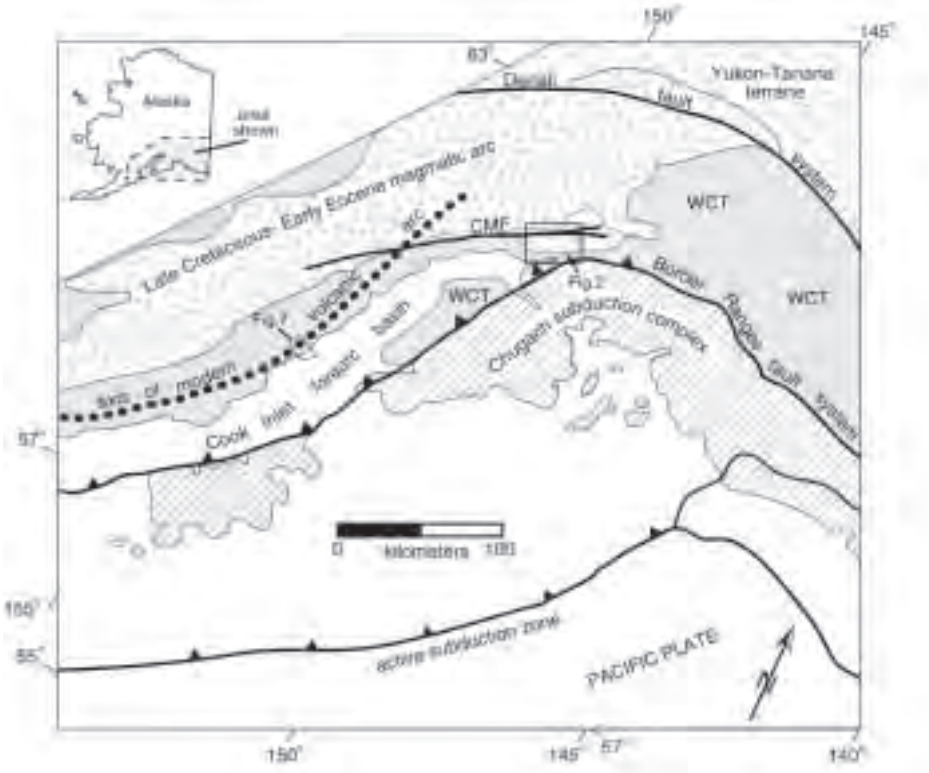

Figure 1. *Generalized map showing major tectonic elements of the southern margin of Alaska. Cook Inlet represents part of an actively subsiding forearc basin located between the modern Aleutian magmatic arc to the north (dotted black line) and the Chugach subduction complex to the south (hatched pattern). Uplifted ancient sedimentary deposits of the forearc basin (open-circled pattern) are exposed in the vicinity of the Castle Mountain fault (CMF). Note that the ancient forearc basin deposits unconformably overlie the allochthonous Wrangellia composite terrane (WCT) and the Late Cretaceous–Eocene magmatic arc. Map adapted from Little (1988). Area of detailed geologic map shown in figure 2 is outlined by rectangle along the eastern part of the Castle Mountain fault.*

composite terrane. Cretaceous forearc basin deposits were either never deposited locally or were uplifted and eroded during the latest Cretaceous and/or Early Paleocene. The Arkose Ridge Formation is overlain by Eocene volcanic rocks and/or Quaternary surficial deposits in the eastern Talkeetna Mountains, and Miocene and younger sedimentary rocks in upper Cook Inlet (Winkler, 1992). In the western Talkeetna Mountains the top of the formation has been eroded and is not exposed (Winkler, 1992). Paleontologic studies of megafossil floras (Martin and Katz, 1912; J. Wolfe *in* Silberman and Grantz, 1984) and K-Ar radiometric dating of interbedded volcanic rocks (Silberman and Grantz, 1984) define the age of the formation as Late

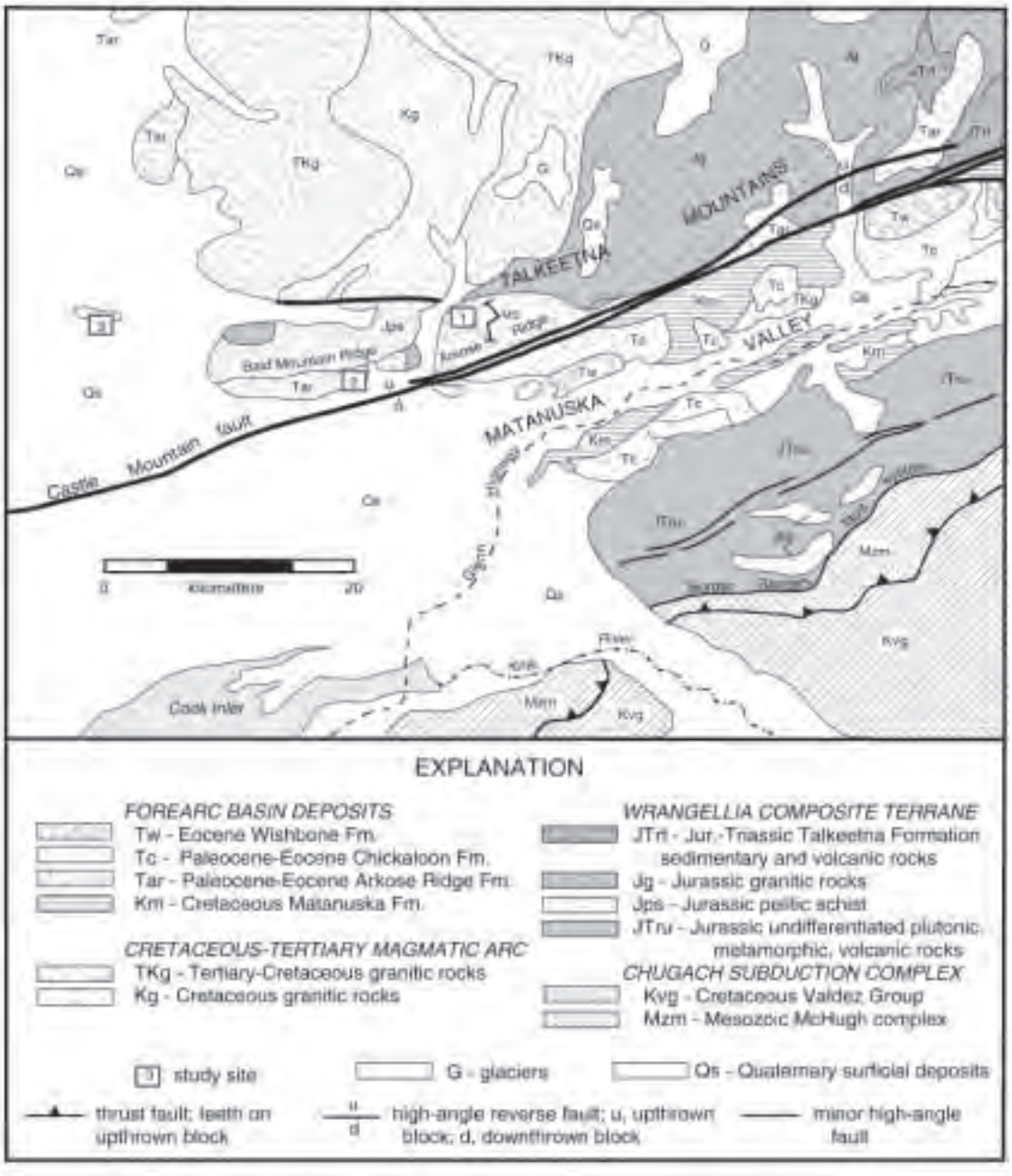

Figure 2. *Generalized geologic map of the Matanuska Valley and western Talkeetna Mountains in the western Anchorage 1x3 degree quadrangle. MS = measured stratigraphic section shown on figure 4. See figure 1 for map location. Geology is from Csejtey and others (1978), Winkler (1992), and this study.*

Paleocene to Middle Eocene (fig. 3; Winkler, 1992). Age-equivalent finer-grained sedimentary strata and volcanic ash of the Chickaloon Formation are exposed between the Castle Mountain and Border Ranges faults in the Matanuska Valley and northern Chugach Mountains (fig. 2). The Chickaloon Formation consists of ~1,500 m of Paleocene–Eocene fluvial–lacustrine mudstone, sandstone, coal, and minor conglomerate (fig. 3; Barnes, 1962; Little, 1988).

PROVENANCE

Compositional data from the Arkose Ridge Formation afford an opportunity to study the petrofacies of forearc basin strata deposited adjacent to an active magmatic arc. The "magmatic arc" provenance field of global sandstone provenance schemes is derived primarily from marine strata deposited in arc-related sedimentary basins (Dickinson, 1988; Marsaglia and

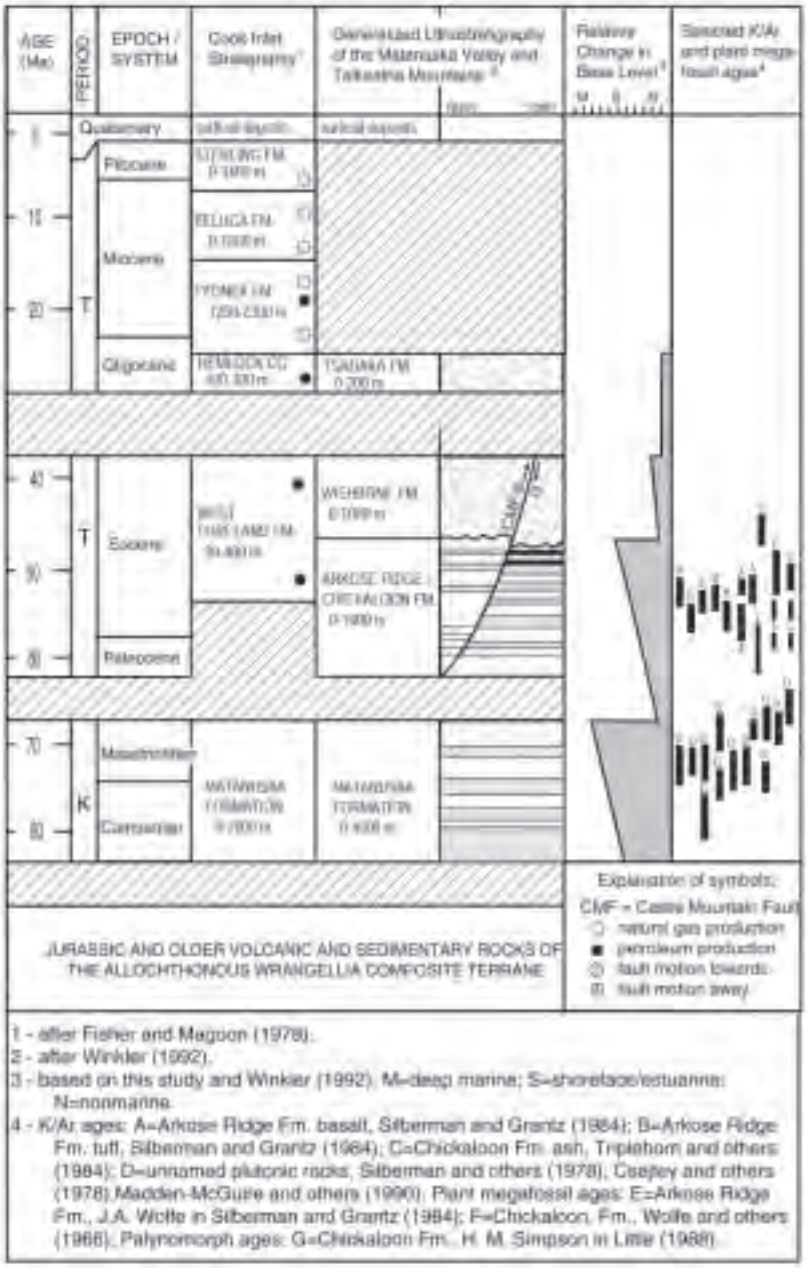

Figure 3. *Age-event diagram showing stratigraphy of Cook Inlet and Matanuska Valley/Talkeetna Mountains, inferred relative base level changes, and published geochronologic and paleontologic data.*

Ingersoll, 1992). Notably underrepresented in the global schemes are data from nonmarine strata deposited proximal to the magmatic arc. We also use our compositional data to better define the Paleocene–Eocene paleogeography of the Cook Inlet–Matanuska Valley forearc region by identifying which source terranes were exposed during deposition of the Arkose Ridge Formation.

METHODS

Our analysis of the Arkose Ridge Formation is from three study sites located in the western Talkeetna Mountains (see fig. 2 for locations). The most laterally and vertically extensive outcrop exposures were observed along the northern flank of Arkose Ridge (fig. 2). A new 1,600+-m-thick measured stratigraphic section from that location forms the basis for most of the compositional and sedimentological data presented in this paper (fig. 4). We recognize three major lithologic successions within the Arkose Ridge Formation based on distinct upsection changes in lithofacies assemblages, sedimentary structures, bed geometries, and bed thicknesses (fig. 4). The sedimentology and depositional systems of each succession is discussed in a section below.

Thirteen sandstone samples were collected over the entire measured section at Arkose Ridge, including each of the three lithologic successions (see fig. 4 for sample distribution). Medium to coarse-grained sandstones were cut into standard petrographic thin sections, stained for potassium and plagioclase feldspar identification, and point-counted using an automated stage. Separate tabulations of grain parameters were kept using both the Gazzi-Dickinson and "traditional" methods (Ingersoll and others, 1984). Recalculated data are presented in table 1 and figure 5 in terms of the Gazzi-Dickinson method so that they can be compared with previous provenance studies such as Dickinson (1988). Two clast counts from conglomerates in the lowermost part of the section at Arkose Ridge were also obtained (fig. 4).

PETROLOGY

Arkose Ridge Formation sandstones are moderately to poorly sorted, contain little matrix, and have angular to subrounded framework grains. Sandstones have average framework grain modes of $Q_{23}F_{67}L_{10}$ and $Qm_{21}F_{68}Lt_{11}$ and average framework mineral modes of $Qm_{23}P_{76}K_{1}$ (table 1). Sandstones classify as feldspathic arenites and arkoses that plot mainly within the "continental block–basement uplift" provenance field (QmFLt and QFL plots on fig. 5). Lithic grain populations consist of igneous and metamorphic varieties ($Lv_{21}Ls_{0}Lm_{79}$). Lathwork grains composed of plagioclase phenocrysts in a dark glassy matrix (fig. 6A) dominate the volcanic lithic population. Foliated phyllosilicate lithic fragments are the dominant metamorphic grain types. There is a pronounced upsection increase in volcanic lithic fragments relative to metamorphic lithic fragments. (fig. 5; successions 1, 2 = $\%Lv_{7}Ls_{0}Lm_{93}$; succession 3 = $\%Lv_{70}Ls_{0}Lm_{30}$). Plutonic rock fragments are common in all Arkose Ridge Formation sandstones and consist predominantly of coarse-grained granitic fragments comprising plagioclase feldspar, monocrystalline quartz, biotite, and muscovite (fig. 6B). Individual plutonic rock fragments comprise several mineral grains greater than 0.0625 mm. Therefore, our point-count tabulations using the Gazzi-Dickinson methodology reflect the individual framework minerals within the rock fragments. For this reason, the lithic populations on table 1 and figure 5 do not include plutonic rock fragments (Ingersoll and others 1984). Granitic clast types with minor amounts of amphibolite, quartz, and siliceous tuff dominate conglomerates from the lower part of the Arkose Ridge Formation (fig. 4).

INTERPRETATION OF COMPOSITIONAL DATA

On the basis of modal composition and paleocurrent data we interpret the Arkose Ridge Formation as being derived from local igneous and metamorphic source terranes exposed north of the Castle Mountain fault (Jg, Jps, Kg, TKg on fig. 2; Csejtey and others, 1978; Winkler, 1992). This interpretation is in agreement with the results of a sandstone petrography study of the Arkose Ridge Formation by Winkler (1978). Igneous clast types constitute more than 80 percent of the conglomerate composition (fig. 4) and are petrographically similar to early Mesozoic plutons exposed immediately north of the studied outcrops (Jg on fig. 2). Diagnostic clast types include quartz–biotite granite, hornblende quartz diorite, hornblende–biotite granodiorite, amphibolite, and foliated quartz diorite. The early Mesozoic granitic rocks likely contributed a large part of the quartz, feldspar, and mica framework grains that are abundant in Arkose Ridge Formation sandstones. On the basis of petrographic characteristics, mica schist fragments containing biotite, muscovite, and chlorite were most likely derived from pelitic schist presently exposed on and around Bald Mountain Ridge (fig. 2). Volcanic lithic fragments common in the upper part of the section are interpreted as being derived from Paleocene–Eocene volcanic rocks, mainly mafic lava flows, along the northern margin of the basin. Paleocene–Eocene extrusive volcanic rocks are exposed throughout the eastern Talkeetna Mountains (Csejtey and others, 1978; Winkler, 1992) but only the plutonic roots of the arc are exposed in the western Talkeetna Mountains (TKg on fig. 2). Volcanic lithic fragments were eroded, mixed with epiclastic nonvolcanic detritus,

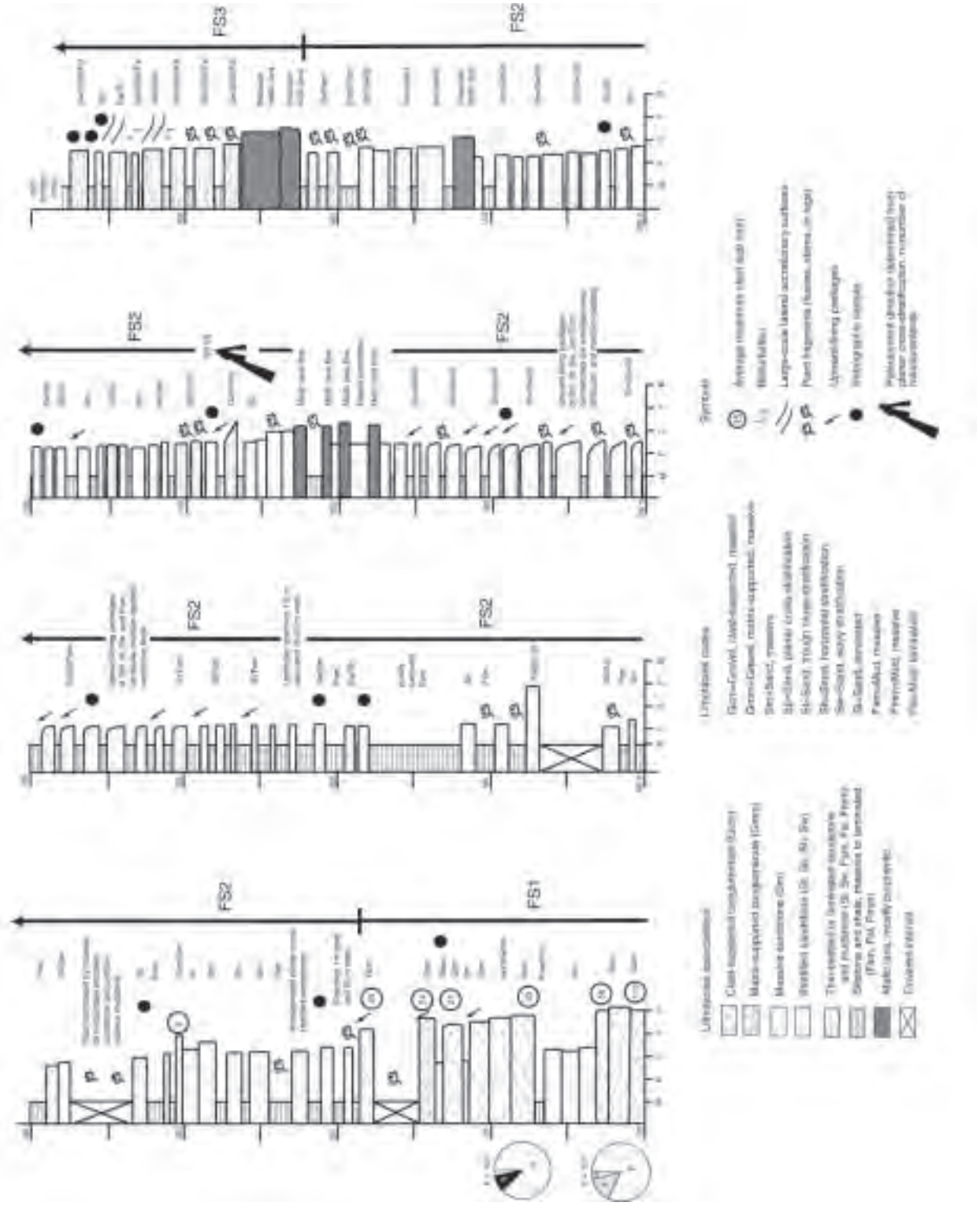
FS3
FS2
FS2
FS2
FS2
FS2
FS2
FS1

Figure 4 (left). *Detailed measured stratigraphic section of the Arkose Ridge Formation using the lithofacies schemes of Miall (1978). See figure 2 for location of measured section. Stratigraphic range of major lithofacies successions shown by black vertical bars: FS1 = succession 1; FS2 = succession 2; FS3 = succession 3. Grain sizes on horizontal scale: M = mud; F = fine-grained sand; C = coarse-grained sand; P = pebble; B = boulder. Rose diagram at 1,060 m represents paleocurrent data collected from planar cross-stratification in succession 2. Solid circles represent sandstone samples collected for modal analysis. Pie diagrams in succession 1 (0 m and 82 m) represent conglomerate clast compositions. Clast compositional data was obtained by counting all pebble-, cobble-, and boulder-sized clasts within a delineated rectangle on an outcrop face. Note the relative abundance of plutonic clasts (P). Other clast types include tuff (T), quartz (Q), minor metamorphic and sedimentary varieties (O). N = number of clasts counted.*

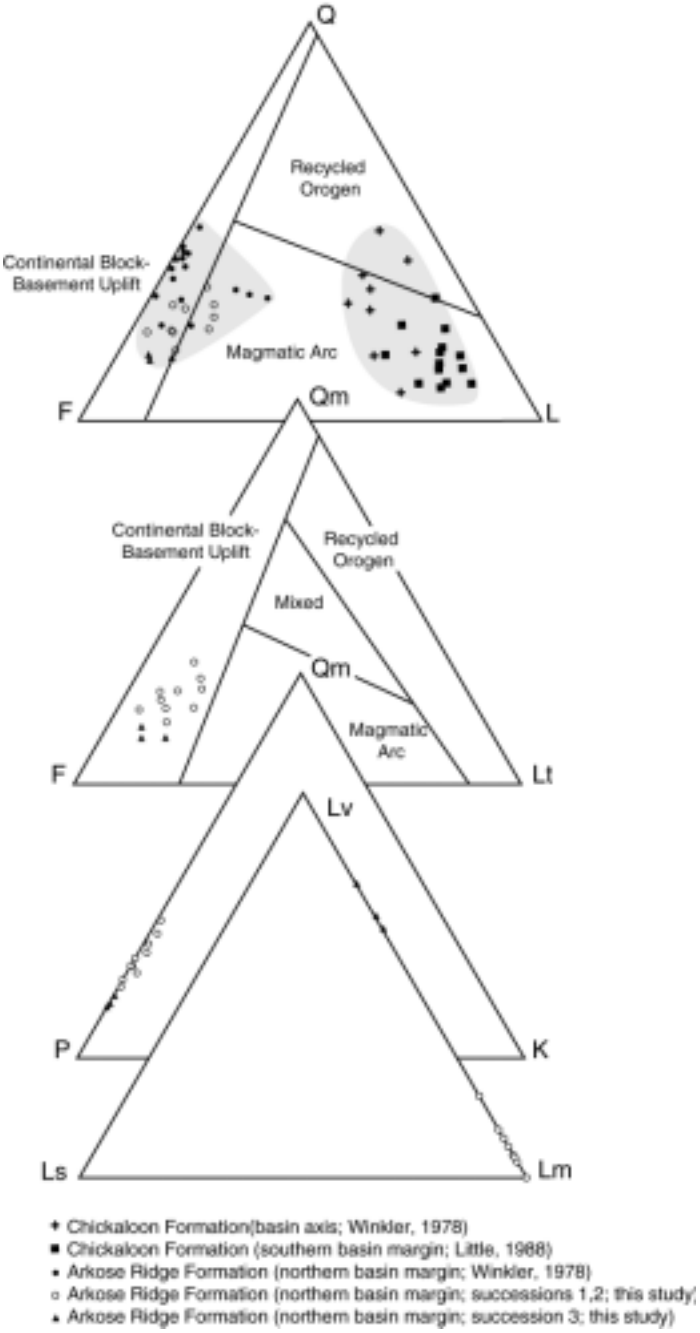

Figure 5 (right). *Ternary diagrams showing modal compositions of Arkose Ridge and Chickaloon Formation sandstones. Each symbol represents one modal analysis of 400 or more framework grains using the Gazzi-Dickinson point-count method (Ingersoll and others, 1984) as part of this study or previous studies (Winkler, 1978; Little, 1988). Q = monocrystalline quartz, chert, and polycrystalline quartz; Qm = monocrystalline quartz; Qt = total quartzose grains; P = plagioclase feldspar; K = potassium feldspar; F = plagioclase and potassium feldspar; Lt = total lithic grains; Lv = volcanic lithic fragments; Lm = metamorphic lithic fragments; Ls = sedimentary lithic fragments; L = lithic grains except quartzose lithic types. "Recycled orogen," "magmatic arc," "continental block-basement uplift," and "mixed" provenance fields from Dickinson and others (1983).*

Table 1. *Recalculated point-count data from the Arkose Ridge Formation*

Stratigraphic position (m)	Facies succession	Q	F	L	Qm	F	Lt	Qm	P	K	Lv	Ls	Lm
LONE1-132	1	28.17	62.91	8.92	24.22	64.27	11.51	27.37	70.73	1.90	8.11	0.00	91.89
LONE1-208	2	22.25	68.50	9.25	19.70	69.19	11.11	22.16	75.57	2.27	5.41	0.00	94.59
LONE1-326	2	26.06	57.75	16.20	24.76	58.57	16.67	29.71	69.14	1.14	5.80	0.00	94.20
LONE1-577	2	33.57	55.48	10.95	31.71	56.83	11.46	35.81	63.36	0.83	0.00	0.00	100.00
LONE1-612	2	29.02	65.12	5.85	24.04	68.29	7.67	26.04	73.96	0.00	4.17	0.00	95.83
LONE1-766	2	22.98	60.39	16.63	19.85	62.85	17.30	24.00	75.69	0.31	0.00	0.00	100.00
LONE1-892	2	22.72	68.64	8.64	21.89	69.15	8.96	24.04	75.96	0.00	0.00	0.00	100.00
LONE1-1071	2	17.63	70.30	12.06	16.12	70.79	13.08	18.55	80.91	0.54	21.15	0.00	78.85
LONE1-1197	2	22.25	74.08	3.67	19.35	75.29	5.36	20.44	79.56	0.00	12.50	0.00	87.50
LONE1-1225	2	29.10	56.22	14.68	27.48	57.51	15.01	32.34	65.87	1.80	10.17	0.00	89.8
Average (successions 1, 2)		25.38	63.94	10.69	22.91	65.27	11.81	26.05	73.08	0.88	6.73	0.00	93.2
LONE1-1570	3	15.85	71.95	12.20	12.13	73.02	14.85	14.24	85.47	0.29	76.00	0.00	24.00
LONE1-1572	3	16.59	76.59	6.83	14.95	76.96	8.09	16.27	83.47	0.27	67.86	0.00	32.14
LONE1-1575	3	15.26	76.99	7.74	12.06	78.42	9.51	13.33	86.67	0.00	64.71	0.00	35.29
Average (succession 3)		15.90	75.18	8.92	13.05	76.13	10.82	14.61	85.20	0.19	69.52	0.00	30.48
Average (all data)		**23.19**	**66.53**	**10.28**	**20.64**	**67.78**	**11.58**	**23.41**	**75.87**	**0.72**	**21.22**	**0.00**	**78.78**
Standard deviation (all data)		5.80	7.52	3.97	5.87	7.31	3.66	6.87	7.29	0.81	28.24	0.00	28.24

Grain parameters: Q=quartzose grains (monocrystalline quartz, chert, and polycrystalline quartz); F=feldspar grains (plagioclase and K-spar); L=lithic grains (sedimentary, volcanic, and metamorphic lithic grains); Qm=monocrystalline quartz; Lt=total lithic grains (chert; polycrystalline quartz; and sedimentary, volcanic, metamorphic lithic grains); Qp=polycrystalline quartz; P=plagioclase feldspar; K=potassium feldspar; Lv=volcanic lithic grains; Lm=metamorphic lithic grains; Ls=sedimentary lithic grains.

and transported southward. The mixing of Cenozoic volcanic detritus with Mesozoic granitic and metamorphic detritus produced a more feldspathic and volcanic lithic-rich petrofacies than found in sandstones from the lower part of the section (fig. 5). Sediment derivation from northern source terranes is consistent with southwestward-directed paleocurrent indicators (1,060 m on fig. 4) and regional textural data that record a southwestward reduction in grain size of Paleocene–Eocene strata from the Talkeetna Mountains to the upper Cook Inlet (Barnes, 1962; Kirschner and Lyon, 1973; Little, 1988; Winkler, 1992; J.M. Trop, unpublished data).

Available compositional data from Paleocene–Eocene forearc basin strata document substantial spatial variation in sandstone petrofacies. Compared to age-equivalent sandstones deposited along the southern margin of the forearc basin, sandstone petrofacies from the Arkose Ridge Formation are more quartzofeldspathic (QFL plot on fig. 5; Winkler, 1978). Sandstones deposited along the southern basin margin are interpreted to have been derived largely from the Chugach subduction complex on the basis of paleocurrent, lithologic, and compositional data (Little, 1988). Uplift and erosion of the subduction complex provided abundant sedimentary and metasedimentary lithic fragments and a paucity of feldspathic framework grains. In contrast, sediment deposited along the northern basin margin received abundant feldspathic detritus from the inactive Mesozoic and active Cenozoic magmatic arcs.

SEDIMENTOLOGY

The Arkose Ridge Formation has been mapped and described, but no detailed sedimentological data have been previously reported. On the basis of the general lithologies and absence of marine megafossils, previous workers interpret the strata as being deposited in nonmarine environments (Winkler, 1992). Measured stratigraphic sections, lithofacies analysis, maximum particle size data, and paleocurrent analysis from our study document three lithofacies successions that better define the depositional systems of the Arkose Ridge Formation. Each succession is described and interpreted below.

DESCRIPTION OF SUCCESSION 1

The lowermost 200 m of the Arkose Ridge Formation is characterized by clast-supported cobble and boulder conglomerate containing poorly sorted, subrounded to rounded clasts (figs. 4, 6C). Average maximum clast sizes range from 6 to 113 cm and progressively decrease upsection (fig. 4). Clasts as large as 360 cm are present locally. Lithofacies assemblages are dominated by amalgamated, massive to crudely bedded conglomerate packages that are 5–15 m thick and laterally continuous at the outcrop scale (10–50 m). Some conglomerate packages fine upwards into 2–5 m thick units of sandstone or, more rarely, mudstone. Sandstones are medium to thick bedded, are laterally persistent, and commonly exhibit medium-scale, planar cross-stratification. Mudstones, which constitute less than 20 percent of succession 1, are generally massive, carbonaceous, and rich in plant debris. Matrix-rich conglomerates, although rare, are also present in succession 1. The matrix-rich conglomerates are laterally continuous and 10–50 cm thick. Clasts in these conglomerates are more poorly sorted and more angular than clasts in the clast-supported conglomerates.

INTERPRETATION OF SUCCESSION 1

The coarse grain size, sedimentary structures, and upward-fining trends of succession 1 indicate that streamflow processes were important during deposition. In particular, lithofacies of this succession are characterized by textures and structures typical of deposits on modern proglacial outwash fans (Boothroyd and Ashley, 1975) and gravelly braided streams (Rust, 1977). We interpret succession 1 to represent deposition on gravelly bedload streams on an alluvial fan and/or alluvial braidplain. Organized conglomerate beds at the base of each fluvial sequence were likely deposited by downstream migration of longitudinal and transverse gravel bars (Nemec and Steel, 1984). Overlying sandstones are interpreted as being deposited in shallow channels and on emergent bars. Thin mudstone sequences record abandonment of gravelly streams and deposition in adjacent floodplain and paludal swamp environments. Rare matrix-rich conglomerates most likely represent debris flows based on the poor sorting, abundant matrix, and absence of internal organization and stratification (Johnson, 1965; Middleton and Hampton, 1976).

DESCRIPTION OF SUCCESSION 2

Overlying the coarse conglomeratic strata of succession 1 is a thick sequence of medium-bedded amalgamated sandstones with interbedded mudstone. Individual sandstone bodies are 0.6–2.0 m thick, lenticular over 10–20 m, and comprised of fine- to medium-grained sandstone (fig. 4). Although individual sandstone beds are lenticular, beds are highly amalgamated forming broad sandstone sheets (figs. 6D, E). Medium-scale planar, trough, and horizontal cross-stratification are common in the sandstones (fig. 6E). Basal scours have relief of ~0.25–0.80 m and commonly include fossilized tree branches and leaves. Succession 2 is characterized by 2–20 m thick upward-fining sequences (fig. 4). Typical sequences consist of

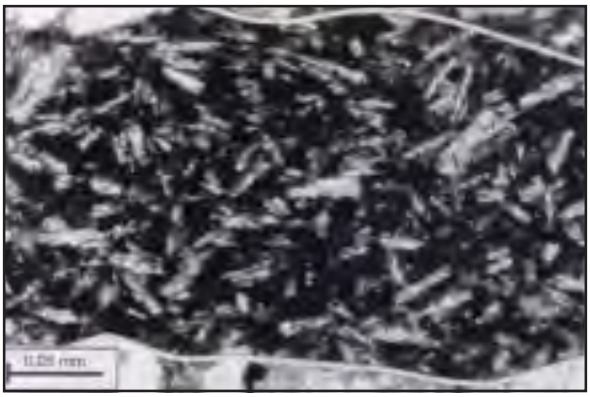

Figure 6A. *Photomicrograph of lathwork volcanic lithic fragment common in the upper part of the Arkose Ridge Formation. Grain boundary is outlined by white line.*

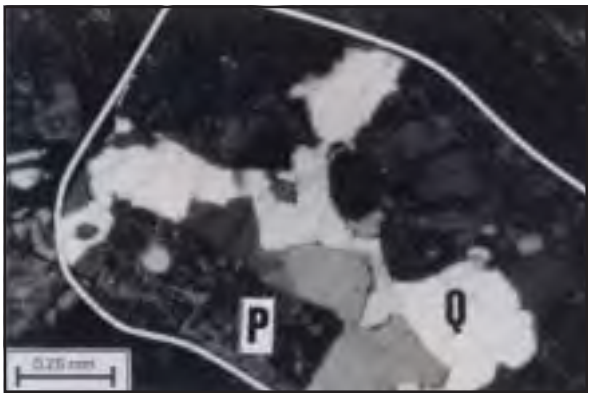

Figure 6B. *Photomicrograph of granitic rock fragment representative of igneous rock fragments throughout the Arkose Ridge Formation. Grain comprises plagioclase feldspar (P) and monocrystalline quartz (Q). Grain boundary is outlined by white line.*

Figure 6C. *Steeply dipping, boulder and cobble conglomerate deposits of succession 1. White line defines bedding. Note person for scale (arrow, upper right center).*

Figure 6D. *Sandstone and lava of succession 2. Exposure includes 20-m-thick lava unit that is outlined by arrows and is darker in color than the sandstone beds. Sandstones consist of highly amalgamated, broad, shallow channels. Exposure is approximately 250 m thick.*

Figure 6E. *Amalgamated sandstone channels typical of succession 2. Large black arrows outline the erosional base of one channel. Top of channel is dominated by trough cross-stratification (arrowhead). Bedding dips to left. Person (upper center) for scale.*

Figure 6F. *Ripple-laminated sandstone with clay drapes. Black arrows point toward a clay drape preserved on a ripple slip face. Note laminated sandstone and mudstone near hammer. Hammer (28 cm) for scale.*

massive to planar cross-stratified sandstones that grade upward into ripple-laminated, fine-grained sandstones which are capped by structureless to laminated mudstones with abundant plant fossil leaves. Mudstone beds are 0.2–10 m thick, structureless to laminated, and laterally persistent at the outcrop scale (10–50 m). Thin interbeds of carbonaceous shale and coal are also present.

Volcanic strata occur in the upper part of succession 2 and consist mostly of mafic lava flows (fig. 4). At Arkose Ridge, lava flows are 5–20 m thick, laterally continuous for 100–300 m, and interbedded with cross-stratified sandstone and mudstone (figs. 4, 6D). Although lava flows are common, pyroclastic volcanic rocks were not recognized at any of the three study sites.

INTERPRETATION OF SUCCESSION 2

Succession 2 is interpreted as being formed by streamflow and volcanic processes on an alluvial fan or braidplain. Evidence for fluvial deposition includes the presence of planar and trough cross-stratification, upward-fining packages, and lenticular bed geometries. The amalgamated sheetlike architecture of channel sandstones and the scale of individual sedimentary structures (25–50 cm high planar foresets) suggest that deposition occurred by migration of transverse and longitudinal sandbars in low-sinuosity braided streams generally less than 150 cm deep (Harms and others, 1982). The amalgamation of sandstone units is attributed to frequent switching of streams across an unconfined depositional surface whereas upward-fining cycles likely resulted from eventual abandonment of channels. Most mudstones were probably deposited by suspension fallout of fine-grained material during major flood events. The thickness and lateral continuity of interbedded volcanic rocks suggest that lava deposition occurred in both channel and interchannel regions of the alluvial fan or braidplain.

DESCRIPTION OF SUCCESSION 3

Succession 3 consists of channelized thin- to medium-bedded sandstone, laminated sandstone and shale, and massive carbonaceous shale. Large-scale, inclined heterolithic strata consisting of laminated siltstone and thin-bedded sandstone are preserved in succession 3. Clay-draped trough and ripple cross-stratification (fig. 6F), flaser bedding, wavy bedding, climbing ripples, and bioturbation are characteristic of succession 3. Plant megafossils are very abundant and exquisitely preserved, particularly in carbonaceous mudstones.

INTERPRETATION OF SUCCESSION 3

The intricate mixture of channelized sandstone and mudstone, in addition to the type, scale, and arrangement of sedimentary structures in succession 3 indicates deposition in a tidally influenced fluvial system (Clifton, 1982; Eisma, 1998), such as the upper reaches of an estuary. Sandstone deposition likely occurred by migration of tidal-fluvial point bars in upper estuary channels, whereas laterally continuous carbonaceous mudstones were deposited in nearby tidal-fluvial marshes and tidal flats. Flaser to wavy bedding and clay-draped sand ripples common throughout succession 3 suggest repeated fluctuations in current velocity, a depositional feature characteristic of tidal regimes (Eisma, 1998). Waxing and waning of current velocity and stand still of currents during high tide produce clay-draped ripples (Reineck and Singh, 1973). Inclined heterolithic strata are characteristic of deposits formed by sandy point bars in micro- to mesotidally influenced reaches of rivers (Smith, 1985; Thomas and others, 1987). Flow reversal indicators, such as herringbone cross-stratification, were not observed in the Arkose Ridge Formation. Almost all tidally influenced rivers, however, are ebb dominant (Barwis, 1978) and numerous workers have demonstrated that the preservation potential of flow reversal indicators in the more upstream reaches of tidally influenced rivers is low (for example, Dorjes and Howard, 1975). The relative abundance of preserved delicate plant-leaf fossils is probably a function of proximity to nearby vegetated terrestrial environments and high sedimentation rates in estuarine environments (Eisma, 1998).

PALEOGEOGRAPHY AND DEPOSITIONAL MODEL

New sedimentological and petrological data indicate that the Paleocene–Eocene Arkose Ridge Formation was deposited proximal to active volcanoes and uplifted plutonic segments of a Mesozoic magmatic arc along the northern margin of the Cook Inlet–Matanuska Valley forearc basin. Lithofacies, paleocurrent, and compositional data indicate that alluvial fan, fluvial, and estuarine depositional systems dispersed sediment southwestward, along the trend of the Paleocene–Eocene magmatic arc (fig. 7a). Three major lithofacies successions in the Arkose Ridge Formation record a transgressive sequence from gravel-rich alluvial fan and fluvial systems below to sandy, braided streams and tidally influenced, sinuous streams above (fig. 7a). The upsection change in depositional environments is attributed to a progressive relative rise in sea level during the Late Paleocene to Middle Eocene. Rising sea level prompted northward (arcward) onlap of finer-grained, tidally influenced deposystems across coarser-grained alluvial fan deposits and lava flows. The transgressive event recorded by the lithofacies of the Arkose Ridge Formation is coeval with global eustatic sea-level curves that illustrate first-order transgression during the Late Paleocene (60–55 Ma) and sea-level highstand during the Early Eocene (55–50 Ma; Haq and others, 1988). Additional extrinsic factors may have contributed to the relative rise in sea-level including variations in tectonic subsidence and sediment supply. A modern analog for our depositional model of the Arkose Ridge Formation is upper Cook Inlet (fig. 7b). Recent lava flows along the Aleutian arc are located within tens of kilometers of their eruptive centers and merge basinward with braided streams, tidally influenced streams, and tidal flats along the Cook Inlet estuary (Kienle and Nye, 1990; Magoon and others, 1976; fig. 7b).

CONCLUSIONS

Sandstone and conglomerate compositional data combined with southwestward-directed paleocurrent indicators suggest that detritus was derived mainly from local source terranes exposed directly north of the Castle Mountain fault system during deposition of the Paleocene–Eocene Arkose Ridge Formation. Compositional data reveal a lower petrofacies rich in metamorphic and granitic detritus and an upper petrofacies with higher proportions of volcanic detritus. Initially, metamorphic-rich detritus was eroded from the plutonic roots of an inactive Mesozoic magmatic arc, whereas erosion along an active Cenozoic magmatic arc provided detritus rich in volcanic lithic fragments during the later stages of sedimentation.

New sedimentological data demonstrate that alluvial fan, fluvial, and estuarine depositional systems deposited the Paleocene–Eocene Arkose Ridge Formation along the arcward margin of the Cook Inlet–Matanuska Valley forearc basin. Progressive upsection changes in sedimentary lithofacies reveal a transgressive

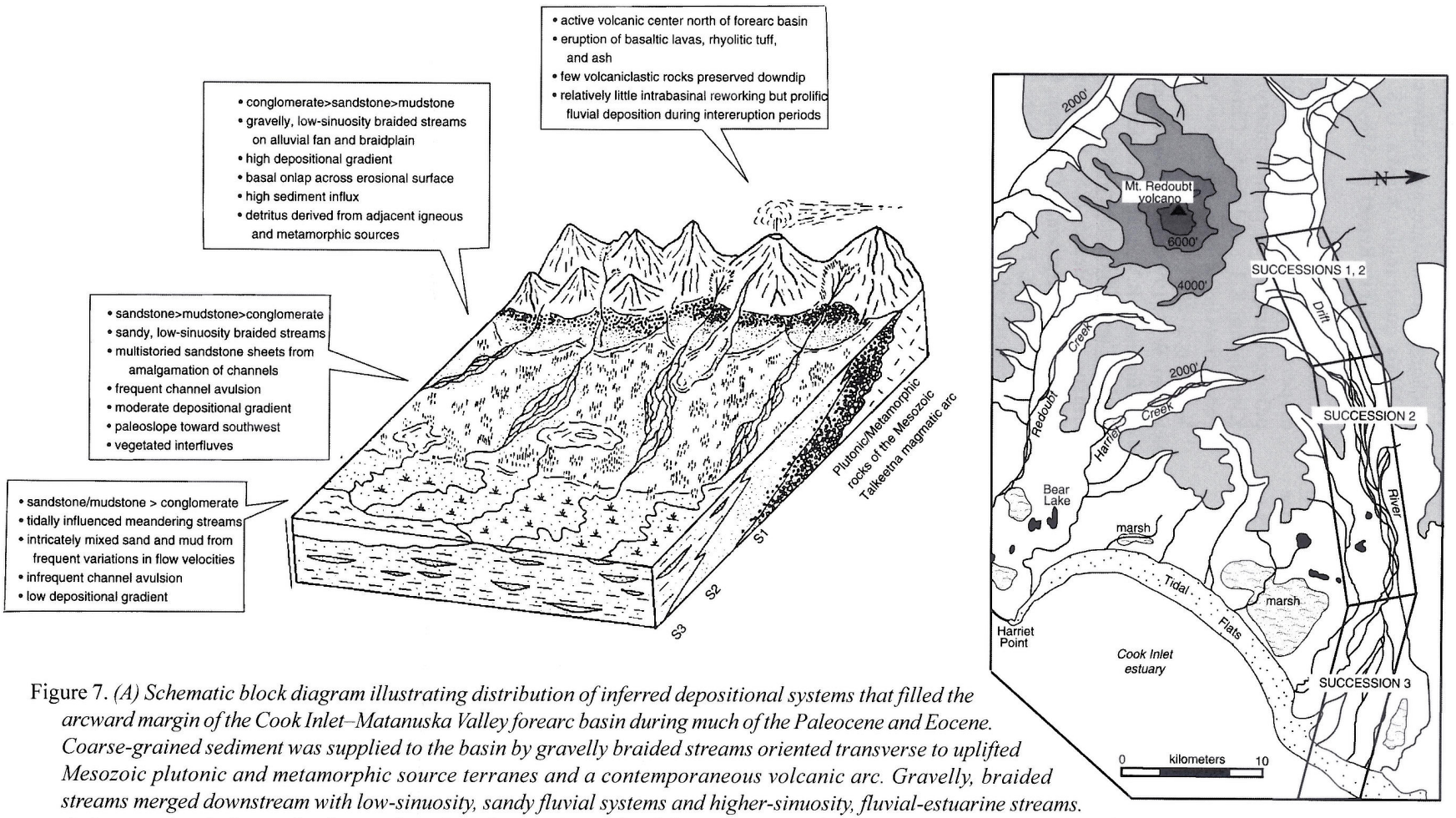

Figure 7. *(A) Schematic block diagram illustrating distribution of inferred depositional systems that filled the arcward margin of the Cook Inlet–Matanuska Valley forearc basin during much of the Paleocene and Eocene. Coarse-grained sediment was supplied to the basin by gravelly braided streams oriented transverse to uplifted Mesozoic plutonic and metamorphic source terranes and a contemporaneous volcanic arc. Gravelly, braided streams merged downstream with low-sinuosity, sandy fluvial systems and higher-sinuosity, fluvial-estuarine streams. An increase in relative sea level caused northward migration of distal deposystems, producing an overall retrogradational lithofacies succession. (B) Modified topographic map of the Kenai B-8 15-minute quadrangle showing modern depositional systems along the southeastern flank of Mt. Redoubt, an active volcano of the Aleutian magmatic arc. Location of map shown in figure 1. This modern setting may be analogous to the depositional environments of the Paleocene–Eocene Arkose Ridge Formation. Braided streams drain the flanks of the calc-alkaline basaltic stratovolcano and merge downstream into progressively finer-grained and more sinuous, tidally influenced streams adjacent to the Cook Inlet estuary. The inferred positions of major lithofacies successions documented in the Arkose Ridge Formation are outlined by rectangles representing succession 1 (S1), succession 2 (S2), and succession 3 (S3).*

depositional sequence from gravel-rich, alluvial fan systems to sandy, braided streams to tidally influenced, sinuous streams. An increase in relative sea level during the Late Paleocene to Middle Eocene resulted in northward onlap of tidally influenced deposystems toward the basin margin and increased preservation of fine-grained sediment. Interbedded volcanic flows in the upper part of the formation indicate relative proximity to active volcanic centers during deposition.

ACKNOWLEDGMENTS

This research was supported by the Donors of the Petroleum Research Fund, administered by the American Chemical Society. The Purdue Research Foundation; the Geological Society of America; and the American Association of Petroleum Geologists provided partial funding. We thank A. Grantz, G. Winkler, and W. Nokleberg for useful discussions on the geology of the Talkeetna Mountains and G. Winkler and D. LePain for critical reviews of the manuscript.

REFERENCES

Barnes, F.F., 1962, Geologic map of the lower Matanuska Valley, Alaska: U.S. Geological Survey Miscellaneous Geologic Investigations Map I–359, scale 1:63,360.

Barwis, J.H., 1978, Sedimentology of some South Carolina tidal-creek point bars, and a comparison with their fluvial counterparts, *in* Miall, A.D., ed., Fluvial Sedimentology: Canadian Society of Petroleum Geologists, Memoir 5, p. 129–160.

Boothroyd, J.C., and Ashley, G.M., 1975, Processes, bar morphology, and sedimentary structures on braided outwash fans, northeastern Gulf of Alaska, *in* Jopling, A.V., and McDonald, B.C., eds., Glaciofluvial and Glaciolacustrine Sedimentation: Society of Economic Paleontologists and Mineralogists, Special Publication 23, p. 193–222.

Busby-Spera, C.J., 1986, Sedimentation and subsidence styles in a Cretaceous forearc basin, southern Vizcaino Peninsula, Baja California, Mexico, *in* Abbott, P.L., ed., Cretaceous stratigraphy of western North America, Society of Economic Paleontologists and Mineralogists, Field Trip Guidebook 46, p. 79–90.

Clifton, H.E., 1982, Estuarine deposits, *in* Scholl, P.A., and Spearing, D.R., eds., Sandstone Depositional Environments: American Association of Petroleum Geologists, Memoir 31, p. 179–184.

Csejtey, Bela, Jr., Nelson, W.H., Jones, D.L., Silberling, N.J., Dean, R.M., Morris, M.S., Lanphere, M.A., Smith, J.G., and Silberman, M.L., 1978, Reconnaissance geologic map and geochronology, Talkeetna Mountains quadrangle, northern part of Anchorage quadrangle, and southwestern corner of Healy quadrangle, Alaska: U.S. Geological Survey Open-File Report 78–558-A, 62 p., 1 sheet, scale 1:250,000.

Dickinson, W.R., 1988, Provenance and sediment dispersal in relation to paleotectonics and paleogeography of sedimentary basins, *in* Kleinspehn, K.L., and Paola, Chris, eds., New Perspectives in Basin Analysis: New York, Springer-Verlag, p. 3–25.

Dickinson, W.R., 1995, Forearc basins, in Busby, C.J., and Ingersoll, R.V., eds., Tectonics of Sedimentary Basins, Cambridge, Blackwell Science, p. 221–262.

Dickinson, W.R., Beard, L.S., Brakenridge, G.R., Erjavec, J.L., Ferguson, R.C., Inman, K.F., Knepp, R.A., Lindberg, F.A., and Ryberg, P.T., 1983, Provenance of North American Phanerozoic sandstones in relation to tectonic setting: Geological Society of America, Bulletin, v. 94, p. 222–235.

Dorjes, Jurgen, and Howard, J.D., 1975, Fluvial-marine transition indicators in an estuarine environment, Ogeechee River–Ossabaw Sound, *in* Estuaries of the Georgia coast, U.S.A., sedimentology and biology: Senckenbergiana Maritima 7, p. 137–179.

Eisma, D, 1998, Intertidal Deposits: River mouths, tidal flats, and coastal lagoons, with contributions by P.L. Boer, G.C. Cadee, K. Dikema, H. Ridderinkhof, and C. Philippart, CRC Press, Boca Raton, Florida, 525 p.

Engebretson, D.C., Cox, Allan, and Gordon, R.G., 1983, Relative motions between oceanic and continental plates in the Pacific basin, *in* Howell, D.G., Jones, D.L., Cox, A., and Nur, A.M., eds., Proceedings of the Circum-Pacific terrane conference, Stanford, California: Stanford University Publications, Geological Sciences, v. 18, p. 80–82.

Fisher, M.A., and Magoon, L.B., 1978, Geologic framework of lower Cook Inlet, Alaska: American Association of Petroleum Geologists Bulletin, v. 62, p. 373–402.

Fuchs, W.A., 1980, Tertiary tectonic history of the Castle Mountain–Caribou fault system in the Talkeetna Mountains, Alaska, Salt Lake City, Utah: University of Utah, Ph.D. thesis, 152 p.

Fulford, M.M., and Busby, C.J., 1993, Tectonic controls on non-marine sedimentation in a Cretaceous forearc basin, Baja California, Mexico, *in* Frostick, L.E, and Steel, R.J., eds., Tectonic controls and signatures in sedimentary successions, Special Publication of the International Association of Sedimentologists, v. 20, p. 301–333.

Grantz, Arthur, 1966, Strike-slip faults in Alaska: U.S. Geological Survey Open-File Report 66–53. 82 p.

Haq, B.U., Hardenbol, Jan, and Vail, P.R., 1988, Mesozoic and Cenozoic chronostratigraphy and cycles of sea-level change, *in* Wilgus, C.K., Hastings, B.S., Ross, C.A., Posamentier, H.W., Van Wagoner, John, Ross, C.A., and Kendall, C.G. St. C., Sea-Level Changes: An Integrated Approach: Society of Economic Paleontologists and Mineralogists Special Publication No. 42, p. 78–108.

Harms, J.C., Southard, J.B., and Walker, R.G., 1982, Structure and sequences in clastic rocks: Society of Economic Paleontologists and Mineralogists, Short Course No. 9, p. 3-1-3-51.

Heller, P.L., and Dickinson, W.R., 1985, Submarine ramp facies model for delta-fed, sand-rich turbidite systems: American Association of Petroleum Geologists Bulletin, v. 69, p. 960–976.

Ingersoll, R.V., 1979, Evolution of the Late Cretaceous forearc basin, northern and central California: Geological Society of America Bulletin, v. 90, p. 813–826.

Ingersoll, R.V., Bullard, T.F., Ford, R.L., Grimm, J.P., Pickle, J.D., and Sares, S.W., 1984, The effect of grain size on detrital modes: A test of the Gazzi-Dickinson point-counting method: Journal of Sedimentary Petrology, v. 54, p. 103–116.

Johnson, A.M., 1965, A model for debris flow: University Park, PA, Ph.D. thesis, Pennsylvania State University.

Kienle, Juergen, and Nye, C.J., 1990, Volcanoes of Alaska, *in* Wood, C.A., and Kienle, Juergen, eds., Volcanoes of North America: Cambridge, MA, p. 8–110.

Kirschner, C.E., and Lyon, C.A., 1973, Stratigraphic and tectonic development of Cook Inlet Petroleum Province, *in* Pitcher, M.G., ed., Arctic Geology: American Association of Petroleum Geologists, Memoir 19, p. 396–407.

Kuenzi, W.D., Horst, O.H., and McGehee, R.V., 1979, Effect of volcanic activity on fluvial-deltaic sedimentation in a modern arc-trench gap, southwestern Guatemala: Geological Society of America Bulletin, v. 90, p. 827–838.

Little, T.A., 1988, Tertiary tectonics of the Border Ranges fault system, north-central Chugach Mountains, Alaska—Sedimentation, deformation, and uplift along the inboard edge of a subduction complex: Stanford, CA, Stanford University, Ph.D. thesis, 565 p.

Little, T. A., 1990, Kinematics of wrench and divergent-wrench deformation along a central part of the Border Ranges fault system, northern Chugach Mountains, Alaska: Tectonics, v. 9, p. 585–611.

MacKevett, E.M., Jr., and Plafker, George, 1974, The Border Ranges fault in south-central Alaska: U.S. Geological Survey Journal of Research, v. 2, p. 323–329.

Madden-McGuire, D.J, Silberman, M.L., and Church, S.E., 1990, Geologic relationships, K-Ar ages, and isotopic data from the Willow Creek gold mining district, southern Alaska, *in* Keays, R.R., Ramsey, W.H.R., and Groves, D.I., eds., Geology of gold deposits—The prospective in 1988: Economic Geology, Monograph 6, p. 242–251.

Magoon, L.B., Adkison, W.L, and Egbert, R.M., 1976, Map showing geology, wildcat wells, Tertiary plant fossil localities, K-Ar age dates, and petroleum operations, Cook Inlet area, Alaska: U.S. Geological Survey Miscellaneous Investigations Map I–1019, 3 sheets, scale 1:250,000.

Marsaglia, K.M., and Ingersoll, R.V., 1992, Compositional trends in arc-related, deep-marine sand and sandstone: A reassessment of magmatic-arc provenance: Geological Society of America Bulletin, v. 104, p. 1637–1649.

Martin, G.C., and Katz, F.J., 1912, Geology and coal fields of the lower Matanuska Valley, Alaska: U.S. Geological Survey Bulletin 500, 98 p.

Miall, A.D., 1978, Lithofacies types and vertical profile models in braided river deposits: a summary, *in* Miall, A.D., ed., Fluvial Sedimentology: Canadian Society of Petroleum Geologists, Memoir 5, p. 597–604.

Middleton, G.V., and Hampton, M.A., 1976, Subaqueous sediment transport and deposition by sediment gravity flows, *in* Stanley, D.J., and Swift, D.J.P., eds., Marine Sediment Transport and Environmental Management: New York, Wiley, p. 197–218.

Morris, W.R., and Busby-Spera, C.J., 1988, Sedimentologic evolution of a submarine canyon in a forearc basin, Upper Cretaceous Rosario Formation, San Carlos, Mexico: American Association of Petroleum Geologists Bulletin, v. 72, p. 717–737.

Morris, W.R., Smith, D.P., and Busby-Spera, C.J., 1989, Deep marine conglomerate facies and processes in Cretaceous forearc basins of Baja California, Mexico, *in* Colburn, I.P., Abbott, P.L., and Minch, John, eds., Conglomerates in basin analysis: A symposium dedicated to A.O. Woodford: Society of Economic Paleontologists and Mineralogists, Pacific Section, v. 62, p. 123–142.

Nemec, W., and Steel, R.J., 1984, Alluvial and coastal conglomerates: Their significant features and some comments on gravelly mass-flow deposits, *in* Koster, E.H., and Steel, R.J., eds., Sedimentology of gravels and conglomerates: Canadian Society of Petroleum Geologists, Memoir 10, p. 1–31.

Oil and Gas Journal, 1998, Independents lead resurgence of drilling in Alaska's Cook Inlet, v. 96, p. 27–29.

Pavlis, T.L., and Crouse, G.W., 1989, Late Mesozoic strike slip movement on the Border Ranges fault system in the eastern Chugach Mountains, southern Alaska, *in* Page, R.A., ed., Special section on northern Chugach Mountains–southern Copper River basin segment of the Alaskan Transect; Part I: Journal of Geophysical Research, B, Solid Earth and Planets, v. 94, p. 4321–4332.

Plafker, George, Jones, D.L, and Pessagno, E.A., Jr., 1977, A Cretaceous accretionary flysch and melange terrane along the Gulf of Alaska margin, *in* Blean, K.M, The United States Geological Survey in Alaska—Accomplishments during 1976: U.S. Geological Survey Circular 751-B, p. B41–B43.

Plafker, George, and Berg, H.C., 1994, Overview of the geology and tectonic evolution of Alaska, *in* Plafker, George, and Berg, H.G., The Geology of Alaska: The Geology of North America, v. G–1, p. 989–1021.

Reineck, H.E., and Singh, I.B., 1973, Depositional Sedimentary Environments, New York, Springer-Verlag, 439 p.

Rust, B.R., 1977, Depositional models for braided alluvium, *in* Miall, A.D., ed., Fluvial Sedimentology, Canadian Society of Petroleum Geologists Memoir 5, p. 605–625.

Silberman, M.L., and Grantz, Arthur, 1984, Paleogene volcanic rocks of the Matanuska Valley area and the displacement history of the Castle Mountain fault, *in* Coonrad, W.L., and Elliot, R.L., eds., The United States Geological Survey in Alaska - Accomplishments during 1981: U.S. Geological Survey Circular 868, p. 82–86.

Silberman, M.L., O'Leary, R.M., Csejtey, Bela, Jr., Smith, J.G., and Connor, C.L., 1978, Geochemical anomalies and isotopic ages in the Willow Creek mining district, southwestern Talkeetna Mountains, Alaska: U.S. Geological Survey Open-File Report 78–223, 33 p.

Smith, D.G., 1985, Modern analogs of the McMurray Formation channel deposits, sedimentology of mesotidal-influenced meandering point bars with inclined beds of alternating mud and sand: Alberta Oil Sands Technology and Research Authority, Final Report for Research Project No. 391, 78 p.

Thomas, R.G., Smith, D.G., Wood, J.M., Visser, J., Calverley-Range, E.A., and Koster, E.H., 1987, Inclined heterolithic stratification—terminology, description, interpretation, and significance: Sedimentary Geology, v. 53, p. 123–179.

Triplehorn, D.M., Turner, D.L., and Naeser, C.W., 1984, Radiometric age of the Chickaloon Formation of south-central Alaska—Location of the Paleocene–Eocene boundary: Geological Society of America Bulletin, v. 95, p. 740–742.

Vessel, R.K., and Davies, D.K., 1981, Nonmarine sedimentation in an active forearc basin: Special Publication of the Society of Economic Paleontologists and Mineralogists, no. 31, p. 31–45.

Winkler, G.R., 1978, Framework grain mineralogy and provenance of sandstones from the Arkose Ridge and Chickaloon Formations, Matanuska Valley, *in* Johnson, K.M., ed., The United States Geological Survey in Alaska - Accomplishments during 1977: U.S. Geological Survey Circular 772-B, p. B70–B73.

Winkler, G.R., 1992, Geologic map and summary geochronology of the Anchorage 1x3 degree quadrangle, southern Alaska: U.S. Geological Survey Miscellaneous Investigations Series Map I–2283, 1 sheet.

Wolfe, J.A., Hopkins, D.M., and Leopold, E.B., 1966, Tertiary stratigraphy and paleobotany of the Cook Inlet region, Alaska: U.S. Geological Survey Professional Paper 398-A, p. A1–A29.

LATE DEVONIAN (LATE FAMENNIAN) RADIOLARIANS FROM THE CHULITNA TERRANE, SOUTH-CENTRAL ALASKA

Mun-Zu Won,[1] Robert B. Blodgett,[2] Karen H. Clautice,[3] and Rainer J. Newberry[4]

ABSTRACT

A late Famennian radiolarian fauna of generally poor (rarely moderate) preservation was extracted from cherts of the "Do" unit in the Chulitna terrane, south-central Alaska. Because of the generally poor state of preservation, this faunal assemblage exhibits both low diversity and low abundance. It contains 13 genera and 20 species. Three species are new: *Palaeoscenidium chulitnaensis*, *Palaeoscenidium planum*, and *Popofskyellum? tetralongispina*. Among the radiolarian species, *Holoeciscus foremanae*, the two new species of *Palaeoscenidium*, and the presence of the species *Ceratoikiscum mirum* indicate that the Do unit radiolarian fauna is of late Famennian age. The faunal composition of the Chulitna terrane is similar to that of late Famennian radiolarian faunas from the Woodford Formation in the Ouachita Mountains of Oklahoma and Arkansas, as well as the Arbuckle Mountains and Criner Hills of Oklahoma. Outside of North America, the Chulitna fauna is similar to that from the Frankenwald, Bavaria, and from the siliceous boulder fauna of the lower Main valley near Frankfurt/Main, Germany (source area: Frankenwald).

INTRODUCTION

The Chulitna terrane, originally defined by Jones and others (1980), has had a significant role in the development of accretionary terrane models of Alaska. Both geologic and paleontologic evidence was marshaled to indicate that some of the rocks originated far to the south of their present location. Despite the prominent position that fossil biota of this terrane have held as evidence of large-scale displacement, most aspects of fossil faunas and floras of this terrane remain unknown (Blodgett and Clautice, 1998).

Chert-rich intervals are common in various positions in the Chulitna terrane stratigraphy. C.D. Blome (in Jones and others, 1980, pl. 2) illustrated Upper Jurassic radiolarians from the argillite, chert, and sandstone unit of the adjacent West Fork terrane. Radiolarians were also noted by E.A. Pessagno, Jr. (in Jones and others, 1980, p. A9) from the argillite, sandstone, and chert unit in the Chulitna terrane. Faunal lists were provided for two separate localities in this unit. One locality was identified as being of Callovian to early Tithonian (Late Jurassic) age and the other of late Valanginian (Early Cretaceous) age. The oldest radiolarian faunas from the Chulitna terrane are of Famennian (late Late Devonian) age, and these were reported from red cherts within the Do unit of Jones and others (1980, p. A3–A4; pl. 1). These authors noted that nine localities in the unit were of Famennian age. However, their report did not provide illustrations or taxonomic descriptions of the radiolarians.

In this paper we present the first illustrations and descriptions of elements of the Famennian radiolarian fauna from the Chulitna terrane.

Late Famennian faunas are fairly well known and reported (Cheng, 1986; Schmidt-Effing, 1988; Braun, 1990; Schwartzapfel and Holdsworth, 1996). However, in these reports, species of some late Famennian radiolarian assemblages were selectively described or misidentified. Therefore, some of those species need to be described and/or revised.

LOCALITY REGISTER

Cherts were collected from many localities in the Do unit of Chulitna terrane in the summer of 1997 by members of the Alaska Division of Geological & Geophysical Surveys field mapping party. Late Devonian radiolarians were recovered by Won from 12 localities and, from those, four localities (fig. 1) yielded specimens that are described in this paper. The initials RB, RN, and HA refer to the collectors, R.B. Blodgett, R.J. Newberry, and E.E. Harris, respectively. All illustrated material and types (abbreviation CH) are retained by Won, Pusan National University, Pusan, Republic of Korea.

[1]Department of Marine Science, Natural Science College, Pusan National University, Pusan, Republic of Korea 609-735.
Email for Mun-Zu Won: mzwon@hyowon.cc.pusan.ac.kr
[2]Departments of Zoology and Geosciences, Oregon State University, Corvallis, Oregon 97331.
[3]Alaska Division of Geological & Geophysical Surveys, 794 University Avenue, Suite 200, Fairbanks, Alaska 99709-3645.
[4]Department of Geology and Geophysics, University of Alaska Fairbanks, P.O. Box 755780, Fairbanks, Alaska 99775-5780.

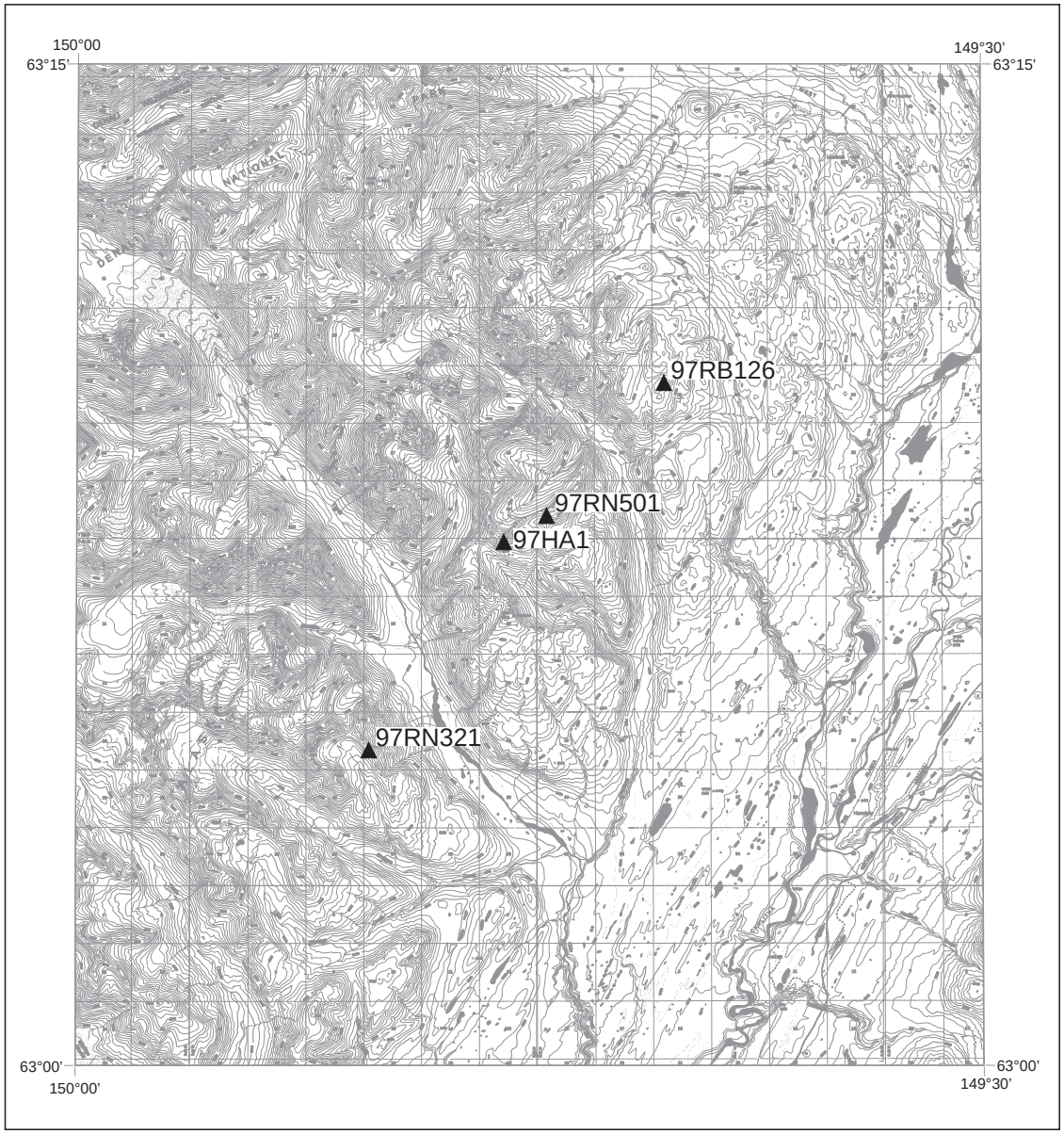

Figure 1. *Index map showing location of fossil localities yielding Famennian radiolarians in the Chulitna terrane, Healy A-6 Quadrangle. Numbered squares are sections, one mile square.*

- 97RB126: Varicolored chert (green, maroon, gray, or light brown) collected from rubble and small outcrop on northwest side of small hill atop mesa in NE¼ SW¼ NW¼ sec. 21, T. 20 S., R. 11 W., Healy A-6 Quadrangle. Lat. 63°10.2' N., Long. 149°40.6' W.
- 97RN321: Red and green chert beds exposed atop small hill along southeast-trending ridge crest in SW¼ NW¼ SW¼ sec. 22, T. 21 S., R. 12 W., Healy A-6 Quadrangle. Lat. 63°04.7' N., Long. 149°50.4' W.
- 97RN501: Chert beds 1 to 3 cm thick with shaly partings. These banded cherts underlie massive sandy tuff exposed on the south side of ridge (at an elevation of about 4,700 ft) in NE¼ NW¼ SW¼ sec. 31, T. 20 S., R. 11 W., Healy A-6 Quadrangle. Lat. 63°08.3' N., Long.149°44.4' W.
- 97HA1: Massive or brecciated maroon chert and greenstone exposed on southeast side of hill in NE¼ NE¼ NW¼ sec. 1, T. 21 S., R. 12 W., Healy A-6 Quadrangle. Lat. 63°07.9' N., Long. 149°45.7' W.

BIOSTRATIGRAPHIC RANGE, CHARACTERISTICS, AND COMPOSITION OF THE RADIOLARIAN ASSEMBLAGE

The Famennian radiolarian assemblage of the Chulitna terrane is low both in diversity and abundance, and many of the specimens have robust skeletons. Late Famennian radiolarian assemblages having a diverse species composition are well known from the Woodford Formation of the Ouachita Mountains of Oklahoma and Arkansas (Cheng, 1986) and from the Arbuckle Mountains and Criner Hills of Oklahoma (Schwartzapfel and Holdsworth, 1996). Late Devonian assemblages of low diversity are also known from the Frankenwald (Schmidt-Effing, 1988) and boulders from the lower Main valley near Frankfurt/Main in Germany (Braun, 1990).

The Chulitna fauna yields *Holoeciscus foremanae* Cheng 1986, *Entactinia variospina* Won 1983, *Plenospongiosa? gourmelonae* Won 1998, *Archocyrtium venustum* Cheng 1986, *Archocyrtium reideli* Deflandre 1972, *Entactinosphaera? palimbola* Foreman 1963, *Popofskyellum? tetralongispina* n. sp., *Palaeoscenidium chulitnaensis* n. sp., *Palaeoscenidium planum* n. sp., *Ceratoikiscum mirum* Cheng 1986, *Ceratoikiscum* sp. cf. *C. sandbergi* Cheng 1986, *Palaeoscenidium* sp., *Entactinia* sp., *Popofskyellum?* sp., *Pylentonema* sp., *Cyrtentactinia?* sp., *Totollum?* sp., *Tetrentactinia?* sp., and *Retentactinia?* sp.

Comments on the general nature of the radiolarian fauna of the Do unit were provided by B.K. Holdsworth, who reported that the fauna included *Entactinosphaera aitpaiensis* Nazarov 1975 and a new species of *Holoeciscus* Foreman 1963, a genus known only from rocks of Famennian age (Jones and others, 1980, p. A4). He assigned the fauna a Famennian age. The new *Holoeciscus* was later named as *Holoeciscus foremanae* by Cheng (1986); it was found in the late Famennian Woodford Formation.

Among the elements of the Chulitna fauna, species of *Entactinia*, *Plenospongiosa? gourmelonae,* and species of *Archocyrtium* are long ranging, extending from the Late Devonian into the Early Carboniferous. *Entactinia variospina* has been reported in rocks as old as the *A. pseudoparadoxa* Zone (Won 1991, 1998) of Early Carboniferous (Tournaisian) in Europe. It also occurs in the late Famennian faunas of east-central Alaska.

From the Chulitna fauna, *Palaeoscenidium planum, Palaeoscenidium chulitnaensis, Holoeciscus foremanae,* and species of *Ceratoikiscum* and *Pylentonema* can be used for determining the stratigraphic range of the fauna. According to observations by Won, one of the newly established species, *Palaeoscenidium planum* n. sp., occurs in the Woodford Formation, Oklahoma, but because of selective treatment of the faunal elements in earlier reports, the species was not previously described. Specimens of *Palaeoscenidium chulitnaensis* n. sp. were first reported by Braun (1990) from the Kieselschiefer-Geröllen fauna, even though he identified this species as *P. cladophorum*. *P. chulitnaensis* n. sp. does not occur in the Woodford Formation but it is present in east-central Alaska together with *P. planum* n. sp. and *H. foremanae*. Species of *Ceratoikiscum* cannot be confidently identified due to poor preservation in the Chulitna fauna. However, one of them most likely belongs to *C. mirum,* and another species is more similar to specimens of *C. sandbergi* identified by Schwartzapfel and Holdsworth (1996) than to those identified by Cheng (1986). *C. sandbergi* itself was established by Cheng (1986) on the basis of poorly preserved specimens and later redefined by Schwartzapfel and Holdsworth (1996). However, it is unclear whether these authors were studying the same species because there are several types (species) with well-developed caveal ribs bearing a distinct rib spine developed near the distal end of each rib, which is one of the diagnostic characteristics of *C. sandbergi*. These types (species) show phylogenetic changes with time in unreported faunas from east-central Alaska. A species of *Pylentonema* with spines arranged as they are in *Quadrapesus* Cheng 1986 was recovered in the Chulitna fauna. The genus *Quadrapesus* is a synonym of *Pylentonema,* because, as Won (1998) has documented, the different position of the spines cannot be a critical criterion at genus-level classifications.

The composition of the fauna discussed in this paper is similar to that of the Kieselschiefer-Geröllen fauna (Braun, 1990) in boulders from the Rhine River valley, Germany. Braun (1990) concluded that there is no possibility that his fauna belongs to the Carboniferous there because the co-occurring conodont, *Bispathodus stabilis,* is known to be limited to Upper Devonian strata. He assigned the fauna to the *Holoeciscus*-2 Zone because of the presence *of Holoeciscus foremanae* and absence of *Pylentonema,* citing the report of Cheng (1986), who stated that *Pylentonema* first occurs at the base of the *Holoeciscus*-3 Assemblage Zone. The Chulitna fauna contains *Pylentonema*. Thus, this fauna is not older than *Holoeciscus*-3 Assemblage or the base of the *Pylentonema* spp.–*Staurentactinia* spp. Interval Zone (Zone I) established by Schwartzapfel and Holdsworth (1996). However, we cannot conclude that the Chulitna fauna is younger than the Kieselschiefer-Geröllen fauna because of the presence of the genus *Pylentonema* in Chulitna fauna and its absence in latter fauna. The absence of a species cannot be critical for determining stratigraphic age, particularly when we consider that some faunas of any age are not well preserved or are of low diversity.

The species composition of the Chulitna fauna described here is also similar to that of Woodford Formation faunas reported by Cheng (1986) and Schwartzapfel and Holdsworth (1996), and of the unreported faunas from east-central Alaska. Schwartzapfel and Holdsworth (1996) reported that *Holoeciscus foremanae* occurs in the Woodford Formation faunas from the *Pylentonema* spp.–*Staurentactinia* spp. Zone (Zone I) to the *Protoalbaillella deflandrei–Holoeciscus* spp. Zone (Zone IV). Schwartzapfel and Holdsworth (1996) stated that the last appearance datum of *Ceratoikiscum sandbergi* is near the top of the *Lapidopiscum* spp.–*Protoalbaillella deflandrei* Zone (Zone III). According to Cheng (1986) *C. mirum* occurs in three strata in the Woodford Formation ranging from the *Lapidopiscum* spp.–*Protoalbaillella deflandrei* Zone (Zone III) to the middle of the *Protoalbaillella deflandrei–Holoeciscus* spp. Zone (Zone IV) of Schwartzapfel and Holdsworth (1996). In contrast to this, Schwartzapfel and Holdsworth (1996) stated that the species occurs from the *Staurentactinia* spp.–*Lapidopiscum* spp. Zone (Zone II) to the *Lapidopiscum* spp.–*Protoalbaillella deflandrei* Zone (Zone III). According to Cheng (1986), the first appearance datum of *Archeocyrtium venustum* and *Archeocyrtium riedeli* is from the *Lapidopiscum* spp.–*Protoalbaillella deflandrei* Zone (Zone III) established by Schwartzapfel and Holdsworth (1966). According to Won's observations of Woodford Formation faunas, the last appearance datum of the *Palaeoscenidium planum* n. sp. is the same as that of *Holoeciscus foremanae* in the Woodford Formation. In unreported late Famennian to early Carboniferous faunas from east-central Alaska, *Plenoentactinia? gourmelone* occurs in faunas equivalent to the *Lapidopiscum* spp.–*Protoalbaillella deflandrei* Zone (Zone III) fauna established by Schwartzapfel and Holdsworth (1996). The last appearance datum of *Entactinosphaera? palimbora* is the middle of Zone III. Consequently, the stratigraphic range of the Chulitna fauna belongs to the *Lapidopiscum* spp.–*Protoalbaillella deflandrei* Zone (Zone III). According to Schwartzapfel and Holdsworth the chronostratigraphic placement of Zone III is uppermost upper Famennian.

Taxonomic descriptions in this paper are limited to the new species.

SYSTEMATIC PALEONTOLOGY

Family Popofskyellumidae Deflandre 1964

Genus *Popofskyellum* Deflandre 1964

Remarks: Cheng (1986) established a new genus, *Kantollum*, whose test is strongly or weakly lobulate and has four or more lobes with strictures at joints. He stated that this genus differs from *Popofskyellum* by the lack of opposed lateral rods. Later, Schwartzapfel and Holdsworth (1996) established a new genus, *Totollum*, most of whose species were once placed under the emended genus *Popofskyellum* by Cheng. *Totollum* is defined as having two subapical horns and two lateral rods, and the genus *Popofskyellum* was re-emended by Schwartzapfel and Holdsworth. In reality, there are species whose characteristics do not match any of these three genera but are intermediate. Thus, more research is needed to correctly relate these genera.

Popofskyellum? tetralongispina Won n. sp.
Figures 2.1-2.3

Derivation of name: tetra (Lat.), four; longus (Lat.), long; spina (Lat.), spine

Holotype: CH554 from locality 97RB126

Diagnosis: A skeleton consisting of a smooth, bell-shaped to conical shell with hexagonal meshwork; four thick and long spines around the apical area. No lateral rods, wings, or rings present.

Description: The skeleton is hexagonally latticed, but the apical area from which the four stout spines arise seems to be unperforated. The skeleton is bell-shaped or somewhat conical and smooth, without undulations or segments. The shape of the hexagonal meshwork can be somewhat compressed in the direction of the long axis, and the mesh is relatively coarse in comparison to that of other species of this genus. There are no lateral rods, lateral wings, or rings. One spine is apical, and the other three are lateral on the apical area. The length and thickness of the spines are similar.

Remarks: This species has no lateral rods and so cannot belong to *Popofskyellum*, according to the emendation by Cheng (1986) or by Schwartzapfel and Holdsworth (1996). They all stated that the genus has no lateral rods. However, this species cannot belong to *Kantollum* (Cheng, 1986) having no lateral rods, because *Kantollum*, in Cheng's definition, is also characterized as being strongly or weakly lobulate with four or more lobes with strictures at joints. In contrast, *P. tetralongispina* n. sp. has a perfectly smooth shell wall. Some specimens of *Kantollum* species, e.g., *K. undulatum* (Cheng, 1986, pl. 1, figs. 8, 13; Schwartzapfel and Holdsworth, 1996, pl. 3, figs. 2, 4, 13), have clear traces of lateral rods. Also a species with two apical horns, which is one of the most characteristic and diagnostic features of *Totollum* (Schwartzapfel and Holdsworth, 1996), has no lateral rods [for example, *Totollum?* sp. cf. *T. deflandrei* (Cheng): Schwartzapfel and Holdsworth 1996, pl. 5, figs. 3, 4], even though *Totollum* is defined as having lateral rods.

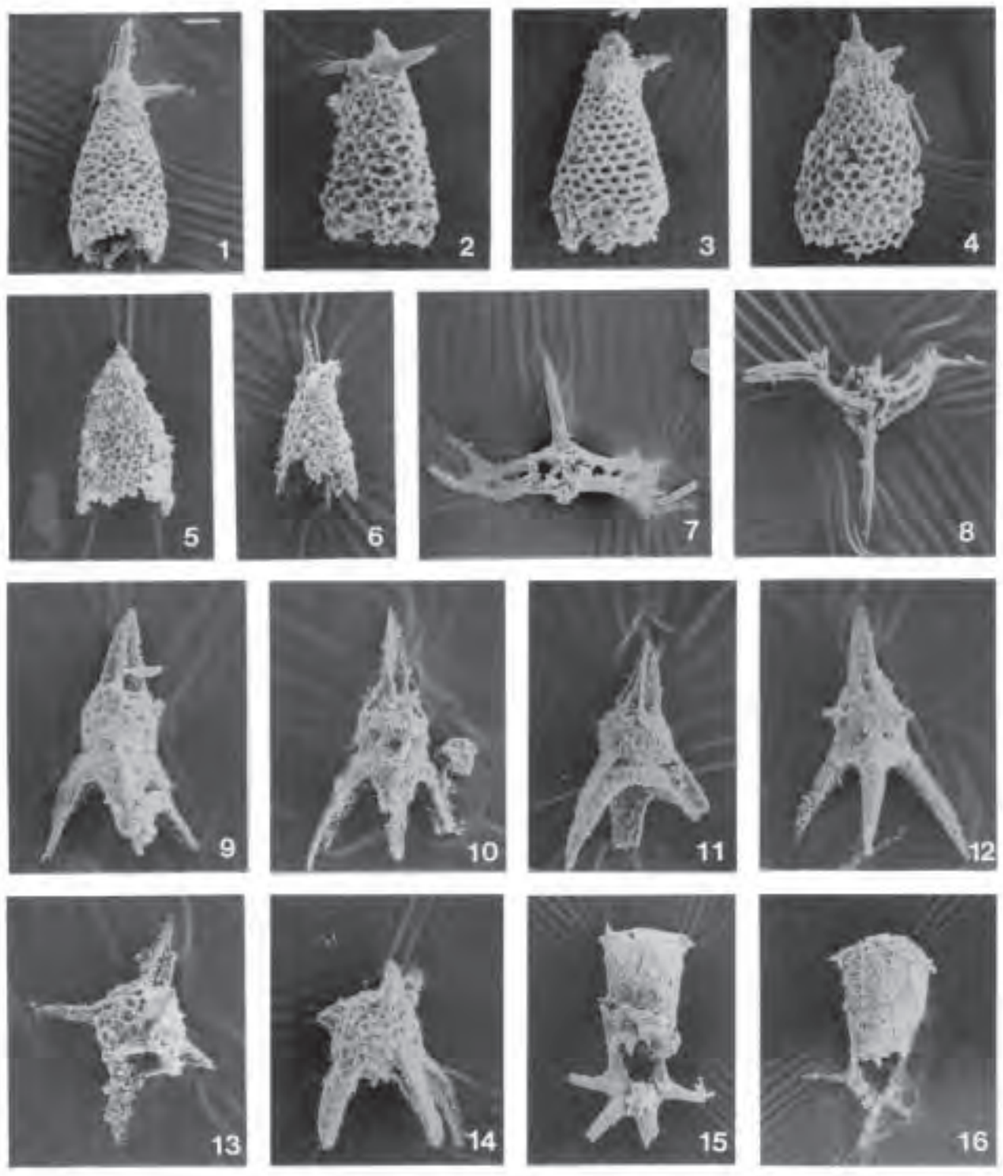

Figure 2

Figure 2. *A distance of 6 mm on these SEM photographs is equivalent to the length in μm indicated in parentheses. All specimens are from locality 97RB126 unless otherwise noted.*

1-3. *Popofskyellum? tetralongispina* n. sp. 1. Holotype, CH554 (33.3 μm). 2. CH507 (33.3 μm). 3. Note somewhat varying shapes of the hexagonal meshes of the shell wall, CH511 (33.3 μm)
4. *Popofskyellum?* sp. CH506 (28.5 μm)
5. *Totollum?* CH469 (28.5 μm) from locality 97RN321
6. *Cyrtentactinia?* CH555 (28.5 μm)
7. *Ceratoikiscum mirum* Cheng 1986 CH451 (33.3 μm)
8 . *Ceratoikiscum* sp. cf. *C. sandbergi* Cheng 1986 CH497 (33.3 μm)
9-10. *Archocyrtium riedeli* Deflandre 1972. 9. CH485 (22.2 μm) from locality 97RN321. 10. CH443 (22.2 μm)
11. *Archocyrtium venustum* Cheng 1986. CH496 (22.2 μm)
12. Specimen having characteristics between *A. venustum* Cheng 1986 and *A. procerum* Cheng 1986 and rudiments of spines on the cephalon, CH444 (22.2 μm)
13, 14. *Pylentonema* sp. CH445 (22.2 μm), CH460 (33.3 μm)
15, 16. *Holoeciscus foremanae* Cheng 1986. 15. CH465 (50 μm). 16. CH471 (22.2 μm) from locality 97RN321

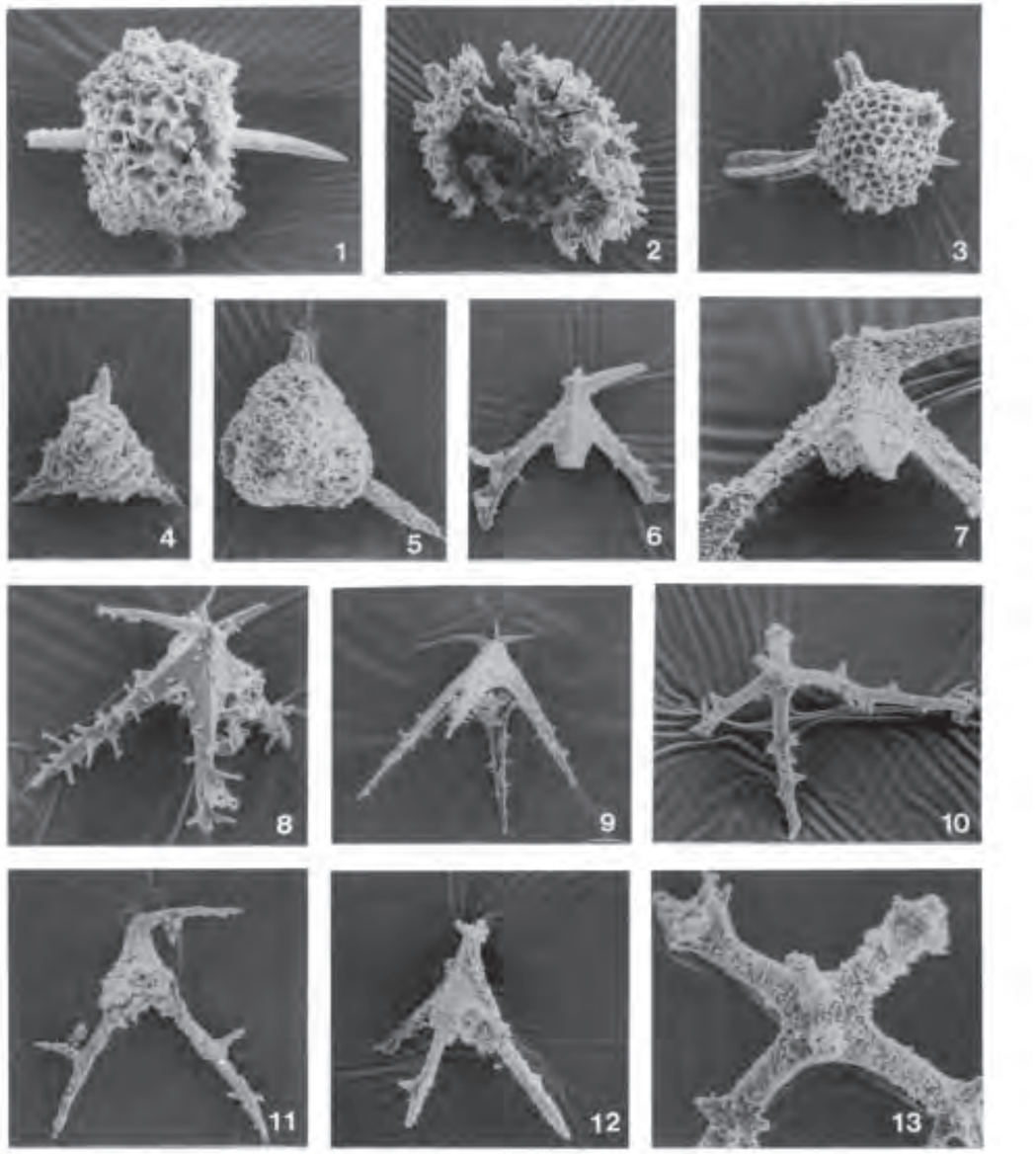

Figure 3

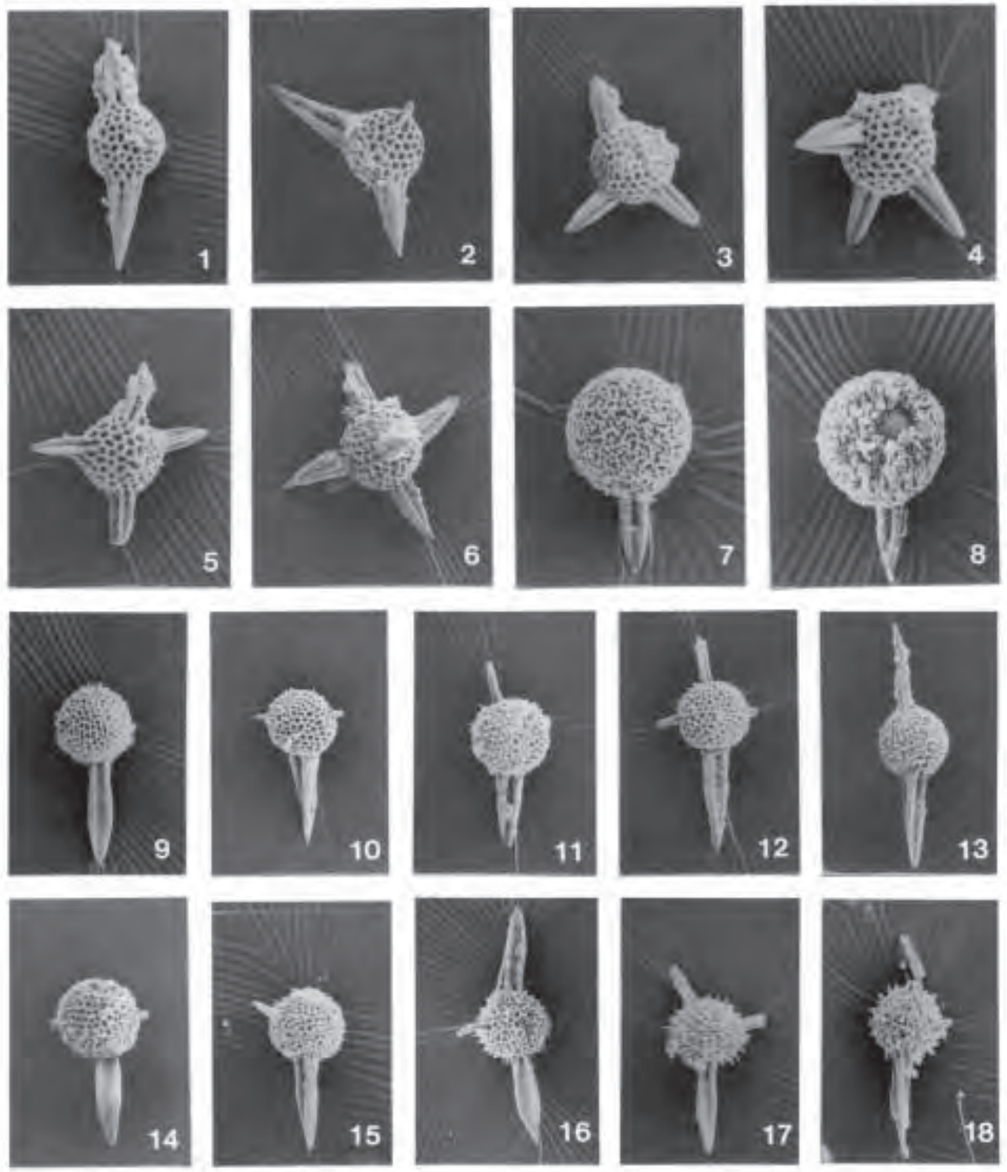

Figure 4

Thus, the absence or presence of the lateral rods might not be a critical characteristic for determining the generic-level classification. The new species, *P. tetralongispina*, is provisionally placed under *Popofskyellum*.

Family Palaeoscenidiidae Riedel 1967
Genus *Palaeoscenidium?* Deflandre 1953

Palaeoscenidium chulitnaensis Won n. sp.
Figures 3.10, 3.13

1990 *Palaeoscenidium cladophorum* Deflandre: Braun; pl. 1, figs. 4, 5

Derivation of name: From the Chulitna terrane where this species was recovered

Holotype: CH498 from locality 97RB126

Diagnosis: A skeleton consisting of six rod-like robust spines bearing spinules. More spinules on four spines than the other two spines. Two pairs of three spines connected at a meeting point.

Description: The skeleton consists of six very robust rod-like spines connected by a meeting point. From each ray spinules are raised. The spinules are somewhat apophysis-like, but the arrangement of the spinules is variable. The spinules arise at one position and are radially distributed, or are gathered in one area or haphazardly along the rays. The number and length of the spinules on each ray are different, but one spine of each pair has many fewer spinules than the other spines. The spinules seem to be connected to spongy tissue, which is not well preserved.

Remarks: Specimens of this species from boulders in the Main valley near Frankfurt/Main (Germany) were identified as *Palaeoscenidium cladophorum* by Braun (1990). However, the new species differs in possessing no tent-like structure and has six spines. Because of the lack of a tent-like structure, this species cannot belong to *Palaeoscenidium*. Also, the spinules of this species seem to be connected to spongy tissue which may not be preserved in the Chulitna fauna. Even if the spongy tissue were preserved and the spinules are equivalent to subfamily retentactininae established by Won (1997), the structure of the spinules differs from that of apophyses and the spines are connected by a meeting point unlike that of retentactininae. Thus, this species is provisionally placed on its higher level assignment.

Palaeoscenidium planum Won n. sp.
Figures 3.6-3.9

Derivation of name: Planus (Lat.), flat

Holotype: W1b-1206 from the Woodford Formation, Oklahoma

Diagnosis: A skeleton characterized by four two-bladed basal spines and four apical spines; one of the two blades of each spine extended and connected with the neighboring spine to form a space that resembles a tent-like structure; spinules developed on the outer side of the blade or along the edge of the blade; two of the apical spines longer than the other two.

Description: The skeleton consists of four basal and four apical spines. Each basal spine is two-bladed. These blades become narrower distally, and the spine is pointed at the tip. The blades are widened proximally, and each of them is connected smoothly to the adjacent spine. The connected parts form a space that is equivalent to the tent-like structure. Each pair of apical spines consists of a long and a short spine,

Figure 3 (left). *A distance of 6 mm on these SEM photographs is equivalent to the length in μm indicated in parentheses. All specimens are from locality 97RB126 unless otherwise noted.*

1, 2. *Retentactinia?* sp. Arrows indicate apophyses. 1. CH480 (44.4 μm). 2. CH466 (40 μm)
3. *Entactinia* sp. CH431(33.3 μm)
4, 5. *Tetrentactinia?* sp. 4. CH433 (33.3 μm) from locality 97RN321A. 5. CH508 (33.3 μm)
6-9. *Palaeoscenidium planum* n. sp. 6, 7. CH452 (40, 16.6 μm) 8. W2b-1223 (27.7 μm) from the Woodford Formation, Oklahoma. 9. Holotype: W1b-1206 (27.7 μm) from the Woodford Formation, Oklahoma; one short spine of left pair of apical spines is not visible
10, 13. *Palaeoscenidium chulitnaensis* n. sp. 10, 13. Holotype: CH498 (40, 16.3 μm) from locality 97RN321
11, 12. *Palaeoscenidium* sp. 11. CH448 (50 μm) from locality 97HA1. 12. CH500 (40 μm)

Figure 4 (left). *A distance of 6 mm on these SEM photographs is equivalent to the length in μm indicated in parentheses. All specimens are from locality 97RB126.*

1-6. *Entactinia variospina* Won 1983. 1. CH534 (50 μm). 2. CH423 (50 μm). 3. CH428 (66.6 μm). 4. CH537 (50 μm). 5. CH426 (50 μm). 6. CH425 (66.6 μm)
7, 8. *Plenospongiosa? gourmelonae* Won 1998. 7. CH436 (40 μm). 8. CH437 (40 μm)
9-18. *Entactinosphaera? palimbola* Foreman 1963. 9. CH563 (66.6 μm). 10. CH478 (66.6 μm). 11. CH461 (66.6 μm). 12. CH475 (66.6 μm). 13. CH420 (66.6 μm). 14. CH417 (66.6 μm). 15. CH565 (66.6 μm). 16. CH562 (66.6 μm). 17. CH477 (66.6 μm). 18. CH459 (66.6 μm)

and they are separated by a very short distance. In each pair, the long spine stands at right angles to the short spine. The two longer spines stand at opposite sides, and the two shorter spines stand at opposite sides. Spinules arise from the outer surface of the blade, at the edges of the blade, or at the edge where the two blades meet.

Remarks: None of the specimens of *P. planum* n. sp. from the Chulitna terrane is perfectly preserved. Thus, some features cannot be observed in the figure illustrating the specimen from the Chulitna terrane. The description of this species is also based on well-preserved specimens, one of which is taken as the holotype, in the Woodford Formation of Oklahoma. However, Cheng (1986) and Schwartzapfel and Holdsworth (1996) did not describe or illustrate this species. This species is rare in the Do unit but according to my observation of Woodford Formation faunas, it generally occurs with *Holoeciscus foremanae* in that formation. This new species is clearly distinguished from the other species of *Palaeoscenidium* by the presence of the two-bladed basal spines.

ACKNOWLEDGMENTS

We are deeply grateful to Katherine Reed and Paula Noble, both of whom provided technical and preliminary editorial reviews as well as valuable suggestions for additions to the manuscript. The siliceous microfossil study was supported by Pusan National University, Korea.

REFERENCES

Blodgett, R.B., and Clautice, K.H., 1998, New insights into the stratigraphy and paleontology of the Chulitna terrane and surrounding area, Healy A-6 Quadrangle, south-central Alaska [abst.]: The Alaska Geological Society, 1998, Science and Technology Conference, "Cutting Edge in Alaska," 2 p.

Braun, Andreas, 1990, Overdevonische Radiolarien aus Kieselschiefer-Geröllen des unteren Maintales bei Frankfurt am Main: Geologisches Jahrbuch Hessen, v. 118, p. 5–27.

Cheng, Y.-N., 1986, Taxonomic Studies on Upper Paleozoic Radiolaria: Taiwan, National Museum of Natural Science, Special Publication 1, 311 p.

Deflandre, Georges, 1953, Radiolaires fossiles, *in* Grassé, P.P., ed., Traité de Zoologie, Paris, Masson & Cie., v. 1, no. 2, p. 389–436.

———1964, La famille des Popofskyellidae fam. nov. et le genre *Popofskyellum* Defl., Radiolaires viséens de la Montagne Noire: Paris, Comptes Rendus Hebdomadaires des Seances de l'Académie des Sciences, v. 259, no. 18, p. 3055–3058.

Deflandre, Georges, 1972, Remarques complémentaires sur la morphologie et la nomenclature de quelques genres de Radiolaires du Paléozoïque: Paris, Comptes Rendus Hebdomadaires des Seances de l'Académie des Sciences, Serie D: Sciences Naturelles, v. 275, no. 1, p. 13–16.

Foreman, H.P., 1963, Upper Devonian Radiolaria from the Huron Member of the Ohio Shale: Micropaleontology, v. 9, no. 3, p. 267–304.

Gourmelon, Francoise, 1987, Les Radiolaires tournaisiens des nodules phosphatés de la Montagne Noire et des Pyrénées Centrales: Brest, France, Biostratigraphie du Paléozoique, v. 6, p. 1–172.

Jones, D.L., Silberling, N.J., Csejtey, Bela, Jr., Nelson, W.H., and Blome, C.D., 1980, Age and structural significance of ophiolite and adjoining rocks in the upper Chulitna district, south-central Alaska: U.S. Geological Survey Professional Paper 1121-A, 21 p.

Nazarov, B.B., 1975, Radiolyarii nizhnego-srednego paleozoya kazakhstana: Trudy Geologicheskie Institut, Akademiya Nauk SSSR, Vypusk 27, 202 p.

Riedel, W.R., 1967, Some new families of Radiolaria: Proceedings of the Geological Society of London, no. 1640, p. 148–149.

Schmidt-Effing, Reinhard, 1988, Eine Radiolarien-Fauna des Famenne (Ober-Devon) aus dem Franken-wald (Bayern): Geologica et Palaeontologica, v. 22, p. 33–41.

Schwartzapfel, J.A., and Holdsworth, B.K., 1996, Upper Devonian and Mississippian Radiolarian Zonation and Biostratigraphy of the Woodford, Sycamore, Caney and Goddard Formations, Oklahoma: Cushman Foundation for Foraminiferal Research; Special Publication 33, 275 p.

Won, M.-Z., 1983, Radiolarien aus dem Unter-Karbon des Rheinischen Schiefergebirges (Deutschland): Palaeontographica, Abteilung A, v. 182, p. 116–175.

———1990, Lower Carboniferous radiolarian fauna from Riescheid, Germany: Journal of the Paleontological Society of Korea, v. 6, no. 2, p. 111–146.

———1991, Phylogenetic study of some species of genus *Albaillella* Deflandre 1952 and a radiolarian zonation in the Rheinische Schiefergebirge, West Germany: Journal of the Paleontological Society of Korea, v. 7, no. 1, p. 13–25.

———1997, Review of the family Entactiniidae (Radiolaria) and taxonomy and morphology of the Entactiniidae in the late Devonian (Frasnian) Gogo formation, Australia: Micropaleontology, v. 43, no. 4, p. 333–369.

———1998, A Tournaisian (Lower Carboniferous) radiolarian zonation and radiolarians of the *A. pseudoparadoxa* Zone from Oese (Rheinische Schiefergebirge), Germany: The Journal of the Korean Earth Science Society, v. 19, no. 2, p. 216–259.

Short Notes on Alaska Geology 1999
Previous Editions of Short Notes on Alaska Geology

Short Notes on Alaskan Geology 1976: **DGGS Geologic Report 51 (out of stock, $3.50 photocopied)**

Reconnaissance geology along the Variegated Glacier, Saint Elias Mountains
Evidence for early Cenozoic orogeny in central Alaska Range
The Shumagin-Kodiak batholith: A Paleocene magmatic arc?
Speculative tectonic evolution of the Cenozoic Shelikof Trough, south-central Alaska
Discovery of blueschists on Kodiak Island
Large kaolinite crystals in the Chignik Formation (Upper Cretaceous), Herendeen Bay
Occurrence of sodic amphibole-bearing rocks in the Valdez C-2 Quadrangle
High-quality coal near Point Hope, northwestern Alaska

Short Notes on Alaskan Geology 1977**: DGGS Geologic Report 55 (out of stock, $5.00 photocopied)**

A Givetian (Late Middle Devonian) fauna from Healy B-4 Quadrangle, central Alaska Range
Probable karst topography near Jade Mountains, southwestern Brooks Range
Tectonic significance of the Knik River schist terrane, south-central Alaska
Geochronology of southern Prince of Wales Island Katmai caldera: Glacier growth, lake rise, and geothermal activity
Geology and K-Ar age of mineralized intrusive rocks from the Chulitna mining district, central Alaska
The Richardson lineament: A structural control for gold deposits in the Richardson mining district, interior Alaska
Boulder Creek tin lode deposits
Comparison of mercury-antimony-tungsten mineralization of Alaska with strata-bound cinnabar-stibnite-scheelite deposits of the Circum-Pacific and Mediterranean regions
Earthquake recurrence and location in the western Gulf of Alaska

Short Notes on Alaskan Geology 1978**: DGGS Geologic Report 61 ($2.00)**

Holocene displacements measured by trenching the Castle Mountain fault near Houston
Bluff Point landslide, a massive ancient rock failure near Homer
Recurrent late Quaternary faulting near Healy
Glaciation of Indian Mountain, west-central Alaska
The Cantwell ash bed, a Holocene tephra in the central Alaska Range
Geochronology of metamorphic and igneous rocks in the Kantishna Hills, Mount McKinley Quadrangle
The Chilikadrotna Greenstone, an Upper Silurian metavolcanic sequence in the central Lake Clark Quadrangle
Tectonic and economic significance of Late Devonian and late Proterozoic U-Pb zircon ages from the Brooks Range

Short Notes on Alaskan Geology 1979-80**: DGGS Geologic Report 63 ($1.00)**

Lead isotope ratios from the Red Dog and Drenchwater Creek lead-zinc deposits, De Long Mountains, Brooks Range
^{40}K-^{40}Ar ages from rhyolite of Sugar Loaf Mountain, central Alaska Range: Implications for offset along the Hines Creek strand of the Denali fault system
Multiple glaciation in the Beaver Mountains, western interior Alaska
Fossil algae in Lower Devonian limestones, east-central Alaska
Tertiary tillites(?) on the northeast flank of Granite Mountain, central Alaska Range
Evidence for suprapermafrost ground-water blockage, Prudhoe Bay oil field

Short Notes on Alaskan Geology 1981: **DGGS Geologic Report 73 ($3.00)**

Alkaline igneous rocks in the eastern Alaska Range
Shear moduli and sampling ratios for the Bootlegger Cove Formation as determined by resonant-column testing
Clinoptilolite and mordenite deposits of possible economic value at Iliamna Lake, Alaska
The Keete Inlet thrust fault, Prince of Wales Island
Two Holocene maars in the central Alaska Range
Radiometric-age determinations from Kiska Island, Aleutian Islands, Alaska
Geochemical signature of the Goon Dip Greenstone on Chicagof Island, southeastern Alaska
Uranium mineralization in the Nenana Coal Field, Alaska
Reconnaissance of rare-metal occurrences associated with the Old Crow batholith, eastern Alaska - north-western Canada
A recent earthquake on the Denali fault in the southeast Alaska Range
Triassic paleomagnetic data and paleolatitudes for Wangellia, Alaska

***Short Notes on Alaskan Geology 1982-83*: DGGS Professional Report 86 ($2.50)**

An unconformity with associated conglomeratic sediments in the Berners Bay area of southeast Alaska
An iron-rich lava flow from the Nenana coal field, central Alaska
Results of shallow seismic survey for ground water at McGrath
Evaluation of a shallow sand-and-gravel aquifer at Eagle River
Correlation of geophysical well logs for a water development in south Anchorage
Garnet compositional estimates as indicators of progressive regional metamorphism in polymetamorphic rocks, Kantishna Hills
Geology of the Miss Molly molybdenum prospect, Tyonek C-6 Quadrangle Glacial geology of the Mt. Prindle area, Yukon-Tanana Upland

***Short Notes on Alaskan Geology 1991*: DGGS Professional Report 111 ($8.00)**

Tin placers associated with the downcutting of fissure basalts, Ray River drainage, Alaska
Geology and geochemistry of the Gagaryah barite deposit, western Alaska Range, Alaska
Geology and geochemistry of Tatlawiksuk Hot Springs, a newly discovered geothermal area in western Alaska
Geology and geochemistry of the Sleitat Mountain tin deposit, southwestern Alaska
Native mercurian-silver, silver, and gold nuggets from Hunter Creek, Alaska
Late Pleistocene volcanic deposits near the Valley of Ten Thousand Smokes, Katmai National Park, Alaska
Deglaciation of the Allison-Sawmill Creeks area, southern shore of Port Valdez, Alaska
Dating Holocene moraines of Canwell Glacier, Delta River valley, central Alaska Range
Gilead sandstone, northeastern Brooks Range, Alaska: An Albian to Cenomanian marine clastic succession
Kikiktat Mountain klippe: A link between the Copter Peak and Nuka Ridge allochthons, northcentral Brooks Range, Alaska
Sample media useful for a systematic geochemical survey of upper Valdez Creek, Alaska

***Short Notes on Alaskan Geology 1993*: DGGS Professional Report 113 ($6.00)**

Mississippian terrigenous clastic and volcaniclastic rocks of the Ellesmerian sequence, upper Sheenjek River area, eastern Brooks Range, Alaska
The penultimate great earthquake in southcentral Alaska: evidence from a buried forest near Girdwood
Geology, alteration, and mineralization of the Vinasale Mountain gold deposit, west-central Alaska
Fumarolic gas chemistry (1982) and thermal spring water chemistry (1985), Crater Peak, Mount Spurr, Alaska
Organic-rich shale and bentonite in the Arctic Creek unit, Arctic National Wildlife Refuge: implications for stratigraphic and structural interpretations
Dating Holocene moraines of Black Rapids Glacier, Delta River valley, central Alaska Range
Paleomagnetism of the Fairbanks basalts, interior Alaska
The Hayes Glacier fault, southern Alaska Range: evidence for post-Paleocene movement
Detachment folds and a passive-roof duplex: examples from the northeastern Brooks Range, Alaska

***Short Notes on Alaskan Geology 1995*: DGGS Professional Report 117 ($15.00)**

Radiocarbon age of probable Hayes tephra, Kenai Peninsula, Alaska
Geochemistry of saline lakes of the northeastern Yukon Flats, eastcentral Alaska
Geometry and deformation of a duplex and its roof layer: Observations from the Echooka anticlinorium, northeastern Brooks Range, Alaska
Late-Wisconsin events in the Upper Cook Inlet region, southcentral Alaska
Stratigraphy and implications of a lakeside section, Glacial Lake, southwestern Kigluaik Mountains, Seward Peninsula, Alaska
Lithofacies, petrology, and petrophysics of the Kemik Sandstone (Lower Cretaceous), eastern Arctic Slope, Alaska
A new species of the conodont *amydrotaxis* From the Early Devonian of southwestern Alaska
Early Devonian and Late Triassic conodonts from Annette and Hotspur Islands, southeastern Alaska
Mineralization and zoning of polymetallic veins in the Beaver Mountains volcano-plutonic complex, Iditarod Quadrangle, westcentral Alaska
Possible thrust windows on the central Seward Peninsula, Alaska

***Short Notes on Alaskan Geology 1997*: DGGS Professional Report 118 ($9.00)**

Geochronologic investigations of magmatism and metamorphism within the Kigluaik Mountains gneiss dome, Seward Peninsula, Alaska
Composite standard correlation of the Mississippian-Pennsylvanian (Carboniferous) Lisburne Group from Prudhoe Bay to the eastern Arctic National Wildlife Refuge, North Slope, Alaska
Enigmatic source of oil from Chukchi Sea, northwestern Alaska
Emsian (late Early Devonian) fossils indicate a Siberian origin for the Farewell Terrane
Growth-position petrified trees overlying thick Nanushuk Group coal, Lili Creek, Lookout Ridge Quadrangle, North Slope, Alaska
Paleotopographic control on deposition of the lower Kayak Shale, northern Franklin Mountains, Brroks Range, Alaska
Cooling history of the Okpilak batholith, northeastern Brooks Range, as determined from potassium-feldspar thermochronometry
First occurrence of a hadrosaur (Dinosauria) from the Matanuska Formation (Turonian) in the Talkeetna Mountains of south-central Alaska
Petrography of the Tingmerkpuk Sandstone (Neocomian), northwestern Brroks Range, Alaska: A preliminary study
Lower to Middle Devonian (latest Emsian to earliest Eifelian) conodonts from teh Alexander Terrane, southeastern Alaska
Preliminary petrography and provenance of six Lower Cretaceous sandstones, northwestern Brooks Range, Alaska

View eastward along the west fork of Atigun River of prominent anticlinal hinge in the Upper Kanayut Conglomerate (Lower Mississippian to Upper Devonian) within the Toyuk thrust zone, a major thrust zone in the central Brooks Range. See Chmielowski and Wallace (this volume), "Duplex structure and Paleocene displacement of the Toyuk thrust zone near the Dalton Highway, north-central Brooks Range." (Photo by Reia M. Chmielowski)

Excavator and bulldozer trench on Lewis Ridge, Donlin Creek property, southwestern Alaska. Trench is approximately 1,300 feet long and part of a 3.7-mile trenching program by Placer Dome Exploration Inc. during the 1997 and 1998 field seasons. Light-colored rocks are igneous dikes and sills, and darker rocks are Kuskokwim Group shale and graywacke. Note the core drill rig in the background to the right of center. (Photo by David Szumigala)